ISTITUTO UNIVERSITARIO DI
STUDI SUPERIORI -
IUSS

UNIVERSITÀ DEGLI STUDI DI PAVIA
Dipartimento di Medicina Molecolare
Unità di Biochimica

PhD in Biomolecular Sciences and Biotechnology - cycle XXXIII

Impaired osteoblasts homeostasis and matrix quality in Osteogenesis Imperfecta are rescued by 4-phenylbutyrate

Tutors:

Prof.ssa Antonella Forlino

Dr.ssa Roberta Besio

PhD experimental thesis by

Nadia Garibaldi

Academic Year 2019/2020

INDEX

INTRODUCTION……..……...…….1

I – Collagen and bone formation…….....2

- **Fibrillar collagen in bone**…….....2
- **Collagen type I: structure and biosynthesis**……..……....3
- **Procollagen I secretion and collagen matrix incorporation**…….…….....6
- **Accessory proteins for collagen I fibrillogenesis**…….....7
- **Osteoblasts: from differentiation to mineralization**……8
- **Osteocytes: the terminal stage of OBs differentiation**……...11
- **Osteoclasts**……12

II: Osteogenesis imperfecta……14

- **Classification of OI forms**…… 14
  - *Defects in collagen type I synthesis and structure*……...14
  - *Collagen post-translational modifications defects*……..15
  - *Defects in collagen chaperoning, processing and crosslinking*……...16

- *Bone formation and mineralization defects*……17
- *Osteoblast differentiation and activity defects*……18
- *Latest OI forms*……....20

- **Intracellular collagen retention and ER stress**……....24

III: OI therapeutic approaches…….....29

- **Anti-resorptive treatments**……...29

- *Bisphosphonates*……..29
- *Denosumab*……..30

- **Bone anabolic treatments**……..30

- *Teriparatide*……30
- *Anti-sclerostin antibody*……...31
- *Anti-TGF-β antibody*……..……..32

- **Cell therapy**……..32

- **Matrix vescicles therapy**…….....33

- **Gene therapy**…….....34

- **4 - Phenylbutyrate**……...……35

IV: murine models of classical Osteogenesis imperfecta……..38

- **Brtl mouse** …….....40

- **Amish mouse**……43

Chapter I

4-PBA ameliorates cellular homeostasis in fibroblasts from Osteogenesis Imperfecta patients by enhancing autophagy and stimulating protein secretion……..…45

Chapter II

Cellular stress due to impairment of collagen prolyl hydroxylation complex is rescued by the chaperone 4-phenylbutyrate …….57

Chapter III

Targeting cellular stress improves osteoblasts homeostasis and matrix in murine models of Osteogenesis Imperfecta……...……72

Chapter IV

Osteoblasts mineralization and collagen matrix are conserved upon specific *Col1a2* silencing ……..……...120

BIBLIOGRAPHY…….134

Introduction

I – Collagen and bone formation

The bone tissue is a specialized form of connective tissue characterized by a specific cellular composition and by a mineralized extracellular matrix (ECM) [1, 2]. It is the main constituent of the skeleton, which serves a mechanical function of body scaffold and protection of internal organs.

The synthesis of the bone tissue is mediated by osteoblasts, which work in tight cooperation with bone-resorbing osteoclasts and with osteocytes, the cells orchestrating all the bone processes [3]. Osteoblasts synthetize the bone ECM, though a process called osteogenesis. Osteoclasts carve out the bone shape and adjust it to the demands of the body growth and metabolism in two processes called modeling and remodeling, respectively. Indeed, bone remodeling is an important step in regulating Ca^{2+} plasma concentration and homeostasis. Fine tuning of this system is crucial for the development of bones, for repairing fractures, and for the correct maintenance of the skeleton throughout life.

The ECM is constituted by an organic fraction called osteoid, mainly (~90%) made of type I collagen, and by an inorganic fraction, the mineral component, consisting largely of hydroxyapatite [Ca_{10} $(PO_4)_6$ $(OH)_2$] needle-like crystals oriented in the same direction as collagen fibrils [4]. While the organic matrix confers to the bone its resistance to traction and pressure, the inorganic one is responsible for its stiffness. The combination of these features produces a bone architecture that is both resistant and lightweight, therefore it is proper to fulfill the bone mechanical functions.

Fibrillar collagen in bone

Collagens are the most abundant proteins in mammals and their structure share, as a common feature, the presence of a triple helix of three α polypeptide chains that can be identical, and form homotrimers, or different, and form heterotrimers [5].

A subgroup of the 28 members of collagen family [5] is constituted by fibrillar collagens, whose precursors assemble into fibrils that constitute an important scaffold for extracellular matrix organization. Collagen type I and type II are of particular interest since they are the most abundant in the body and the main components of the organic bone matrix and of cartilage, respectively. Once secreted, collagen type I assembles into microfibrils of five molecules that closely interact with the adjacent microfibrils, leading to the quasi-hexagonal

packing of collagen molecules and allowing the subsequent mineral deposition that constitutes a hallmark of bone ECM [6].

Along with bones, collagen type I is also one of the principal components of tendons, skin, ligaments, cornea, and many interstitial connective tissues [7].

Collagen type I: structure and biosynthesis

Collagen type I is a heterotrimer composed by two α1 and one α2 chains, coded by *COL1A1* and *COL1A2* genes, respectively, which assemble into a procollagen molecule made of a central triple helix flanked by a C-telopeptide and a N-telopeptide. The telopeptides contain hydroxylysine residues that are important for collagen crosslinks formation, and are respectively flanked by a C-terminal and a N-terminal globular non-collagenous propeptide [8, 9] (**Fig.1**).

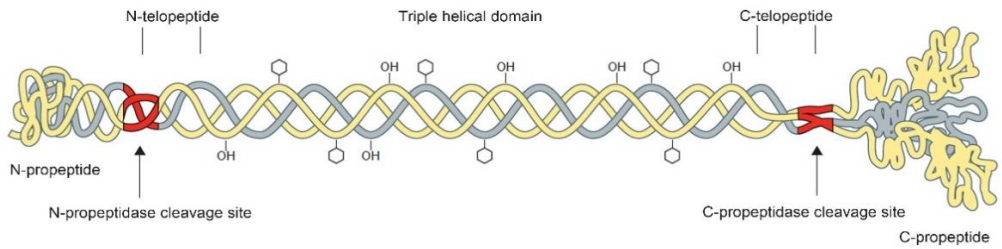

Figure 1: **procollagen type I structure, modified from [10]**. Two α1 and one α2 chains assemble and form a procollagen molecule, constituted by a central triple helical domain flanked by N- and C-terminal telopeptides and propeptides. Proline and lysine hydroxylations and hydroxylysine glycosylations along the helical regions of both chains are necessary for the correct folding of the triple helix.

Procollagen type I chains are co-translationally translocated into the lumen of the endoplasmic reticulum (ER) [11]. Following their synthesis, the C-terminal propeptides of each chain remain temporarily attached to the ER membrane, where they work as nucleation sites for the triple helix formation. When the chains are still unfolded, they undergo a series of post-translational modifications by several enzymes: prolyl 4-hydroxylase 1 (P4H1) is responsible for the C4 hydroxylation of helical proline residues in position Y of the Gly-Xaa-Yaa repeats, important for helix stability by favouring water-bridged intramolecular hydrogen bonding; prolyl 3-hydroxylases 1 and 2 (P3H1 and P3H2) are responsible for the

3-hydroxylation of proline residues in specific X positions; lysyl hydroxylases 1 and 2 (LH1 and LH2), which act on collagen triple helix and telopeptides respectively, turn lysine residues in hydroxylysines, providing the substrates for successive intracellular glycosylation and extracellular covalent cross link formation.

Among the collagen-specific modifications, the 3-hydroxylation of proline 986 in each of the α1 chains of procollagen I, performed by the prolyl 3-hydroxylation complex, is particularly important because it facilitates the formation and stabilization of procollagen triple helices [12, 13]. Besides the 3-hydroxylase activity, the complex also works as a chaperone for collagen folding [14-16], and it is composed of three proteins: prolyl 3-hydroxylase 1 (P3H1), encoded by *P3H1* gene, cartilage-associated protein (CRTAP), encoded by *CRTAP* gene, and peptidyl-prolyl *cis-trans* isomerase B (Cyclophilin B or CyPB), encoded by *PPIB* gene [17].

P3H1 catalyzes the hydroxylation of proline, imparting the enzymatic function of the complex. CRTAP does not have enzymatic activity, but participates to P3H1 activity as a helper protein by facilitating its association with nascent procollagen chains [18]. CyPB is a *cis-trans* isomerase that allows the proline residues to reach the *trans* conformation, thus accelerating protein folding [19]. To this purpose, it directly interacts with procollagen molecules, catalysing *cis-trans* proline conversion. It is also involved in procollagen export and secretion along with heat shock protein 47 (HSP47) [20]. Its role in prolyl 3-hydroxylation complex is still not completely understood and its absence does not affect the other two proteins of the complex. CyPB does not only participate to P3H1 complex, but also exists independently of it, playing a role in other collagen modifying complexes [21-23] and in inflammation, viral infection, and cancer [24].

Together with their hydroxylating functions, P4H1 and prolyl-3 hydroxylation complex interact with collagen as chaperones to ensure the correct collagen triple helix folding, by making it thermodynamically favorable [25].

Following the necessary modifications, procollagen chains associate, after the formation of stabilizing intra-chain disulphide bonds, and fold into a triple helix from the C-terminus to the N-terminus. Once folded, the procollagen molecule is stabilized in the ER by specific chaperones such as HSP47, which binds procollagen at the consensus binding sequence Gly-Xaa-Arg in the triple helix, where it avoids local unfolding and incorrect intracellular

aggregation of the chains [26]; furthermore it carries out its chaperoning function during procollagen progression from the ER to the ER-Golgi intermediate compartment [27].

Another important chaperone binding procollagen triple helix is FKBP65, that has an important peptidyl-prolyl *cis-trans* isomerase activity and interacts with HSP47, promoting an increase in collagen folding rate [28]. It also modulates LH2 enzymatic activity, which is important for the formation of collagen cross-links [29]. HSP47, FKBP65 and LH2 interact form a complex stabilized by the ER-resident chaperone BIP, that regulates type I procollagen telopeptide lysyl hydroxylation [30, 31] (**Fig.2**). It is demonstrated that FKBP65 also interacts with triple helical collagen, as it delays collagen type I fibril formation, at least in *in vitro* experiments [32]. The chaperones lead to the retention of unfolded collagen molecules within the ER and to the progression towards the secretory pathway of correctly folded molecules.

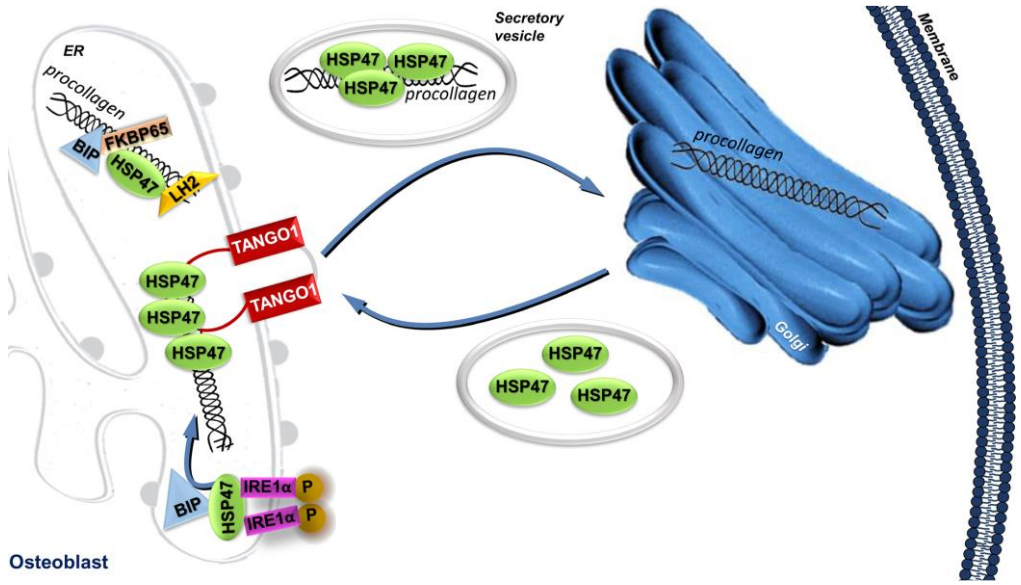

Figure 2: **procollagen I chaperoning and trafficking from ER to Golgi [33]**.
In the ER, HSP47 interacts with FKBP65 and LH2. The stability of this complex is regulated by the master effector of the Unfolded Protein Response (UPR) pathway, BIP. Upon binding to HSP47, procollagen trafficking toward Golgi is mediated by the formation of large COPII vesicles derived by the HSP47 anchorage to the SH3 domain of the ER protein TANGO1. Once reaching the Golgi, HSP47 releases its cargo in a pH-dependent manner and it is recycled back to the ER thanks to the presence of a C-terminal RDEL retention signal.

Procollagen I secretion and collagen matrix incorporation

Procollagen I is a large molecule, therefore a special COPII-based trafficking system is required for its transport from the ER to the Golgi apparatus.

HSP47 collagen-specific chaperone is one of the key players in this process, as it binds the folded triple helical regions of collagen molecules, thus stabilizing their structure [34]. Furthermore a recent study demonstrated that at low molar ratios HSP47 preferentially binds collagen I in proximity of the N-terminal region, while at higher molar ratios it uniformly distributes along pro-collagen I [35]. Together with its collagen chaperone role, HSP47 also carries a binding site for a specific domain of the ER protein transmembrane protein transport and Golgi organization 1 (TANGO1) [36, 37], which mediates collagen entrance into secretory vesicles that progress towards the Golgi compartment. In particular after recruiting its homolog and coreceptor cTAGE5, which lacks the ER-resident domain, TANGO1 promotes large carrier formation at ER exit sites (ERES) by assembling into rings around the budding membrane to prevent premature coat formation. Then it links, by direct binding, large cargo proteins to the COPII coat proteins Sec23-Sec24 [38]. COPII vesicles grow, incorporating the cargo proteins, and build two superimposed layers: an inner coat of Sec23/24 proteins and an outer cage made of Sec13/31 proteins [39]. Once the vesicle is completed, COPII proteins detach thanks to GTP hydrolysis, and allow vesicle fusion with the ER-Golgi intermediate compartment (ERGIC).

In the Golgi apparatus, procollagen is transported in post-Golgi tubular-saccular carriers by the detachment of large regions of the trans Golgi [40-42] and bundles of procollagen are then released from the trans-face of the Golgi to form secretory vesicles, as shown by ultrastructural studies in human fibroblasts [43-45]. Finally, the secretory vacuoles fuse with the plasma membrane, releasing collagen molecules in the ECM. Here two further maturation processes take place. The first one is a proteolytic cleavage mediated by two specific zinc- proteases, ADAM metallopeptidase domain 2 (ADAMTS2) and bone morphogenetic protein 1 (BMP-1), that remove the globular N- and C-terminal propeptides, respectively. The cleavage strongly reduces collagen solubility, leading to its spontaneous self-assembly into fibrils [46].

In addition, an enzymatic oxidative deamination, performed by lysyl-oxidase (LOX), occurs to the telopeptidyl lysine and hydroxylysine residues producing reactive telopeptidyl-aldehydic residues. These residues react with another aldehyde or with amine groups derived

from unmodified lysine and hydroxylysine residues, initiating a series of non-enzymatic condensation reactions that result in the formation of covalent intra- and intermolecular cross-links, important for the biomechanical functions of collagen fibrils [47] (**Fig.3**).

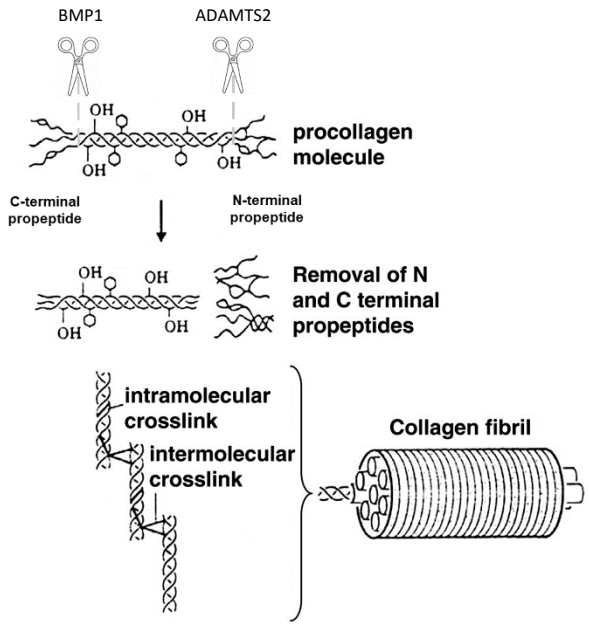

Figure 3: **procollagen I extracellular processing and incorporation into fibrils, modified from [48]**. Once procollagen has been released in the ECM, BMP1 and ADAMTS2 proteases cut the C- and N- terminal propeptides, respectively, producing a mature collagen I molecule that crosslinks with other molecules, forming a network of collagen fibrils.

Accessory proteins for collagen I fibrillogenesis

Several proteins are required for the correct formation of collagen I fibrils, which is a very accurate and complex process. A crucial one is fibronectin, a glycoprotein that is secreted as a disulfide-bonded dimer and carries three types of repeating modules, necessary to make interactions with cells, ECM components and other fibronectin molecules. Polymerization of fibronectin also requires the participation of integrins, transmembrane receptors that facilitate adhesion between cells and the ECM. Collagen I is known to interact with fibronectin and integrins, which are sort of organizers of fibrils formation, however their specific sites of interactions require further studies [49]. Fibril formation takes place thanks to molecules working as nucleators and regulating collagen I fibrils diameter, among them a relevant role is covered by the heterotrimeric fibrillar collagen type V, in which a portion

of the N-propeptide is retained after processing and serves to nucleate fibrils formation [50-52], and fibrillar collagen type III, whose molecules are strictly linked to collagen I fibers in the matrix [53].

Type XII and XIV FACIT collagens are also present in tissues containing collagen I, particularly they can be spliced into different variants that can confer specific properties to the fibrils and regulate their diameter [52].

Lastly the regulatory function of fibrils formation, in terms of rate of assembly, size, and structure of fibrils, is provided by multiple proteins and small molecules such as small leucine rich proteoglycans (SLRPs), consisting of a core protein and covalently attached glycosaminoglycan (GAG), that participate to the stability of collagen fibrils by protecting them from proteolysis and directly bind regulating factors such as TGFβ. SLRPs include decorin, biglycan, fibromodulin and lumican [54].

Osteoblasts: from differentiation to mineralization

Osteoblasts (OBs), cuboidal cells whose activity is highest during embryonic skeletal formation and growth, are the cells responsible for both collagen deposition and mineralization of the ECM, the two processes required for bone formation [3]. Osteoprogenitor cells originate from pluripotent mesenchymal stem cells (MSCs) of the bone marrow (**Fig.4**). MSCs give origin to other cell lineages, such as myoblasts, chondrocytes or adipocytes, thus, the activation of master transcriptional regulators is required to ensure the proper differentiation. For OBs, the main upstream regulator is Runt-related transcription factor 2 (RUNX2), a factor activated by phosphorylation operated by the mitogen-activated protein kinase (MAPK) pathway and producing MSCs conversion to pre-OBs [55]. At first, RUNX2 upregulates specific OBs differentiation-inducing pathways, including Hedgehog, Wnt/β-catenin and bone morphogenetic proteins (BMPs) pathways [3]. Furthermore, it directly regulates the zinc-finger transcription factor SP7, also called Osterix (OSX), that leads to mature matrix-producing OBs, further enhancing RUNX2 expression and promoting the expression of collagen I, alkaline phosphatese (ALP) and bone sialoprotein (BSP) during early maturation stages, and osteonectin (ON), osteopontin (OPN), osteocalcin (OCN) and other bone matrix proteins in late OBs differentiation stages [56].

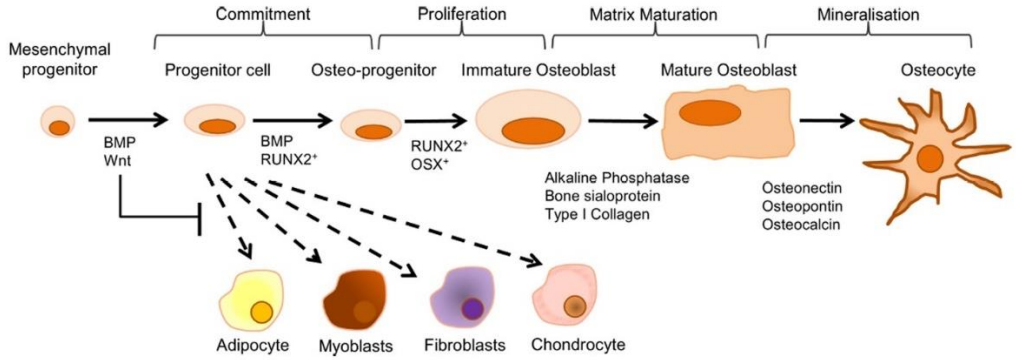

Figure 4: **osteoblasts differentiation, modified from [57]**. Signaling by members of the canonical Wnt/ β-catenin pathway directs the mesenchymal stem cell fate toward the osteoblast lineage by inducing the osteogenic transcription factors RUNX2 and OSX. Immature osteoblasts still have the potential to divide. They express high level of ALP, BSP and type I collagen. Differentiation progresses towards the nonproliferating mature osteoblasts stage, characterised by increased expression of ALP and several non-collagen proteins, in which matrix maturation takes place. At the completion of bone formation, a subset of osteoblasts can undergo further differentiation, upon being embedded in the bone matrix, and become osteocytes. The remaining osteoblasts are thought to either undergo apoptosis or become inactive bone-lining cells.

OBs-produced collagen I fibrils in bone ECM form a network that works as a scaffold for mineralization [58], as they line up head-to-tail to form repeating arrays which confers flexibility to the nonmineralized tissues. Nevertheless, the bone matrix also needs specific inorganic components, in particular calcium and phosphate, but also carbonate, magnesium, sodium and potassium in minor quantities, in order to complete its mineralization process. The negatively charged carboxyl and carbonyl groups distributed on collagen molecules constitute the nucleation sites where calcium and phosphate ions bind, triggering the formation of the hydroxyapatite (HA) crystals [58].

To the purpose of mineral deposition, the extracellular membrane-invested particles named matrix vesicles (MVs) play a crucial role. They originate by polarized budding and pinching-off from specific regions of the outer plasma membranes of OBs. The first crystals of hydroxyapatite form on the inner surfaces of vesicles membranes, following Ca^{2+} and PO_4^{3-} uptake performed by ion channels and transporters [59]. Then the activity of MVs membrane-located proteins such as phosphatases, in particular ALP, and of calcium-binding molecules promote the growth of mineral crystals, which are released from the vesicles in

the ECM. The extracellular environment supplies additional Ca^{2+} and PO_4^{3-} ions to continue crystal growth [60].

ALP in particular is responsible for the regulation of phosphate production, which is essential for mineralization [61]. ALP is an ectoenzyme attached to the outer face of the plasma membrane through a phosphatidyl inositol-glycophospholipid anchor [62] and it is highly expressed in osteoblasts and chondrocytes of the calcifying cartilage.

Because extracellular inorganic pyrophosphate inhibits hydroxyapatite formation, ALP hydrolyzes pyrophosphate and provides inorganic phosphate to promote mineralization [63].

Once in the ECM, the mineral particles at first align in parallel to the fibril axis of the collagen and deposit within the empty spaces between collagen molecules and collagen fibrils, subsequently crystals spread throughout the matrix [64].

Several non-collagenous molecules, found tightly associated with collagen, are also required for the formation and maturation of mineralized tissues, such as proteoglycans, hyaluronic acid and chondroitin sulphate, contributing to the bone construction [65, 66]. Other important molecules are released by osteoblasts in the collagen fibers network: osteonectin (ON), also named SPARC or secreted protein acidic and rich in cysteine, binds to collagen and HA crystals and releases calcium ions, enhancing mineralization of the collagen matrix in bone [67]; BSP is a highly glycosylated and sulphated phosphoprotein that binds hydroxyapatite and works as a promoter and nucleator of *de novo* mineralization [68]; osteopontin (OPN), also called bone sialoprotein I, is a secreted acidic protein that binds calcium-based biominerals and inhibits mineralization to regulate crystals growth [69]; lastly, osteocalcin (OCN), also known as bone gamma-carboxyglutamic acid-containing protein (BGLAP), in its carboxylated form is packaged into intracellular vesicles for secretion into the bone matrix [70] where it binds calcium ions in hydroxyapatite, allowing to locally increase its concentration [71].

ON and BSP are expressed strongly in the osteogenetic phases in which the bone matrix is still not calcified, while OPN and OCN start to be expressed when the bone matrix is already calcified [72]. In particular, mature OCN is secreted by OBs into the bone micro-environment and aligns its specific calcium-binding residues with the calcium ions in hydroxyapatite, inhibiting the precipitation of calcium salts and consequently inhibiting bone mineral crystals formation [73]; in addition, OCN serves as a chemotactic signal for osteoclasts and stimulates their differentiation, maturation, and activity, proving to be

essential in bone turnover [74]. The mineralized matrix, together with the complex network of non-collagenous proteins that constitute the bone matrix and contribute to its organization, is essential to reinforce the bone tissue, to augment its strength and to confer its structural and biomechanical properties. Its composition varies depending on ageing and dietary factors.

Osteocytes: the terminal stage of OBs differentiation

Once OBs have completed their differentiation and mineralization of the surrounding matrix, they express late stage genes, such as *DMP1*, encoding for dentin matrix acidic phosphoprotein 1, and *SOST*, encoding for sclerostin, an inhibitor of Wnt/β-catenin pathway and of bone mineralization [56]. At this point they complete their differentiation path remaining progressively trapped into the bone matrix, in small cavities named bone lacunae, and turning into osteocytes.

These are the most abundant cells in adult bones, incapable of dividing by mitosis and extremely long-lived compared to OBs and OCs, as they survive for decades in the bone matrix. They are characterized by thin cytoplasmic extroflexions that extend in bone canaliculi digged through the matrix, reaching the bone surface and bone vasculature, and they are surrounded by a fluid, still not well characterised, that allows exchanges of nutrient and gaseous substances and cellular communication by circulation of signaling molecules [2, 75].

Although being terminally differentiated and quiescent cells, osteocytes cover essential functions for bone homeostasis. They have a mechanosensory role since they control adaptive responses to mechanical loading of the skeleton, they orchestrate bone remodeling by regulating both OBs and osteoclast function, and, lastly, they integrate hormonal and mechanical signals in the regulation of bone mass [75].

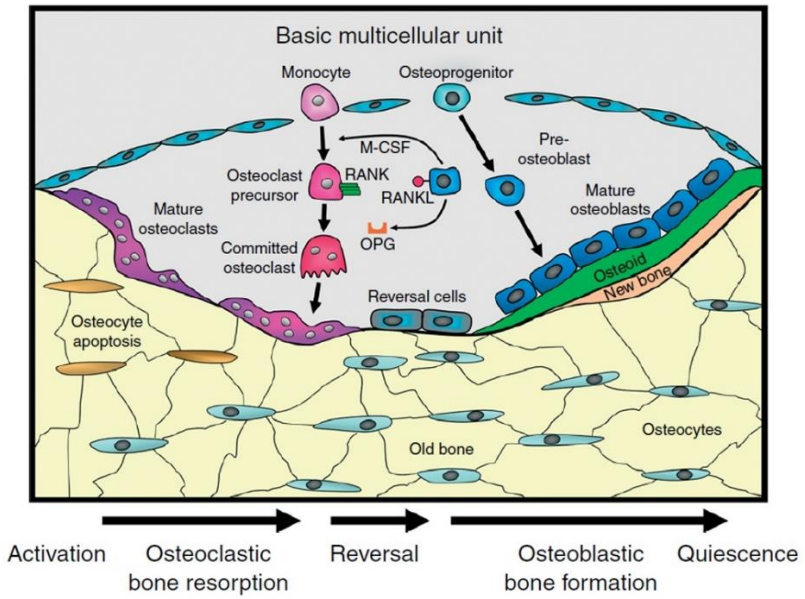

Figure 5: **schematic representation of the basic multicellular unit of the bone remodeling cycle [76]**. Osteoblasts, that differentiate from osteoprogenitor cells, deposit bone matrix and gradually remain embedded in the mineralized matrix. Over time they complete their differentiation into osteocytes, entering in a quiescent state but retaining the ability to sense mechanical stimuli and to exchange signals among each other, playing a role in bone remodeling regulation. Osteoclasts differentiate from the hematopoietic stem cell lineage and are recruited on the bone, where they are responsible for the reabsorption of the mineralized matrix.

Osteoclasts

Bone tissue undergoes continuous cycles of formation and reabsorption, whose balance is influenced by mechanical loading on the musculoskeletal system, as well as by the interaction with other biological systems such as the endocrine, nervous and immune systems [77].

The cells responsible for the reabsorption process are the osteoclasts (OCs), that differentiate from monocyte/macrophage lineage cells, derived from hematopoietic stem cells (HSCs) [78].

The differentiation process starts when parathyroid hormone (PTH), secreted in response to low Ca^{2+} blood serum levels, binds its receptors on stromal cells, OBs and osteocytes, where it inhibits OCs precursors inhibitor Osteoprotegerin (OPG) and induces the production of two main OCs differentiation factors, receptor activator of nuclear factor kappa-B ligand (RANKL) and macrophage colony-stimulating factor (M-CSF) [79, 80] .

In particular RANKL is a member of the tumor necrosis family (TNF) able to bind its receptor RANK on the surface of OCs progenitors, while M-CSF is a cytokine that binds its transmembrane tyrosine kinase-receptor c-fms (colony-stimulating factor 1 receptor), also located on OCs precursors' surface [2]. Once bound to the respective receptors, they activate a differentiation-inducing cascade, including NF-κB and MAPK downstream signaling pathways, that result in the activation of NFATc1 (Nuclear factor of activated T-cells, cytoplasmic 1), an essential nuclear regulator factor for osteoclastogenesis enhancement [81, 82].

As osteoclastogenesis proceeds, OC progenitors fuse to generate large multinucleated cells, that reach the bone surface through chemotaxis, make contact with it using podosomes and adhere to it through specific integrin receptors [2].

Here, where OCs ruffled border is in adhesion to the bone surface, these cells display an erosive activity on the bone matrix by acidification of the extracellular environment around them. In particular, the secretion of H^+ and Cl^- ions degrades the bone inorganic component and exposes the organic matrix to enzymatic degradation, operated by cathepsin K (CTSK) and matrix metalloproteinases (MMPs) [78].

When intracellular Ca^{2+} concentration arises, following matrix resorption and Ca^{2+} ions release, OCs motility is suppressed and they trigger the destruction of resorbing cytoskeletal structures. Then OCs progressively undergo apoptosis, resulting in suppression of the bone-resorption activity [83].

II: Osteogenesis imperfecta

Osteogenesis imperfecta (OI) is a group of rare and phenotypically heterogeneous skeletal dysplasias, in which 85% of cases are caused by dominant autosomal mutations in the type I collagen coding genes, affecting collagen quantity or structure [84]. However, in the past decade, numerous recessive (mostly), dominant and X-linked OI forms have been identified, triggered by mutations in a wide variety of genes encoding for proteins that are involved in type I collagen synthesis, processing, secretion and post-translational modifications, as well as proteins that regulate differentiation and activity of bone-forming cells [9].

OI is also known as brittle bone disease, as the primary clinical manifestations include low bone mass, bone fragility, deformity of long bones, ribs and spine, vertebral compressions and growth deficiency. In addition, OI patients can display various secondary features, such as blue sclerae, hearing loss, dentinogenesis imperfecta, malocclusion, basilar invagination, pulmonary function impairment, cardiac valve abnormalities, muscle weakness, ligamentous laxity and respiratory impairment [9]. A typical OI hallmark is the presence of bone tissue alterations, which are similar almost in every OI type and have been reported both in OI murine models and in OI patients' biopsies: impaired bone modeling due to increased number and surface of OCs; reduced collagenic matrix production and altered crosslinks among collagen fibrils; bone matrix hypermineralization [85].

Classification of OI forms

The different forms of OI were classified into five groups, based on the function of the genes affected by the mutations [9].

Defects in collagen type I synthesis and structure

OI type I to IV are the classic forms of OI, based on Sillence classification and are characterised by autosomal dominant transmission [86]. These forms are caused by mutations affecting collagen type I α1 and α2 chains coding genes, *COL1A1* and *COL1A2*, and can have two main outcomes: a reduced number of otherwise normal collagen molecules, namely quantitative defect, resulting in mild OI type I, and structural or qualitative defects generated when mutations alter the collagen structure, leading to the severe OI type III, the moderately severe type IV and the lethal OI type II [87].

Structural defects are mainly caused by point mutations that substitute the glycine within the Gly-Xaa-Yaa repeat with a bulkier amino acid that causes steric hindrance; 20-25% of mutations happen in the 3′ or 5′ splice sites and cause exon skipping in *COL1A1* and *COL1A2*; around 5% of mutations localize in the C-propeptide domain of procollagen [9].
Structural defects lead to a delay in collagen folding in the ER, where collagen chains are excessively exposed to post-translational-modifying enzymes [88]. The majority of the overmodified molecules are secreted and form fibrils with an impaired structure, thus participating to the assembly of an abnormal and functionally impaired ECM, while a fraction of these molecules is retained in the ER causing intracellular stress [15].
The differences in OI clinical outcome depend: 1. on the nature of the substituting amino acid, since bulkier charged residues strongly alter the protein structure; 2. on the position of the mutations along the chain, where mutations in the C-terminus impair the triple helix formation and cause a more serious phenotype compared to N-terminus mutations as happens for mutations located in the Major Ligand Binding Site; 3. lastly, on collagen I stoichiometry, as *COL1A2* substitutions lead to less severe outcomes that *COL1A1* ones [84].

Collagen post-translational modifications defects

Procollagen I molecules are subjected to a variety of post translational modifications in the ER to ensure their correct folding before the steps of secretion and incorporation in ECM collagen fibrils, like the 3-hydroxylation of proline 986 operated by prolyl-3 hydroxylation complex. Defects in each of the members of the 3-hydroxylyation complex result in a different form of OI.
In particular, OI type VII is caused by null or missense mutations in *CRTAP* [18, 89], whereas loss-of-function mutations in *P3H1* are responsible for OI type VIII.
Because P3H1 and CRTAP are mutually protective, the absence of one of them causes also the loss of the other [90, 91], therefore distinguishing the two OI forms is challenging from a clinical point of view. They share a phenotype that can range from severe to lethal, characterized by rhizomelia, neonatal fractures and broad undertubulated long bones [18, 92].
Instead, OI type IX is caused by missense mutations in *PPIB*, resulting in a phenotype that overlaps OI type VII and VIII ones with the exception of rhizomelia [19, 93].

The absence of either CRTAP, P3H1 and CyPB causes the complete lack or strong reduction of the α1(I)3-Hyp986, associated to delayed collagen type I folding, increase triple helical overmodification and decreased collagen secretion, as demonstrated in OI dermal fibroblasts [17, 94]. Only in one case a homozygous mutation in the starting codon of *CyPB* in two OI siblings was associated with normal α1(I)Pro986 hydroxylation and normal modification of the collagen helix [95]. In each of the three OI forms, overmodified collagen molecules assemble into irregular fibrils that impair mineralization and affect bone properties [15].

Defects in collagen chaperoning, processing and crosslinking

The ER contains specific chaperones required for collagen folding. The two most important ones are heat shock protein 47 (HSP47), encoded by *SERPINH1*, and FK506-binding protein 10 (FKBP65), encoded by *FKBP10*, both binding preferentially the triple helix of newly folded procollagen molecules.

Mutations identified in *SERPINH1* gene cause the severe to lethal OI type X [96]. Studies conducted in a Hsp47 knock-out murine model have highlighted the crucial role of the protein in collagen processing and secretion, demonstrating also that its mutation leads to ER enlargement and to the activation of ER stress and apoptosis [97].

Recessive mutations in *FKBP10* gene are causative of OI type XI, characterised by a remarkable phenotypic variability. From an intracellular point of view, collagen I trimer stability is impaired causing partial procollagen retention in the ER and subsequent organelle dilation [98, 99]. A peculiarity of collagen secreted by FKBP65-deficient cells is the severe underhydroxylation of C-telopeptide lysine residues that are crucial for collagen crosslinking, as it positively modulates LH2 enzymatic activity that is critical for the formation of hydroxylysine-aldehyde derived intermolecular collagen cross-links [29]. The alteration of cross-linking process explains ECM impairment and insufficiency in this OI form [99].

Heterozygous missense mutations in *FKBP10* and in LH2-coding gene procollagen-lysine, 2-oxoglutarate 5-dioxygenase 2 (*PLOD2*) have been identified as causative of autosomal recessive Bruck Syndrome I and II, characterised by bone fragility, congenital joint contractures with webbing (pterygia), scoliosis, and osteoporosis [100, 101]. No specific differences in clinical phenotype were noticed and reported between Bruck syndrome patients with mutations in *PLOD2* or *FKBP10* [102].

Following their secretion in the ECM, collagen molecules need an extracellular processing step of N- and C- propeptides removal to become mature and assembly into matrix fibers. The cleavage function is solved by the enzymes ADAMTS2 and BMP1, respectively [9].
The most common dominant mutations in the N-terminal propeptide cleavage site alter its structure and hide the site to ADAMTS2 recognition. This results in the retention of the N-propeptide, which alters its intracellular functions and its extracellular interaction with cytokines that regulate bone development [103].
On the other hand, mutations affecting C-propeptide cleavage site or BMP1 cause C-propeptide retention in the extracellular matrix where it works as a mineral nucleator, thus promoting abnormally high mineralization. Dominant mutations that affect collagen I chains C-terminal cleavage site are responsible of a mild form of OI [104], while mutations affecting the cleavage enzyme BMP1 impair the processing of collagen I C-propeptide and result in the more severe OI type XII [105]. This difference is due to the broad BMP1 effect on ECM assembly and structure, where it processes the C- propeptides of different collagen types [106, 107], it cleaves the collagen and elastin crosslinking enzyme pro-lysyl oxidase [108] but also small leucine-rich proteoglycans [109, 110], and lastly it activates multiple cytokines [111],

Bone formation and mineralization defects

Two OI forms arise from defects in genes that are particularly important in the regulation of bone mineralization.
IFITM5 encodes for the bone restricted ifitm-like protein (BRIL), whose molecular mechanism in bone is still unclear, but it is known to be a positive regulator of mineralization [112].
SERPINF1 encodes for the pigment epithelium-derived factor (PEDF), which enhances the expression of osteogenic genes, induces human MSCs differentiation and OBs mineralization *in vitro* and negatively regulates OCs maturation [113-115]. PEDF interacts with several matrix components, such as collagen, hyaluronan and heparan sulphate proteoglycans, and also with the OBs differentiation and matrix mineralization- promoting vascular endothelial growth factor (VEGF) [116, 117].
Dominant mutation in the 5' untranslated region of *IFITM5* generates a new start codon, adding five residues (MALEP) to the N-terminal of the protein, thus causing OI type V, the

only dominant OI form after the classic ones involving *COL1A1* and *COL1A2* [118]. Elongated BRIL leads to the peculiar formation of a hyperplastic callus [119, 120].

Recessive mutations that lead to the absence or the synthesis of a non-functional PEDF are causative of atypical collagen fibrils arrangement and consequently of OI type VI, characterized by decreased bone mineral density [121].

A heterozygous BRIL p.Ser40Leu mutation causing Golgi retention of the mutant protein [122] was also identified, and patients interestingly displayed the typical bone histology pattern described in OI type VI instead of OI type V. Fibroblasts and osteoblasts carrying BRIL p.Ser40Leu have impaired PEDF secretion, revealing a cross talk between the two proteins, despite their opposite effects on bone mineralization [123]. However, the connection between BRIL and PEDF functions is still obscure and requires further elucidation.

Osteoblast differentiation and activity defects

This last class of OI-causing defects includes mutations in genes that are involved in the differentiation or activity of OBs.

SP7 gene encodes for osteoblast-specific transcription factor SP7 (Osterix), which is specifically expressed in cortical and trabecular osteoblasts and at a lower level in the prehypertrophic chondrocytes of the growth plate. It is essential for OBs differentiation, as demonstrated in osterix- null mice that have reduced expression of osteoblast differentiation and proliferation markers such as collagen, bone sialoprotein, and osteocalcin; furthermore they display bone-bending deformities and impaired mineralization [124]. Only two pathogenic variants have been identified in *SP7*, that cause recessive OI type XVII, characterised by an osteoporotic phenotype and reduced bone mineral density [125, 126].

The first mutation is a homozygous single nucleotide deletion inducing a premature stop codon in the final exon of the gene, that produces a truncated protein whose DNA-binding properties are altered and impair SP7-mediated transcription regulation [126]. The second mutation identified in *SP7* was a homozygous substitution involving the change of an arginine residue with a cysteine in exon 2 that disrupts the protein function, but further studies are required to explore the pathogenicity of this variant [125].

TMEM38B gene encodes for the ubiquitous voltage-dependent cation channel TRIC-B, whose function is to maintain ER membrane potential by allowing K^+ flow to balance the

release of Ca^{2+}, therefore it is an important regulator of calcium flux [33]. Ca^{2+} is involved in cell signaling, as it works as a cofactor for several proteins, including the collagen-modifying enzymes lysyl-hydroxylases, and it affects the function of second messenger. Mutations in TRIC-B, that can be homozygous deletions, splice site mutations and nonsense variants, decrease both resting state Ca^{2+} content in the cytoplasm and its release from intracellular compartments in osteoblasts, causing recessive OI type XIV [127]. Both OBs and OCs activities are impaired by TRIC-B mutation, producing a skeletal dysfunction.

Wingless-type MMTV integration site family 1 (WNT1) is a secreted glycoprotein that upon binding to low density lipoprotein receptor-related proteins 5 and 6 (LRP5 and LRP6) and to the seven-transmembrane protein Frizzled, mediates the release from a cytosolic degradation complex of the second messenger β-catenin, which moves to the nucleus and serves a regulatory function of OBs differentiation and activity [128]. Mutations in *WNT1* impair bone cell homeostasis, as well as β-catenin translocation to the nucleus: heterozygous defects cause an osteoporotic phenotype, while homozygous mutations cause OI type XV, characterised by poor bone turnover [129].

MBTPS2 gene encodes for the Golgi membrane protease S2P, that works in concert with S1P protease. S2P is part of the regulated intramembrane proteolysis (RIP process) in osteoblasts and operates the cleavage of the N-terminal domain of several different transcription factors.

Mutations is S2P, mainly located in proximity of the metal ion binding domain of the protease, are the cause of recessive X-linked OI type XIX, in which collagen secretion and crosslinking are altered and produce an impaired extracellular matrix [130].

Among the transcription factors constituting the substrate of S2P and S1P, *CREB3L1*, a member of the CREB family is particularly interesting, in fact it encodes for old astrocyte specifically induced substance (OASIS), an ER-bound transcription factor that binds the promoter of *COL1A1* and enhances the transcription of collagen I gene but also other matrix proteins such as bone sialoproteins. Mutations in OASIS cause lower secretion of non-collagenous matrix proteins and ER enlargement, constituting the molecular basis of the osteopenic phenotype of OI type XVI [131].

This class of OI defects also includes OI type XVII caused by mutations in the secreted protein acidic and rich in cysteine SPARC, that is a matricellular calcium-binding protein and an intracellular chaperone. In the ER SPARC interacts with HSP47 to ensure that only

correctly folded procollagen molecules exit the ER [132], whereas in the bone matrix, it binds collagen and crystals of hydroxyapatite and releases Ca^{2+} ions, participating to collagen scaffold mineralization. In particular, the calcium binding site of SPARC contains specific residues able to form an intramolecular saline bridge, essential for the interaction with fibrillar collagen in a collagen-binding pocket [133].

Homozygous missense mutations in *SPARC* lead to a delay in collagen secretion, post-translational overmodifications and to a skeletal phenotype characterized by bone fragility, altered mineral composition, lower collagen content and smaller fibrils [134]. More recent studies demonstrated that SPARC is also involved in bone marrow stem cells differentiation towards OBs [135].

Latest discovered OI forms

In the last decade new pathogenic mutations have been identified in genes that previously had not been considered to be linked to OI. Although their inclusion into one of the above reported functional groups needs further characterization, the patients carrying these mutations present the well characterized OI clinical phenotype.

A new form of X-linked osteoporosis, with an OI overlapping phenotype, was identified in five families carrying pathogenic variants in the gene encoding for plastin 3 (PLS3) [136], a key protein in the formation of actin bundles throughout the cytoskeleton [137]. Its presence is reported in OBs, in particular in matrix vesicles [138], in osteoclasts, in which PLS3 participates to the arrangement of large actin filaments contained in podosomes [139], and in osteocytes dendrites, which suggests the protein involvement in osteocytes mechanosensing function [136].

PLS3 defects, triggered in particular by missense mutations, deletions and small insertions, result in a premature stop codon or a frameshift impairing PLS3 function [33]. In individuals with *PLS3* mutations, collagen I has normal structure and a normal level of synthesis, nevertheless the patients display a phenotype of severe bone fragility, osteoporosis and impairment in bone mineralization. PLS3 alter both bone forming and bone reabsorption processes, leading occasionally to decreased mineralization, occasionally to its increase, with a still undefined mechanism [140, 141].

As discussed in the previous chapter, collagen trafficking from the ER to the ERGIC compartment requires a complex machinery involving COPII proteins, such as SEC24D

(SEC24 homolog D, COPII coat complex component), that takes part in COPII coat formation around ER-exiting vesicles. A *SEC24D* nonsense mutation and a missense mutation have been discovered in skin fibroblasts from a young patient with a syndromic form of OI, clinically classified as Cole-Carpenter syndrome. The missense mutation affected a highly conserved amino acid of the protein and led to a mildly defective ER export of procollagen, but most importantly to ER retention of cargo trafficking molecules, leading to dilation of ER cisternae [142]. Further missense substitutions in *SEC24D* have been identified in two Chinese families [143], and in a young Chinese patient, carrying both a frameshift-causing mutation in exon 2 and a mutation affecting the last base of exon 19 [144]. The outcome in each patient is a phenotype of impaired bone mineral density, skeletal malformations and other typical OI clinical signs, therefore suggesting that *SEC24D* mutations can be considered as causative of a new form of autosomal recessive OI.

Terminal nucleotidyltransferase 46 member A gene (*FAM46A*) encodes for a soluble protein member of the nucleotidyltransferases (NTase) fold superfamily whose function is not yet defined in humans [145]. Nevertheless its expression in primary osteoblasts and mineralized bone tissue and its modulatory function on BMP signaling suggest a role in bone development and homeostasis [146, 147].

Variants in *FAM46A*, in particular a loss-of-function mutation or a homozygous duplication, causing a premature stop codon and the absence of the protein, were identified as causative of an autosomal recessive OI form [148, 149]. The main clinical manifestations of the patients are overlapping with the Stuve-Wiedemann syndrome phenotype and include spontaneous fractures, osteopenia, bowing of the lower limbs and joint hyperlaxity [149, 150].

More recently, mutations causing another novel autosomal recessive OI form have been discovered in mesoderm development gene *MESD* [151]. The gene encodes for an ER chaperone for the canonical WNT signaling receptors LRP5 and LRP6 and its absence impairs the two receptors trafficking to the cell surface [152]. Despite the need of further evaluations, it was demonstrated that OI-associated *MESD* homozygous mutations occur in the last exon of the gene and remove a highly conserved ER retention domain, producing a frameshift or a truncated protein, this results in the impairment of MESD retain or recycle in the ER, in the reduction of the protein's chaperone efficiency [153, 154], and ultimately

impairs WNT signaling [151]. Individuals affected by this OI form present a progressively deforming OI phenotype with early onset osteoporosis [151, 155].

Another recent OI-associated mutation is in coiled-coil domain containing 134 gene (*CCDC134*) [156], encoding for a secreted protein involved in the negative regulation of extracellular single-regulated kinases (ERK) and c-Jun N-terminal kinases (JNK) signaling pathways [157]. A homozygous variant in *CCDC134* was retrieved in three patients from two unrelated families, presenting pseudarthroses, severe bone fragility and other typical OI hallmarks. The mutation is responsible for the absence of the protein and the consequent increase of Erk1/2 phosphorylation, leading to decreased OPN mRNA, lower *COL1A1* expression and reduced mineralization in patient osteoblasts matrix [156].

Lastly, bi-allelic pathogenic *KDELR2* variants were recently identified as causative of OI in four families. *KDELR2* gene encodes for KDEL endoplasmic reticulum protein retention receptor 2, which regulates the COPI retrograde transport-mediated recycling of proteins carrying a KDEL-like peptide from the Golgi to the ER [158]. The identified mutations lead to the inactivation of the receptor and result in hindered KDELR2-mediated Golgi-ER transport. Importantly, the peculiarity of individuals deficient of KDELR2 is the inability of HSP47 to bind KDELR2 and detach from collagen type I molecules, therefore HSP47 remains bound to collagen molecules in the extracellular environment, undermining fibrils formation and the construction of bone matrix organic scaffold [159].

Mutated gene	Encoded protein	OI type	Inheritance	OMIM
Impairment of collagen synthesis and structure				
COL1A1 or	Collagen alpha-1(I) chain (α1(I)) or	I, II, III or IV	AD	166200, 166210,
COL1A2	Collagen alpha-2(I) chain (α2(I))			259420, 166220
Abnormal collagen post-translational modification				
CRTAP	Cartilage-associated protein (CRTAP)	VII	AR	610682
P3H1	Prolyl-3 hydroxylase I (P3H1)	VIII	AR	610915
PPIB	Peptidyl-prolyl cis-trans isomerase B or Cyclophilin B (PPIase B or CyPB)	IX	AR	259440
Compromised collagen processing and crosslinking				
SERPINH1	Serpin H1 (also known as HSP47)	X	AR	613848
FKBP10	65 kDa FK506-binding protein 65 (FKBP65)	XI	AR	610968
PLOD2	Lysyl hydroxylase 2 (LH2)	n.c.	AR	609220
BMP1	Bone morphogenetic protein 1 (BMP1)	XII	AR	614856
Compromised bone mineralization				
IFITM5	Bone-restricted interferon-induced transmembrane protein-like protein (BRIL)	V	AD	610967
SERPINF1	Pigment epithelium-derived factor (PEDF)	VI	AR	613982
Altered osteoblast differentiation and function				
SP7	Transcription factor SP7, also known as osterix (OSX)	XIII	AR	613849
TMEM38B	Trimeric intracellular cation channel type B (TRIC-B)	XIV	AR	615066
WNT1	Proto-oncogene Wnt1 (WNT1)	XV	AR AD	615220 Unknown
MBTPS2	Membrane-bound transcription factor site-2 protease (S2P)	XIX	XR	200294
CREB3L1	Old astrocyte specifically induced substance (OASIS)	XVI	AR	616229
SPARC	Secreted protein acidic and cysteine rich (SPARC, also known as osteonectin)	XVII	AR	616507
Other OI types				
PLS3	Plastin 3 (PLS3)	n.c.	XR	Unknown
SEC24D	SEC24 homolog D, COPII coat complex component (SEC24D)	n.c. n.c.	AR	Unknown
FAM46A	Terminal nucleotidyltransferase 46 member A (FAM46A)	XVIII	AR	611357
MESD	Mesoderm development protein (MESD)	XX	AR	607783
CCDC134	Coiled-coil domain containing 134 (CCDC134)	n.c.	AR	Unknown
KDELR2	KDEL endoplasmic reticulum protein retention receptor 2	n.c.	AR	Unknown

AD: autosomal dominant; AR: autosomal recessive; XR: X-linked recessive; n.c.: not classified yet

Table 1: **Genetic classification of Osteogenesis imperfecta** (modified from Marini *et al*., 2017).

Intracellular collagen retention and ER stress

Despite OI outcome was traditionally attributed only to the presence of structural abnormal collagen in the ECM, recently it has been recognized that also intracellular collagen retention and accumulation play a key role in modulating the phenotype severity in OI, as they represent a great perturbation in the maintenance of cellular homeostasis [160, 161].

In classic OI forms, mutations in the α chains of collagen I cause the delay in its folding and the prolonged exposure to post-translational modifying enzymes in the ER, that causes in turn the partial retention of mutated molecules [162]. Procollagen I retention takes place also in case of mutations in non-collagen genes, impairing collagen folding or post-translational modifications [17, 163]. Abnormal type I collagen has been isolated and found to be retained in the intracellular environment in tissues and fibroblast cultures from several OI patients, showing functional abnormalities such as reduced helical stability, reduced secretion, increased degradation, and excessive lysines modification [164, 165], but also in patients' OBs, in which collagen modification appeared more pronounced than in collagen molecules extracted from the same individuals' fibroblasts [166].

When the rate of misfolding exceeds the capacity of cells to degrade or secrete misfolded molecules, intracellular accumulation of procollagen becomes massive, leading to the enlargement of ER cisternae, as described in different murine models of OI, and impairing OBs maturation and function [167-169].

The ER compartment is responsible for the quality control of a huge amount of proteins, especially the ones that enter the secretory pathway, in particular it manages protein folding and processing and ensures that improperly folded proteins do not proceed to the cell surface; furthermore, to avoid potentially toxic accumulation of misfolded and unfolded proteins, the ER balances its burden of incoming proteins with its capacity to fold and process them [170]. Disruption of this balance, as in the case of procollagen I accumulation, results in ER stress and initiates a variety of responses that work to restore and/or increase ER function.

The first cellular response to ER stress is the activation of the adaptive signal transduction pathway unfolded protein response (UPR), that induces the expression enhancement of several ER chaperones to facilitate the correct folding and assembly of ER proteins, in order to avoid aggregation and to regulate stress signaling and protein degradation [170-172]. They can be divided into three categories. The first are chaperones of the heat shock protein (HSP) family that include binding immunoglobulin protein (BIP), also known as glucose

regulated protein 78 (GRP78), carrying a peptide-binding domain that binds to the unfolded proteins by recognizing exposed hydrophobic residues [173, 174]. BIP does not only act as a single chaperone, but it also works in concert with other ER molecules, forming an ER multi-protein complex that can bind to unfolded protein substrates [175].

The second category is made of chaperone lectins, containing the ER membrane protein calnexin and the soluble ER lumen protein calreticulin, which recognize nascent proteins subjected to a correct N-linked glycosylation process and drive them to folding and assembly steps [176]. The last group includes substrate-specific chaperones, such as the collagen-specific one HSP47 [171]. Additionally, there are at least two groups of folding catalysts, namely thiol oxidoreductases, such as protein disulphide isomerase (PDI) and peptidyl prolyl *cis-trans* isomerases (PPIs) [171]. In particular the enzyme PDI is a multi-domain, multi-functional member of the thioredoxin superfamily [177], which catalyses thiol-disulphide oxidation, reduction and isomerization and promotes native disulphide bonds formation, furthermore it interacts directly with non-native proteins and folds them [178].

Among ER chaperones, the protein BIP is crucial to the UPR pathway since it contributes to the activation of UPR three main branches, each including an ER-resident transmembrane protein as a proximal signal sensor: protein kinase R (PKR)-like endoplasmic reticulum kinase (PERK), inositol-requiring enzyme 1 α (IRE1 α) and activating transcription factor 6 (ATF6) [179].

The UPR initiators are usually maintained in an inactive state through binding to BIP. Upon ER stress, BIP dissociates from the sensors since it is recruited to bind unfolded proteins to solve its chaperone function. This dissociation activates the three UPR sensors, triggering UPR pathway to relieve the stress and to block further damage [171], however the exact mechanism by which each protein senses the increases in the luminal concentration of unfolded proteins is not known [161]. Recent studies of BIP interaction with UPR sensors have proposed that also other regulatory BIP-independent mechanisms are involved in UPR activation following ER stress [180, 181]. For example in OI patients' fibroblasts, BIP interaction with procollagen I was demonstrated only in the presence of C-propeptide mutations and not always in the presence of triple helical glycine substitutions [182], suggesting in the latter case the activation of an unusual UPR pathway [161].

Following activation, PERK dimerizes, promoting its autophosphorylation, and activation, and phosphorylates the eukaryotic translation-initiation factor 2α (eIF2α), which attenuates

the rate of general translation, thus preventing further protein synthesis [183, 184] and activates the activating transcription factor 4 (ATF4), responsible for the transcriptional expression regulation of genes involved in stress resistance [185] (**Fig.6**).

Instead activated IRE1α has endoribonuclease activity and splices a 26-base intron from the mRNA encoding the X-box binding protein 1 (XBP-1) [186], a transcription factor with target genes involved in protein folding and endoplasmic-reticulum-associated degradation pathway (ERAD); in addition, IRE1α is involved in mRNA degradation RIDD (regulated Ire1α dependent mRNA decay) and it can trigger the activation of an anti-apoptotic response by binding TNF receptor associated factor (TRAF) [187, 188] (**Fig.6**). Recently HSP47 was identified as a regulator of IRE1α activation and downstream signaling, in particular it was demonstrated that HSP47 directly interacts with IRE1α luminal domain and favours the release of BIP, thus increasing the oligomerization status of IRE1a [31].

Lastly, release from BIP allows ATF6 to translocate from ER to Golgi, where it is cleaved by the proteases S1P and S2P, and the cleaved ATF6 migrates into the nucleus and upregulates genes that augment ER folding capacity, like BIP itself, folding enzymes, such as PDI, and lipid biosynthesis, to allow ER volume to increase [189] (**Fig.6**).

Thus, UPR progresses through transient attenuation of translational and transcriptional induction of ER chaperones, folding enzymes, and proteins involved in ERAD to alleviate protein aggregation in the ER as an adaptive response [190].

The excessive crowding of misfolded procollagen chains in the ER requires the activation of a degradation response in the attempt to rescue cellular homeostasis. A basal degradation (~ 15% in fibroblasts) is present in all cells under conditions that permit normal folding of the procollagen triple helix, but degradation increases significantly in OI cells which synthesize high amount of structurally abnormal procollagen [191].

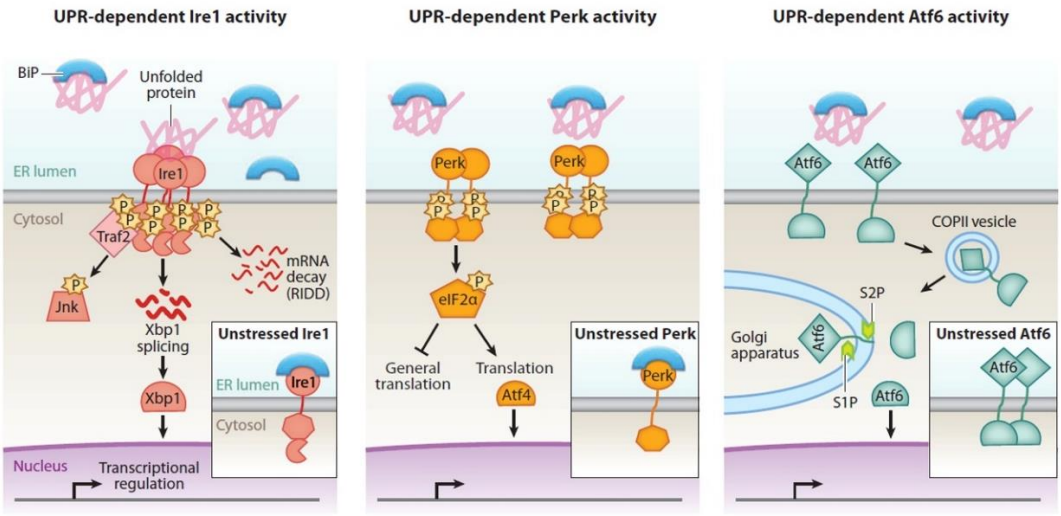

Figure 6: the three signaling branches of UPR [170]. UPR activation is mediated by the detachment of BIP from three ER stress sensors IRE1α, PERK and ATF6. IRE1α alternatively splices the mRNA encoding for the transcription factor XBP1 that regulates stress genes expression, in addition it is involved in RIDD pathway for mRNA decay; PERK autophosphorylates and activates eIF2α, which in turn activates ATF4, attenuating the rate of general translation; ATF6 translocates from ER to Golgi, where it is cleaved by the proteases S1P and S2P and in its cleaved form migrates to the nucleus, where it regulates the expression of proteins involved in folding and in ER functions rescue.

Whereas aggregates of unfolded procollagen chains are eliminated through the ERAD pathway, insoluble misfolded procollagens aggregates accumulated in the ER are degraded through autophagy [192]. Autophagy is a catabolic process responsible for the elimination of cellular dysfunctional components, such as organelles, exogenous viruses, and bacteria in the cytoplasm [193, 194], that consists of three steps: formation of an autophagosome with a double membrane, sequestration of cytoplasmic constituents, and fusion of the autophagosome with lysosomes, where encapsulated constituents are degraded by proteases. Today the aspects of where in the cell procollagen molecules are recognized and how they are captured for autophagic degradation still have to be properly dissected [192]. A recent study has been performed in normal OBs and OBs expressing bone pathology-causing mutant molecules to investigate about procollagen trafficking. The study highlighted that while the majority of procollagen molecules selected for degradation are sent through autophagy, a subset of folded/misfolded molecules are diverted to lysosomes from peculiar ERESs that are engulfed by nearby lysosomes through a noncanonical, autophagic process resembling microautophagy. Thus a novel pathway for regulating procollagen homeostasis,

which is initiated at ERESs and involves an unconventional mode of autophagic degradation, has been identified [195].

Although the general output of the UPR is to restore ER homeostasis, chronic ER stress can induce apoptosis, in particular, through the intrinsic mitochondrial apoptosis pathway [196]. Apoptosis consists in a programmed cell death resulting in the clearance of cells with minimal damage to surrounding tissues [197]. Multiple signals link ER stress to apoptosis, particularly several transcriptional targets of the UPR are proapoptotic, one of them is CHOP, a B-cell lymphoma 2 (Bcl-2) inhibitor that is upregulated by the PERK effector ATF4 and whose deficiency leads to decreased apoptosis under ER stress [198].

Apoptosis can also be induced by IRE1α through multiple mechanisms, including activation of JNK pathway [199] or by sustained activation of the RIDD pathway [200], furthermore IRE1α directly interacts with the proapoptotic proteins Bax and Bak, regulating apoptotic signaling [201].

The identification of procollagen intracellular accumulation as causative of a strong stress response in bone cells and of OI phenotype is crucial, both to better understand OI-causing molecular mechanism and to define novel potential targets for OI therapy.

III: OI therapeutic approaches

There is no definitive cure for OI, which is treated with the available therapeutic approaches used for osteoporosis. Bone mass, quality and architecture are crucial features to confer to the bone its integrity and strength, therefore the aim of the most used current therapeutics is to improve bone architecture and increase bone mass using anti-resorptive or anabolic treatments, even if they do not address the underlying matrix defect [202].

Anti-resorptive treatments

Bisphosphonates

Among the most used compounds for treating OI are the anti-resorptive drugs bisphosphonates (BPs), such as alendronate, zoledronic acid and pamidronate, which are synthetic analogues of pyrophosphate and inhibit OCs function. Once administered, these compounds bind to the hydroxyapatite crystals, for which they have a high binding affinity, and, following uptake by OCs impair their activity of survival [203, 204].

BPs can be divided into the two categories nitrogenous and non-nitrogenous, the first ones inhibit protein prenylation and consequently disrupt OCs formation, survival and cytoskeletal dynamics, the second group trigger osteoclast apoptosis initiation by replacing the terminal pyrophosphate moiety of ATP, which is essential for cellular metabolism. Both cases result in the blockage of bone resorption and in a consequent increase of bone mass [205]. BPs-treated bones, even if made with poor OI-quality matrix, are proved to be effective in increasing bone mineral density (BMD), to maximize mobility and to improve functional outcomes in adult patients [206-208] and with a greater beneficial effect, in children [209-211]. Although their demonstrated efficacy, the main issues about BPs therapy are their long-time persistence in the skeleton [212], that affect the correct bone turnover and skeletal remodeling in the treated children during growth, and the possibility of delayed tooth eruption and impaired fractures and osteotomies healing following prolonged administration [9]. In adults in particular, BPs delay fracture healing [213] and may increase the risk of atypical femoral fractures [214]. For these reasons, despite bisphosphonates represent the standard cure for OI patients, further studies are needed in order to assess their long-term safety and to optimize their administration guidelines.

Denosumab

Another anti-resorptive approach FDA-approved to treat osteoporosis, Denosumab, a fully humanized monoclonal antibody against RANKL, is being considered for OI patients' treatment. It specifically inhibits RANKL, an important cytokine that binds to its RANK receptor on immature monocytes and induces their differentiation into mature OCs [215, 216]. RANKL inhibition was first tested in the osteogenesis imperfecta mouse (oim) model, in which it ameliorated bone biomechanical parameters such as bone density and stiffness and cortical thickness, on the other hand it did not show any effect on the number of fractures [217]. Regarding patients, the antibody was tested in the FREEDOM phase III clinical trial in postmenopausal women with osteoporosis for ten years, revealing its positive effect in promoting BMD, reducing fractures incidence and showing very mild adverse effects [218]. The role of Denosumab in patients still has to be dissected properly and its use is debated, as RANKL plays a role in the immune system and could negatively affect the response to infections [219]. However, its administration in different trials involving boys with OI resulted in decreased bone resorption and increased BMD in lumbar spine with very mild adverse effect [220-222], thus the antibody seems a promising alternative to bisphosphonates therapy.

Bone anabolic treatments

Teriparatide

Teriparatide (TPD), a recombinant form of parathyroid hormone (hPTH 1-34), is a FDA-approved anabolic agent for the treatment of osteoporosis that increases BMD and reduces vertebral and non-vertebral fractures in postmenopausal women by stimulating OBs over OCs function [223]. TPD studies were conducted in mild and severe forms of OI, nonetheless they are limited to adult patients. Its use is not approved in pediatric population due to its theoretical risk for osteosarcoma, as reported in rat studies and in two clinical cases [202, 224]. In mild OI forms, the compound increased both bone formation and resorption markers in serum and augmented BMD, and no effect was observed in self-reported fractures [225, 226]. Further evaluations are needed to assess the role of TPD administration on fracture rate, however a recent report of an atypical femoral fracture healing in a 70 year-old type I OI patient suggested a potential beneficial effect even on this aspect [227].

On the other hand, patients affected by the more severe forms of OI type III and IV displayed no difference or improvement after 18 months of TPD treatment [228].

Anti-sclerostin antibody

The most promising anabolic therapy at the moment implies the use of an antibody against sclerostin, or secreted cystine knot-containing protein, a protein mainly produced by osteocytes that binds to the WNT ligands co-receptors LRP5 and LRP6, where it works as an antagonist of bone formation [229]. Blocking sclerostin results in the activation of the canonical Wnt/β-catenin pathway and consequently in the stimulation of OBs differentiation and activity with a beneficial effect on the skeleton.

This therapy brought to the improvement of bone mass, architecture and biomechanical parameters in murine models of OI [230-233]. In particular it was demonstrated in the oim mouse model of type III OI that sclerostin antibody treatment significantly decreases fracture incidence in the axial skeleton, without impairing the body weight, stature and growth of tested animals. In *Col1a1*$^{+/G349C}$ mice (Brtl) the administration of the antibody led to improved bone mass, reduced long-bone fragility and increased femoral stiffness and strength [230, 231].

On the other hand, contradictory effects were retrieved in the treatment of growing and adult *Col1a1*$^{+/Jrt}$ mice, representing a model for more severe OI, in fact no significant treatment-associated differences were detected in serum markers of bone formation or resorption, plus higher trabecular bone volume and cortical thickness were detected in growing, but not in adult mice [232]. Due to its efficacy in ameliorating different aspects of impaired bones, the use of sclerostin antibody could have a powerful impact on OI treatment, but other studies are required to assess its safety and the therapy duration in OI patients [234].

The most recent study on the Brtl murine model of OI type IV, combined bisphosphonates and sclerostin antibody in the same treatment, hypothesizing a stronger effect on bone mass compared to the two therapies administered separately. The main outcome was a robust gain both in femoral trabecular thickness and number, especially when the two drugs were given together in multiple cycles, and also improved vertebral stiffness, trabecular bone mass and bone biomechanical functions [235]. Though further evaluation is needed, this indicates that a combination of the anti-resorptive and the anabolic therapies could be an interesting solution to improve bone quality in OI patients.

Anti-TGF-β antibody

The balance between OBs and OCs activity is the basis of the bone remodeling process [236]. TGF-β factor, that is secreted by OBs and stored in inactive form in the bone matrix, is a coordinator of this process. Following OCs' bone resorption, TGF-β is released in its active form and it triggers the SMAD signaling network, that plays important role in skeletal development upon binding to the cell surface receptors TGFBR1/2 [237].

The alteration of the OI bone cellular balance, due to the increased OCs and reduced OBs activity, leads to the impairment of TGF-β storage, resulting in uncontrolled activation of its signaling pathway further busting the pathological bone phenotype. It has been reported that excessive TGF-β1 signaling results in a low bone mass phenotype in an animal model with a osteoporosis-like phenotype [238] and in murine models of OI [239, 240]. Because TGF-β pharmacological inhibition ameliorated the bone phenotype at least in animal models and because fresolimumab, an antibody against the three isoforms of TGF-β, has been well tolerated in phase I clinical trial in patients with primary focal segmental glomerulosclerosis and idiopathic pulmonary fibrosis [241], the drug is being tested in a phase I clinical trial for OI patients [202].

Cell therapy

Mosaic carriers of an OI-causing mutation do not present a clinical skeletal phenotype, even in presence of a high number of mutant osteoblasts [242]. This constitutes the grounds of OI cell-based therapy, in which pluripotent normal cells with osteoblast differentiation potential are transplanted into affected individuals that will then recapitulate the mosaic healthy phenotype.

Studies for transplantation were conducted both in murine models and in humans. In particular, i*n utero* transplantation of green fluorescent protein (GFP)-expressing whole bone marrow in heterozygous Brtl mouse revealed that engrafted cells differentiated to trabecular and cortical bone cells and synthesized a great amount of normal matrix since they made up to 20% of all type I collagen in the host bone. The transplantation also reduced perinatal lethality and improved the bone architecture parameters of treated Brtl femora at 2 months of age [243].

Several clinical trials for bone marrow transplantation (BMT) in severe OI patients have been attempted. In a first trial of five children that received bone marrow transplantation, three of them showed donor cells engraftment, a significant increase in bone mineral content and in body length with a rate similar to healthy controls. A following trial was performed on six children with severe OI who underwent BMT, that were infused with gene-marked, donor marrow- derived MSCs. Five of them displayed engraftment in bone and increased growth rate, suggesting that post-transplant treatment with allogeneic MSCs enhances the therapeutic effects of BMT [244].

Only in two cases MSCs transplantation was performed *in utero* in patients. In the first case, a female fetus diagnosed with severe OI, the engraftment was successful, but since the child was also treated with bisphosphonates, it was difficult to dissect the effects of the two approaches [245].

The second case, in a more recent study, involved prenatal transplantation of two OI patients with human fetal MSC (hfMSC) and postnatal boosting with same-donor MSCs. In both patients, the treatment resulted in reduced fracture incidence and increased growth rate as compared to non-treated OI patients [246].

All the transplanted individuals displayed improved linear growth, bone structure and integrity following transplantation, therefore cell therapy studies pave the way for a novel potential OI treatment, nevertheless some important issues still need to be addressed, in particular bone engraftment efficiency, the use of bone-specific delivery systems and the age of treatment [204, 247].

Matrix vesicles therapy

Besides to differentiate into target tissue cells, MSCs are responsible for the production of trophic factors, such as growth factors and cytokines, which can activate and support endogenous cells, even though the detailed mechanism of these therapeutic effects has not been fully elucidated [248].

MSCs can release extracellular vesicles (EVs) like exosomes, derived from early endosomes, and microvesicles, that have large dimensions and shed from the plasma membrane [249-251], both containing bioactive molecules, such as proteins and RNAs, and deliver signals for intercellular communication. Therefore MSC-derived EVs play an

important role in the therapeutic effects observed in the treatment of several diseases [249, 252-254].

Regarding OI animal models in particular, in the past years MSCs infusion has proven to induce the production of a factor into the serum, which then stimulates chondrocyte proliferation in the growth plate from where bone growth occurs [255], but most importantly even infusion of conditioned medium from MSC cultures can initiate this multistep pathway and stimulate chondrocyte proliferation [255].

A recent study has proved that EVs also have the potential to serve as a cell-free therapy equivalent to MSC therapy that, instead of creating mosaicism, boosts the activity of endogenous cells and bypasses many of the limitations of cell-based therapies, such as variable therapeutic potency between MSC donors and safety concerns [256]. Indeed OI mice were treated with conditioned medium from murine and human MSCs revealing that chondrocyte proliferation was not stimulated by soluble proteins in the medium, but by RNAs contained in EVs, in particular miRNAs, which stimulate bone growth [256].

Identifying the miRNAs and other molecules responsible for this outcome is a further critical step before EV therapy can be considered as a novel cell-free therapy for OI.

Gene therapy

The only resolutive cure for OI is gene therapy, based on inactivating or correcting the expression of the mutated genes. In severe classical OI forms carrying *COL1A1* or *COL1A2* mutations, characterized by a structural qualitative collagen defect, the silencing strategy would result in the production of collagen only from the healthy allele and thus in the transition to a mild, quantitative OI type [204]. Antisense oligonucleotides, ribozymes, small interfering RNA (siRNA) and short hairpin RNA (shRNA) can be used to target mutated transcripts [257].

The transfection of antisense oligodeoxynucleotides in cultured human fibroblasts from an OI type IV patient with a *COL1A2* point mutation resulted in a significant *in vitro* suppression of the mutant protein.

In 2004 the first *COL1A1* allele-specific silencing using siRNA was performed in OI patients carrying a known *COL1A1* mutation. MSCs from the patients were transfected with an adeno-associated virus containing a construct that would target and disrupt the mutant allele [258]. Two later studies used siRNAs to obtain type I collagen allele-specific silencing, the

first in human bone-derived cells *in vitro*, in which a mutation-independent approach was used to target heterozygous single nucleotide polymorphisms (SNPs) or insertion/deletion polymorphisms in the *COL1A1* and *COL1A2* genes [259, 260]; the second in the Brtl mouse fibroblasts, in which allele-specific silencing of mutant *Col1a1* using shRNAs subcloned in a lentiviral vector reduced the amount of mutant collagen by 40% [261]. Although partially successful, this therapeutic approach carries many uncertainties, such as the safety of the vectors utilized for the delivery, possible insertional mutagenesis and duration of the effects [202]. In addition, silencing approaches have been tested mainly *in vitro*, and further *in vivo* studies are needed on appropriate animal models before moving on to clinical trials.

Despite different aspects of this therapy are uncertain, some recent studies open new possibilities, one of them is the development of a bone delivery system that could allow the siRNA targeting directly to the bone tissue by systemic injection [262]; another recent research investigated the use of viral vectors expressing target tissue-specific shRNAs, aptamer-shRNA chimeras and atelocollagen-bound siRNAs [263, 264].

Gene therapy is a developing field in OI treatment that opens some appealing possibilities for the future, such as the combination of gene and cell therapy. MSC gene targeting and generation of induced pluripotent stem cells (iPSCs) could in fact be used to treat OI skeletal abnormalities by transplanting patient-specific bone-forming cells that no longer express the mutant gene. A proof of the success of this combination was obtained in an *in vivo* trial, in which OI patient MSCs were corrected and the derived iPSCs were transplanted in an animal model where they produced normal collagen and successfully formed bone [265].

Another promising therapeutic approach for OI is gene editing using the new CRISPRs/Cas9 system. It has not been used in OI yet, but it has been recently tested in animal models of other diseases, in which gene editing Cas9-guide RNA complexes were successfully delivered *in vivo* [266-268]. The use of this tool, that would allow to precisely edit any mutation in an allele-specific manner, could radically change the way we treat human Mendelian disorders.

4-Phenylbutyrate

Among the currently available therapies for OI, the anti-resorptive and the anabolic ones are the most used, nevertheless there is a limitation in their molecular mechanism: they only address the problem at the level of the extracellular matrix, by promoting its production or

by inhibiting its resorption, and without addressing its quality issue. None of these therapies focuses on the amelioration of bone intracellular environment, which is stressed by the accumulation of unfolded collagen molecules.

To this purpose, recently the compound 4-phenylbutyrate (4-PBA) has gained increasing attention.

From a molecular point of view, 4-PBA is an aromatic fatty acid that in humans is oxidized into phenylacetate (PAA) in the liver by β-oxidation and is eliminated by conjugation with glutamine to form phenylacetylglutamine, which is excreted in the urine [269], thus acting as an ammonia scavenger. 4-PBA is FDA-approved for patients with urea cycle disorders and hyperammonemia, in which defects in the excretion of waste nitrogen induce the accumulation of glutamine and alanine [270, 271].

4-PBA is also a member of histone deacetylase inhibitors (HDACI), a class of proteins that restore positive charges on histones by removing acetyl groups and induce transcriptional repression through chromatin condensation [272], indeed hyperacetylated histones are linked to transcriptionally active domains, while hypoacetylated histones are generally associated with transcriptionally silent loci [273].

An important function of 4-PBA is its chaperone-like activity that facilitates protein folding and stabilizes already folded molecules by binding them and protecting their structure against proteolytic degradation and thermal denaturation [274-276]. Its chaperone ability was first identified in diseases such as cystic fibrosis [277] and type 2 diabetes associated to obesity [278] where 4-PBA was able to alleviate ER stress and UPR activation, as shown by decreased expression of specific proteins from these pathways [279], to restore the function of mutated proteins retained in the ER and to promote their progression to the intracellular trafficking pathway [277, 280].

The chaperone function of the compound has been studied in several disease models over the years, such as α1-antitripsin deficiency [281, 282], glaucoma [283], cataract [284], cholestasis [285], Wilson disease [286], Parkinson's disease [287].

Regarding in particular its role in bone cells, it is reported that 4-PBA increases histone acetylation, stimulates ALP activity and promotes cell proliferation and maturation in OBs cultures [288, 289].

The established link between 4-PBA treatment and ER stress, together with its beneficial effect on bone-forming cells, makes the compound an appealing opportunity to address OI-

causing intracellular molecular mechanism. The compound has already been successfully used to rescue the cellular phenotype of hemorrhagic stroke caused by intracellular accumulation of mutant collagen type IV [290].

The first study of 4-PBA in OI has been conducted *in vivo* in an OI Chihuahua zebrafish (*Danio rerio*) model of classical severe OI [291]. Our group demonstrated that ER enlargement was ameliorated upon 4-PBA administration, which increased the amount of extracellular collagen and improved OI fish skeletal mineralization and morphology. The expression of early and late osteoblast markers was investigated in order to evaluate if the inhibitory effect of 4-PBA on histone deacetylases affected the transcription of osteoblasts specific genes. No difference was retrieved, indicating that the inhibitory effect of 4-PBA on histone deacetylases was not significant at the used concentration [292].

Two more recent studies conducted by our group aimed at elucidating the effect of the intracellular retention of mutant collagen on cellular functions both in dominant and recessive OI patients' fibroblasts, and to investigate whether this condition could be rescued by 4-PBA. The results of our researches will be discussed in the next chapters.

Interestingly, a recent study performed on a knockout mouse model with an osteoblast-specific mutation impairing autophagy, revealed that OBs from this model displayed ER stress and impaired bone formation and mineralization activities, altering bone mass phenotype [293]. 4-PBA administration was able to reverse the expression of ER stress markers and to induce the expression of OBs-specific differentiation and mineralization markers, revealing a beneficial effect of the drug on bone forming cells metabolism [293].

IV: murine models of classical Osteogenesis Imperfecta

The use of animal models is crucial in the study of bone diseases like OI, because it is not possible to routinely perform molecular analyses on patients' bone tissue. Indeed, the acquisition of bone samples with a bone biopsy is an invasive procedure, as the brittleness of OI patients' bones would increase the recovery time, the risk of secondary fractures and pain.

Since mice are mammals, their anatomy and physiology resemble the human ones, therefore their use as models of diseases allows a deeper understanding of the disorders pathobiology. I focused my attention on currently available OI murine models carrying mutations in collagen genes, reproducing classic OI forms (**Table 2**).

In the past decades, several murine models of classic OI displaying a bone phenotype have been developed. The Mov-13 transgenic mouse carries a *Col1a1* null allele, thus homozygous mice do not produce type I collagen and are lethal, while heterozygous mice deposit reduced amounts of normal type I collagen in the ECM and display an osteopenic phenotype and abnormal skeletal biomechanics [294, 295].

Another transgenic model is the human *COL1A1*-minigene mouse, containing a construct that expresses a version of human *COL1A1* missing the central 41 exons, encoding a significant portion of the triple-helical domain. The resulting shortened human proα1(I) chains associate with normal murine proα1(I) and proα2(I) chains, depleting the amount of normal type I collagen and altering ECM organization [296, 297].

In 1988, an OI type II transgenic mouse model expressing a mutated *COL1A1* gene, that resulted in perinatal lethality, was generated by site-directed mutagenesis. The mutation was introduced in the triple helical domain of *COL1A1* gene, at residue 859 [298, 299]. Fetuses displayed short and wavy ribs, poor bone mineralization, underdeveloped skeletons, and pliable limbs, in addition the bones presented large cavities, indicating a high level of resorption [298, 300].

Alongside transgenic ones, some OI models were generated by chemically induced mutations, such as the abnormal gait 2 ($Aga2^{+/-}$) mouse (T to A transversion within intron 50 in *Col1a1*), exhibiting an abnormal gait as a result of excessive hind-limb deformity and expressing a mutation affecting *Col1a1* whose equivalent genetic mutation has never been identified in humans [169]. The heterozygous mice ($Aga2^{+/-}$) expressed a range of phenotypic variation from severe osteopenia (model of OI type III), characterized by

disorganized trabecular bone and collagen structure leading to skeletal deformities and fracture, to perinatal death (model of OI type II). On the other hand, homozygous Aga2$^{-/-}$ mice died in utero [169, 298].

The second known classical OI model generated by chemically induced mutation is the Col1a1$^{Jrt/+}$ mouse, carrying a T to C transition that results in the skipping of exon 9 of *Col1a1* gene and in a consequent 18-amino acid deletion in the main triple helical domain of collagen α1 chain.

Col1a1$^{Jrt/+}$ mice display lower BMD, decreased bone parameters, and are more prone to fractures, in addition they display high bone turnover and impaired extracellular matrix, showing abnormalities in matrix composition and collagen fibrillogenesis and hindered mineralization. It is the first reported model that combines the phenotype of OI and Ehlers Danlos syndrome [301].

Less models with mutations in α2(I) collagen chain are available respect to α1(I), one of them is the osteogenesis imperfecta murine (*oim*) model, that carries a mutation in the gene coding for *Col1a2* and exhibits a skeletal disease with clinical and biochemical features of severe OI type III. It is the only naturally occurring OI mouse model and its frame-shift mutation in the region of the gene that encodes the terminal portion of the proα2(I) C-propeptide leads to the synthesis of non-functional proα2(I) chains [302-304].

Despite their utility, these models are not optimal for studies of OI pathophysiology because they lack the combination of typical glycine substitution mutations and autosomal dominant inheritance retrieved in human patients. Furthermore, some of these models are perinatal lethal (OI type II) or show not physiologic levels of mutant mRNA expression.

Two existing models of moderately severe OI type IV, the Brtl and the Amish, carrying respectively a mutation in *Col1a1* and *Col1a2*, combine all these features, therefore they represent a powerful tool to study the outcome of mutations in the two collagen I chains.

Mouse model	Generation	Mutated gene	OI type	Molecular defect	Protein defect
Mov-13	transgenic	*Col1a1*	I-II	retrovirus integration in first intron of *Col1a1*	null allele and reduced α1(I) chains production
human *COL1A1* - minigene model	transgenic	*COL1A1*	II-IV	missing central region containing 41 exons	shortened pro-α1(I) chain
G859C	transgenic	*COL1A1*	II	insertion of synthetic oligodeoxyribonucleotide	G859C
Aga2$^{+/-}$	chemically induced mutation	*Col1a1*	II-III	T to A transversion within intron 50	ablation of C244 and 48 amino acids frameshift
Col1a1 $^{Jrt/+}$	chemically induced mutation	*Col1a1*	IV	T to C transition in splice donor of exon 9	18 amino acids deletion in Col1a1 triple helical domain
oim	naturally occurring	*Col1a2*	I-III	G deletion at nucleotide 3983	frameshift mutation and 48 amino acids alteration
Col1a1 $^{+/G349C}$ (Brtl)	gene targeting	*Col1a1*	IV	G-to-T transversion at nucleotide 1456	G349C
Col1a2 $^{+/G610C}$ (Amish)	gene targeting	*Col1a2*	I-IV	G-to-T transversion at nucleotide 2098	G610C

Table 2: **list of the currently available murine models of classical OI, carrying mutations in collagen I genes.**

Brtl mouse

The Col1a1$^{+/G349C}$ mouse (Brtl) is a knock-in murine model for OI, generated using the Cre/*lox* system. Brtl is heterozygous for a G-to-T transversion at nucleotide 1456 in exon 23 of *Col1a1* allele, changing glycine 349 to a cysteine [305], faithfully reproducing a mutation previously characterized in an OI type IV proband [166] (**Table 2**). Brtl mice have a smaller size than wild type (wt) littermates and present a phenotypic variability, some mice have moderately severe outcome, some show perinatal lethality of OI type II. Indeed 30% of the pups die within hours of birth from respiratory insufficiency [305], therefore reproducing the phenotype described in some patients who carry identical mutations, but have different clinical severity [306].

The surviving heterozygous mutant mice display growth deficiency, impaired mineralization of the skeleton, bone fragility and deformity, in addition their growth pattern with normal size at birth followed by growth deficiency by 4–5 weeks of age, reproduces the early childhood growth pattern reported for moderately severe OI patients [305, 307]. Brtl femurs at 6 months of age displayed a significantly lower BMD and mineral-to-matrix ratio than wt counterparts, together with an altered bone geometry, diminished cortical thickness and reduced stiffness and strength of the bone, nevertheless all these parameters improved after the mice pubertal stage [308].

Further studies in Brtl femora revealed that the bone phenotype of the model is mainly due to an imbalance in the bone remodeling cells, as OCs number and function were increased, while mineral apposition was decreased during growth, pointing to a decline in the production of matrix by OBs [309]. *In vitro* impairment of osteoblastogenesis was also demonstrated in Brtl osteogenic precursors, which have reduced expression of the typical bone differentiation markers and skew towards adipocytic differentiation, leading to a consequent reduction of committed osteoprogenitors in the bone marrow [310].

Despite G349C mutation in α1(I) chains proved to have no effect on the thermal stability or rate of thermal denaturation of mutant collagen and on collagen-collagen recognition and interaction, it leads to the formation of smaller diameter collagen I fibers *in vitro* and it disrupts crystalline organization of tendon fibers *in vivo*. Three different types of collagen I molecules can be found in Brtl ECM, with none, one or both α1 mutated chains, and such heterogeneity causes small variations in molecular alignment of fibers, thus limiting their growth, altering their structure and impairing their interactions with other matrix molecules and resulting in an altered ECM [311].

A fraction of the collagen molecules is partially retained in the ER but interestingly the molecules with both mutated chains are secreted faster and more efficiently [312].

A peculiarity of the mutated chains is the presence of a reactive -SH group, located on the cysteine 349 residue, that can cause the formation of a S-S dimer between two mutated chains or can be the source of abnormal interaction with other molecules, playing a detrimental role in the extracellular matrix. The free -SH is also one of the causes of the selective retention and degradation of triple helices with a single mutated chain, characterized by reduced stability and increased susceptibility to non-specific proteolytic degradation [312, 313].

Interestingly, the expression of the ER-resident collagen-specific molecular chaperone HSP47, known to be augmented in several OI cases, is increased also in Brtl cells [314]. Studies conducted on mutant *Col1a1* silencing revealed a significant reduction in HSP47 expression, arising the speculation that the suppression of mutated collagen may also ameliorate the ER stress caused by aberrant collagen retention [261].

In spite of a good skeletal and molecular characterization of the model, the main unsolved issue in Brtl mice is the phenotypic variability between non-lethal and lethal pups, in fact the molecular mechanism underneath this diversity still remains obscure. Lethal mice

present a severe undermineralization of bones compared to surviving mice, especially in calvaria, propensity to fractures of the long bones and severe deformity [305].

Microarray and proteomic studies on Brtl calvarial bones revealed that both extracellular and intracellular factors are involved in the modulation of the different phenotype. At the intracellular level, mice with lethal phenotype showed a bone specific up-regulation of the pro-apoptotic protein Gadd153/Chop, while mice with moderately severe OI showed an increased level of chaperones, proteasomal subunits and metabolic enzymes, highlighting a difference in the ability to handle cellular malfunction. On the other hand, the ECM lethal Brtl mice presented increased expression of cartilaginous proteins and diminished expression of bone matrix proteins, suggesting an alteration in their extracellular matrix composition and a delay in skeletal development [315]. Differences were also retrieved in protein expression profiles of fibroblasts form lethal and surviving mice, particularly the surviving ones presented the expression of specific chaperones, the reduction of the proteasomal components and the downregulation of cytoskeletal proteins involved in membrane trafficking, cell migration, and cell division [316].

Indeed the cytoskeleton was identified as one of the possible causes of the different phenotype: calvarial and long bone osteoblasts from Brtl lethal pups present a strongly disorganized cytoskeleton assembly that affects cell proliferation, collagen deposition, and integrin and TGF-β signaling [240]. The downregulation of the intermediate filament vimentin, whose disassembly is causative of cytoskeletal collapse [316-318], the transcriptional upregulation of the regulatory factor stathmin, promoting the disassembly of microtubules, [316, 318], and the deregulation of cofilin-1, inducing F-actin depolymerization and inhibiting G-actin polymerization [319], constitute the basis of lethal mice cytoskeletal abnormality. The consequences of these alterations also include a reduction in cell proliferation and decreased expression of the early osteoblast transcription factor RUNX2, with consequent impairment of bone structural properties [240].

These data revealed that the intracellular machinery in lethal mice is less effective to cope with the cellular stress, suggesting that a modulation of cellular pathways can mitigate/ameliorate the OI phenotype.

Amish mouse

The *Col1a2*$^{+/G610C}$ mouse (Amish) is also a knock-in murine model for OI type IV carrying a *COL1A2* variant, precisely a G-to-T transversion at nucleotide 2098 that alters the glycine 610 to cysteine (**Table 2**). This substitution replicates the one of an American Old Order Amish family identified through the Amish Family Osteoporosis Study (AFOS) [320] and by the Anabaptist Genealogy Database (AGDB4), which was queried to recognize a putative founder couple of the affected family [321].

Knock-in mice were produced using embryonic stem cells targeting and Cre/lox P technology. Homozygous pups did not survive after birth because of severe bone pathology and undermineralization [168]. Heterozygous pups survived to weaning and their bones were more brittle and prone to fractures compared to their wt counterparts, being characterised by an osteopenic phenotype represented by decreased bone volume, reduced cortical thickness, and fewer and more dispersed trabeculae [168, 322].

Mineral properties of the Amish mice are normal at 10 days and show a more brittle bone phenotype with aging. Because the process of endochondral bone formation is active in the post-natal period from birth to 10 days, while from 10 days to 2 months endochondral ossification and appositional bone growth take place, appositional bone growth is identified as the aberrant process, due to its dependence on type I collagen structure [322].

On the extracellular side, despite that most of the mutated molecules are secreted in the ECM, a fraction of these molecules is not incorporated into the matrix, in fact the number of incorporated collagen molecules carrying the mutated chain is less than the total mutated molecules secreted by OBs [167], and collagen molecules thermal stability is reduced in comparison with healthy mice [168]. G610C mutation ultimately results in a poor organization of collagen fibers in the ECM [323]. A surprising aspect in the Amish mice is their ability to secrete a significant fraction of type I collagen mutant α1(I) homotrimer in addition to α2(I)-G610C containing heterotrimeric collagen.

Importantly, the mutation in α2 chain is responsible for the impairment of procollagen I folding, in fact procollagen I chains from heterozygous mice were overhydroxylated and overglycosylated and they accumulated in the ER cisternae, which were found to be dilated [167].

The expression of the key UPR transducer BIP was found unchanged, highlighting the activation of an alternative stress response instead of a canonical UPR pathway. The main

outcome is a malfunction in the OBs, displaying impaired differentiation and reduced activity, in particular lower mineral deposition *in vitro* [167].

Because ER-accumulated misfolded procollagen is primarily degraded by lysosomes through autophagy, the modulation of this pathway constitutes an appealing OI target [167]. In a recent study, a low protein diet was administered to Amish mice with the aim of stimulating the autophagic pathway and verifying if it would have affected the bone material quality over time. Despite the fact that diet had beneficial effects on OBs precursors differentiation and maturation and on mineralization of the newly deposited bone, it suppressed overall animal growth, reduced mineral apposition rate, and reduced the absolute bone strength and toughness both in Amish and wt mice, demonstrating that a prolonged autophagy activation is detrimental to bone cells homeostasis [323].

Analyses of the femoral geometric and biomechanical properties of Amish mice revealed reduced marrow cavity diameter in females and increased cortical bone width in males, as well as decreased whole bone biomechanical strength and reduced femoral length in both sexes. Tibia analyses also revealed decreased trabecular bone volume/total volume (BV/TV) and trabecular number [324].

Raman spectroscopy performed on Amish femora showed elevated mineral-to-collagen ratio and reduced collagen content compared to healthy mice [325].

In conclusion, the Brtl and Amish models proved to be faithfully representative of classic OI features and constitute a powerful tool to investigate the molecular pathways involved in OI pathogenesis and to test the efficiency of OI therapies.

Chapter 1

4-PBA ameliorates cellular homeostasis in fibroblasts from Osteogenesis Imperfecta patients by enhancing autophagy and stimulating protein secretion

Mutations in α1 or α2 chains of collagen type I cause classical dominant forms of OI and lead to the alteration of the structure and function of the extracellular matrix. While the majority of mutated molecules are secreted in the ECM, a fraction is intracellularly retained in the ER. In this work, using OI patient fibroblasts carrying mutations in both chains we demonstrated that retained collagen molecules are responsible for ER enlargement and consequent activation of the unfolded protein response (UPR), mainly through the eukaryotic translation initiation factor 2 alpha kinase 3 (PERK) branch. Cells carrying α1(I) mutations react to the stress by upregulating autophagy, while cells with α2(I) mutations only occasionally trigger the autodegradative response. Despite the autophagy activation to face stress conditions, apoptosis occurs in all mutant cells.

To decrease the stress, OI fibroblasts were treated with the chemical chaperone and histone deacetylase inhibitor 4-PBA. The drug proved to inhibit UPR, to enhance autophagy and to promote protein secretion, thus contributing to the clearance of ER cisternae crowding and restoring cellular functionality. Interestingly, we observed a selective effect of 4-PBA on collagen secretion, as it was stimulated only in the fibroblasts carrying mutations closer to the C-terminus of the molecule.

This paper provides proof that intracellular stress can be a target for OI pharmacological therapy and that 4-PBA administration is a promising strategy to rescue OI cells homeostasis.

I contributed to the revision process of this work, in particular I performed cell cultures and cells samples preparations, such as protein lysates. I also performed part of the western blots.

BBA - Molecular Basis of Disease 1864 (2018) 1642–1652

Contents lists available at ScienceDirect

BBA - Molecular Basis of Disease

journal homepage: www.elsevier.com/locate/bbadis

4-PBA ameliorates cellular homeostasis in fibroblasts from osteogenesis imperfecta patients by enhancing autophagy and stimulating protein secretion

Roberta Besio[a], Giusy Iula[a], Nadia Garibaldi[a], Lina Cipolla[b], Simone Sabbioneda[b], Marco Biggiogera[c], Joan C. Marini[d], Antonio Rossi[a], Antonella Forlino[a,*]

[a] Department of Molecular Medicine, Biochemistry Unit, University of Pavia, Pavia 27100, Italy
[b] Istituto di Genetica Molecolare, Consiglio Nazionale delle Ricerche, Pavia 27100, Italy
[c] Department of Biology and Biotechnology, University of Pavia, 27100 Pavia, Italy
[d] Bone and Extracellular Matrix Branch, NICHD, National Institute of Health, Bethesda, MD 20892, USA

ARTICLE INFO

Keywords:
Collagen
Osteogenesis imperfecta
Autophagy
Endoplasmic reticulum stress
Chemical chaperone
Unfolded protein response

ABSTRACT

The clinical phenotype in osteogenesis imperfecta (OI) is attributed to the dominant negative function of mutant type I collagen molecules in the extracellular matrix, by altering its structure and function. Intracellular retention of mutant collagen has also been reported, but its effect on cellular homeostasis is less characterized. Using OI patient fibroblasts carrying mutations in the α1(I) and α2(I) chains we demonstrate that retained collagen molecules are responsible for endoplasmic reticulum (ER) enlargement and activation of the unfolded protein response (UPR) mainly through the eukaryotic translation initiation factor 2 alpha kinase 3 (PERK) branch. Cells carrying α1(I) mutations upregulate autophagy, while cells with α2(I) mutations only occasionally activate the autodegradative response. Despite the autophagy activation to face stress conditions, apoptosis occurs in all mutant fibroblasts. To reduce cellular stress, mutant fibroblasts were treated with the FDA-approved chemical chaperone 4-phenylbutyric acid. The drug rescues cell death by modulating UPR activation thanks to both its chaperone and histone deacetylase inhibitor abilities. As chaperone it increases general cellular protein secretion in all patients' cells as well as collagen secretion in cells with the most C-terminal mutation. As histone deacetylase inhibitor it enhances the expression of the autophagic gene *Atg5* with a consequent stimulation of autophagy. These results demonstrate that the cellular response to ER stress can be a relevant target to ameliorate OI cell homeostasis.

1. Introduction

Osteogenesis imperfecta (OI) is one of the more common of the rare hereditary skeletal dysplasias, with an incidence of 1:15–20,000 [1]. The OI phenotype, ranging from very mild osteoporosis to perinatal lethality, is characterized by reduced bone mineral density, deformed bones and frequent fractures in the absence of or in response to minor trauma [2]. Classical OI (types I to IV, based on Sillence classification) is a dominantly inherited bone dysplasia caused by mutations in the *COL1A1* and *COL1A2* genes, encoding for α1 and α2 chains of type I collagen, respectively [3]. Type I collagen is the most abundant protein of skin and bone extracellular matrix (ECM). The delay in type I collagen folding due to glycine substitution in the procollagen chains is responsible for a prolonged exposure of the chains to the endoplasmic reticulum (ER) enzymes responsible for post-translational modifications [1]. Thus, in OI cells trimeric collagen molecules are synthesized with increased proline and lysine hydroxylation and hydroxylysine glycosylation [4]. The overmodification is broadly dependent on the position of the mutation along the chains. Since collagen folds in a zipper like fashion, from the C- to the N-terminal end, it was previously thought that this contributed to the severity of the phenotype of mutations at the C- terminus of the α1(I) chain. Now this outcome is understood to be influenced by the major ligand-binding region (MLBR) near the C-terminus as well as by the particular substituting amino acid [5,6]. The overmodification remains useful as a measure of delayed folding of helices containing mutant chains.

* Corresponding author at: Department of Molecular Medicine, Biochemistry Unit, University of Pavia, Via Taramelli 3B, 27100 Pavia, Italy.
E-mail addresses: roberta.besio@unipv.it (R. Besio), giusy.iula01@universitadipavia.it (G. Iula), nadia.garibaldi01@universitadipavia.it (N. Garibaldi), lina.cipolla@igm.cnr.it (L. Cipolla), simone.sabbioneda@igm.cnr.it (S. Sabbioneda), marco.biggiogera@unipv.it (M. Biggiogera), marinij@mail.nih.gov (J.C. Marini), antrossi@unipv.it (A. Rossi), aforlino@unipv.it (A. Forlino).

https://doi.org/10.1016/j.bbadis.2018.02.002
Received 13 December 2017; Received in revised form 6 February 2018; Accepted 8 February 2018
Available online 10 February 2018

The mutated type I collagen is predominantly secreted in the ECM, but partially retained intracellularly [2]. While the detrimental effect of its presence in the ECM has been widely investigated and considered the major cause of the OI bone phenotype, its intracellular role is less well understood [2]. An accumulation of mutant collagen in the ER was detected alongside a 40% matrix insufficiency in the Brtl murine model for classical OI, carrying a heterozygous α1(I)-G349C substitution [7]. Similarly, ER enlargement was described in the dominant OI murine model Amish, carrying an α2(I)-G610C substitution and in the heterozygous Aga2 OI murine model carrying a C-terminal single nucleotide deletion responsible for a frameshift changing the last 90 amino acids of the proα1(I) [8–10]. Enlargement of the ER cisternae was also detected in recessive OI caused by mutations in the collagen specific chaperones FK506 binding protein 10 (FKBP10) and SERPINH1 known to be involved in collagen folding and secretion [11,12].

Ishida et al. demonstrated that monomeric proα chains are degraded by the ER-associated degradation (ERAD) pathway, whereas procollagen aggregates, caused by the presence of C-propeptide or triple helical mutations, not impairing trimeric collagen assembly, are eliminated by autophagy [13]. Similarly, Miringian et al. observed the autophagic, but not the proteosomal degradation of mutant collagen in primary osteoblasts obtained from the Amish OI murine model [9].

The type and regulation of the cellular response to the intracellular accumulation of mutant collagen is still an open question. The unfolded protein response (UPR), an evolutionary conserved adaptive response, is generally activated to maintain the functional integrity of the ER under stress conditions (14). The UPR consists of three major signaling cascades initiated by three ER-resident proteins: ER to nucleus signaling 1 (ERN1/Ire1α), activating transcription factor-6 (ATF6) and eukaryotic translation initiation factor 2 alpha kinase 3 (PERK) [14].

Earlier studies by Chessler and Lamande using fibroblasts obtained from OI patients revealed that the retained abnormal collagen is interacting with the UPR sensor BIP, pointing to the activation of the unfolded protein response [15,16]. However, BIP interaction was demonstrated only in the presence of C-propeptide mutations and not in the presence of triple helical glycine substitutions, suggesting in the latter case the activation of an as yet undefined UPR pathway [17].

When ER stress persists and the UPR fails to restore normal cell homeostasis, programmed cell death may occurs [18]. In this contest, the response to ER stress becomes an important modifier of disease severity [17]. Indeed, chemical chaperones, molecules able to help protein folding, had been proposed and used in preclinical and clinical trials to treat diseases caused by intracellular accumulation of misfolded proteins [19]. Among the chemical chaperones already approved by the FDA, although for a different indication, 4-phenylbutyric acid (4-PBA) is appealing to treat collagen-related disorders associated with ER stress [20]. Indeed 4-PBA has been successfully used for rescue the cellular phenotype of hemorrhagic stroke due to intracellular mutant collagen type IV [21]. In the OI context, we recently demonstrated a skeletal amelioration in the *Chihuahua* zebrafish model of classical OI following 4-PBA treatment [22].

The aim of the present study was to elucidate the effect of the intracellular retention of mutant collagen on cellular functions and to investigate whether this condition could be a valid target to rescue OI cellular homeostasis. OI patients' fibroblasts were chosen for the analyses since they are more accessible than osteoblasts and produce a high level of type I collagen. Although OI affects mainly bone tissue, skin abnormalities were reported in patients using skin quantitative magnetic resonance microimaging and histological analysis [23,24]. Moreover similar altered pathways were identified in bone and skin in the Brtl mouse, and the same alterations were also detected in primary OI fibroblasts [25–27]. For our studies we selected fibroblasts from patients who carry glycine substitutions by various amino acids in different locations along the α1(I) or α2(I) chains (Table 1). Of note, two cell lines obtained from independent patients carrying an identical glycine substitution (G667R), but causing lethal (OI type II) or non-lethal (OI type III) outcome, respectively, were also available.

Table 1
Patients fibroblasts used in the study.

	Glycine substitution[a]	Genetic mutation	Protein mutation[b]	OI type[c]	Ref.
α1(I)	**G226S**	c.1210G > A	p.G404S	III	6
	G478S	c.1966G > A	p.G656S	II	28
	G667R	c.2533G > A	p.G845R	III	Marini p.c.
	G667R	c.2533G > A	p.G845R	II	Marini p.c.
	G994D	c.3515G > A	p.G1172D	II	28
α2(I)	**G319 V**	c.1226-7GA > TT	p.G409 V	II	28
	G640C	c.2188G > T	p.G730C	II/III	29
	G697C	c.2359G > T	p.G787C	II	28
	G745C	c.2503G > T	p.G835C	III	30
	G859S	c.2845G > A	p.G949S	III	6

p.c. personal communication
[a] position of mutated glycine into the collagen helix considering the initial gly of the triple helix as amino acid 1.
[b] amino acid number considering the initial methionine codon as amino acid 1.
[c] OI type based on Sillence's classification.

2. Materials and methods

2.1. Human fibroblasts

Human fibroblasts from skin biopsy of OI patients, carrying mutations in *COL1A1* ($n = 5$) or in *COL1A2* ($n = 5$) genes, and three age matched controls were obtained after informed consent and used up to passage P10 (Table 1) [6,28–30]. Cells were grown at 37 °C in humidified atmosphere containing 5% CO_2 and cultured in Dulbecco Modified Eagle's Medium (D-MEM) (4.5 g/l glucose) (Lonza) supplemented with 10% Fetal Bovine Serum (FBS) (Euroclone), 4 mM glutamine (Euroclone), 100 μg/ml penicillin and streptomycin (Euroclone). For each experiment, except where differently stated, 2.5×10^4 cells/cm^2 were plated and harvested after 5 days with no media change. For drug treatment cells were incubated for 15 h with 5 mM 4-PBA (Sigma-Aldrich). The lysosome was blocked using 10 μM chloroquine (Sigma-Aldrich) for 6 h.

2.2. Steady state and chase collagen analysis

Labelling of collagen with L-[2,3,4,5-^{3}H]-proline (PerkinElmer) was used to evaluate collagen over-modification. 2.5×10^4 fibroblasts/cm^2 were plated into 6-wells-plate and grown for 24 h. Cells were then incubated for 2 h with serum-free D-MEM containing 4 mM glutamine, 100 μg/ml penicillin and streptomycin and 100 μg/ml (+)-sodium L-ascorbate (Sigma-Aldrich) to stimulate collagen production. For steady state experiments the labelling was performed for 18 h in the same media using 28.57 μCi of ^{3}H-Pro/ml. For chase experiments the labeling was performed for 4 h using 47.14 μCi of ^{3}H-Pro/ml, then the labeling media was replaced with serum-free D-MEM containing 2 mM proline (Sigma-Aldrich), 4 mM glutamine, 100 μg/ml penicillin and streptomycin and 100 μg/ml (+)-sodium L-ascorbate (chase media). Collagen was collected at 0.5, 1, 2, 3 and 4 h after the pulse. Collagen extraction was performed as previously reported [31]. Briefly, medium and cell lysate fractions were digested o/n with 100 ng/ml of pepsin in 0.5 M acetic acid at 4 °C. Collagen was then precipitated using 2 M NaCl, 0.5 M acetic acid. Collagen was resuspended in Laemmli buffer (62 mM Tris HCl, pH 6.8, 10% glycerol, 2% sodium dodecyl sulphate, 0.02% bromophenol blue) and the radioactivity (counts for minute, CPM) was measured using a liquid scintillation analyzer (PerkinElmer TRI-CARB 2300 TR).

For steady state analyses equal amounts of ^{3}H-labeled collagen from each patient cells were loaded on 6% urea-SDS gel in non-reducing condition. For chase analyses the same volume of ^{3}H-labeled collagens

from each time point was electrophoresed. The gels were fixed in 45% methanol, 9% glacial acetic acid, incubated for 1 h with enhancer (PerkinElmer, 6NE9701), washed in deionized water, and dried. ^{3}H gel radiographs were obtained by direct exposure of dried gels to hyperfilm (Amersham) at −80 °C. The radiographs were acquired by VersaDoc 3000 (BioRad) and α1 band intensity was evaluated by Quantity One software (BioRad). For chase analyses the ratio between the collagen in the media and the total collagen (medium plus cell layer collagen) was evaluated by measuring the density of the α1(I) band to quantify the percentage of collagen secretion. Each chase experiment was run at least in duplicate.

2.3. Transmission electron microscopy analysis

For transmission electron microscopy analysis, fibroblasts from controls and patients were trypsinized and centrifuged at 1000*g* for 3 min. The pellet was fixed with 1% glutaraldehyde in the culture medium for 2 h at room temperature. The cells were rinsed in PBS and then in H_2O. Finally, the fibroblasts were fixed in 2% (*w/v*) OsO_4 in H_2O for 2 h at room temperature (RT), rinsed in distilled water and embedded in 2% agarose in H_2O. The specimens were then dehydrated in acetone and finally infiltrated with Epoxy resin overnight (o/n), and polymerized in gelatin capsules at 60 °C for 24 h. Thin sections (60–70 nm thick) were cut on a Reichert OM-U3 ultramicrotome with a diamond knife and collected on 300-mesh nickel grids. The grids were stained with saturated aqueous uranyl acetate by lead citrate and observed with a Zeiss EM900 electron microscope, operated at 80 kV with objective aperture of 30 μm.

2.4. Protein lysates

Fibroblasts were washed with PBS, scraped in PBS, centrifuged at 1000*g* for 4 min and lysed and sonicated in RIPA buffer (150 mM NaCl, 1% IGEPAL® CA-630, 0.5% sodium deoxycholate, 0.1% SDS, and 50 mM Tris, pH 8) supplemented with protease inhibitors (13 mM benzamidine, 2 mM *N*-ethylmalemide, 5 mM ethylenediaminetetraacetic acid, 1 mM phenylmethylsulfonyl fluoride and 2 mM $NaVO_3$). Proteins were quantified by RC DC Protein Assay (BioRad). Bovine Serum Albumine (BSA) (Sigma-Aldrich) was used as standard.

2.5. Western blot

Proteins from human fibroblasts lysates (10–50 μg) were separated on SDS-PAGE with the acrylamide percentage ranging from 6% to 15% depending on the size of the analyzed protein. The proteins were electrotransferred from the gel to a PVDF membrane (GE Healthcare) at 100 V for 2 h on ice in 19 mM Tris HCl, 192 mM glycine and 20% (*v*/v) methanol. The membranes were then blocked with 5% (*w/v*) BSA in 20 mM TrisHCl, 500 mM NaCl, pH 7.5 (TBS), 0.05% (v/v) Tween-20 (Sigma-Aldrich) (TBS-T) at RT for 1 h. After washing with TBS-T the membranes were incubated with 1:1000 primary antibody against the specific protein BIP (Cell Signaling), IRE1α (Cell Signaling), PERK (Cell Signaling), PDI (Cell Signaling), p-PERK (Thr980) (Cell Signaling); LC3A/B (Cell Signaling), ATG5 (Cell Signaling), ATG12 (Cell Signaling) and ATG16L1 (Cell Signaling); Caspase-3 (Cell Signaling), Cleaved Caspase-3 (Cell Signaling); ATF4 (Novus Biological); p-IRE1α (Ser724) (Novus Biological), ATF6 (Abcam); acetyl hystone H3J (ThermoFisher); in 5% BSA in TBS-T o/n at 4 °C. The appropriate secondary antibody anti-mouse (Cell Signaling), anti-rabbit (Cell Signaling) or anti-goat (Santa Cruz Biotechnology), was added at dilution of 1:2000 in 5% BSA in TBS-T for 1 h at RT. Anti-β-actin antibody (Santa Cruz Biotechnology) diluted 1:1000 in 5% BSA in TBS-T was used for protein loading normalization. The signal was detected by ECL Western blotting detection reagents (GE Healthcare) and images were acquired with ImageQuant LAS 4000 (GE Healthcare), using the ImageQuant LAS 4000 1.2 software. Bands intensity was evaluated by densitometry, using ImageQuant TL analysis software. For each gel, the intensity of the control band was set equal to one and the expression of the mutant samples was expressed as fold difference. For each cell line, three independent lysates were collected and technical triplicates were performed.

2.6. LC3 immunofluorescence

1.5×10^4 fibroblasts were plated on sterile glass coverslips (Marienfeld) in 24 well plate in triplicate. After 5 days, cells were treated for 6 h with 10 μM chloroquine. After the treatment, the medium was removed and cells were fixed with cold 100% CH_3OH for 15 min at −20 °C, washed 3 times with PBS and blocked 1 h in 1% BSA in PBS containing 0.3% TritonX100. Then, cells were incubated with LC3 primary antibody (Cell Signaling) diluted 1:500 in 1% BSA, 0.3% TritonX100 in PBS o/n at 4 °C. Cells were washed 3 times with PBS and incubated with secondary antibody (AlexaFluor 488 coniugated F(ab') fragment anti- rabbit IgG, Immunological Sciences) diluted 1:2000 in 1% BSA, 0.3% Tritonx100 in PBS for 2 h at RT. Nuclei were stained with 4′,6-diamidino-2-phenylindole (DAPI) (Sigma-Aldrich). The samples were analyzed by TCS SP2- Leica confocal microscope (Leica). The total area of punctate signal per cell was measured by the Leica software LAS4.5.

2.7. Fluorescence activated cell sorting (FACS)

To analyze apoptosis the FACS Annexin V/Dead Cell Apoptosis Kit (Invitrogen) was used following manufacturer instruction. As positive control for the activation of apoptosis cells were treated with 20 μM thapsigargin (Sigma-Aldrich) for 24 h in serum-free D-MEM. Samples were analyzed by Cell Sorter S3 (Biorad), 1×10^4 events for each sample, measuring the fluorescence emission at 510–540 nm and > 565 nm.

2.8. Protein secretion

OI patients' fibroblasts were plated in 24 well plate and after 5 days without changing the medium were labeled with 5 uCi/ml [35S] EXPRESS35S Protein Labeling Mix (PerkinElmer) in D-MEM without L-methionine, L-cystine, and L-glutamine for 1 h at 37 °C. Total proteins from medium and cell layer were precipitated with 10% trichloroacetic acid. Proteins were washed with acetone twice and resuspended in 60 mM Tris HCl, pH 6.8, 10% sodium dodecyl sulphate. The radioactivity (counts for minute, CPM) of the samples was measured using a liquid scintillation analyzer (TRI-CARB 2300 TR). The percentage of protein secretion was calculated based on the ratio between the CPM in the media and the CPM in medium and cell layer, evaluated in 5 technical replicates.

2.9. Expression analysis

Total RNA was extracted from patients fibroblasts using TriReagent (Sigma–Aldrich) according to the manufacturer's protocol. DNase digestion was performed using the Turbo DNA Free Kit (Ambion, Applied Biosystems), and RNA integrity was verified on agarose gel. cDNA was synthetized and qPCR was performed on the Mx3000P Stratagene thermocycler using commercially available TaqMan primers and TaqMan Universal PCR Master Mix (Applied Biosystems). All reactions were performed in triplicate. Expression level for *ATG5* (ThermoFisher, Hs00169468_m1) was evaluated. *GAPDH* (ThermoFisher, Hs99999905_m1) and *ACTB* (ThermoFisher, HS99999903) were used as normalizer. Relative expression levels were calculated using the ΔΔCt method.

2.10. XBP1 splicing analyses

cDNA from control and patients cells was used as a template for PCR amplification across the region of the *XBP1* cDNA (NM_005080.3) containing the intronic target of IRE1α ribonuclease using 0.3 μM sense (nt 396-425; 5′-TCA GCT TTT ACG AGA GAA AAC TCA TGG CCT-3′) and antisense primers (nt 696-667; 5′-AGA ACA TGA CTG GGT CCA AGT TGT CCA GAA-3′). Following a 30 min incubation at 50 °C, reactions were cycled 30 times at 94 °C, 60 °C and 72 °C for 30 s at each temperature. Reaction products were electrophoresed on 7% TBE acrylamide gels and visualized by ethidium bromide staining.

2.11. Statistic analysis

Statistic differences between patients and controls were evaluated by two-tailed Student's test. Technical triplicates were performed, except when otherwise specified, and values were expressed as mean ± standard deviation. A p value < 0.05 was considered significant.

3. Results

3.1. Mutant overmodified type I collagen causes ER cisternae enlargement

Electrophoretic analysis of ^{3}H-proline labeled type I collagen obtained from patient and control primary fibroblasts was used to demonstrate increased glycosylation level associated with glycine substitutions (Fig. 1A). Steady-state collagen gels revealed the typical delayed broader and/or double α(I) bands in both media and cell lysates obtained from cells carrying the α1-G478S, α1-G667RII, α1-G667RIII, α1-G994D, α2-G319 V, α2-G745C, α2-G640C and α2-G697C mutations. In agreement with the collagen folding direction, from C- to N-terminus, only the cells carrying an N-terminal mutation, the α1-G226S, produced normal migrating collagen chains (Fig. 1A). The exception to the C-/N-terminal rule is represented by α2-G859S fibroblasts where normal migrating α bands were detected, likely given the proximity of the mutated residue to a highly flexible region more permissive for folding [32].

Electron microscopy imaging performed on cells representative for α1 and α2 mutations revealed ER dilatation and the presence of large vacuoles, resembling autophagosome vesicles, since double membrane and presence of residual material were occasionally detectable (Fig. 1B).

3.2. Retained mutant procollagen activates the unfolded protein response

Expression of chaperones and proteins involved in the unfolded protein response (UPR) pathway was evaluated (Supplementary Table 1). The expression of BIP, the best characterized activator of the UPR sensors, was increased in 3 out of 5 cells carrying mutations in the collagen I α1 chain and in 3 out of 5 cells with mutations in the collagen I α2 chain (Fig. 2A-B). Interestingly, upregulation of BIP was detected in α1-G667RII associated with a lethal phenotype, while its expression was normal in α1-G667RIII cells from a patient with a moderate severe phenotype (Fig. 2A).

Protein disulfide isomerase (PDI), which catalyzes the formation and isomerization of disulfide bonds and it is known to interact with single collagen α chains, was upregulated in all α1(I) mutated cells, with the exception of the α1-G667RII (Fig. 2A). By contrast, in the α2(I) mutated cells PDI expression was unchanged (Fig. 2B).

The activation of the UPR sensors PERK and IRE1α by phosphorylation and of ATF6 by proteolytic cleavage was then investigated. p-PERK/PERK ratio was increased in all mutant fibroblasts with α1(I) and α2(I) mutations independently from the location/type of the mutation, with the exception of α2-G640C (Fig. 2A–B). Consistently, the expression of activating transcription factor 4 (ATF4), the effector in the PERK pathway, was increased with the exception of the most N-terminal α1-G226S line (Fig. 2A–B).

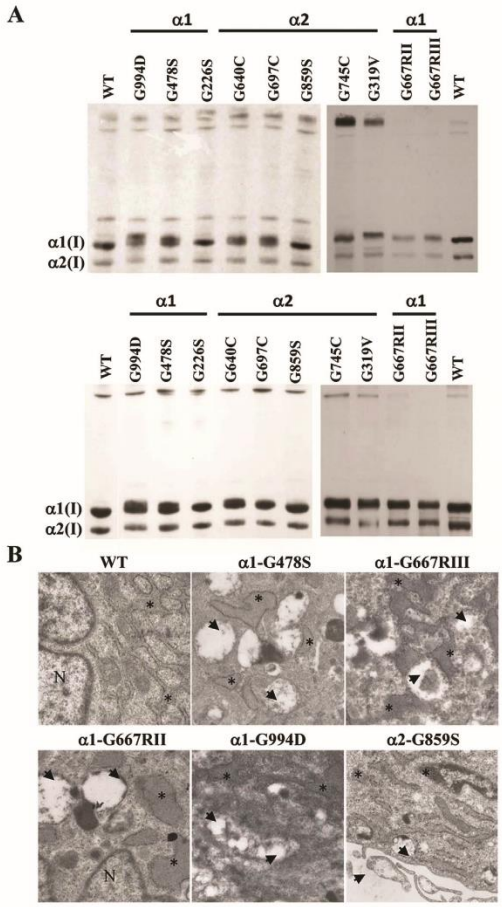

Fig. 1. Mutations in type I collagen genes lead to collagen overmodifications and ER enlargement. (A) Electrophoretic analyses of type I collagen extracted from patients' fibroblasts with dominant OI. Fibroblasts were labeled with ^{3}H-Proline for 18 h. Type I collagen was extracted from cell layer (upper panel) and medium (lower panel) fractions and analyzed by SDS-PAGE. Representative radiographs are shown. A typical broadening or doubling of the α(I) bands in both fractions is observed in all cells except the very N-terminal mutation α1-G226S and the α2-G859S. (B) Transmission electron microscopy analysis of OI fibroblasts revealed the presence of ER enlargement (*) and of cellular vacuolization (arrow). N = nucleus. Magnification 20,000×.

The IRE1α branch was activated in the α1(I) mutated cells α1-G667RIII and α1-G994D and in all cells with mutations in α2, with the exception of α2-G640C, as demonstrated by the level of p-IRE1αI and by the IRE1α- mediated splicing of *XBP1* (Fig. 2A, B, C).

No difference in the level of cleaved ATF6 was detectable in any cells (Fig. 2A-B).

Based on our data, mutant collagen synthesis and intracellular retention cause disruptions of ER homeostasis and determine the activation of the unfolded protein response in OI fibroblasts with mutations in both the α1 and α2 chains. The α2-G640C cells represent the only exception to this rule being characterized by the presence of overmodified collagen without UPR activation.

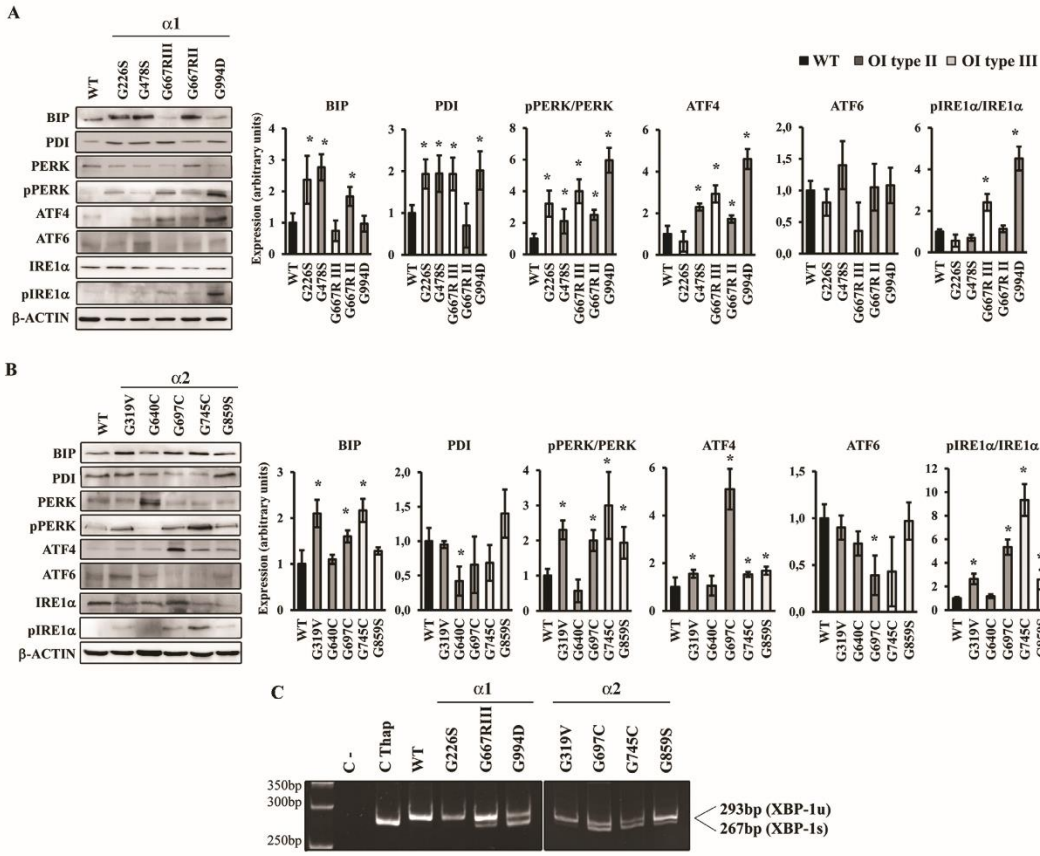

Fig. 2. Mutations in type I collagen genes activates the unfolded protein response in OI patients' fibroblasts. Western blot analyses of the collagen chaperone PDI and of proteins involved in the UPR (BIP, PERK, p-PERK, ATF4, ATF6, IRE1α and p-IRE1α) in cells with mutations in the α1 (A) and α2 chains (B). UPR resulted activated in all patients fibroblasts except in α2-G640C. (C) RT-PCR amplification of XBP1 mRNA from control and patients cells. The spliced XBP1-1s form of XBP1 transcript is found in patients cells with α1-G667RIII, α1-G994D, α2-G319V,α2-G697C, α2-G745C and α2-G859S mutations. Complete splicing is detected in control fibroblasts treated with thapsigargin (Thap). OI type II: lethal osteogenesis imperfecta. OI type III: non-lethal osteogenesis imperfecta. C-: negative control. * $p < 0.05$.

3.3. OI fibroblasts react to cellular stress by upregulating autophagy

Since autophagy is the first cell response to dysfunctional cellular components [33–35], its activation in OI fibroblasts, consequent to the presence and/or intracellular accumulation of mutated collagen, was evaluated. By Western blotting experiments we observed that the expression level of ATG5-12 complex, necessary for autophagosome elongation, was significantly increased in the cell lines α1-G226S, α1-G667RII and α1-G667RIII and the expression of ATG16, which together with ATG5-12 promotes elongation and closures of the autophagosome, was increased in all cells with mutations in α1(I), whereas no upregulation was detected in α2(I) cells (Fig. 3A-B). However, the levels of ATG5-12 and ATG16 are not always correlated to autophagy activation [36]. The terminal fusion of an autophagosome with its target membrane involves LC3-I processing to LC3-II due to the conjugation with phosphatidylethanolamine. The measurements of static and dynamic LC3IIA/B levels in the absence/presence of chloroquine were performed to monitor autophagy (Fig. 3). In static conditions the expression of LC3-II was upregulated in α1-G226S, α1-G478S and α1-G667RII cells (Fig. 3A) while following chloroquine treatment the level of LC3-II increased in all the α1 mutated lines indicating a general accumulation of LC3 due to the block in autophagic flux (Fig. 3C). In α2(I) fibroblasts a LC3-II accumulation was detected in untreated α2-G319V, α2-G697C and α2-G859S (Fig. 3B) and confirmed under dynamic conditions for α2-G697C and α2-G859S (Fig. 3D).

To independently validate the activation of the autophagic pathway, LC3 immunofluorescence was analyzed in OI fibroblasts in the presence of chloroquine. The LC3 signal was significantly increased compared to controls in α1-G478S, α1-G667RIII, α1-G667RII, α1-G994D, α2-G697C, and α2-G859S cells while it remained unchanged in α2-G640C (Fig. 4), in agreement with the Western blot data.

3.4. Cellular stress causes activation of apoptosis

Given that the persistence of ER stress could activate apoptosis as an extreme cellular response to stress, we investigated the level of cleaved caspase 3 showing in all OI mutant cells an increased level of this executioner protease, indicative of apoptosis occurrence (Fig. 5A).

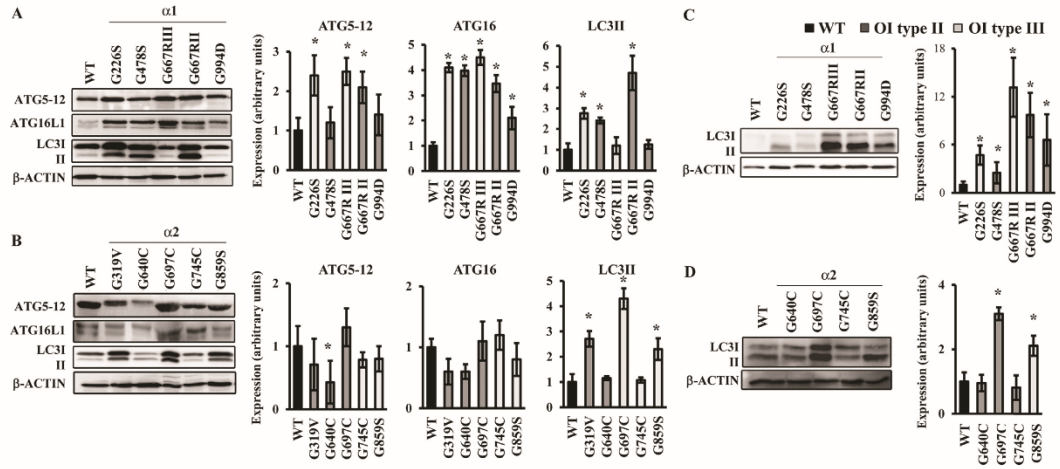

Fig. 3. OI cells react to cellular stress by activating autophagy. (A–B) Western blot analyses of proteins involved in the autophagic pathway (ATG5-12, ATG16L1, LC3-I/LC3-II) in OI fibroblasts with mutations in *COL1A1* (A) and *COL1A2* (B) genes. Protein components involved in the formation of the autophagosome are upregulated in patients with α1(I) mutations. The terminal autophagic marker LC3 is upregulated in the majority of cases. (C-D) LC3 Western blot analyses in the presence of chloroquine in OI fibroblasts with mutations in *COL1A1* (C) and *COL1A2* (D) genes. The terminal marker of autophagy evaluated in dynamic conditions is increased in all patients' cells except in α2-G640C and α2-G745C. OI type II: lethal osteogenesis imperfecta. OI type III: non-lethal osteogenesis imperfecta. * $p < 0.05$.

Fluorescence Activated Cell Sorting (FACS) of annexin V/dead positive cells confirmed the activation of apoptosis in the OI fibroblasts. A higher percentage of apoptotic cells compared to controls was detected in α1-G478S ($p = 0.269$), α1-G667RIII ($p = 0.046$), α1-G667RII ($p = 0.004$), α1-G994D ($p = 0.002$) and α2-G640C ($p = 0.032$), α2-G697C (p = 0.046) and α2-G859S ($p = 0.008$) (Fig. 5B).

3.5. The chemical chaperone 4-PBA ameliorates OI fibroblasts homeostasis

To evaluate if the alleviation of the stress could ameliorate OI patient cells homeostasis, controls and patients fibroblasts were treated with 4-PBA, a well-known chemical chaperone that is FDA-approved as ammonia scavenger for urea cycle disorders [37]. The effect of the drug was evaluated by Western blotting measuring the expression p-PERK, as marker for UPR, and the activation of caspase 3, as signature for apoptosis. The levels of these markers were compared in treated versus untreated cells and in treated OI cells versus untreated controls. None of the selected markers were significantly changed in WT cells after 4-PBA treatment (Supplementary Table 2).

4-PBA treatment decreased the p-PERK/PERK level in 4 out of 5 cell lines with mutations in α1 chain, reaching values comparable to controls in α1-G667RIII and in α1-G994D (Fig. 6A). A normalization of the PERK activation did not occur in the α1-G667RII (Fig. 6A). Regarding cells with mutations in the α2 chain, 4-PBA decreased the level of p-PERK/PERK to controls value in α2-G697C and α2-G745C (Fig. 6B).

Interestingly, the level of cleaved caspase 3 was decreased with respect to untreated cells reaching normal levels in all treated α1 cells, with the exception of the very N-terminal one α1-G226S (Fig. 6A), and in α2-G640C and α2-G859S (Fig. 6B).

Thus, 4-PBA treatment generally restored control values for pPERK/PERK and of the terminal caspase 3 in most of the cells with mutations in the α1 collagen chain. The treatment of α2 mutated cells was effective for these parameters in α2-G697C and α2-G745C.

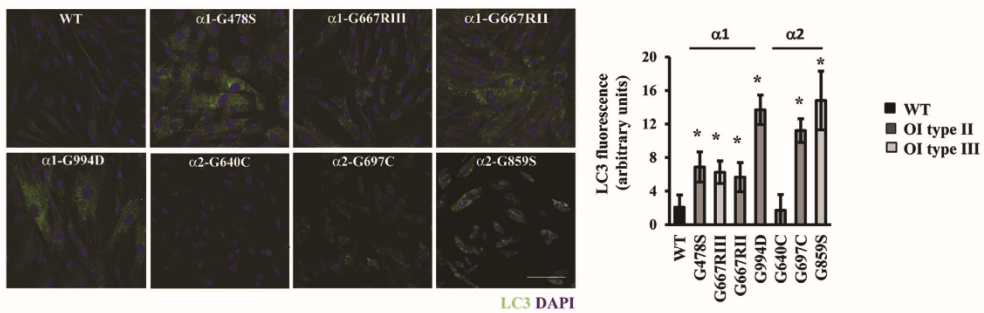

Fig. 4. Autophagy activation in OI cells. Autophagy was evaluated in control and OI fibroblasts α1-G478S, α1-G667RIII, α1-G667RII, α1-G994D, α2-G640C, α2-G697C and α2-G859S by LC3 immunofluorescence in the presence of chloroquine. Representative confocal images of WT and mutant fibroblasts incubated with LC3 antibody are shown. Quantitation of the total area of punctate signal per cell confirms the activation of autophagy. DAPI (nuclei) in blue and LC3 in green. Magnification 40×, zoom 4×. OI type II: lethal osteogenesis imperfecta. OI type III: non-lethal osteogenesis imperfecta. * $p < 0.05$.

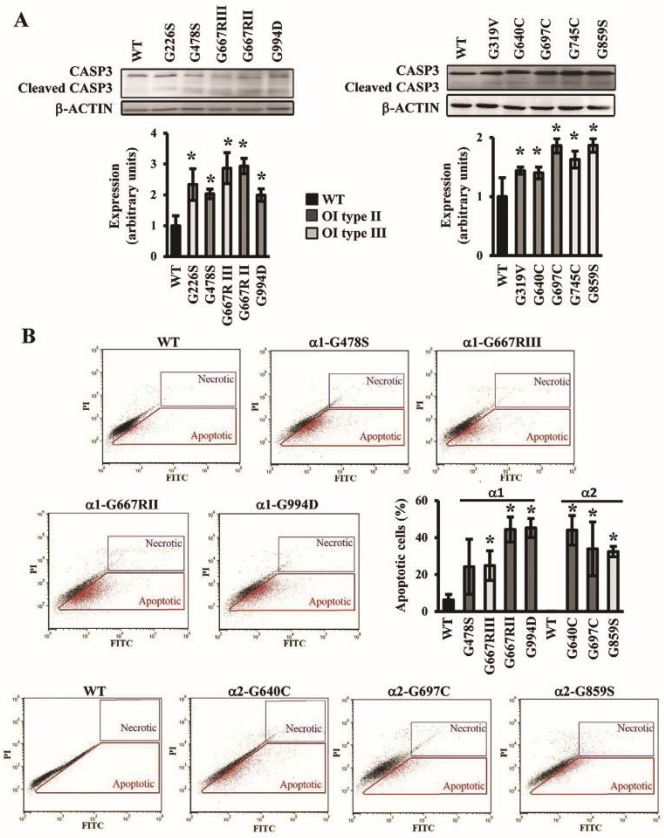

Fig. 5. Activation of apoptosis in OI patients cells. (A) Western blot analyses of the terminal marker of apoptosis cleaved caspase 3. (B) FACS analysis detection of apoptotic cells by concurrent staining with annexin V (FITC) and propidium iodide (PI). The fraction of apoptotic events in the cells is shown in representative plots and quantified in the histogram as mean ± SEM. Apoptosis is activated in all tested OI patients cells. OI type II: lethal osteogenesis imperfecta. OI type III: non-lethal osteogenesis imperfecta. * $p < 0.05$.

3.6. 4-PBA stimulates protein secretion and autophagy

In order to understand the molecular basis of the positive 4-PBA action on mutant cellular homeostasis we investigated in our system the chaperone and histone deacetylase inhibitory activity of the drug.

Upon 4-PBA administration protein secretion was increased in all OI cells (Fig. 7A), compared to severely reduced secretion in basal condition (with the exception of the α1-G640C), as evaluated by protein labeling with ^{35}S-L-methionine and ^{35}S-L-cysteine.

To analyze specifically type I collagen secretion, chase experiments with ^{3}H-Pro metabolic labeling were performed and delayed secretion of collagen in all the analyzed OI fibroblasts was shown (Fig. 7B). 4-PBA treatment was able to clearly enhance collagen secretion in the α1-G994D fibroblasts, the cells with the most C-terminal mutation and the one with the strongest intracellular retention.

Since epigenetic modifications play a crucial role in the regulation of gene expression to maintain cell homeostasis [38], and since 4-PBA has a known effect on histone modifications [39], histone H3 acetylation was investigated. 4-PBA increased the level of the H3 modification in all control and mutant cells with the exception of the α1-G478S (Fig. 8A). This increase was associated with the upregulation of the expression of the autophagic gene *ATG5* with the only exception of α1-G478S, as shown by qPCR data (Fig. 8B, Supplementary Fig. 1). Importantly mRNA data were supported by protein data which revealed increased LC3-II levels in all α1 and α2 cells treated with 4-PBA clearly indicating a stimulation of autophagy (Fig. 8C).

Thus in the analyzed OI fibroblasts 4-PBA, stimulating both protein secretion and autophagy, helps the clearance of the engorged cells with positive effects on cell homeostasis and a reduction of cell death.

4. Discussion

The symptoms of skeletal dysplasias have been previously attributed to the dominant negative effect of structural abnormal collagen on extracellular matrix. Only recently, the cellular malfunction caused by mutated proteins retention in the endoplasmic reticulum has been demonstrated to play a key role in modulating the phenotype severity in several diseases including skeletal disorders due to mutations in ECM molecules such as the fibrillar collagen types II and X [17,40]. Here, we utilize fibroblasts from 10 OI patients producing structurally abnormal type I collagen, 5 each with glycine substitutions in the α1(I) and α2(I) chains, to investigate the effect of its intracellular retention (Table 1). Type I collagen is the major protein component of the ECM of bone and skin and is the most abundant protein synthesized by fibroblasts. We

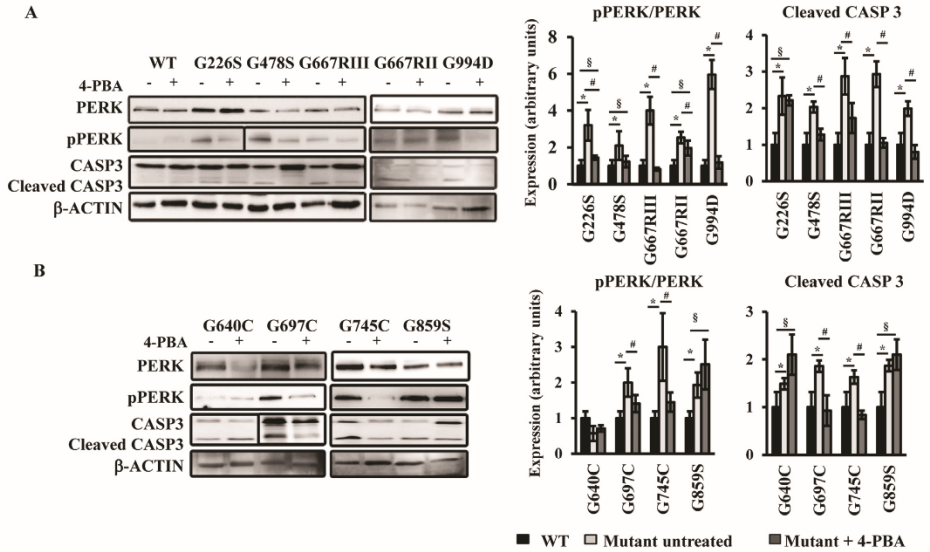

Fig. 6. 4-PBA ameliorates OI fibroblasts homeostasis. To alleviate the stress and to ameliorate OI patients' cells homeostasis, fibroblasts with mutations in *COL1A1* (A) and *COL1A2* (B) genes were treated with 5 mM 4-PBA for 15 h. The effect of the drug was evaluated following by Western blotting the expression of p-PERK, as markers for UPR, and the expression of cleaved caspase 3, as signature for apoptosis. The levels of these proteins were compared in treated versus untreated cells and in treated OI cells versus untreated controls. 4-PBA treatment mainly restores control values for what concern the activation of the UPR sensor PERK and the activation of the terminal caspase 3 in cells with mutations in the α1 collagen chain. The treatment on α2 mutated cells was effective on α2-G697C and α2-G745C. * $p < 0,05$ mutant fibroblasts respect to control fibroblasts. # $p < 0,05$ treated fibroblasts respect to untreated mutant fibroblasts. § $p < 0,05$ treated fibroblasts respect to untreated control fibroblasts.

demonstrated the activation of the PERK UPR branch, with increased p-PERK/PERK ratio and increased expression of its downstream effector ATF4 (Fig. 2A-B). The activation of the UPR branch mediated by PERK has been described in the Amish murine model for dominant OI, carrying the α2(I)-G610C substitution [9], in the OI Dachshund dog homozygous for a defect in HSP47 [41], and in human OI type XIV patients lacking the expression of TRIC-B [42]. However, we also demonstrated the activation of the IRE1α UPR branch, especially, though not exclusively, in fibroblasts with α2(I) substitutions, which has not been previously reported in OI. Both PERK and IRE1α are type I transmembrane proteins sharing similar ER luminal domain structure and cytosolic Ser/Thr kinase domain, thus what determines the activation of one or the other or both pathways is difficult to dissect. The type and duration of intracellular insult as well as the structural differences between IRE and PERK lumen sensing domain were hypothesized as possible modulators of their response to cell stress [43]. Interestingly, the activation of IRE1α is reported to occur first following an ER insult favoring cytoprotective response, and to be attenuated during persistent ER stress, whereas PERK signaling, including translational inhibition and proapoptotic activation, is maintained and associated with cell death. Based on this observation, we can speculate that a prolonged presence of higher amount of mutated collagen due to α1 mutations, 75% compared to 50% mutant molecules when the mutation is in α2, is causing a more severe stress following misfolded protein retention. The ER lumen domain of the three UPR sensors PERK, Ire1α and ATF6 is associated with BIP, the major ER chaperone that upon ER stress is released to favor proper protein folding [44]. The puzzling behavior of BIP in OI cells has contributed to confusion concerning UPR activation as consequence of aberrant type I collagen. Immunoprecipitation studies demonstrated that retained mutant procollagen in OI primary fibroblasts is bound by BIP in presence of C-propeptide mutations, but not in presence of mutations in the triple helical domain [15,16]. Western blot analyses of primary osteoblasts from the OI Aga2 mouse model, harboring a proα1(I) C-terminal frameshift and from the α2(I)-G610C mouse revealed an upregulation of BIP in the former, but not in the latter. Interestingly, we found that BIP was upregulated in 3 of 5 helical mutations in α1(I) and α2(I) chains (Fig. 2A-B). It is possible that the use of fibroblasts, and the different type/position of substitution may explain the diverse response compared with the Amish model. In addition, based on the IRE1 crystal structure and detailed kinetic studies of BIP interaction with various UPR sensors, it has been proposed that other regulatory mechanisms or components in addition to BIP are involved in UPR activation following ER stress [45,46].

When UPR fails to reduce the ER overload, autophagy, a highly conserved cellular process regulating the turnover of cytoplasmic materials via a lysosome-dependent pathway, may be activated [47]. Indeed, in OI fibroblasts the prolonged stress caused by the continuous synthesis and intracellular accumulation of mutant collagen causes autophagy upregulation (Figs. 3–4). Our observation is in agreement with the literature data which identify autophagy as the preferential degradation pathway to eliminate over-glycosylated trimeric procollagen I molecules [9,13,48]. Autophagy is significantly activated in all mutant *COL1A1* cells, but only in two mutant *COL1A2* cells. Considering the stoichiometric composition of type I collagen, it may be that a minimal threshold of mutant molecules is required to activate autophagy, although we cannot exclude a role for the type/position of the α2(I) mutation in modulating autophagy, since 2 of the 5 α2(I) mutations increased this degradation pathway (Figs. 3–4). Autophagy has a well-known cytoprotective role in various disorders and its cell protective role in presence of ER stress has been as well reported [47,49,50]. The failure of autophagy to rescue cellular homeostasis in OI cells sets in motion the path to apoptotic death (Fig. 5). Similarly, the intracellular accumulation of abnormal proα1(I) in the Aga2 OI mouse induces caspases-12 and 3 activation, leading to osteoblast apoptosis [10], while in the Amish mouse model upregulation of the

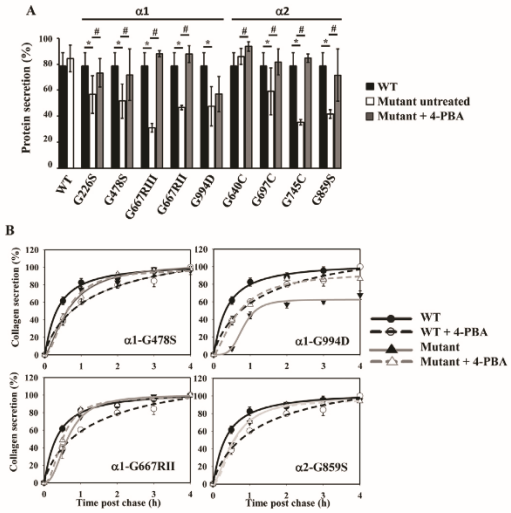

Fig. 7. 4-PBA ameliorates OI fibroblasts homeostasis by stimulating protein secretion. (A) After 4-PBA treatment OI patients' fibroblasts were labeled with [35S] EXPRESS35S Protein Labeling Mix for 1 h and total proteins were extracted from medium and cell layer. Determination of the total counts incorporated in cell layer and medium revealed that 4-PBA increases protein secretion in all cells lines. (B) Collagen secretion was evaluated by incubating the cells for 4 h with 47.14 μCi of ^{3}H-Pro/ml, and extracting the collagen from both medium and cell layer fractions at the indicated time points. Samples were run on SDS-PAGE and the ratio between the densitometric value of collagen α1(I) in the media and the total collagen α1(I) (collagen present in medium and in cell layer) was evaluated and shown in the plot. Collagen secretion is delayed in all mutant cells tested compared to controls. Collagen intracellular retention was significant in α1-G994D cells. 4-PBA increased collagen secretion in α1-G994D cells.

general stress response protein CHOP was detected, promoting apoptosis [9]. It is interesting that we detected apoptosis even in the α1-G226S fibroblasts, which have minimal overglycosylation because of the N-terminal location of this glycine substitution. G226 is located in close proximity to a HSP47 binding site, which has recently been reported to play a role in collagen sorting from the ER [5,51]. Thus, it is tempting to hypothesize that autophagy and apoptosis of G226S cells may reflect an effect on collagen sorting, since the collagen structure and modifications are minimally altered. The demonstration of apoptosis in α2-G640C cells is more puzzling, since neither UPR nor autophagy activation were detected. We can speculate that the substituting cysteine might form detrimental disulphide bonds between procollagen molecules or other ER resident proteins, impairing mutant collagen secretion from the ER. Of note, among the available OI fibroblasts we had the opportunity to analyze cells carrying an identical α1-G667R substitution, but isolated from patients with markedly different phenotypes, severe OI type III (α1-G667RIII) or lethal OI type II (α1-G667RII). The α1-G667RIII cells, but not the G667RII, showed upregulation of PDI, a chaperone favoring collagen chain recognition and folding, and of IRE1α, the more cytoprotective UPR transducer (Fig. 2A). These data may be relevant to the mechanism of their phenotypic variability. Especially in the α1(I) chain, patients with identical substitution of the same glycine residue may have lethal or non-lethal phenotypes, which is problematic for genetic counselling. In the Brtl OI mouse model, the α1(I) G349C substitution generates distinct moderate and lethal outcomes. Using bone and skin samples, we excluded that Brtl phenotype variability was due to differences in collagen structure, physical properties or interaction between mutant collagen helices [7]. Instead, using microarray and proteomic analysis, we found different intracellular responses to mutant collagen retention in the two phenotypes [25,26]. Similarly, we have confirmed in patients cells that the ability to manage cell stress can affect cellular homeostasis in the presence of identical mutations. No specific differences in cellular homeostasis were identified between the other lethal and non-lethal cells carrying different mutations.

Chemical chaperones have been used to alleviate cellular stress in several conditions with perturbed ER homeostasis. This is an appealing approach since several molecules with chaperone function are FDA-approved for other indications and already have a good safety record [52–54]. The chemical chaperone 4-phenylbutyric acid (4-PBA) is FDA-approved for urea cycle disorders based on its ammonia scavenger activity [37]. 4-PBA is also able to increase ER folding capacity by facilitating proper folding and decreasing the accumulation and aggregation of misfolded proteins in the ER lumen [20]. Interestingly, amelioration of the cellular phenotype upon 4-PBA treatment was previously reported in dermal fibroblasts with *COL4A2* mutations [21]. Here, 4-PBA treatment of cells with α1(I) mutations decreased or/and normalized PDI and p-PERK/PERK expression and decreased apoptosis (Fig. 6). Only fibroblasts carrying the α1-G226S and α2-G859C OI mutations showed no effect on apoptosis (Fig. 6). This may be related to the proximity of these substitutions to the HSP47 binding sites on collagen. The overall effect of 4-PBA on cells with α2(I) mutations was more subtle than for α1(I) mutations, pointing to a possible effect of the mutant chain itself. Both stress and apoptotic markers were decreased in cells with α2-G697C and α2-G745C mutations (Fig. 6B). Not surprisingly, no effect was found in α2-G640C, in which no UPR was detected in the basal state and for which the molecular basis of apoptosis need to be further evaluated. The molecular basis of 4-PBA effect on our *in vitro* system is related to both chaperone and autophagy effects. Following drug administration, we saw an increase of general protein secretion in all cells, which had been severely reduced in untreated cells, perhaps related to effects of mutant collagen on the general ER folding machinery (Fig. 7A). In the cells with the most C-terminal mutation, we also detected improved collagen secretion (Fig. 7B). We conclude that 4-PBA facilitates the ER folding machinery, impaired in stress condition, ameliorating cell homeostasis as demonstrated by the reduced PERK and apoptosis activation. This effect may also account for the amelioration in collagen secretion although probably in a mutation dependent manner. Our recent corroborative data in the *Chihuahua* (*Chi/+*) zebrafish model for classical OI displayed an increased amount of type I collagen in the *Chi/+* tail upon tail clip and regrowth in the presence of 4-PBA [22].

Treated mutant fibroblasts showed a significant increase of LC3II expression, highlighting a role for 4-PBA as autophagic inducer and suggesting a complementary process of autophagy may favor the degradation of retained unfolded proteins [55]. Indeed 4-PBA-mediated autophagy upregulation has been recently described in hepatocyte cells [56] and induction of autophagy rescued the bone matrix deposition by cultured osteoblasts of the OI Amish model [9]. Moreover, autophagy was reported to play an essential role in protecting cells against the toxicity of TGF-β induced type I procollagen accumulation in the ER [57]. Furthermore, inhibition of autophagy by specific inhibitors or RNAi-mediated knockdown of an autophagy-related gene significantly stimulated accumulation of aggregated procollagen trimers in the ER, while its activation with rapamycin resulted in reduction of aggregates [13,50].

The question to be addressed was how 4-PBA could act as autophagy inducer in our *in vitro* model. Since the upregulation of *ATG5* expression following 4-PBA administration was previously reported in human macrophages infected by *Mycobacterium tuberculosis* we investigated the other known function of 4-PBA as histone deacetylase inhibitor [39,58]. We found that 4-PBA-increased levels of histone H3 acetylation (Fig. 8A) was associated with significantly increased expression of the autophagic gene *ATG5* (Fig. 8B). Although mRNA or protein expression levels are not considered appropriate indicators for

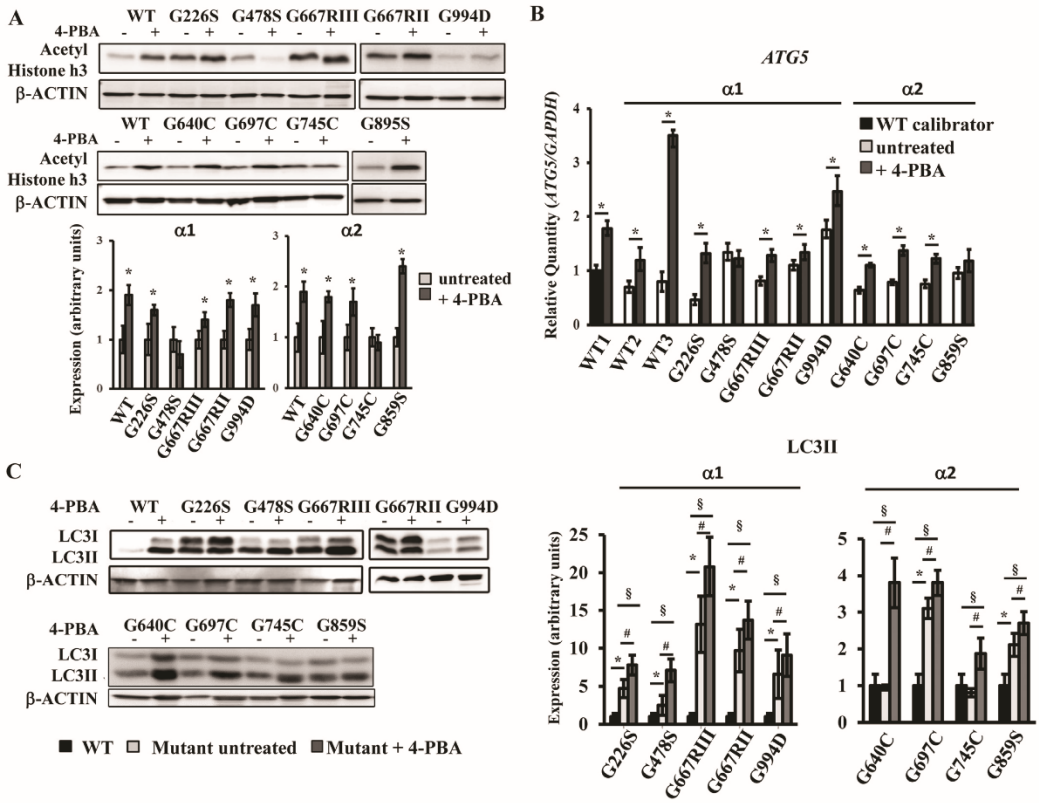

Fig. 8. 4-PBA ameliorates OI fibroblasts homeostasis by stimulating autophagy. (A) Histone H3 acetylation was investigated by Western blot analyses. 4-PBA increased the level of the H3 modification in all cells with the exception of the α1-G478S. (B) The expression of the autophagic gene *ATG5*, evaluated by qPCR, was increased by the treatment in all cells with the exception of α1-G478S. (C) LC3 Western blot analyses in the presence of chloroquine revealed increased LC3-II levels in all α1 and α2 cells after the 4-PBA treatment, clearly indicating a stimulation of autophagy.

monitoring autophagy, *ATG5* upregulation associated with increased autophagy (Fig. 8C) suggests that a transcriptional regulation of autophagic genes may be activated by 4-PBA histone deacetylase inhibitory activity.

Our study identified ER stress and autophagy as two potential targets for OI treatment. The data suggest that chaperone activity and autophagy may act as critical modifiers of the severity of collagen I disease. Manipulation of cellular pathways to modulate the OI phenotype may be easier than targeting the structural abnormalities in matrix, and may produce significant amelioration in clinical severity.

Supplementary data to this article can be found online at https://doi.org/10.1016/j.bbadis.2018.02.002.

Funding

This work was supported by Fondazione Cariplo [grant No. 2013-0612], Telethon [grant No. GGP13098] and the European Community, FP7, 'Sybil' project [grant No. 602300] to AF; and by Associazione Italiana per la Ricerca sul Cancro [Start-up grant No. 12710] and the European Commission [grant No. PCIG10-GA-2011-303806] to SS.

Transparency document

The http://dx.doi.org/10.1016/j.bbadis.2018.02.002 associated with this article can be found, in online version.

Acknowledgements

We thank Dr. Patrizia Vaghi, Centro Grandi Strumenti, University of Pavia, Italy, for technical assistance with confocal microscopy, Mr. Angelo Gallanti for technical assistance with cell culture and Prof. Ivana Scovassi for the careful reading of the manuscript.

The authors report no conflict of interest.

References

[1] A. Forlino, J.C. Marini, Osteogenesis imperfecta, Lancet 387 (2016) 1657–1671.
[2] A. Forlino, W.A. Cabral, A.M. Barnes, J.C. Marini, New perspectives on osteogenesis imperfecta, Nat Rev Endocrinol 7 (2011) 540–557.
[3] D.O. Sillence, A. Senn, D.M. Danks, Genetic heterogeneity in osteogenesis imperfecta, J. Med. Genet. 16 (1979) 101–116.
[4] Y. Taga, M. Kusubata, K. Ogawa-Goto, S. Hattori, Site-specific quantitative analysis of overglycosylation of collagen in osteogenesis imperfecta using hydrazide chemistry and SILAC, J. Proteome Res. 12 (2013) 2225–2232.
[5] S.M. Sweeney, J.P. Orgel, A. Fertala, J.D. McAuliffe, K.R. Turner, G.A. Di Lullo, S. Chen, O. Antipova, S. Perumal, L. Ala-Kokko, et al., Candidate cell and matrix

interaction domains on the collagen fibril, the predominant protein of vertebrates, J. Biol. Chem. 283 (2008) 21187–21197.
[6] J.C. Marini, A. Forlino, W.A. Cabral, A.M. Barnes, J.D. San Antonio, S. Milgrom, J.C. Hyland, J. Korkko, D.J. Prockop, A. De Paepe, et al., Consortium for osteogenesis imperfecta mutations in the helical domain of type I collagen: regions rich in lethal mutations align with collagen binding sites for integrins and proteoglycans, Hum. Mutat. 28 (2007) 209–221.
[7] A. Forlino, N.V. Kuznetsova, J.C. Marini, S. Leikin, Selective retention and degradation of molecules with a single mutant alpha1(I) chain in the Brtl IV mouse model of OI, Matrix Biology: Journal of the International Society for Matrix Biology 26 (2007) 604–614.
[8] E. Daley, E.A. Streeten, J.D. Sorkin, N. Kuznetsova, S.A. Shapses, S.M. Carleton, A.R. Shuldiner, J.C. Marini, C.L. Phillips, S.A. Goldstein, et al., Variable bone fragility associated with an Amish COL1A2 variant and a knock-in mouse model, J. Bone Miner. Res. 25 (2010) 247–261.
[9] L.S. Mirigian, E. Makareeva, E.L. Mertz, S. Omari, A.M. Roberts-Pilgrim, A.K. Oestreich, C.L. Phillips, S. Leikin, Osteoblast malfunction caused by cell stress response to procollagen misfolding in a2(I)-G610C mouse model of osteogenesis imperfecta, JBMR 31 (2016) 1608–1616.
[10] T.S. Lisse, F. Thiele, H. Fuchs, W. Hans, G.K. Przemeck, K. Abe, B. Rathkolb, L. Quintanilla-Martinez, G. Hoelzlwimmer, M. Helfrich, et al., ER stress-mediated apoptosis in a new mouse model of osteogenesis imperfecta, PLoS Genet. 4 (2008) e7.
[11] H.E. Christiansen, U. Schwarze, S.M. Pyott, A. AlSwaid, M. Al Balwi, S. Alrasheed, M.G. Pepin, M.A. Weis, D.R. Eyre, P.H. Byers, Homozygosity for a missense mutation in SERPINH1, which encodes the collagen chaperone protein HSP47, results in severe recessive osteogenesis imperfecta, Am. J. Hum. Genet. 86 (2010) 389–398.
[12] Y. Alanay, H. Avaygan, N. Camacho, G.E. Utine, K. Boduroglu, D. Aktas, M. Alikasifoglu, E. Tuncbilek, D. Orhan, F.T. Bakar, et al., Mutations in the gene encoding the RER protein FKBP65 cause autosomal-recessive osteogenesis imperfecta, Am. J. Hum. Genet. 86 (2010) 551–559.
[13] Y. Ishida, K. Nagata, Autophagy eliminates a specific species of misfolded procollagen and plays a protective role in cell survival against ER stress, Autophagy 5 (2009) 1217–1219.
[14] C. Hetz, E. Chevet, S.A. Oakes, Proteostasis control by the unfolded protein response, Nat. Cell Biol. 17 (2015) 829–838.
[15] S.D. Chessler, P.H. Byers, BiP binds type I procollagen pro alpha chains with mutations in the carboxyl-terminal propeptide synthesized by cells from patients with osteogenesis imperfecta, J. Biol. Chem. 268 (1993) 18226–18233.
[16] S.R. Lamande, S.D. Chessler, S.B. Golub, P.H. Byers, D. Chan, W.G. Cole, D.O. Sillence, J.F. Bateman, Endoplasmic reticulum-mediated quality control of type I collagen production by cells from osteogenesis imperfecta patients with mutations in the pro alpha 1 (I) chain carboxyl-terminal propeptide which impair subunit assembly, J. Biol. Chem. 270 (1995) 8642–8649.
[17] R.P. Boot-Handford, M.D. Briggs, The unfolded protein response and its relevance to connective tissue diseases, Cell Tissue Res. 339 (2010) 197–211.
[18] K.Y. Tsang, D. Chan, J.F. Bateman, K.S. Cheah, In vivo cellular adaptation to ER stress: survival strategies with double-edged consequences, J. Cell Sci. 123 (2010) 2145–2154.
[19] F.E. Cohen, J.W. Kelly, Therapeutic approaches to protein-misfolding diseases, Nature 426 (2003) 905–909.
[20] T. Iannitti, B. Palmieri, Clinical and experimental applications of sodium phenylbutyrate, Drugs in R&D 11 (2011) 227–249.
[21] L.S. Murray, Y. Lu, A. Taggart, N. Van Regemorter, C. Vilain, M. Abramowicz, K.E. Kadler, T. Van Agtmael, Chemical chaperone treatment reduces intracellular accumulation of mutant collagen IV and ameliorates the cellular phenotype of a COL4A2 mutation that causes haemorrhagic stroke, Hum. Mol. Genet. 23 (2014) 283–292.
[22] R. Gioia, F. Tonelli, I. Ceppi, M. Biggiogera, S. Leikin, S. Fisher, E. Tenedini, T.A. Yorgan, T. Schinke, K. Tian, et al., The chaperone activity of 4PBA ameliorates the skeletal phenotype of Chihuahua, a zebrafish model for dominant osteogenesis imperfecta, Hum. Mol. Genet. 26 (2017) 2897–2911.
[23] B.G. Ashinsky, K.W. Fishbein, E.M. Carter, P.C. Lin, N. Pleshko, C.L. Raggio, R.G. Spencer, Multiparametric classification of skin from osteogenesis imperfecta patients and controls by quantitative magnetic resonance microimaging, PLoS One 11 (2016) e0157891.
[24] M. Balasubramanian, G.J. Sobey, B.E. Wagner, L.C. Peres, J. Bowen, J. Bexon, M.K. Javaid, P. Arundel, N.J. Bishop, Osteogenesis imperfecta: ultrastructural and histological findings on examination of skin revealing novel insights into genotype-phenotype correlation, Ultrastruct. Pathol. 40 (2016) 71–76.
[25] A. Forlino, C. Tani, A. Rossi, A. Lupi, E. Campari, B. Gualeni, L. Bianchi, A. Armini, G. Cetta, L. Bini, et al., Differential expression of both extracellular and intracellular proteins is involved in the lethal or nonlethal phenotypic variation of BrtlIV, a murine model for osteogenesis imperfecta, Proteomics 7 (2007) 1877–1891.
[26] L. Bianchi, A. Gagliardi, R. Gioia, R. Besio, C. Tani, C. Landi, M. Cipriano, A. Gimigliano, A. Rossi, J.C. Marini, et al., Differential response to intracellular stress in the skin from osteogenesis imperfecta Brtl mice with lethal and non lethal phenotype: a proteomic approach, J. Proteome 75 (2012) 4717–4733.
[27] L. Bianchi, A. Gagliardi, S. Maruelli, R. Besio, C. Landi, R. Gioia, K.M. Kozloff, B.M. Khoury, P.J. Coucke, S. Symoens, et al., Altered cytoskeletal organization characterized lethal but not surviving Brtl+/− mice: insight on phenotypic variability in osteogenesis imperfecta, Hum. Mol. Genet. 24 (2015) 6118–6133.
[28] M. Mottes, M. Gomez Lira, F. Zolezzi, M. Valli, V. Lisi, P. Freising, Four new cases of lethal osteogenesis imperfecta due to glycine substitutions in COL1A1 and genes. Mutations in brief no. 152. Online, Hum. Mutat. 12 (1998) 71–72.
[29] M. Gomez-Lira, A. Sangalli, P.F. Pignatti, M.C. Digilio, A. Giannotti, E. Carnevale, M. Mottes, Determination of a new collagen type I alpha 2 gene point mutation which causes a Gly640 Cys substitution in osteogenesis imperfecta and prenatal diagnosis by DNA hybridisation, J. Med. Genet. 31 (1994) 965–968.
[30] G. Venturi, E. Tedeschi, M. Mottes, M. Valli, M. Camilot, S. Viglio, F. Antoniazzi, L. Tato, Osteogenesis imperfecta: clinical, biochemical and molecular findings, Clin. Genet. 70 (2006) 131–139.
[31] M. Valli, M. Mottes, R. Tenni, A. Sangalli, M. Gomez Lira, A. Rossi, F. Antoniazzi, G. Cetta, P.F. Pignatti, A de novo G to T transversion in a pro-alpha 1 (I) collagen gene for a moderate case of osteogenesis imperfecta. Substitution of cysteine for glycine 178 in the triple helical domain, J. Biol. Chem. 266 (1991) 1872–1878.
[32] E. Makareeva, E.L. Mertz, N.V. Kuznetsova, M.B. Sutter, A.M. DeRidder, W.A. Cabral, A.M. Barnes, D.J. McBride, J.C. Marini, S. Leikin, Structural heterogeneity of type I collagen triple helix and its role in osteogenesis imperfecta, J. Biol. Chem. 283 (2008) 4787–4798.
[33] D.R. Green, B. Levine, To be or not to be? How selective autophagy and cell death govern cell fate, Cell 157 (2014) 65–75.
[34] Z. Yin, C. Pascual, D.J. Klionsky, Autophagy: machinery and regulation, Microb Cell 3 (2016) 588–596.
[35] L. Galluzzi, E.H. Baehrecke, A. Ballabio, P. Boya, J.M. Bravo-San Pedro, F. Cecconi, A.M. Choi, C.T. Chu, P. Codogno, M.I. Colombo, et al., Molecular definitions of autophagy and related processes, EMBO J. 36 (2017) 1811–1836.
[36] S. Barth, D. Glick, K.F. Macleod, Autophagy: assays and artifacts, J. Pathol. 221 (2010) 117–124.
[37] S. Matoori, J.C. Leroux, Recent advances in the treatment of hyperammonemia, Adv. Drug Deliv. Rev. 90 (2015) 55–68.
[38] A. Portela, M. Esteller, Epigenetic modifications and human disease, Nat. Biotechnol. 28 (2010) 1057–1068.
[39] D.M. Fass, R. Shah, B. Ghosh, K. Hennig, S. Norton, W.N. Zhao, S.A. Reis, P.S. Klein, R. Mazitschek, R.L. Maglathlin, et al., Effect of inhibiting histone deacetylase with short-chain carboxylic acids and their hydroxamic acid analogs on vertebrate development and neuronal chromatin, ACS Med. Chem. Lett. 2 (2010) 39–42.
[40] K. Gawron, Endoplasmic reticulum stress in chondrodysplasias caused by mutations in collagen types II and X, Cell Stress Chaperones 21 (2016) 943–958.
[41] U. Lindert, M.A. Weis, J. Rai, F. Seeliger, I. Hausser, T. Leeb, D. Eyre, M. Rohrbach, C. Giunta, Molecular consequences of the SERPINH1/HSP47 mutation in the dachshund natural model of osteogenesis imperfecta, J. Biol. Chem. 290 (2015) 17679–17689.
[42] W.A. Cabral, M. Ishikawa, M. Garten, E.N. Makareeva, B.M. Sargent, M. Weis, A.M. Barnes, E.A. Webb, N.J. Shaw, L. Ala-Kokko, et al., Absence of the ER Cation Channel TMEM38B/TRIC-B disrupts intracellular calcium homeostasis and dysregulates collagen synthesis in recessive osteogenesis imperfecta, PLoS Genet. 12 (2016) e1006156.
[43] J.B. DuRose, A.B. Tam, M. Niwa, Intrinsic capacities of molecular sensors of the unfolded protein response to sense alternate forms of endoplasmic reticulum stress, Mol. Biol. Cell 17 (2006) 3095–3107.
[44] J. Li, M. Ni, B. Lee, E. Barron, D.R. Hinton, A.S. Lee, The unfolded protein response regulator GRP78/BiP is required for endoplasmic reticulum integrity and stress-induced autophagy in mammalian cells, Cell Death Differ. 15 (2008) 1460–1471.
[45] J. Zhou, C.Y. Liu, S.H. Back, R.L. Clark, D. Peisach, Z. Xu, R.J. Kaufman, The crystal structure of human IRE1 luminal domain reveals a conserved dimerization interface required for activation of the unfolded protein response, Proc. Natl. Acad. Sci. U. S. A. 103 (2006) 14343–14348.
[46] M. Carrara, F. Prischi, P.R. Nowak, M.M. Ali, Crystal structures reveal transient PERK luminal domain tetramerization in endoplasmic reticulum stress signaling, EMBO J. 34 (2015) 1589–1600.
[47] M. Ogata, S. Hino, A. Saito, K. Morikawa, S. Kondo, S. Kanemoto, T. Murakami, M. Taniguchi, I. Tanii, K. Yoshinaga, et al., Autophagy is activated for cell survival after endoplasmic reticulum stress, Mol. Cell. Biol. 26 (2006) 9220–9231.
[48] K. Kawasaki, R. Ushioda, S. Ito, K. Ikeda, Y. Masago, K. Nagata, Deletion of the collagen-specific molecular chaperone Hsp47 causes endoplasmic reticulum stress-mediated apoptosis of hepatic stellate cells, J. Biol. Chem. 290 (2015) 3639–3646.
[49] B. Levine, G. Kroemer, Autophagy in the pathogenesis of disease, Cell 132 (2008) 27–42.
[50] A. Bartolome, C. Guillen, M. Benito, Autophagy plays a protective role in endoplasmic reticulum stress-mediated pancreatic beta cell death, Autophagy 8 (2012) 1757–1768.
[51] Y. Ishikawa, S. Ito, K. Nagata, L.Y. Sakai, H.P. Bachinger, Intracellular mechanisms of molecular recognition and sorting for transport of large extracellular matrix molecules, Proc. Natl. Acad. Sci. U. S. A. 113 (2016) E6036–E6044.
[52] E. Makareeva, N.A. Aviles, S. Leikin, Chaperoning osteogenesis: new protein-folding disease paradigms, Trends Cell Biol. 21 (2011) 168–176.
[53] M.D. Briggs, P.A. Bell, M.J. Wright, K.A. Pirog, New therapeutic targets in rare genetic skeletal diseases, Expert Opin Orphan Drugs 3 (2015) 1137–1154.
[54] T.T. Ashburn, K.B. Thor, Drug repositioning: identifying and developing new uses for existing drugs, Nat. Rev. Drug Discov. 3 (2004) 673–683.
[55] L. Galluzzi, J.M. Bravo-San Pedro, B. Levine, D.R. Green, G. Kroemer, Pharmacological modulation of autophagy: therapeutic potential and persisting obstacles, Nat. Rev. Drug Discov. 16 (2017) 487–511.
[56] A.U. Nissar, L. Sharma, M.A. Mudasir, L.A. Nazir, S.A. Umar Jr., P.R. Sharma, R.A. Vishwakarma, S.A. Tasduq, Chemical chaperone 4-phenyl butyric acid (4PBA) reduces hepatocellular lipid accumulation and lipotoxicity through induction of autophagy, J. Lipid Res. 58 (2017) 1855–1868.
[57] S.I. Kim, H.J. Na, Y. Ding, Z. Wang, S.J. Lee, M.E. Choi, Autophagy promotes intracellular degradation of type I collagen induced by transforming growth factor (TGF)-beta1, J. Biol. Chem. 287 (2012) 11677–11688.
[58] R.S. Rekha, S.S. Rao Muvva, M. Wan, R. Raqib, P. Bergman, S. Brighenti, G.H. Gudmundsson, B. Agerberth, Phenylbutyrate induces LL-37-dependent autophagy and intracellular killing of *Mycobacterium tuberculosis* in human macrophages, Autophagy 11 (2015) 1688–1699.

Chapter 2

Cellular stress due to impairment of collagen prolyl hydroxylation complex is rescued by the chaperone 4-phenylbutyrate

Recessive OI types VII, VIII and IX are caused by mutations in CRTAP, prolyl-3-hydroxylase 1 (P3H1) and cyclophilin B (PPIB), respectively, components of the ER-resident prolyl-3 hydroxylation complex, which performs the hydroxylation of Pro986 in α1 chains of collagen I. Mutations in one of the components of the complex hinder the correct collagen folding and prolong its exposure to ER post-translational modifying enzymes, leading to the synthesis of overmodified collagen molecules that are retained in the ER.

In this work we studied the effects of mutations in the proteins of the complex on cellular homeostasis, using primary fibroblasts from seven recessive OI patients. We assessed the activation of UPR and apoptosis, as well as we proved ER cisternae enlargement and an altered proteostasis. Given the beneficial effect of 4-PBA in human fibroblasts of dominant OI, we tested the effect of the drug also in recessive OI cells. The compound ameliorated intracellular morphology, it was beneficial in lowering UPR and apoptosis activation and it promoted general protein secretion and autophagy. We also demonstrated that 4-PBA rescuing ability is due to its chaperone role rather than its autophagy-promoting ability, since it was able to restore ER functions and to reduce stress in presence of a pharmacological inhibitor of autophagy. This work provides a deeper insight into the molecular mechanism of the drug and identifies intracellular stress as a target shared by dominant and recessive OI forms.

I actively participated to the experimental part of this work. In particular, I performed part of the cell cultures, protein lysates preparations, RNA extraction and retrotranscription and immunofluorescences. I also took part in the review and editing phases of the work.

© 2019. Published by The Company of Biologists Ltd | Disease Models & Mechanisms (2019) 12, dmm038521. doi:10.1242/dmm.038521

RESEARCH ARTICLE

Cellular stress due to impairment of collagen prolyl hydroxylation complex is rescued by the chaperone 4-phenylbutyrate

Roberta Besio[1], Nadia Garibaldi[1,2], Laura Leoni[1], Lina Cipolla[3], Simone Sabbioneda[3], Marco Biggiogera[4], Monica Mottes[5], Mona Aglan[6], Ghada A. Otaify[6], Samia A. Temtamy[6], Antonio Rossi[1] and Antonella Forlino[1,*]

ABSTRACT

Osteogenesis imperfecta (OI) types VII, VIII and IX, caused by recessive mutations in cartilage-associated protein (*CRTAP*), prolyl-3-hydroxylase 1 (*P3H1*) and cyclophilin B (*PPIB*), respectively, are characterized by the synthesis of overmodified collagen. The genes encode for the components of the endoplasmic reticulum (ER) complex responsible for the 3-hydroxylation of specific proline residues in type I collagen. Our study dissects the effects of mutations in the proteins of the complex on cellular homeostasis, using primary fibroblasts from seven recessive OI patients. In all cell lines, the intracellular retention of overmodified type I collagen molecules causes ER enlargement associated with the presence of protein aggregates, activation of the PERK branch of the unfolded protein response and apoptotic death. The administration of 4-phenylbutyrate (4-PBA) alleviates cellular stress by restoring ER cisternae size, and normalizing the phosphorylated PERK (p-PERK):PERK ratio and the expression of apoptotic marker. The drug also has a stimulatory effect on autophagy. We proved that the rescue of cellular homeostasis following 4-PBA treatment is associated with its chaperone activity, since it increases protein secretion, restoring ER proteostasis and reducing PERK activation and cell survival also in the presence of pharmacological inhibition of autophagy. Our results provide a novel insight into the mechanism of 4-PBA action and demonstrate that intracellular stress in recessive OI can be alleviated by 4-PBA therapy, similarly to what we recently reported for dominant OI, thus allowing a common target for OI forms characterized by overmodified collagen.

This article has an associated First Person interview with the first author of the paper.

KEY WORDS: Osteogenesis imperfecta, Endoplasmic reticulum stress, Chemical chaperone, Unfolded protein response, 4-PBA

[1]Department of Molecular Medicine, Biochemistry Unit, University of Pavia, 27100 Pavia, Italy. [2]Istituto Universitario di Studi Superiori - IUSS, 27100 Pavia, Italy. [3]Istituto di Genetica Molecolare, Consiglio Nazionale delle Ricerche, 27100 Pavia, Italy. [4]Department of Biology and Biotechnology, University of Pavia, 27100 Pavia, Italy. [5]Department of Neuroscience, Biomedicine and Movement, University of Verona, 37134 Verona, Italy. [6]Department of Clinical Genetics, Human Genetics & Genome Research Division, Center of Excellence for Human Genetics, National Research Centre, Cairo 12622, Egypt.

*Author for correspondence (aforlino@unipv.it)

R.B., 0000-0003-1430-2934; S.S., 0000-0001-8551-5465; M.B., 0000-0003-3834-6712; M.M., 0000-0002-7390-2246; M.A., 0000-0002-0908-0639; G.A.O., 0000-0003-2313-7387; S.A.T., 0000-0002-6452-823X; A.R., 0000-0002-2460-8761; A.F., 0000-0002-6385-1182

Received 8 January 2019; Accepted 20 May 2019

INTRODUCTION

Osteogenesis imperfecta (OI) is a collagen-related heritable disorder affecting several connective tissues, but is mainly characterized by skeletal deformity and bone fragility (Marini et al., 2017). Together with the dominant forms caused by mutations in type I collagen and representing over 85% of OI cases, recessive and X-linked OI have been described since 2006. These forms are characterized by defects in proteins involved in collagen type I folding, post-translational modifications, intracellular trafficking, extracellular processing or osteoblasts maturation (Forlino and Marini, 2016; Lindert et al., 2016).

Synthesis of type I collagen includes a complex intracellular and extracellular series of events preceding mature collagen fibril formation and involves several molecular players. Briefly, two proα1 and one proα2 chains are synthesized in the endoplasmic reticulum (ER) and linked in a trimeric molecule thanks to specific C-terminal recognition sequences and covalent disulfide bridges occurring in close proximity to the ER membrane. During their translation and before triple-helical folding, the α-chains undergo various post-translational modification events, including hydroxylation of proline in C-4 and C-3 and of lysine residues (Ishikawa and Bächinger, 2013). Proline-4 hydroxylation, catalyzed by prolyl-4-hydroxylase B (P4HB), affects almost all the proline residues placed in the Y position of the collagen triplet unit (Gly-X-Y). 4(R)-hydroxy-L-proline (4-Hyp) residues are fundamental for helix stability by favoring water-bridged intramolecular hydrogen bonding. The hydroxylation of triple helical and telopeptide lysine residues, performed by lysyl hydroxylase 1 and lysyl hydroxylase 2, respectively, provides the substrates for successive intracellular glycosylation and extracellular covalent crosslink formation. The role of 3(S)-hydroxy-L-proline (3-Hyp) instead is still poorly defined (Hudson and Eyre, 2013; Pokidysheva et al., 2014). Very few proline residues in collagen type I are 3-hydroxylated, likely excluding their role in collagen stability (Marini et al., 2007). In α1(I), only Pro986 is always present as 3-Hyp and this post-translational modification is performed by prolyl-3-hydroxylase 1 (P3H1) that is associated in a 1:1:1 ratio with cartilage-associated protein (CRTAP) and cyclophilin B (CyPB) to form a complex active in the ER (Ishikawa et al., 2009). The relevance of 3-Hyp in collagen folding as well as in proper fibril formation was proposed following the identification of three recessive OI forms characterized by the lack of α1(I)Pro986 C-3 hydroxylation and caused by mutations in one of the three genes encoding the proteins of the ER complex (Marini et al., 2007). Defects in CRTAP, the helper protein of the complex, are responsible for OI type VII (OMIM # 610682), and patients show a moderate to lethal phenotype with growth deficiency, rhizomelia, severe osteoporosis and neonatal fractures (Morello et al., 2006). OI type VIII (OMIM # 610915) is the consequence of mutations in P3H1, the protein of the complex that catalyzes α1(I)Pro986 C-3 hydroxylation. OI type VIII patients usually show a severe to lethal phenotype with the symptoms overlapping those of type VII (Cabral

et al., 2007). Importantly, CRTAP and P3H1 are mutually stabilizing in the ER (Chang et al., 2010).

Mutations in *PPIB* are responsible for OI type IX (OMIM # 259440). *PPIB* encodes for CyPB, the peptidyl-prolyl *cis-trans* isomerase that catalyzes the isomerization of the peptide bonds involving proline residues, the rate-limiting step reaction in collagen folding. The phenotype of OI type IX patients ranges from moderate to lethal, partially overlapping OI type VII and VIII forms, but without rhizomelia (Barnes et al., 2010; van Dijk et al., 2009).

The absence of CRTAP, P3H1 and CyPB, associated with complete lack or reduced α1(I)3-Hyp986, delays collagen type I folding, causing overmodification of the helical region and decreased collagen secretion at least in OI dermal fibroblasts (Marini et al., 2007). A still open question to understand the molecular basis of these OI recessive forms is whether the OI phenotype is caused by the absence of 3-Hyp in the bone matrix or by a defect in intracellular collagen folding and secretion, or a combination of both. Interestingly, in a knock-in mouse in which the P3H1 catalytic site was inactivated, but the enzyme was still able to complex with CRTAP, a mild bone phenotype was present (Homan et al., 2014).

The overmodified collagen molecules secreted in the extracellular matrix (ECM) in OI type VII, VIII and IX assemble in irregular fibrils, which impair proper mineralization, affecting bone properties, but their intracellular effects are still unknown (Forlino et al., 2011). Interestingly, using a functional proteomic approach on lysates obtained from primary fibroblasts of patients with mutations in *CRTAP*, *P3H1* or *PPIB*, we demonstrated an altered cytoskeleton and altered nucleoskeletal assembly, pointing to an impairment of the intracellular compartment (Gagliardi et al., 2017).

No effective therapy is available for any of the OI forms, and bisphosphonates, the most commonly used drugs, are anti-catabolic molecules that impair osteoclast activity and bone remodeling, improving bone mineral density, but without positive effects on bone properties (Besio and Forlino, 2015). Thus, the search for new and, likely, common pharmacological targets for multiple OI forms is an urgent patient need. We used seven primary fibroblast lines obtained from recessive OI type VII, VIII and IX patients to evaluate how cells react to the presence of overmodified collagen because of mutations in the components of the collagen prolyl-3-hydroxylase complex. We demonstrated that mutant collagen accumulates in the ER, causing unfolded protein response (UPR) activation and apoptotic death. We proved that the administration of the chemical chaperone 4-phenylbutyrate (4-PBA) ameliorates cellular homeostasis by mainly favoring protein secretion.

RESULTS

Primary fibroblasts from seven previously described (*PPIB*) recessive OI patients with mutations in the components of the

Table 1. List of the human primary fibroblast cells used in the study

Patient	Gene	Protein	Gene mutation	Protein mutation	OI type	Clinical phenotype	Reference
CRTAP-1	*CRTAP*	CRTAP	c.118_133del16insTACCC/ c.118_133del16insTACCC	Glu40Tyrfs*117	VII	Short stature, long-bone fractures and deformities, vertebral deformities, rhizomelia, grayish sclerae	Valli et al., 2012
CRTAP-2	*CRTAP*	CRTAP	c.-1677_471+1592del/c.-1677_471+1592del	Not reported	VII	Short stature, long-bone fractures and deformities, vertebral deformities, scoliosis, pectus carinatum, wormian bone, osteoporosis, joint hypermobility, rhizomelia, faint blue sclerae at birth	Caparros-Martin et al., 2013
CRTAP-3	*CRTAP*	CRTAP	c.804_809delAGAAGT/ c.804_809delAGAAGT	Glu269_Val270del	VII	Short stature, long-bone fractures and deformities, rib fractures, vertebral deformities, compression and fractures, scoliosis, osteopenia, no rhizomelia, grayish sclerae	Amor et al., 2011
P3H1-1	*P3H1*	P3H1	c.2148delC	Glu719Asnfs*747	VIII	Short stature, long-bone fractures and deformities, vertebral deformities, osteopenia	Our unpublished data
P3H1-2	*P3H1*	P3H1	c.1223+2T>G/c.1223+2T>G	Not reported	VIII	Short stature, long-bone fractures and deformities, pectus carinatum, wormian bones, vertebral deformities, scoliosis, osteoporosis, joint hypermobility, faint blue sclerae at birth	Caparros-Martin et al., 2013
P3H1-3	*P3H1*	P3H1	c.765C>A/c.2055+18G>A	Tyr255Ter splice site	VIII	22-week-old fetus: severe skeletal dysplasia characterized by short, bowed and deformed long bones	Our unpublished data
CyPB	*PPIB*	CyPB	c.497A>C/c.497A>C	His166Pro	IX	Short stature, long-bone fractures and deformities, pectus carinatum, flaring of ribs, wormian bones, vertebral deformities, kyphoscoliosis, osteoporosis, joint hypermobility, dusky color of the sclerae	Caparros-Martin et al., 2013

Disease Models & Mechanisms (2019) 12, dmm038521. doi:10.1242/dmm.038521

3-hydroxylation complex were selected for the study. Three patients carry mutations in *CRTAP* (CRTAP-1, CRTAP-2 and CRTAP-3), three in *P3H1* (P3H1-1, P3H1-2 and P3H1-3) and one in *PPIB* (CyPB) (Table 1).

In CRTAP-1, in which the mutation is predicted to cause a frameshift resulting in a premature stop codon, and in CRTAP-2, in which a large genomic deletion including exon 1 was described, a strongly reduced (0.036±0.019) and no CRTAP expression, respectively, were detected by quantitative real-time PCR (qPCR), suggesting the activation of nonsense-mediated decay (Fig. 1A). Similarly, a reduced P3H1 expression (0.146±0.03) was present in P3H1-2 cells carrying an intronic mutation in intron 7, predicted to impair normal splicing. Indeed, no exon 6-8 amplicon was detected by reverse-transcription PCR (RT-PCR), but a band with higher molecular weight, compatible with the retention of the intronic sequence, was detected (Fig. 1B).

A reduction of about 50% of *P3H1* transcript was demonstrated in P3H1-3, a compound heterozygous for an allele carrying a missense mutation and a second allele predicted to impair the translation of the KDEL ER-retention signal. The defect in the P3H1-1 patient, the only one not molecularly characterized yet, was identified as a single-nucleotide deletion (c.2148delC) in *P3H1* exon 15. The mutation causes a frameshift and the introduction of a premature stop codon at position 747 (Glu719Asnfs*747). Only a slightly reduced *P3H1* expression (0.78±0.03) was detected (Fig. 1A). As expected, no impairment of CRTAP expression was found in CRTAP-3, carrying the homozygous deletion of 6 nucleotides (nt) responsible for the in frame removal of amino acids Glu269 and Val270, or in CyPB, carrying a homozygous single base-pair substitution generating the His166Pro in CyPB (Fig. 1A).

At the protein level, all cells from patients carrying mutations in *CRTAP* showed the absence of both CRTAP and P3H1 expression and, similarly, patients with mutations in *P3H1* showed no P3H1 and CRTAP expression, as expected given the mutual protection of these proteins in the complex (Chang et al., 2010). By contrast, the level of the third component, CyPB, was not affected (Fig. 1C). No CyPB expression was detectable in *PPIB* mutant cells despite normal transcript level, but the level of CRTAP and P3H1 proteins were within the normal range (CRTAP 1.00±0.19; P3H1 1.00±0.28).

Mutations in the components of the prolyl 3-hydroxylation complex impair collagen structure and cell survival

The impairment of the 3-hydroxylation complex is known to affect type I collagen folding, causing its increased hydroxylation and glycosylation (Forlino and Marini, 2016). In all analyzed OI cells, the presence of collagen overmodification was confirmed by electrophoretic analysis of ^{3}H-labeled type I collagen. Steady-state collagen gels revealed the typical broadening of the α(I) bands in both cell-layer and medium fractions (Fig. 2A). Furthermore, an increase of collagen retention was detected in mutant cells

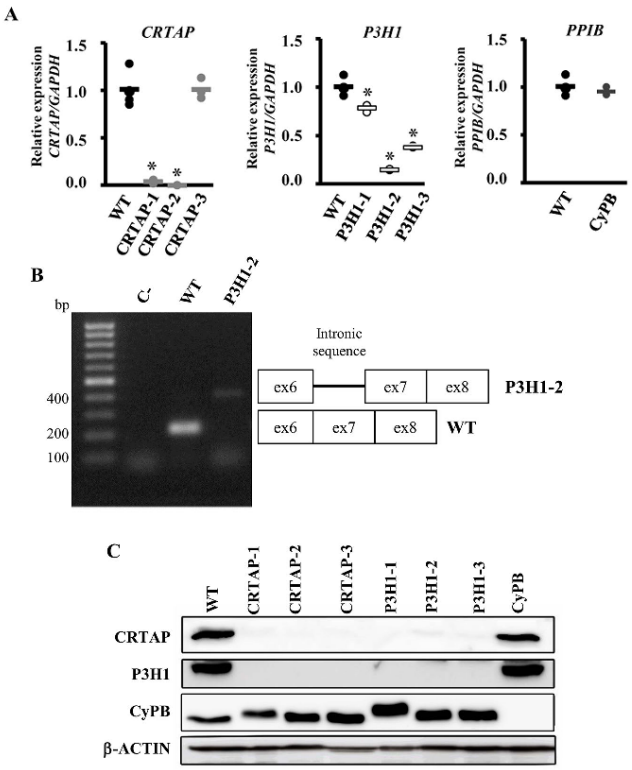

Fig. 1. Loss of mutant CRTAP, P3H1 and CyPB in OI patient fibroblasts. (A) Quantitation of *CRTAP*, *P3H1* and *PPIB* expression evaluated by qPCR. Mutations in *CRTAP*, *P3H1* and *PPIB* caused a close to complete absence of the mutated transcripts in CRTAP-1, CRTAP-2 and P3H1-2 patients, and a reduced mRNA level in P3H1-1 and P3H1-3. *P<0.05. WT values are represented as black dots; CRTAP as gray dots; P3H1 as white dots; CyPB as dark gray dots. (B) Amplification of the exon 6-exon 8 region of *P3H1* transcript generated the expected 217 bp amplicon in control cells (WT), whereas, in the P3H1-2 patient, the presence of a higher molecular weight (~400 bp) band compatible with intronic retention was detected. C-, RT-PCR negative control. (C) Representative western blot to evaluate the expression of CRTAP, P3H1 and CyPB in control (WT) and mutant cell lysate fractions (CRTAP-1, CRTAP-2, CRTAP-3, P3H1-1, P3H1-2, P3H1-3, CyPB). Loss of the mutated protein in patient's cells was demonstrated. Patients with mutations in *CRTAP* showed also no P3H1 expression and patients with mutations in *P3H1* showed no CRTAP expression, as a consequence of their mutual protection in the complex.

Disease Models & Mechanisms (2019) 12, dmm038521. doi:10.1242/dmm.038521

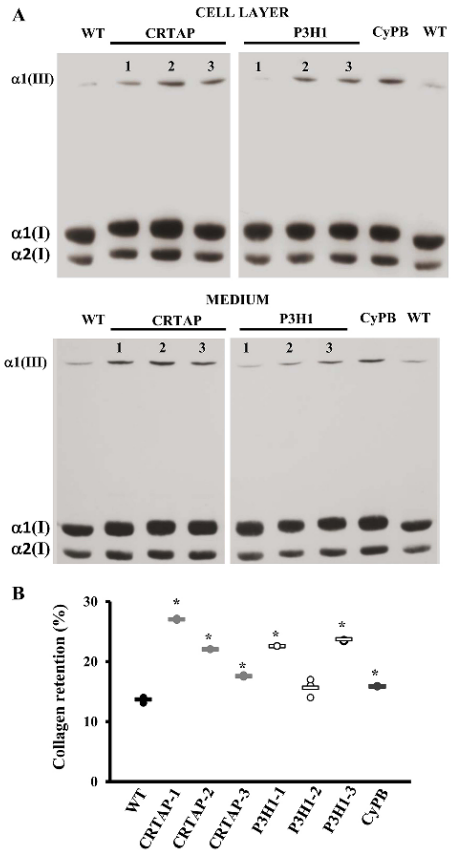

Fig. 2. Mutations in the collagen prolyl-3-hydroxylation complex lead to collagen overmodifications and collagen intracellular retention. (A) Representative SDS-urea-PAGE fluorographies of ^{3}H-labeled collagen extracted from the cell layer and medium of control (WT) and patient (CRTAP-1, CRTAP-2, CRTAP-3, P3H1-1, P3H1-2, P3H1-3, CyPB) fibroblasts. In mutant samples, broader and slower α(I) bands demonstrated the overglycosylation of type I collagen. (B) The percentage of intracellular collagen retention was evaluated as a ratio between the CPM in the cell layer and in medium plus cell layer. Collagen molecules in mutant cells were more intracellularly retained compared to WT. **P*<0.05. WT values are represented as black dots; CRTAP as gray dots; P3H1 as white dots; CyPB as dark gray dots.

compared to controls, and kinetic analysis showed a decrease in collagen secretion (Fig. 2B and Fig. S1).

Electron microscopy imaging revealed the presence of large vacuoles, resembling autophagosome vesicles since double membranes were occasionally detectable, and the ER cisternae were clearly enlarged compared to control cells. The ER looked normal in P3H1-2 cells (Fig. 5B).

Apoptosis occurrence was demonstrated in all OI mutant cells by the increased level of cleaved caspase 3 (Fig. 3A) and confirmed by fluorescence activated cell sorting (FACS) upon annexin V/Dead-positive cell labeling. Indeed, an higher percentage of apoptotic cells compared to controls (4.31±0.78%) was detected by FACS in CRTAP-2, CRTAP-3, P3H1-2, P3H1-3 and CyPB fibroblasts (49.00±5.2%, 35.74±3.57%, 22.86±2.83%, 53.93±2.17 and 20.42±1.11%, respectively) (Fig. 3B and Fig. S2).

UPR is activated in fibroblasts from patients with recessive OI

Given the intracellular presence of overmodified collagen molecules in the recessive patients' fibroblasts, we investigated the expression of the chaperones binding immunoglobulin protein (BIP) and protein disulfide isomerase (PDI) and the activation of the three branches of the UPR: the eukaryotic translation initiation factor 2 alpha kinase 3 (PERK) branch, the inositol-requiring enzyme 1α (IRE1 α) branch and the activating transcription factor 6 (ATF6) branch.

Four out of seven cell lines showed an increased level of both BIP, the best-characterized activator of the UPR sensors, and PDI, which catalyzes the formation and isomerization of disulfide bonds necessary for protein native state and which is known to interact with single collagen α chains (Fig. 3C) (Wilson et al., 1998).

The phosphorylated PERK (p-PERK):PERK ratio was significantly increased in all mutant cells with the exception of P3H1-2, in which a trend was detectable. Consistently, in these cell lines the expression of activating transcription factor 4 (ATF4), the effector of p-PERK, was also increased (Fig. 3C), confirming the activation of the UPR branch. No activation of the ATF6 and IRE1α branches was identified since no difference in cleaved ATF6 was detected and the IRE1α-mediated splicing of *XBP1* in mutants was comparable to controls (Fig. 3D).

Based on these data, we demonstrated that mutations in the prolyl-3-hydroxylation complex, causing the synthesis of overmodified collagen, lead to the disruption of ER homeostasis and consequent activation of the PERK branch of the UPR in OI fibroblasts.

Recessive OI fibroblasts react to cellular stress by activating autophagy

Given the presence and/or intracellular accumulation of overmodified collagen molecules and with autophagy being the first cell response to constitutive dysfunctional cellular components, its activation was investigated, evaluating the expression of the terminal autophagic marker, the microtubule-associated protein 1A/1B-light chain 3 (LC3-II). The expression of LC3-II was upregulated in all cases except in patient P3H1-2 (Fig. 4A). Following chloroquine treatment, the expression of LC3-II was increased compared to wild type (WT) in CRTAP-2, CRTAP-3, P3H1-2 and CyPB cells, indicating a general accumulation of LC3-II due to the block in autophagic flux (Fig. 4B). The quantitation of LC3 immunofluorescence in OI fibroblasts treated with chloroquine was performed to validate the activation of the autophagic pathway by an independent assay. As expected, the LC3 signal was significantly increased compared to controls in CRTAP-2, CRTAP-3, P3H1-2 and CyPB cells, in agreement with the western blot data (Fig. 4C).

4-PBA ameliorates recessive OI fibroblasts homeostasis

To alleviate cellular stress due to intracellular retention of overmodified collagen molecules, patient fibroblasts and control cells were treated with 4-PBA, a well-known chemical chaperone, FDA-approved as an ammonia scavenger for urea cycle disorders (Matoori and Leroux, 2015). The effect of the drug was evaluated following the activation of the PERK branch of the UPR and the activation of caspase 3, as a signature for apoptosis, by western blotting. Their levels were compared in control and OI treated versus untreated cells and in treated OI cells versus untreated controls. None of the selected markers was significantly changed in WT after 4-PBA

Disease Models & Mechanisms (2019) 12, dmm038521. doi:10.1242/dmm.038521

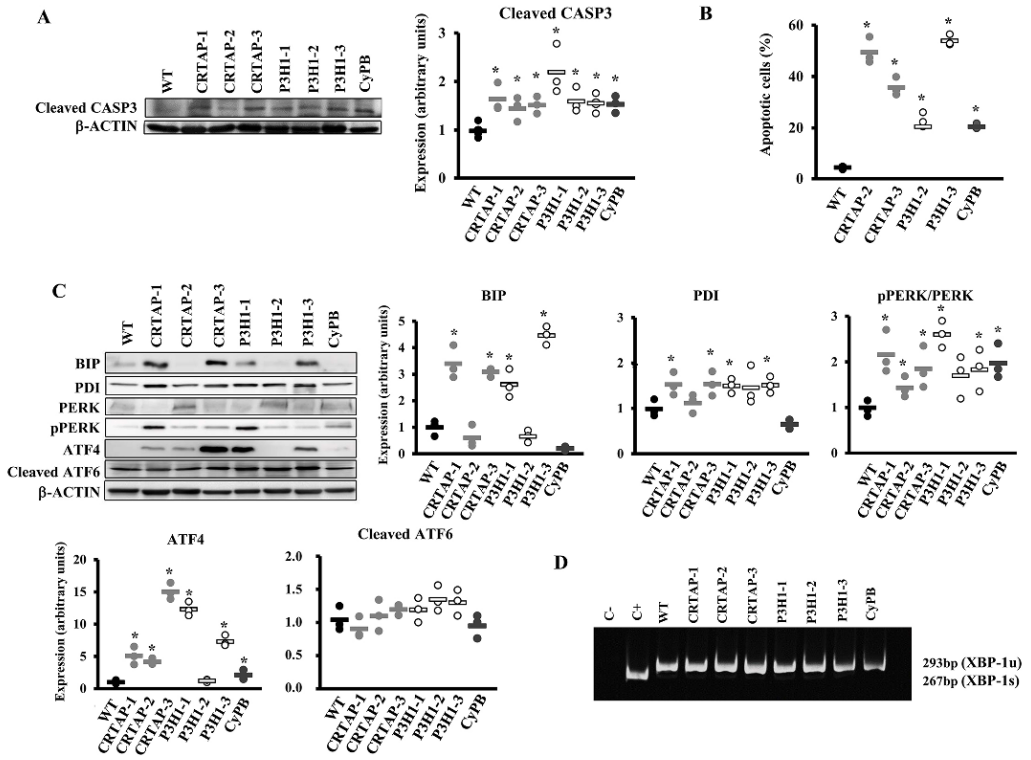

Fig. 3. Activation of apoptosis and the UPR in recessive OI patient fibroblasts. (A) Representative western blot (left) to evaluate the expression of cleaved caspase 3 (CASP3), a terminal marker for apoptosis and the dot plot of the quantitation analysis (right). β-actin was used for normalization. (B) Quantitative analysis of the fraction of apoptotic events in the cell lines following FACS analysis upon cells staining with annexin V (FITC) and propidium iodide (PI). Apoptosis is activated in all tested OI patients' cells. (C) Representative western blots (left) and dot plots of the quantitative analysis (right and bottom) of the collagen chaperone PDI and of proteins involved in the UPR (BIP, PERK, p-PERK, ATF4, ATF6) in control (WT) cells and in cells with mutations in CRTAP, P3H1 or CyPB. The PERK branch of the UPR was upregulated in all patients' fibroblasts with the exception of patient P3H1-2. β-actin was used for normalization. WT values are represented as black dots; CRTAP as gray dots; P3H1 as white dots; CyPB as dark gray dots. *P<0.05. (D) RT-PCR amplification of *XBP1* mRNA from control (WT) and patient cells. The spliced XBP1-1s form of XBP1 transcript (XBP-1u) is not detectable in patient cells. Fibroblasts treated with thapsigargin were used as positive control (C+).

administration (data not shown). Interestingly, following the treatment, p-PERK:PERK and cleaved caspase 3 levels were decreased to or even less than control values in all cases (Fig. 5A). The positive effect of the drug on recessive OI cellular homeostasis was further confirmed by the reduction of ER cisternae size, as evaluated by transmission electron microscopy (Fig. 5B). No rescue of CRTAP and CyPB was instead detected after the treatment in the patients with normal transcript level, indicating that the 4-PBA effect is not due to rescue of folding of the mutant proteins (Fig. 5C).

4-PBA chaperone function rescues recessive OI cell homeostasis

In order to determine the mechanism of action of 4-PBA, we investigated in our system the effect of the drug on collagen secretion and on general protein secretion. Collagen secretion was unaffected by the treatment, as were collagen post-translational modifications (data not shown). However, protein labeling with ^{35}S-L-methionine and ^{35}S-L-cysteine revealed an increased total protein secretion upon 4-PBA administration in all the cells tested in which it was severely affected in the basal condition, namely CRTAP-1, P3H1-1, P3H1-2 and P3H1-3 (Fig. 6A), indicating its chaperone activity.

Interestingly, an increased LC3-II level in all mutant cells treated with 4-PBA was detected, clearly supporting a 4-PBA stimulatory effect on autophagy in OI recessive cells (Fig. 6B). In order to determine whether the rescue of the cellular homeostasis following 4-PBA treatment was due to its chaperone function or to its autophagy-stimulating ability, ER proteostasis, PERK activation and cell survival were monitored in the absence or presence of chloroquine, a pharmacological inhibitor of autophagy. Thioflavin T (ThT), a small molecule that exhibits increased fluorescence when it binds to protein aggregates, was used to quantify ER proteostasis (Beriault and Werstuck, 2013). Enhanced ThT fluorescence was detectable in mutant cells compared to control, indicating the accumulation of intracellular misfolded material (Fig. 7A). 4-PBA treatment significantly reduced the ThT fluorescence, proving the reduction of protein accumulation (Fig. 7A). Importantly, this effect of 4-PBA was evident also when inhibiting autophagy with chloroquine (Fig. 7A). Furthermore, the p-PERK:PERK ratio and

Disease Models & Mechanisms (2019) 12, dmm038521. doi:10.1242/dmm.038521

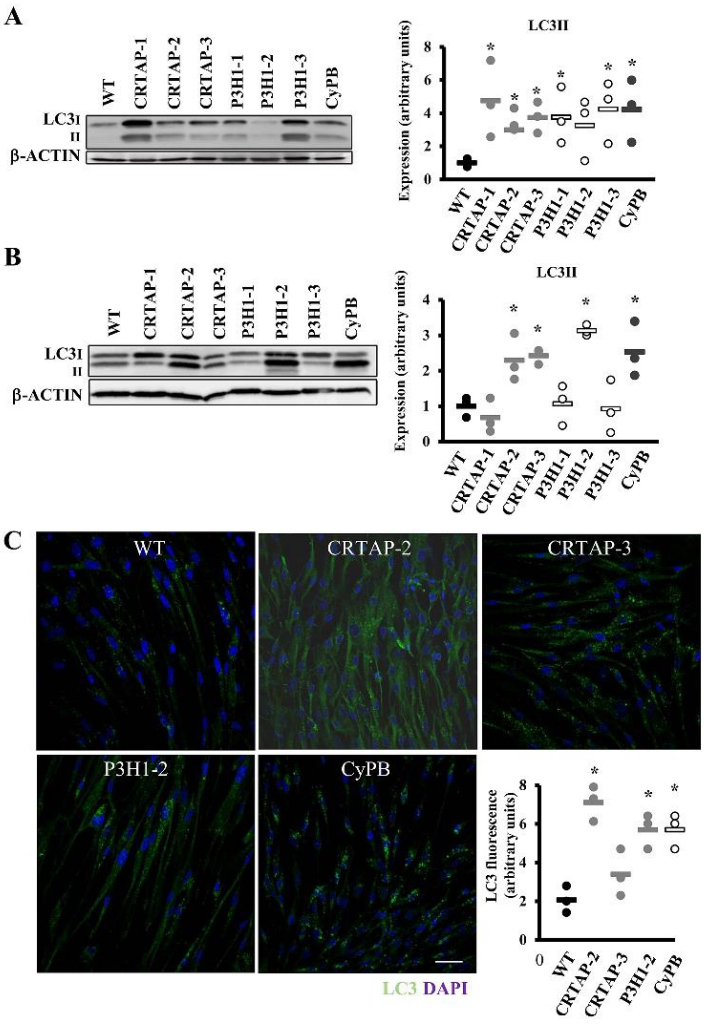

Fig. 4. Recessive OI cells react to cellular stress by activating autophagy. (A) Representative western blot (left) and dot plot of the quantitative analysis (right) of the terminal autophagic marker LC3 in control (WT) and in cells with mutations in CRTAP, P3H1 or CyPB. LC3-II is upregulated in all cases except in patient P3H1-2. β-actin was used for normalization. (B) Representative LC3 western blot (left) performed on cell lysates obtained following chloroquine incubation from WT and mutant samples, and dot plot of the quantitative analysis (right). The terminal marker of autophagy evaluated in dynamic conditions is increased in CRTAP-2, CRTAP-3, P3H1-2 and CyPB. β-actin was used for normalization. (C) Representative LC3 immunofluorescence images of WT and mutant fibroblasts treated with chloroquine. Quantitation of the total area of punctate signal per cell confirms the activation of autophagy. DAPI (nuclei) in blue and LC3 in green. Magnification 40×, zoom 4×. WT values are represented as black dots; CRTAP as gray dots; P3H1 as white dots; CyPB as dark gray dots. **P*<0.05. Scale bar: 40 µm.

apoptosis were decreased by 4-PBA when autophagy was impaired, finally corroborating the primary chaperone function of the drug in rescuing cell homeostasis (Fig. 7B,C).

To evaluate whether other chemical chaperones could have a similar effect on OI cells, tauroursodeoxycholic acid (TUDCA), approved for cholestasis (Wagner and Trauner, 2016), was used. TUDCA did not show any effect on p-PERK, apoptosis and autophagy levels, thus suggesting a specificity of 4-PBA in the rescue of recessive OI fibroblasts homeostasis (Fig. S3).

DISCUSSION

In the past 10 years, the prolyl-3-hydroxylation complex has been demonstrated to be crucial for proper type I collagen folding and post-translational modifications (Marini and Blissett, 2013). Mutations in any of its components, CRTAP, P3H1 and CyPB, are associated with recessive forms of moderate to lethal OI, characterized by the presence of abnormal ECM and impaired mineralization associated with bone fragility (Marini et al., 2017). Here, we move our attention from the extra- to the intracellular space and describe the effect of overmodified type I collagen on cellular homeostasis of seven recessive OI cases, three carrying mutations in *CRTAP*, three in *P3H1* and one in *PPIB*, using skin fibroblasts in which no mutant protein was detectable (Fig. 1C).

Overmodified type I collagen in recessive OI mutants causes UPR and apoptosis activation

In all cell lines, the presence of overmodified collagen was demonstrated by metabolic labeling and electrophoretic analysis

Disease Models & Mechanisms (2019) 12, dmm038521. doi:10.1242/dmm.038521

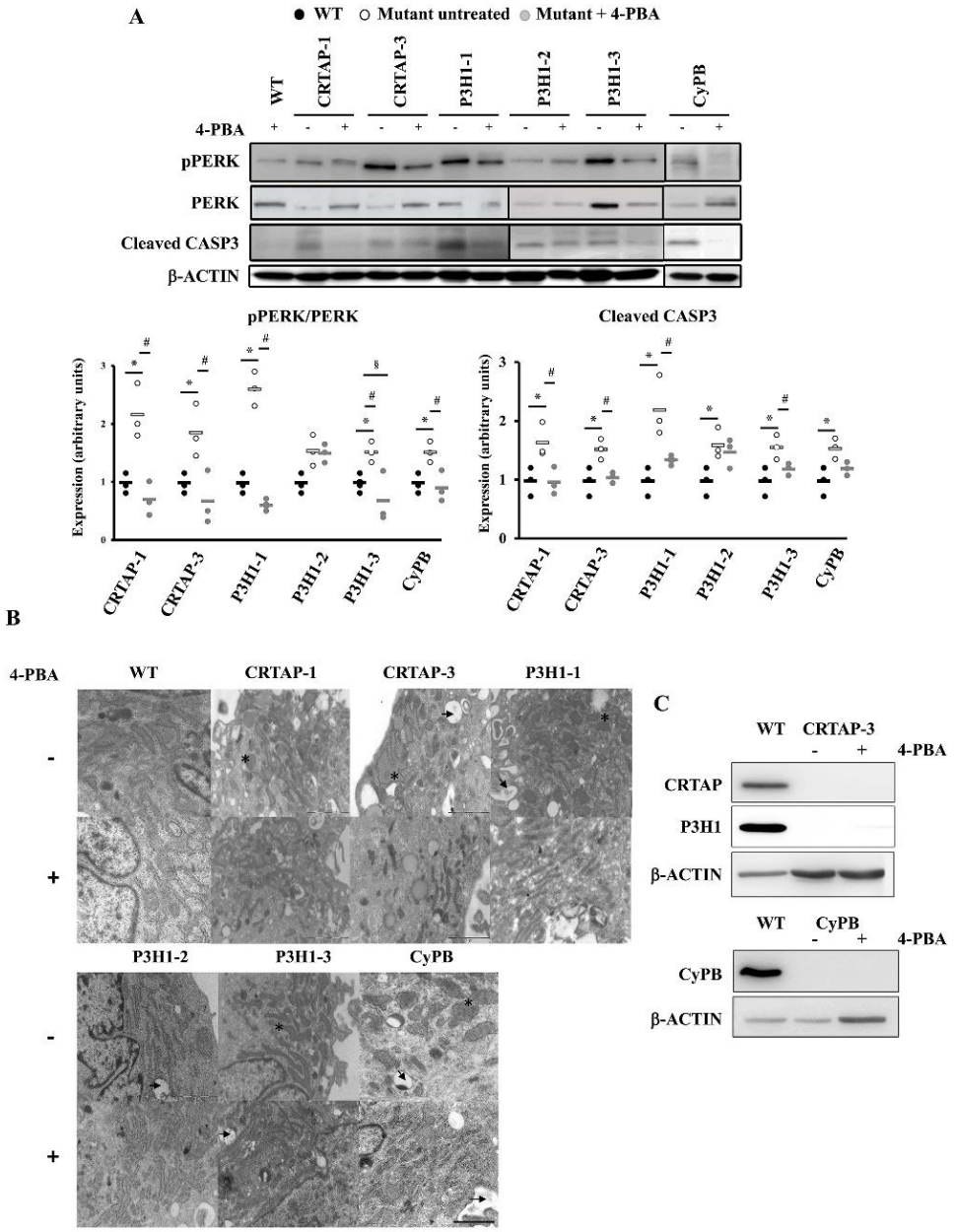

Fig. 5. See next page for legend.

(Fig. 2A). Likely due to the increased accumulation of type I collagen molecules in the ER, cisternae enlargement and cellular vacuolization were detected (Fig. 5B). Interestingly, in the presence of similar broadening of the α-bands, significant intracellular collagen retention and ER enlargement was not clearly evident in P3H1-2 cells, suggesting a variable ability of the cells to handle

Disease Models & Mechanisms (2019) 12, dmm038521. doi:10.1242/dmm.038521

Fig. 5. 4-PBA ameliorates recessive OI fibroblast homeostasis. (A) Representative western blots (top) and dot plot of the quantitative analysis (bottom) of p-PERK and cleaved caspase 3 (CASP3) in the absence (–) or presence (+) of 4-PBA incubation in control (WT) cells and in cells with mutations in CRTAP, P3H1 or CyPB. The levels of these proteins were compared in treated versus untreated cells and in treated OI cells versus untreated controls. β-actin was used for normalization. **P*<0.05 mutant fibroblasts with respect to control fibroblasts. #*P*<0.05 treated mutant fibroblasts with respect to untreated mutant fibroblasts. §*P*<0.05 treated mutant fibroblasts with respect to untreated control fibroblasts. p-PERK:PERK and cleaved caspase 3 levels were decreased to or even less than control values in all cases, with the exception of P3H1-2. WT untreated values are shown as black dots, mutants untreated as white dots and mutants treated as gray dots. (B) Transmission electron microscopy representative images of OI patient fibroblasts in the absence (–) or presence (+) of 4-PBA. The analyses revealed ER enlargement (*) and cellular vacuolization (arrow) in mutant cells with the exception of P3H1-2. 4-PBA treatment reduced the ER cisternae enlargement. Magnification 20,000×. (C) Representative western blot of CRTAP and P3H1 in control (WT) and CRTAP-3 cell lysates, and of CyPB in WT and CyPB lysates. No protein rescue was detected after the treatment in the two mutant cell lines, in which normal transcript level was detected. β-actin was used for normalization. Scale bar: 2 µm.

overmodified type I collagen, either due to a different level of collagen overmodification or to the effect of modifiers affecting collagen secretion (Fig. 2, Fig. 5B). Indeed, although collagen electrophoretic analysis is a quick and simple tool to reveal post-translational overmodifications, it does not allow the detection of subtle differences (Barnes et al., 2006; Cabral et al., 2007) that have been previously demonstrated in OI patients and may potentially impact on protein secretion (Amor et al., 2011; Barnes et al., 2006; Marini et al., 2007; Taga et al., 2013). Furthermore, the functional role of collagen O-glycosylation is not clearly defined yet and, if some information is available regarding its possible extracellular effect on increasing collagen stability against proteolytic degradation, control of lateral growth of the fibrils, interaction with non-collagenous proteins and the cross-linking process, nothing has been reported so far on its intracellular effect (Perdivara et al., 2013).

Following collagen folding in the ER, its secretion requires the assembly of specific large COPII vesicles, whose formation depends on a large number of proteins and lipids. Thus, it is not surprising that the complex collagen secretory machinery may be tuned by the action of modifiers (Vollmann et al., 2017).

To maintain the functional integrity of ER under stress conditions, the evolutionarily conserved adaptive response, the UPR, is generally turned on. Indeed, UPR activation affecting cell homeostasis and likely modulating disease severity was reported in the presence of mutations in ECM molecules, including the fibrillar collagen type II and X (Boot-Handford and Briggs, 2010). In recessive OI cells, the PERK branch of the UPR is activated, as demonstrated by an increased p-PERK:PERK ratio and upregulation of its effector ATF4 (Fig. 3C). In the presence of ER stress, BIP, the master regulator of activation of the UPR branches, is released from the UPR sensors to favor protein folding and this event activates the specific ER cellular response. Interestingly, three out of seven OI cell lines did not show upregulation of BIP, hinting at other regulatory proteins being involved in the ER stress response in the presence of overmodified type I collagen retention, as suggested in previous reports (Besio et al., 2018; Forlino et al., 2007; Mirigian et al., 2016). UPR activation is not sufficient for cell homeostasis and CRTAP-2, CRTAP-3, P3H1-2 and CyPB recessive OI fibroblasts also showed upregulated autophagy (Fig. 4), which is often activated to regulate the lysosome-dependent turnover of cell materials to reduce the ER overload (Galluzzi et al., 2017; Green and Levine, 2014). Surprisingly, autophagy was also stimulated in P3H1-2 cells in which no reduction of collagen secretion, no UPR activation and no ER cisternae enlargement were detectable. The splice-site mutation in this cell line (c.1223+2T>G), predicted to cause exon 7 removal, should result in the translation of a shorter P3H1 (p.Asp391Valfs46) that could indeed be eliminated through

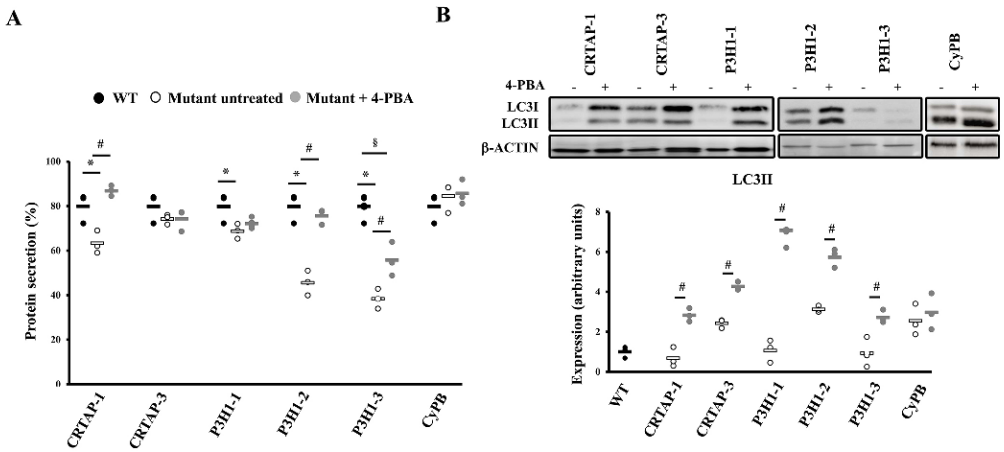

Fig. 6. 4-PBA stimulates protein secretion and autophagy. (A) Dot plot representing the amount of general protein secreted in the absence or presence of 4-PBA treatment in WT and OI patient fibroblasts. In the samples in which protein secretion was impaired in the basal condition, it was rescued by 4-PBA treatment. (B) Representative western blot to evaluate LC3 expression (top) in control (WT) and patient cells in the absence (–) and presence (+) of 4-PBA, and dot plot of the quantitative analysis (bottom). An increase of LC3-II levels in cells after 4-PBA treatment was detected. **P*<0.05 mutant fibroblasts with respect to control fibroblasts. #*P*<0.05 treated mutant fibroblasts with respect to untreated mutant fibroblasts. §*P*<0.05 treated mutant fibroblasts with respect to untreated control fibroblasts. β-actin was used for normalization. WT untreated values are shown as black dots, mutants untreated as white dots and mutants treated as gray dots.

Disease Models & Mechanisms (2019) 12, dmm038521. doi:10.1242/dmm.038521

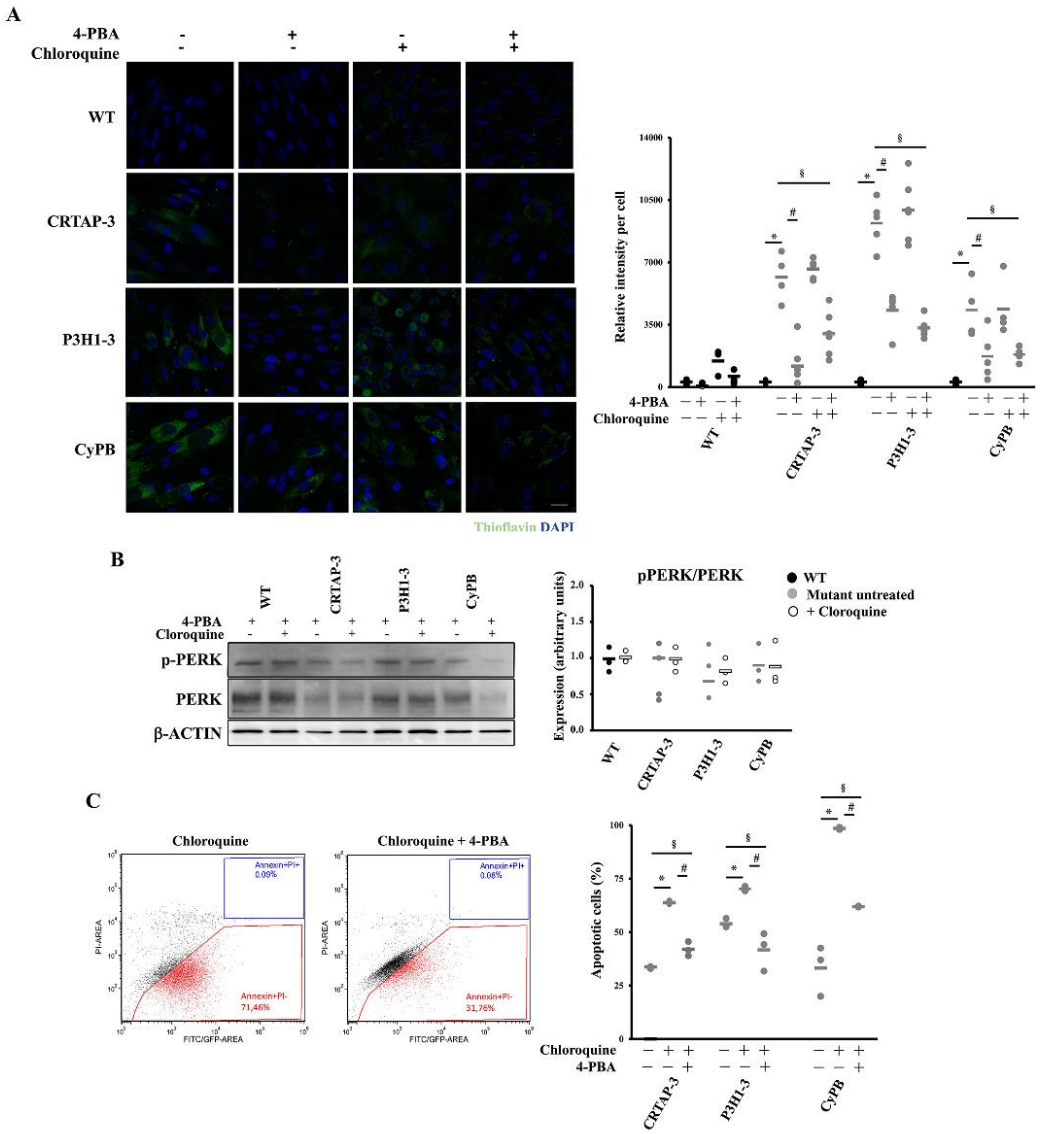

Fig. 7. 4-PBA chaperone function is mainly responsible for homeostasis rescue in the recessive OI cells. (A) ER proteostasis was evaluated using thioflavin T (ThT). Representative immunofluorescence images are shown on the left and the fluorescence quantitation graph is reported on the right. Mutant cells revealed an increased fluorescence compared to control, indicating the intracellular accumulation of misfolded proteins. 4-PBA treatment significantly reduced the ThT fluorescence, proving its chaperone role also following autophagy inhibition with chloroquine. WT is shown in black, mutants in gray. (B) Representative western blot to evaluate pPERK:PERK expression in the absence (–) and presence (+) of 4-PBA and of chloroquine and quantitative analysis. 4-PBA normalized the p-PERK:PERK ratio even when autophagy was impaired. β-actin was used for normalization. WT untreated values are shown as black dots, mutants untreated as gray dots, cells treated with chloroquine as white dots. (C) Representative FACS plots and quantitative analysis of the fraction of apoptotic events following staining with annexin V (FITC) and propidium iodide (PI) in the absence (–) and presence (+) of chloroquine and of 4-PBA. Even when autophagy was impaired, 4-PBA decreased apoptosis. **P*<0.05 mutant fibroblasts treated with chloroquine with respect to untreated. #*P*<0.05 mutant fibroblasts treated with 4-PBA and chloroquine with respect to treated with chloroquine. §*P*<0.05 mutant fibroblasts treated with 4-PBA and chloroquine with respect to untreated fibroblasts. Scale bar: 20 µm.

autophagy. Nevertheless, the strong reduction of RNA expression demonstrated the activation of nonsense-mediated decay, likely minimizing the amount of protein synthesis. Despite autophagy activation, apoptosis was promoted in all analyzed cell lines (Fig. 3A).

Common pathways are activated in recessive and classical forms of OI

The reported overmodified collagen retention, UPR activation and cell death found in recessive OI type VII, VIII and IX resemble what was previously detected in the OI forms due to mutations in *COL1A1* and *COL1A2* genes and characterized by the synthesis of structurally altered collagen molecules. In particular, in fibroblasts from patients with classical OI forms, we recently demonstrated that the intracellular-retained overglycosylated collagen causes ER cisternae enlargement, and the inefficiency of the UPR to counteract the constitutive synthesis of mutant collagen brought cells to death (Besio et al., 2018). In our system, we also described autophagy activation as a general mechanism associated with *COL1A1* mutations, but detectable only in few cases with mutations in *COL1A2* (Besio et al., 2018). We hypothesized that endogenous autophagy in OI cells could be linked to the presence of a higher amount of mutant collagen since, due to its stoichiometry, 75% of trimers will be overmodified in the presence of mutant α1, versus 50% when α2 chains are mutated. Interestingly, in the analyzed recessive cells, in which all the collagen type I is overmodified, not all patients had the same autophagic response. Although we cannot exclude a mutation or site-dependent effect of structural defects in collagen chains, these new results support the hypothesis of a role for modifiers in modulating cell response to stress. Indeed, in a previous study using skin and bone samples from the Brtl mouse, a model for dominant OI carrying a G349C substitution in α1(I) and either a moderate or a lethal outcome, we found in mice with non-lethal outcome a better ability to react to mutant collagen retention. Such capacity was associated with an increased expression of chaperone proteins (Bianchi et al., 2012; Forlino et al., 2007). Some years later, we confirmed a different ability to manage cell stress and thus to guarantee cell homeostasis in patients cells carrying identical mutation, but different outcome (Besio et al., 2018).

Of note, independently from the autophagic cellular response, apoptosis is upregulated in both dominant and recessive mutant cells. Thus, apoptotic pathway activation represents a hallmark of unsolved cell stress, both in dominant and in recessive forms of the disease (Besio et al., 2018; Bianchi et al., 2012; Galluzzi et al., 2017; Green and Levine, 2014; Mirigian et al., 2016). P3H1-2 represents an exception to this rule since, in this cell line, apoptosis is not activated by sustained ER stress due to mutant collagen retention, but possibly as a consequence of sustained autophagy.

4-PBA: a potential common therapy for recessive and classical forms of OI

The identification of novel targets for disease treatment is of valuable significance to develop novel therapies. The recognition of altered pathways common to several diseases is even more relevant for rare diseases with a limited number of affected patients. We previously proved that 4-PBA successfully ameliorates classical OI cell homeostasis *in vitro* using OI patients' fibroblasts, and bone phenotype *in vivo* using the OI zebrafish model *Chihuahua* (Besio et al., 2018; Gioia et al., 2017). The drug activated autophagy and increased general protein secretion in OI dominant fibroblasts, and improved bone mineralization and bone histomorphometric parameters in the zebrafish model. 4-PBA is an FDA-approved drug for urea cycle disorders; thus, its repositioning for a different disease will definitely speed up the bench-to-bedside transition (Matoori and Leroux, 2015). Nevertheless, the multiple recognized functions of 4-PBA need to be taken into consideration for a proper data interpretation. Associated to its ammonia scavenger role, 4-PBA has a recognized chaperone function, favoring ER protein folding and thus attenuating the UPR in the presence of ER stress caused by misfolded protein accumulation (Pettit and Fellner, 2014), and it acts as a histone deacetylase inhibitor, modulating chromatin accessibility and thus gene expression (Butchbach et al., 2016). Interestingly, at least in yeast cells, 4-PBA attenuates the UPR by accelerating the degradation of the ER-stress sensor Ire1, rather than by restoring the global protein folding; indeed, UPR attenuation was detectable even in the absence of ER stress (Daosukho et al., 2007; Mai et al., 2018).

Here, we dissected whether the positive effect of 4-PBA was due to its autophagy-stimulating ability or to its chaperone function, and finally proved its relevance in assisting protein secretion.

Taking all these findings into consideration, our results prove and extend the potential use of 4-PBA as chemical chaperone to the OI forms characterized by overmodified collagen production. For the first time, we demonstrated the potential pharmacological benefit of this drug for the recessive forms of OI with defects in the 3-hydroxylation complex. In almost all the analyzed fibroblasts carrying mutations in the P3H1 complex, 4-PBA administration reduced PERK activation and decreased apoptosis (Fig. 5A). The improved general protein secretion detected in the recessive OI resembles the findings described in dominant cases. The restoration of normal ER cisternae size (Fig. 5B) and the reduced ThT fluorescence (Fig. 7A) further supports the reduction of misfolded protein accumulation.

Of note, treatment of CyPB mutant cells seems to act in a different way. Drug administration reduced apoptotic death, but neither autophagy nor protein secretion were significantly augmented. CyPB is involved in other intracellular complexes. It is a binding partner for lysyl hydroxylase isoforms, thus affecting collagen hydroxylation and crosslinks, and interacts with BIP and PDI, thus having a relevant role in the folding of the collagen C-propeptides and on the kinetics of collagen chain association (Gruenwald et al., 2014; Heard et al., 2016; Terajima et al., 2016). Indeed, *PPIB*-null cells showed a delay in trimer association together with the increased post-translational modification present also in *CRTAP*- and *P3H1*-null cells (Pyott et al., 2011; van Dijk et al., 2009). With the limit of the use of a single cell line, mainly due to the extreme rarity of OI type IX, we can hypothesize that the multiple roles of CyPB may be differentially and specifically affected/modulated by 4-PBA treatment, and further experiments will be necessary to shed light on the mechanism.

Study limitations

As a cellular model, we used primary fibroblasts from recessive OI patients. Since skin biopsy has limited invasiveness, a large body of literature is available on OI biochemical characterization based on this cell type, and fibroblasts share with osteoblasts the production of a high amount of collagen type I and several biochemical pathways (Bianchi et al., 2012). Furthermore, a skin phenotype is often described in OI patients (Balasubramanian et al., 2016). Nevertheless, OI is mainly a bone disorder and the bone-forming cells are known to produce even higher amounts of collagen type I, with a higher glycosylation level compared to fibroblasts (Sarafova et al., 1998). Indeed, how osteoblasts react to mutant collagen retention has been recently addressed using calvarial osteoblasts

from the OI knock-in murine model α2(I)-G610C. The misfolded procollagen was found accumulated in the ER, causing an unusual cell stress, which was neither activating a conventional UPR nor causing ER overload, although EIF2α was found phosphorylated (Mirigian et al., 2016). Interestingly, in a more recent paper using the same OI murine model, ER-stress-related genes were found upregulated in hypertrophic chondrocytes expressing type I collagen (Scheiber et al., 2019). Further investigation in different murine models and, likely, in human osteoblasts are necessary.

For proper interpretation of our results, it should also be considered that the *in vitro* growth and expansion of the cells could have imposed an artificial 'stress' that we cannot exclude to have some effects on the activation of specific UPR branches. Anyway, all controls and mutant cell lines were similarly expanded, likely supporting the truthfulness of the described differences. To properly translate *in vitro* data to patients, *in vivo* validation is needed. We recently demonstrated in osteoblasts from the OI zebrafish model *Chihuahua* an ER cisternae enlargement associated with mutant collagen type I synthesis and we proved that 4-PBA was indeed restoring ER cisternae size, likely favoring collagen secretion (Gioia et al., 2017). The identification of the involved pathways in mammals needs further investigation.

In conclusion, we identified ER stress as a common potential target for the treatment of recessive OI carrying mutations in components necessary for collagen post-translational modifications and for the cure of classical dominant OI. The finding that the same chemical chaperone is effective in cells synthesizing overmodified collagen increases the potential clinical use of 4-PBA for multiple OI forms.

MATERIALS AND METHODS

Human fibroblasts

Seven human primary dermal fibroblasts from skin biopsies of OI patients carrying mutations in one of the genes coding for the three members of the collagen prolyl 3-hydroxylation complex – *CRTAP* (CRTAP-1, CRTAP-2, CRTAP-3) (Amor et al., 2011; Caparros-Martin et al., 2013; Valli et al., 2012), *P3H1* (P3H1-1, P3H1-2 and P3H1-3) (Caparros-Martin et al., 2013) and *PPIB* (CyPB) (Caparros-Martin et al., 2013) – and three pediatric controls (Promo Cell) were obtained after informed consent and used up to passage 10 (P10) (Table 1). Cells were grown at 37°C in humidified atmosphere containing 5% CO_2 and cultured in Dulbecco's modified Eagle's medium (DMEM; 4.5 g/l glucose; Lonza) supplemented with 10% fetal bovine serum (FBS; Euroclone), 4 mM glutamine (Euroclone), 100 µg/ml penicillin and streptomycin (Euroclone). No ascorbic acid was added to expansion media. For each experiment, except where differently stated, 2.5×10^4 cells/cm² were plated and harvested after 5 days with no media change. For drug treatment, cells were incubated for 15 h with 5 mM 4-PBA (Sigma-Aldrich) or with 0.96 mM TUDCA (Sigma-Aldrich). The lysosome fusion with autophagosome was blocked using 10 µM chloroquine (Sigma-Aldrich) for 6 h.

Sequencing

Genomic DNA from P3H1-1 was extracted from fibroblasts by standard procedure. Exons were amplified by PCR and Sangers' sequencing was performed.

Expression analysis

Total RNA was extracted from patients' fibroblasts using TriReagent (Sigma-Aldrich) according to the manufacturer's protocol. DNase digestion was performed using the Turbo DNA Free Kit (Ambion, Applied Biosystems), and RNA integrity was verified on agarose gel. cDNA was synthetized and qPCR was performed on the Mx3000P Stratagene thermocycler using Syber Green Master Mix (Applied Biosystems) with custom primers. For *CRTAP* (NM_006371.4) the forward primer was 5′-CCCAGACCTGAAGCAGTT-3 (nt 1180-1197) and the reverse primer was 5′-TTCTCCCTCATCATCATCCATT-3′ (nt 1278-1257). The *PPIB* (NM_000942 .4) forward primer was 5′-GGAGAGAAAGGATT-TGGCTAC-3′ (nt 413-433) and the reverse primer was 5′-CAGGCTGTC-TTGACTGTCGTGA-3′ (nt 651-630). The *P3H1* (NM_001243246.1) forward primer was 5′-CGGGTGGCTGGCGGTTCCG-3′ (nt 78-96) and the reverse primer was 5′-ACCTCGGCTTGGGAGGCAGC-3′ (nt 184-165). All reactions were performed in triplicate. *GAPDH* was used as normalizer. The *GAPDH* (NM_002046.5) forward primer was 5′-ATAC-CAGGAAATGAGCTTGACAAA-3′ (nt 1035-1057) and the *GAPDH* reverse primer was 5′-TCCTCTGACTTCAACAGCGACAC-3′ (nt 1130-1107). Relative expression levels were calculated using the ΔΔCt method.

Protein lysates

Fibroblasts were washed and scraped in PBS, centrifuged at 1000 ***g*** for 4 min, lysed and sonicated in RIPA buffer (150 mM NaCl, 1% IGEPAL® CA-630, 0.5% sodium deoxycholate, 0.1% SDS, and 50 mM Tris, pH 8) supplemented with protease inhibitors (13 mM benzamidine, 2 mM N-ethylmalemide, 5 mM ethylenediaminetetraacetic acid, 1 mM phenylmethylsulfonyl fluoride and 2 mM $NaVO_3$). Proteins were quantified by RC DC Protein Assay (Bio-Rad). Bovine serum albumin (BSA) (Sigma-Aldrich) was used as standard.

Western blot

Proteins from human fibroblast lysates (10-50 µg) were separated on SDS-PAGE with acrylamide percentage ranging from 6 to 15%, depending on the size of the analyzed protein (Table S1). The proteins were electrotransferred to a PVDF membrane (GE Healthcare) at 100 V for 2 h on ice in 19 mM Tris-HCl, 192 mM glycine and 20% (v/v) methanol. The membranes were then blocked with 5% (w/v) BSA in 20 mM Tris-HCl, 500 mM NaCl, pH 7.5 (TBS), 0.05% (v/v) Tween-20 (Sigma-Aldrich) (TBS-T) at room temperature (RT) for 1 h. After washing with TBS-T, the membranes were incubated with 1:1000 primary antibody against the specific proteins CRTAP (generously provided by Dr Lee Brendan, Baylor College of Medicine,TX, USA), P3H1 (NovusBio), CyPB (Proteintech), BIP (Cell Signaling), PERK (Cell Signaling), PDI (Cell Signaling), p-PERK (Thr980; Cell Signaling), LC3A/B (Cell Signaling), cleaved caspase-3 (Cell Signaling), ATF4 (Novus Biological), ATF6 (Abcam) in 5% BSA in TBS-T overnight at 4°C. The appropriate secondary antibody anti-mouse (Cell Signaling), anti-rabbit (Cell Signaling) or anti-goat (Santa Cruz Biotechnology) was added at dilution of 1:2000 in 5% BSA in TBS-T for 1 h at RT. Anti-β-actin antibody (Santa Cruz Biotechnology) diluted 1:1000 in 5% BSA in TBS-T was used for protein loading normalization. The signal was detected by ECL western blotting detection reagents (GE Healthcare) and images were acquired with ImageQuant LAS 4000 (GE Healthcare), using the ImageQuant LAS 4000 1.2 software. Band intensities were evaluated by densitometry, using ImageQuant TL analysis software. For each gel, the intensity of the control band was set equal to one, and the expression of the mutant samples was expressed as fold difference. For each cell line, three independent lysates were collected and technical triplicates were performed.

Collagen analysis

Labeling of collagen with L-[2,3,4,5-^{3}H]-proline (PerkinElmer) was used to evaluate collagen overmodification and secretion. A total of 2.5×10^4 fibroblasts/cm² were plated into 6-well plates and grown for 24 h. Cells were then incubated for 2 h with serum-free DMEM containing 4 mM glutamine, 100 µg/ml penicillin and streptomycin, and 100 µg/ml (+)-sodium L-ascorbate (Sigma-Aldrich) to stimulate collagen production. For steady-state experiments, the labeling was performed for 18 h in the same media using 28.57 µCi of ^{3}H-Pro/ml. For chase experiments, the labeling was performed for 4 h using 47.14 µCi of ^{3}H-Pro/ml, then the labeling media was replaced with serum-free DMEM containing 2 mM proline (Sigma-Aldrich), 4 mM glutamine, 100 µg/ml penicillin and streptomycin, and 100 µg/ml (+)-sodium L-ascorbate (chase media). Collagen was collected at 0.5, 1, 2 and 3 h after the chase. Collagen extraction was performed as previously reported (Forlino et al., 2019; Valli et al., 1991). Briefly, medium and cell lysate fractions were digested overnight with 100 ng/ml of pepsin in 0.5 M acetic acid at 4°C. Collagen was then precipitated using 2 M NaCl, 0.5 M acetic acid. Collagen was resuspended in Laemmli buffer (62 mM Tris-HCl, pH 6.8, 10% glycerol, 2% sodium dodecyl sulfate, 0.02% Bromophenol Blue) and

the radioactivity [counts per minute (CPM)] was measured using a liquid scintillation analyzer (PerkinElmer TRI-CARB 2300 TR).

For steady-state analyses, equal amounts of ^{3}H-labeled collagen from each patient's cells were loaded on 6% urea-SDS gels in a non-reducing condition. For chase analyses, the same volume of ^{3}H-labeled collagens from each time point was electrophoresed. The gels were fixed in 45% methanol, 9% glacial acetic acid, incubated for 1 h with enhancer (PerkinElmer, 6NE9701), washed in deionized water and dried. ^{3}H gel radiographs were obtained by direct exposure of dried gels to hyperfilm (Amersham) at −80°C. The radiography films were digitalized by VersaDoc 3000 (Bio-Rad). To quantify the intracellular collagen retention, the ratio between the CPM in the cell layer and the CPM in medium plus cell layer was evaluated. To quantify the percentage of collagen secretion, the ratio between the density of the α1(I) band in the media and the total collagen (medium plus cell layer) was evaluated by Quantity One software (Bio-Rad) (Ciccocioppo et al., 2013).

To analyze the effect of 4-PBA on collagen secretion, cells were labeled for 18 h in the absence or presence of 5 mM 4-PBA using 28.57 µCi of ^{3}H-Pro/ml. Collagen extraction from the media was performed as previously reported and an equal volume was loaded on the SDS-urea-PAGE. The ratio between the density of the α1(I) band in the medium was evaluated on the digitalized fluorography, and the value was normalized to the DNA extracted from the cell layer.

Transmission electron microscopy analysis

For transmission electron microscopy analysis, fibroblasts from controls and patients were trypsinized and centrifuged at 1000 ***g*** for 3 min. The pellet was fixed with 1% glutaraldehyde in the culture medium for 2 h at RT. The cells were rinsed in PBS and then in H_2O. Finally, the fibroblasts were fixed in 2% (w/v) OsO_4 in H_2O for 2 h at RT, rinsed in distilled water and embedded in 2% agarose. The specimens were dehydrated in acetone and finally infiltrated with epoxy resin overnight and polymerized in gelatin capsules at 60°C for 24 h. Thin sections (60-70 nm thick) were cut on a Reichert OM-U3 ultramicrotome with a diamond knife and collected on 300-mesh nickel grids. The grids were stained with saturated aqueous uranyl acetate by lead citrate and observed with a Zeiss EM900 electron microscope, operated at 80 kV with objective aperture of 30 µm.

XBP1 splicing analyses

cDNA from control and patients cells was used for PCR amplification across the region of the *XBP1* cDNA (NM_005080.3) containing the intronic target of IRE1α ribonuclease using 0.3 µM sense (nt 396-425; 5′-TCAGCTTTTACGAGAGAAAACTCATGGCCT-3′) and antisense (nt 696-667; 5′-AGAACATGACTGGGTCCAAGTTGTCCAGAA-3′) primers. Following a 30 min incubation at 50°C, reactions were cycled 30 times at 94°C, 60°C and 72°C for 30 s at each temperature. Reaction products were electrophoresed on 8% TBE acrylamide gels and visualized by ethidium bromide staining.

LC3 immunofluorescence

A total of 1.5×10^{4} fibroblasts were plated on sterile glass coverslips (Marienfeld) in 24-well plates in triplicate. After 5 days, cells were treated for 6 h with 10 µM chloroquine. Following the treatment, the medium was removed and cells were fixed with cold 100% CH_3OH for 15 min at −20°C, washed three times with PBS and blocked for 1 h in 1% BSA in PBS containing 0.3% Triton X-100. Then, cells were incubated with LC3 primary antibody (Cell Signaling) diluted 1:500 in 1% BSA, 0.3% Triton X-100 in PBS overnight at 4°C. Cells were washed three times with PBS and incubated with secondary antibody [Alexa-Fluor-488-conjugated F(ab′) fragment anti-rabbit IgG, Immunological Sciences] diluted 1:2000 in 1% BSA, 0.3% Triton X-100 in PBS for 2 h at RT. Nuclei were stained with 4′,6-diamidino-2-phenylindole (DAPI; Sigma-Aldrich). The samples were analyzed using an SP5-Leica confocal microscope (Leica). The total area of punctate signal per cell was measured by the Leica software LAS4.5.

Thioflavin-T labeling

A total of 1.5×10^{4} fibroblasts were plated on sterile glass coverslips (Marienfeld) in 24-well plates. After 4 days, cells were incubated with 5 µM Thioflavin T (ThT; Sigma-Aldrich) for 15 h in the presence or absence of 4-PBA and in the presence or absence of chloroquine. The medium was removed and cells were fixed with 4% paraformaldehyde in PBS for 20 min at RT. Nuclei were stained with DAPI (Sigma-Aldrich). The samples were analyzed using an SP8-Leica confocal microscope (Leica). The excitation and emission settings were: DAPI (Ex. MP laser 800 nm, Em. 410-530 nm), ThT (Ex. 458 nm, Em. 480-520 nm). The total area of punctate signal per cell was measured using the Leica software LAS4.5.

Fluorescence activated cell sorting (FACS)

To analyze apoptosis, the FACS Annexin V/Dead Cell Apoptosis Kit (Invitrogen) was used following the manufacturer's instructions. As positive control for the activation of apoptosis, cells were treated with 20 µM thapsigargin (Sigma-Aldrich) for 24 h in serum-free DMEM. Samples were analyzed by Cell Sorter S3 (Bio-Rad); 1×10^{4} events for each sample were considered measuring the fluorescence emission at 510-540 nm and >565 nm. For autophagy inhibition, 50 µM chloroquine was used.

Protein secretion

OI patients' fibroblasts were plated in 24-well plates and labeled with 5 µCi/ml [^{35}S] EXPRESS35S Protein Labeling Mix (PerkinElmer) in DMEM without L-methionine, L-cystine and L-glutamine for 1 h at 37°C. Total proteins from medium and cell layer were precipitated with 10% trichloroacetic acid. Proteins were washed with acetone twice and resuspended in 60 mM Tris-HCl, pH 6.8, 10% sodium dodecyl sulphate. The radioactivity (CPM) of the samples was measured using a liquid scintillation analyzer (TRI-CARB 2300 TR). The percentage of protein secretion was calculated based on the ratio between the CPM in the media and the CPM in medium and cell layer, evaluated in five technical replicates.

Statistical analysis

Statistical differences between patients and controls were evaluated by two-tailed Student's *t*-test. Statistical differences between controls, patients and treated patients and between the different treatments were evaluated by one-way ANOVA using Sigma plot 11.0 (Fisher). All data passed tests for normality and equal variance. Technical triplicates were performed and values were expressed as mean±s.d. A P-value <0.05 was considered significant.

Acknowledgements

We thank Prof. Brendan Lee (College of Medicine Houston, TX, USA) for providing the anti-CRTAP antibody; Prof .Roy Morello for providing the CRTAP-3 cell line; Dr Patrizia Vaghi (Centro Grandi Strumenti, University of Pavia, Italy) for technical assistance with confocal microscopy; and Mr Angelo Gallanti for technical assistance with cell culture.

Competing interests

The authors declare no competing or financial interests.

Author contributions

Conceptualization: R.B., A.F.; Methodology: R.B., N.G., L.L., L.C., S.S., M.B.; Validation: R.B., N.G., L.L., L.C., S.S., M.B.; Formal analysis: R.B., A.F.; Investigation: R.B., A.F.; Resources: M.M., M.A., G.A.O., S.A.T., A.F.; Data curation: R.B., A.F.; Writing - original draft: R.B., A.R., A.F.; Writing - review & editing: R.B., N.G., L.L., L.C., S.S., M.B., M.M., M.A., G.A.O., S.A.T., A.R., A.F.; Supervision: A.F.; Project administration: A.F.; Funding acquisition: A.F., A.R.

Funding

The work was supported by Fondazione Cariplo [grant no. 2013-0612], Fondazione Telethon [grant no. GGP13098] and the FP7 Ideas: European Research Council "Sybil" project [grant no. 602300].

Supplementary information

Supplementary information available online at
http://dmm.biologists.org/lookup/doi/10.1242/dmm.038521.supplemental

References

Amor, I. M. B., Rauch, F., Gruenwald, K., Weis, M., Eyre, D. R., Roughley, P., Glorieux, F. H. and Morello, R. (2011). Severe osteogenesis imperfecta caused by a small in-frame deletion in CRTAP. *Am. J. Med. Genet. A* **155**, 2865-2870. doi:10.1002/ajmg.a.34269

Balasubramanian, M., Sobey, G. J., Wagner, B. E., Peres, L. C., Bowen, J., Bexon, J., Javaid, M. K., Arundel, P. and Bishop, N. J. (2016). Osteogenesis

imperfecta: ultrastructural and histological findings on examination of skin revealing novel insights into genotype-phenotype correlation. *Ultrastruct. Pathol.* **40**, 71-76. doi:10.3109/01913123.2016.1140253

Barnes, A. M., Chang, W., Morello, R., Cabral, W. A., Weis, M. A., Eyre, D. R., Leikin, S., Makareeva, E., Kuznetsova, N., Uveges, T. E. et al. (2006). Deficiency of cartilage-associated protein in recessive lethal osteogenesis imperfecta. *N. Engl. J. Med.* **355**, 2757-2764. doi:10.1056/NEJMoa063804

Barnes, A. M., Carter, E. M., Cabral, W. A., Weis, M. A., Chang, W., Makareeva, E., Leikin, S., Rotimi, C. N., Eyre, D. R., Raggio, C. L. et al. (2010). Lack of cyclophilin B in osteogenesis imperfecta with normal collagen folding. *N. Engl. J. Med.* **362**, 521-528. doi:10.1056/NEJMoa0907705

Beriault, D. R. and Werstuck, G. H. (2013). Detection and quantification of endoplasmic reticulum stress in living cells using the fluorescent compound, Thioflavin T. *Biochim. Biophys. Acta* **1833**, 2293-2301. doi:10.1016/j.bbamcr.2013.05.020

Besio, R. and Forlino, A. (2015). Treatment options for osteogenesis imperfecta. *Expert Opin. Orphan Drugs* **3**, 165-181. doi:10.1517/21678707.2015.1006197

Besio, R., Iula, G., Garibaldi, N., Cipolla, L., Sabbioneda, S., Biggiogera, M., Marini, J. C., Rossi, A. and Forlino, A. (2018). 4-PBA ameliorates cellular homeostasis in fibroblasts from osteogenesis imperfecta patients by enhancing autophagy and stimulating protein secretion. *Biochim. Biophys. Acta* **1864**, 1642-1652. doi:10.1016/j.bbadis.2018.02.002

Bianchi, L., Gagliardi, A., Gioia, R., Besio, R., Tani, C., Landi, C., Cipriano, M., Gimigliano, A., Rossi, A., Marini, J. C. et al. (2012). Differential response to intracellular stress in the skin from osteogenesis imperfecta Brtl mice with lethal and non lethal phenotype: a proteomic approach. *J. Proteomics* **75**, 4717-4733. doi:10.1016/j.jprot.2012.01.038

Boot-Handford, R. P. and Briggs, M. D. (2010). The unfolded protein response and its relevance to connective tissue diseases. *Cell Tissue Res.* **339**, 197-211. doi:10.1007/s00441-009-0877-8

Butchbach, M. E. R., Lumpkin, C. J., Harris, A. W., Saieva, L., Edwards, J. D., Workman, E., Simard, L. R., Pellizzoni, L. and Burghes, A. H. M. (2016). Protective effects of butyrate-based compounds on a mouse model for spinal muscular atrophy. *Exp. Neurol.* **279**, 13-26. doi:10.1016/j.expneurol.2016.02.009

Cabral, W. A., Chang, W., Barnes, A. M., Weis, M. A., Scott, M. A., Leikin, S., Makareeva, E., Kuznetsova, N. V., Rosenbaum, K. N., Tifft, C. J. et al. (2007). Prolyl 3-hydroxylase 1 deficiency causes a recessive metabolic bone disorder resembling lethal/severe osteogenesis imperfecta. *Nat. Genet.* **39**, 359-365. doi:10.1038/ng1968

Caparros-Martin, J. A., Valencia, M., Pulido, V., Martinez-Glez, V., Rueda-Arenas, I., Amr, K., Farra, C., Lapunzina, P., Ruiz-Perez, V. L., Temtamy, S. et al. (2013). Clinical and molecular analysis in families with autosomal recessive osteogenesis imperfecta identifies mutations in five genes and suggests genotype-phenotype correlations. *Am. J. Med. Genet. A* **161**, 1354-1369. doi:10.1002/ajmg.a.35938

Chang, W., Barnes, A. M., Cabral, W. A., Bodurtha, J. N. and Marini, J. C. (2010). Prolyl 3-hydroxylase 1 and CRTAP are mutually stabilizing in the endoplasmic reticulum collagen prolyl 3-hydroxylation complex. *Hum. Mol. Genet.* **19**, 223-234. doi:10.1093/hmg/ddp481

Ciccocioppo, R., Vanoli, A., Klersy, C., Imbesi, V., Boccaccio, V., Manca, R., Betti, E., Cangemi, G. C., Strada, E., Besio, R. et al. (2013). Role of the advanced glycation end products receptor in Crohn's disease inflammation. *World J. Gastroenterol.* **19**, 8269-8281. doi:10.3748/wjg.v19.i45.8269

Daosukho, C., Chen, Y., Noel, T., Sompol, P., Nithipongvanitch, R., Velez, J. M., Oberley, T. D. and St Clair, D. K. (2007). Phenylbutyrate, a histone deacetylase inhibitor, protects against Adriamycin-induced cardiac injury. *Free Radic. Biol. Med.* **42**, 1818-1825. doi:10.1016/j.freeradbiomed.2007.03.007

Forlino, A. and Marini, J. C. (2016). Osteogenesis imperfecta. *Lancet* **387**, 1657-1671. doi:10.1016/S0140-6736(15)00728-X

Forlino, A., Tani, C., Rossi, A., Lupi, A., Campari, E., Gualeni, B., Bianchi, L., Armini, A., Cetta, G., Bini, L. et al. (2007). Differential expression of both extracellular and intracellular proteins is involved in the lethal or nonlethal phenotypic variation of BrtlIV, a murine model for osteogenesis imperfecta. *Proteomics* **7**, 1877-1891. doi:10.1002/pmic.200600919

Forlino, A., Cabral, W. A., Barnes, A. M. and Marini, J. C. (2011). New perspectives on osteogenesis imperfecta. *Nat. Rev. Endocrinol.* **7**, 540-557. doi:10.1038/nrendo.2011.81

Forlino, A., Tonelli, F. and Besio, R. (2019). Steady-state and pulse-chase analyses of fibrillar collagen. *Methods Mol. Biol.* **1952**, 45-53. doi:10.1007/978-1-4939-9133-4_4

Gagliardi, A., Besio, R., Carnemolla, C., Landi, C., Armini, A., Aglan, M., Otaify, G., Temtamy, S. A., Forlino, A., Bini, L. et al. (2017). Cytoskeleton and nuclear lamina affection in recessive osteogenesis imperfecta: a functional proteomics perspective. *J. Proteomics* **167**, 46-59. doi:10.1016/j.jprot.2017.08.007

Galluzzi, L., Bravo-San Pedro, J. M., Levine, B., Green, D. R. and Kroemer, G. (2017). Pharmacological modulation of autophagy: therapeutic potential and persisting obstacles. *Nat. Rev. Drug Discov.* **16**, 487-511. doi:10.1038/nrd.2017.22

Gioia, R., Tonelli, F., Ceppi, I., Biggiogera, M., Leikin, S., Fisher, S., Tenedini, E., Yorgan, T. A., Schinke, T., Tian, K. et al. (2017). The chaperone activity of 4PBA ameliorates the skeletal phenotype of Chihuahua, a zebrafish model for dominant osteogenesis imperfecta. *Hum. Mol. Genet.* **26**, 2897-2911. doi:10.1093/hmg/ddx171

Green, D. R. and Levine, B. (2014). To be or not to be? How selective autophagy and cell death govern cell fate. *Cell* **157**, 65-75. doi:10.1016/j.cell.2014.02.049

Gruenwald, K., Castagnola, P., Besio, R., Dimori, M., Chen, Y., Akel, N. S., Swain, F. L., Skinner, R. A., Eyre, D. R., Gaddy, D. et al. (2014). Sc65 is a novel endoplasmic reticulum protein that regulates bone mass homeostasis. *J. Bone Miner. Res.* **29**, 666-675. doi:10.1002/jbmr.2075

Heard, M. E., Besio, R., Weis, M. A., Rai, J., Hudson, D. M., Dimori, M., Zimmerman, S. M., Kamykowski, J. A., Hogue, W. R., Swain, F. L. et al. (2016). Sc65-null mice provide evidence for a novel endoplasmic reticulum complex regulating collagen lysyl hydroxylation. *PLoS Genet.* **12**, e1006002. doi:10.1371/journal.pgen.1006002

Homan, E. P., Lietman, C., Grafe, I., Lennington, J., Morello, R., Napierala, D., Jiang, M.-M., Munivez, E. M., Dawson, B., Bertin, T. K. et al. (2014). Differential effects of collagen prolyl 3-hydroxylation on skeletal tissues. *PLoS Genet.* **10**, e1004121. doi:10.1371/journal.pgen.1004121

Hudson, D. M. and Eyre, D. R. (2013). Collagen prolyl 3-hydroxylation: a major role for a minor post-translational modification? *Connect. Tissue Res.* **54**, 245-251. doi:10.3109/03008207.2013.800867

Ishikawa, Y. and Bächinger, H. P. (2013). A molecular ensemble in the rER for procollagen maturation. *Biochim. Biophys. Acta* **1833**, 2479-2491. doi:10.1016/j.bbamcr.2013.04.008

Ishikawa, Y., Wirz, J., Vranka, J. A., Nagata, K. and Bächinger, H. P. (2009). Biochemical characterization of the prolyl 3-hydroxylase 1. cartilage-associated protein cyclophilin B complex. *J. Biol. Chem.* **284**, 17641-17647. doi:10.1074/jbc.M109.007070

Lindert, U., Cabral, W. A., Ausavarat, S., Tongkobpetch, S., Ludin, K., Barnes, A. M., Yeetong, P., Weis, M., Krabichler, B., Srichomthong, C. et al. (2016). MBTPS2 mutations cause defective regulated intramembrane proteolysis in X-linked osteogenesis imperfecta. *Nat. Commun.* **7**, 11920. doi:10.1038/ncomms11920

Mai, C. T., Le, Q. G., Ishiwata-Kimata, Y., Takagi, H., Kohno, K. and Kimata, Y. (2018). 4-Phenylbutyrate suppresses the unfolded protein response without restoring protein folding in Saccharomyces cerevisiae. *FEMS Yeast Res.* **18**, doi:10.1093/femsyr/foy016.

Marini, J. C. and Blissett, A. R. (2013). New genes in bone development: what's new in osteogenesis imperfecta. *J. Clin. Endocrinol. Metab.* **98**, 3095-3103. doi:10.1210/jc.2013-1505

Marini, J. C., Cabral, W. A., Barnes, A. M. and Chang, W. (2007). Components of the collagen prolyl 3-hydroxylation complex are crucial for normal bone development. *Cell Cycle* **6**, 1675-1681. doi:10.4161/cc.6.14.4474

Marini, J. C., Forlino, A., Bächinger, H. P., Bishop, N. J., Byers, P. H., Paepe, A. D., Fassier, F., Fratzl-Zelman, N., Kozloff, K. M., Krakow, D. et al. (2017). Osteogenesis imperfecta. *Nat. Rev. Dis. Primers* **3**, 17052. doi:10.1038/nrdp.2017.52

Matoori, S. and Leroux, J.-C. (2015). Recent advances in the treatment of hyperammonemia. *Adv. Drug Deliv. Rev.* **90**, 55-68. doi:10.1016/j.addr.2015.04.009

Mirigian, L. S., Makareeva, E., Mertz, E. L., Omari, S., Roberts-Pilgrim, A. M., Oestreich, A. K., Phillips, C. L. and Leikin, S. (2016). Osteoblast malfunction caused by cell stress response to procollagen misfolding in alpha2(I)-G610C mouse model of osteogenesis imperfecta. *J. Bone Miner. Res.* **31**, 1608-1616. doi:10.1002/jbmr.2824

Morello, R., Bertin, T. K., Chen, Y., Hicks, J., Tonachini, L., Monticone, M., Castagnola, P., Rauch, F., Glorieux, F. H., Vranka, J. et al. (2006). CRTAP is required for prolyl 3- hydroxylation and mutations cause recessive osteogenesis imperfecta. *Cell* **127**, 291-304. doi:10.1016/j.cell.2006.08.039

Perdivara, I., Yamauchi, M. and Tomer, K. B. (2013). Molecular characterization of collagen hydroxylysine O-glycosylation by mass spectrometry: current status. *Aust. J. Chem.* **66**, 760-769. doi:10.1071/CH13174

Pettit, R. S. and Fellner, C. (2014). CFTR modulators for the treatment of cystic fibrosis. *P. T.* **39**, 500-511.

Pokidysheva, E., Boudko, S., Vranka, J., Zientek, K., Maddox, K., Moser, M., Fassler, R., Ware, J. and Bachinger, H. P. (2014). Biological role of prolyl 3-hydroxylation in type IV collagen. *Proc. Natl. Acad. Sci. USA* **111**, 161-166. doi:10.1073/pnas.1307597111

Pyott, S. M., Schwarze, U., Christiansen, H. E., Pepin, M. G., Leistritz, D. F., Dineen, R., Harris, C., Burton, B. K., Angle, B., Kim, K. et al. (2011). Mutations in PPIB (cyclophilin B) delay type I procollagen chain association and result in perinatal lethal to moderate osteogenesis imperfecta phenotypes. *Hum. Mol. Genet.* **20**, 1595-1609. doi:10.1093/hmg/ddr037

Sarafova, A. P., Choi, H., Forlino, A., Gajko, A., Cabral, W. A., Tosi, L., Reing, C. M. and Marini, J. C. (1998). Three novel type I collagen mutations in osteogenesis imperfecta type IV probands are associated with discrepancies between electrophoretic migration of osteoblast and fibroblast collagen. *Hum. Mutat.* **11**, 395-403. doi:10.1002/(SICI)1098-1004(1998)11:5<395::AID-HUMU7>3.0.CO;2-4

Scheiber, A. L., Guess, A. J., Kaito, T., Abzug, J. M., Enomoto-Iwamoto, M., Leikin, S., Iwamoto, M. and Otsuru, S. (2019). Endoplasmic reticulum stress is induced in growth plate hypertrophic chondrocytes in G610C mouse model of

osteogenesis imperfecta. *Biochem. Biophys. Res. Commun.* **509**, 235-240. doi:10.1016/j.bbrc.2018.12.111

Taga, Y., Kusubata, M., Ogawa-Goto, K. and Hattori, S. (2013). Site-specific quantitative analysis of overglycosylation of collagen in osteogenesis imperfecta using hydrazide chemistry and SILAC. *J. Proteome Res.* **12**, 2225-2232. doi:10.1021/pr400079d

Terajima, M., Taga, Y., Chen, Y., Cabral, W. A., Hou-Fu, G., Srisawasdi, S., Nagasawa, M., Sumida, N., Hattori, S., Kurie, J. M. et al. (2016). Cyclophilin-B modulates collagen cross-linking by differentially affecting lysine hydroxylation in the helical and telopeptidyl domains of tendon type I collagen. *J. Biol. Chem.* **291**, 9501-9512. doi:10.1074/jbc.M115.699470

Valli, M., Mottes, M., Tenni, R., Sangalli, A., Gomez Lira, M., Rossi, A., Antoniazzi, F., Cetta, G. and Pignatti, P. F. (1991). A de novo G to T transversion in a pro-alpha 1 (I) collagen gene for a moderate case of osteogenesis imperfecta. Substitution of cysteine for glycine 178 in the triple helical domain. *J. Biol. Chem.* **266**, 1872-1878. doi:10.1007/bf00219169

Valli, M., Barnes, A. M., Gallanti, A., Cabral, W. A., Viglio, S., Weis, M. A., Makareeva, E., Eyre, D., Leikin, S., Antoniazzi, F. et al. (2012). Deficiency of CRTAP in non-lethal recessive osteogenesis imperfecta reduces collagen deposition into matrix. *Clin. Genet.* **82**, 453-459. doi:10.1111/j.1399-0004.2011.01794.x

van Dijk, F. S., Nesbitt, I. M., Zwikstra, E. H., Nikkels, P. G. J., Piersma, S. R., Fratantoni, S. A., Jimenez, C. R., Huizer, M., Morsman, A. C., Cobben, J. M. et al. (2009). PPIB mutations cause severe osteogenesis imperfecta. *Am. J. Hum. Genet.* **85**, 521-527. doi:10.1016/j.ajhg.2009.09.001

Vollmann, E. H., Cao, L., Amatucci, A., Reynolds, T., Hamann, S., Dalkilic-Liddle, I., Cameron, T. O., Hossbach, M., Kauffman, K. J., Mir, F. F. et al. (2017). Identification of novel fibrosis modifiers by in vivo siRNA silencing. *Mol. Ther. Nucleic Acids* **7**, 314-323. doi:10.1016/j.omtn.2017.04.014

Wagner, M. and Trauner, M. (2016). Recent advances in understanding and managing cholestasis. *F1000Res* **5**, 705. doi:10.12688/f1000research.8012.1

Wilson, R., Lees, J. F. and Bulleid, N. J. (1998). Protein disulfide isomerase acts as a molecular chaperone during the assembly of procollagen. *J. Biol. Chem.* **273**, 9637-9643. doi:10.1074/jbc.273.16.9637

Chapter 3

Targeting cellular stress improves osteoblasts homeostasis and matrix in murine models of osteogenesis imperfecta

Collagen type I misfolding and intracellular accumulation were observed in OI and the consequent activation of unfolded protein response and apoptosis was demonstrated in patients' fibroblasts, highlighting the relevance of intracellular mutant collagen in the onset of the pathology. The bone forming cells osteoblasts are the most affected cells in OI, producing high amounts of collagen type I, which assembles into fibrils in the ECM and form a scaffold for mineral deposition. Indeed, perturbed cellular homeostasis and an impaired bone matrix quality are present in OI OBs. We hypothesized that targeting OI OBs homeostasis could be a potential strategy to promote their anabolic activity and, likely, to ameliorate extracellular matrix quality. To this purpose, my main PhD project was to assess the effect of the chemical chaperone 4-PBA in OBs from two well established murine models of dominant OI, the Col1a1$^{+/G349C}$ (Brtl) and the Col1a2$^{+/G610C}$ (Amish) mice, carrying a triple helical glycine substitution in α1 and in α 2 chain, respectively, reproducing mutations previously characterized in OI type IV probands.

The drug proved to rescue cell homeostasis by reducing UPR and apoptotic markers expression and, as for patients' fibroblasts, it improved intracellular morphology by stimulating protein secretion. Importantly, given its ability to reduce collagen I expression and to stimulate its secretion, 4-PBA exerted beneficial effects on extracellular matrix collagen content and maturation. Of relevance, a bone cell-specific action was proven since the drug promoted OI osteoblasts mineralization by increasing alkaline phosphatase expression and activity.

Our results demonstrated 4-PBA efficacy in osteoblasts and proved the drug as a promising candidate to complement current therapy for OI management.

The present manuscript, just submitted to Matrix Biology, constitutes the main project of my PhD and I carried out every phase of the work. I took part in each experiment and in the relative analyses, as well as in the paper writing.

Targeting cellular stress improves osteoblast homeostasis, matrix collagen content and mineralization in two murine models of osteogenesis imperfecta

Running title: Matrix amelioration upon targeting cellular stress

Nadia Garibaldi[a,b], Barbara M. Contento[a], Gabriele Babini[c], Jacopo Morini[c], Stella Siciliani[d], Marco Biggiogera[d], Mario Raspanti[e], Joan C. Marini[f], Antonio Rossi[a], Antonella Forlino[a,*], Roberta Besio[a,*]

[a]Department of Molecular Medicine, Biochemistry Unit, University of Pavia, Pavia, Italy; [b]Istituto Universitario di Studi Superiori - IUSS, Pavia, Italy; [c]Department of Physics, University of Pavia, Pavia, Italy; [d]Department of Biology and Biotechnology, University of Pavia, Pavia, Italy; [e]Department of Medicine and Surgery, University of Insubria, Varese, Italy; [f]Bone and Extracellular Matrix Branch, NICHD, National Institute of Health, Bethesda, MD 20892, USA

[*]These authors contributed equally to the work

Corresponding Authors:
Roberta Besio, PhD
Department of Molecular Medicine, Biochemistry Unit
University of Pavia
via Taramelli 3b - 27100 Pavia, Italy
Phone: +39-0382-987233
e-mail: roberta.besio@unipv.it

Antonella Forlino, PhD
Department of Molecular Medicine, Biochemistry Unit
University of Pavia
Via Taramelli 3B
27100 Pavia, Italy
Phone: +39-0382-987235
e-mail: aforlino@unipv.it

Abstract

Most cases of dominantly inherited osteogenesis imperfecta (OI) are caused by glycine substitutions in the triple helical domain of type I collagen α chains, which delay collagen folding, and cause the synthesis of collagen triple helical molecules with abnormal structure and post-translational modification. A variable extent of mutant collagen ER retention and other secondary mutation effects perturb osteoblast homeostasis and impair bone matrix quality. Amelioration of OI osteoblast homeostasis could be beneficial both to osteoblast anabolic activity and to the content of the extracellular matrix they deposit. Therefore, the effect of the chemical chaperone 4-phenylbutyrate (4-PBA) on cell homeostasis, collagen trafficking, matrix production and mineralization was investigated in primary osteoblasts from two murine models of moderate OI, *Col1a1*$^{+/G349C}$ and *Col1a2*$^{+/G610C}$. At the cellular level, 4-PBA prevented intracellular accumulation of collagen and increased protein secretion, reducing aggregates within the mutant cells and normalizing ER morphology. At the extracellular level, increased collagen incorporation into matrix, associated with greater maturation of collagen fibrils, was observed in osteoblasts from both models. 4-PBA also promoted OI osteoblast mineral deposition by increasing alkaline phosphatase expression and activity. Targeting osteoblast stress with 4-PBA improved both cellular and matrix abnormalities in culture, supporting further *in vivo* studies of its effect on bone tissue composition, strength and mineralization as a potential treatment for classical OI.

Keywords: collagen, osteogenesis imperfecta, endoplasmic reticulum stress, chemical chaperone, unfolded protein response

Introduction

Bone modeling and remodeling require the anabolic activity of osteoblasts (OBs), which are responsible for the synthesis of the extracellular matrix (ECM). Bone ECM, mainly consisting of type I collagen with contributions from several non-collagenic molecules, is the scaffold on which mineral deposition and cell interaction occur, thus its integrity is essential to guarantee proper bone structure and biomechanical properties, as well as cell-cell and cell-matrix communication [1]**.** Indeed, many inherited skeletal dysplasias are associated with mutations in bone ECM components and their pathogenic mechanism is generally attributed to impaired ECM assembly and function [2-6]. In the last decade it has been appreciated that bone cellular dysfunction also contributes to pathological mechanisms. Mutated proteins may be retained in the endoplasmic reticulum (ER) causing cellular stress that may affect the clinical outcome [2, 4, 7-12]. One example of this cellular effect is the intracellular accumulation of mutant collagen type I in classical osteogenesis imperfecta (OI).

OI is among the most common hereditary skeletal dysplasias, characterized by reduced bone mineral density, bone deformity and frequent fragility fractures from minimal or no trauma [13]. Individuals with OI display a broad phenotypic range, from mild osteoporosis to perinatal lethality sometimes even in the presence of identical mutations, and the molecular basis of this phenotypic variability is still unknown [14-17]. Classical OI (types I to IV based on the Sillence classification [18]) is a dominantly inherited disease due to mutations in the *COL1A1* and *COL1A2* genes encoding the α chains of type I collagen. The most common defects are glycine substitutions responsible for the folding delay of the α chains and of their prolonged exposure to the post translational modifying enzymes, thus causing the synthesis of abnormal collagen molecules with increased proline and lysine hydroxylation and hydroxylysine glycosylation [11, 19-21]. In cells from many patients and in various OI murine models, the misfolded collagen is partially retained intracellularly, altering cell homeostasis and provoking a cell stress response which could function

as a modulator of OI [11, 13, 22-24]. Indeed, in the OI murine model Brtl, carrying an α1(I)-G349C substitution and having either a moderate or a lethal outcome, the significant difference in expression of ER stress-related proteins indicated involvement of the intracellular machinery in modulating or responding to OI severity, which makes this pathway a potential novel target for OI therapy [16, 25].

Current pharmacological treatments for OI rely almost exclusively on the use of bisphosphonates, a class of antiresorptive drugs inhibiting osteoclast differentiation and/or activity, used in the management of osteoporosis [26]. Despite success in increasing DXA bone density [27-30], the efficacy of these treatments to reduce the fracture risk is controversial and questions about effective dose, cycling intervals and efficacy and safety of long-term use in developing bones of children with OI remain to be answered [31, 32]. Thus, the identification of novel targets for new pharmacological approaches is an urgent clinical need for these patients.

4-phenylbutyrate (4-PBA), a chemical chaperone already approved by the FDA as an ammonia scavenger, was used in preclinical and clinical trials to treat diseases caused by intracellular accumulation of misfolded proteins [33-38] . Its chaperone ability was first identified in diseases such as cystic fibrosis [39] and type 2 diabetes associated to obesity [40] where 4-PBA was able to alleviate ER stress and UPR activation, and to restore intracellular trafficking [39, 41, 42]. We have recently demonstrated that 4-PBA treatment rescues cellular homeostasis through reduction of cell stress in patient fibroblasts carrying mutations in both collagen and non-collagenous genes [23, 24] and leads to skeletal improvement in the zebrafish *Chihuahua* model of classical OI [43].

For in depth studies of the effectiveness of innovative therapies, models that more faithfully recapitulate human anatomy and physiology than do zebrafish are preferable, and murine models are often the best choice [44, 45]. *Col1a1*$^{+/G349C}$ (Brtl) and *Col1a2*+/^{G610C} (Amish) mice are well established models of a classical form of OI, carrying a triple helical glycine substitution in α1(I) and in α2(I) chain, respectively. Brtl and Amish reproduce glycine substitutions previously

characterized in OI probands and they model the majority of the patient defects [46-48]. Both mice reproduce the growth deficiency, lower bone mineral density and altered mineral-to-matrix ratio and bone geometry underlying bone deformity and fragility, which are typical of individuals affected by OI [46, 49-52]. The imbalance between formation and resorption in bone remodeling, in favour of the latter, is a significant contributor to the bone phenotype in OI. Indeed in the Brtl model, osteoclast number and function are increased, while mineral apposition is decreased during growth, pointing to a decline in osteoblast activity [53]. Brtl mesenchymal stem cells show impaired osteoblastogenesis and a preference towards adipocytic differentiation [25]. Appositional bone growth is also compromised in the Amish model [51], in which osteoblasts are characterized by malfunction, impaired differentiation and lower mineral deposition [11]. Intracellular mutant collagen retention associated with ER cisternae enlargement and altered organization of collagen fibers in the ECM are common features in both models [21, 54].

In the present study, primary osteoblasts from Brtl and Amish OI murine models were used to investigate their baseline response to mutant collagen intracellular retention and to evaluate the effect of the chemical chaperone 4-PBA on cellular homeostasis and extracellular matrix deposition.

Results

Osteoblasts homeostasis is altered in OI murine models

In order to investigate the cellular response to the synthesis of mutant collagen in primary OI osteoblasts, we performed qPCR-based transcriptomic analyses evaluating the expression of genes involved in three major stress related pathways: unfolded protein response (UPR), autophagy, and apoptosis. The UPR was strongly activated in both OI murine models, with 77 upregulated genes in Amish mouse and 40 in Brtl (**Fig. 1A**). The expression of several chaperones was enhanced in both models. *Cct7*, encoding a chaperone involved in folding newly translated polypeptides, and *Calr*, encoding the ER luminal protein calreticulin that binds misfolded proteins and prevents their progression through the secretory pathway, displayed increased expression compared to controls. Also upregulated were genes encoding for proteins involved in protein disulphide isomerization (*Erp44*) and ER quality control of polypeptide folding (*Edem1*, *Prkcsh*, *Rpn1*). In addition, numerous members of the heat shock protein family were upregulated, specifically *Dnajb2*, *Dnajc3*, *Hspa1l*, *Hspa2*, *Hsph1* and, importantly, *Hspa5*, encoding for the ER chaperone and UPR initiator BIP (**Fig 1A**). Interestingly, the upregulated genes included UPR players *Atf6* (ATF6 branch) and *Eif2ak3* (PERK branch), with its effector *Atf4.* ATF4 protein was also increased in both models, confirming PERK branch activation (**Fig. 1B**), while IRE1α- mediated splicing of *Xbp1* was detectable only in Brtl OBs (**Fig. 1C**), indicating that in this model cell stress triggers a more general response involving multiple UPR branches. The expression of numerous genes involved in ubiquitination processes and in misfolded proteins degradation (*Amfr*, *Herpud1*, *Ubxn4*, *Uggt1*, *Uggt2*, *Usp14*, *Vimp*, *Vcp*) was increased in Amish cells (**Fig. 1A**).

Autophagy was activated in both models, although only Brtl mice displayed a substantial upregulation of autophagic genes (**Fig. 1A**). Among the 39 upregulated genes in Brtl OBs, many were involved in autophagosome formation and growth. In particular, we observed enhanced expression of several family members of

autophagy related genes (ATG), including the key autophagic factors *Atg12, Atg16l1 and Atg16l2*, involved in autophagic vesicles formation. Furthermore, we observed augmented level of *Map1lc3a*, encoding for the terminal autophagic marker LC3 that participates to autophagosome membrane expansion. Immunofluorescence analyses revealed an increased level of LC3 (**Fig. 1D**) and western blot performed on cell lysates following chloroquine treatment showed significantly increased LC3II expression in both models (**Fig. 1E**). Importantly, the autophagic flux, calculated as the ratio between LC3II level in chloroquine treated and untreated samples [55], was increased in both models (**Fig. 1F**).

Finally, apoptosis activation was evaluated, revealing both in Brtl and Amish a considerable number of upregulated genes (**Fig. 1A**). Several death domain receptor genes, encoding initiator proteins that trigger the apoptotic cascade, in particular several members of Tumor Necrosis Factor (TNF) receptor superfamily *Tnfrsf10b*, *11b* and *1a*, were increased in both models. Brtl cells also displayed activation of the two death domain receptors *Fadd*, recruited by TNF proteins and activators of initiator caspases, and *Dapk1*, involved in autophagy-dependent apoptosis regulation.

Interestingly, anti-apoptotic factors were also upregulated, predominantly in Brtl cells, such as genes of the Bcl-2 family (*Bcl10, Bcl2, Bcl2a1a, Bcl2l1, Bcl2l11*) together with their enhancers *Bag1, Bag3* and *Bnip2* genes encoding the BCL-2 interacting proteins. Different members of the caspase family, responsible for the apoptotic cascade, were increased in both Brtl and Amish. Apoptosis initiators such as *Casp2*, *Casp8* and *Casp9* were activated preferentially in Brtl, while the effector caspases *Casp4*, Casp7, *Casp12* and *Casp14* were activated in Amish OBs. Importantly, *Casp6*, one of the main effector caspases, and *Casp3*, the caspase in charge of apoptosis execution, were upregulated in both models (**Fig. 1A**). Although the pathway was triggered in both models, Brtl cells had increased expression of a larger number of genes (Brtl n=54; Amish n=38). Immunofluorescence of cleaved caspase 3 (**Fig. 2D**) and FACS quantification of apoptotic cells with annexin V and

propidium iodide confirmed the activation of apoptosis in both models (Brtl 1.94 ± 0.43 fold differences respect to WT, $p<0.05$; Amish 1.55 ± 0.48 fold differences respect to WT, $p< 0.05$).

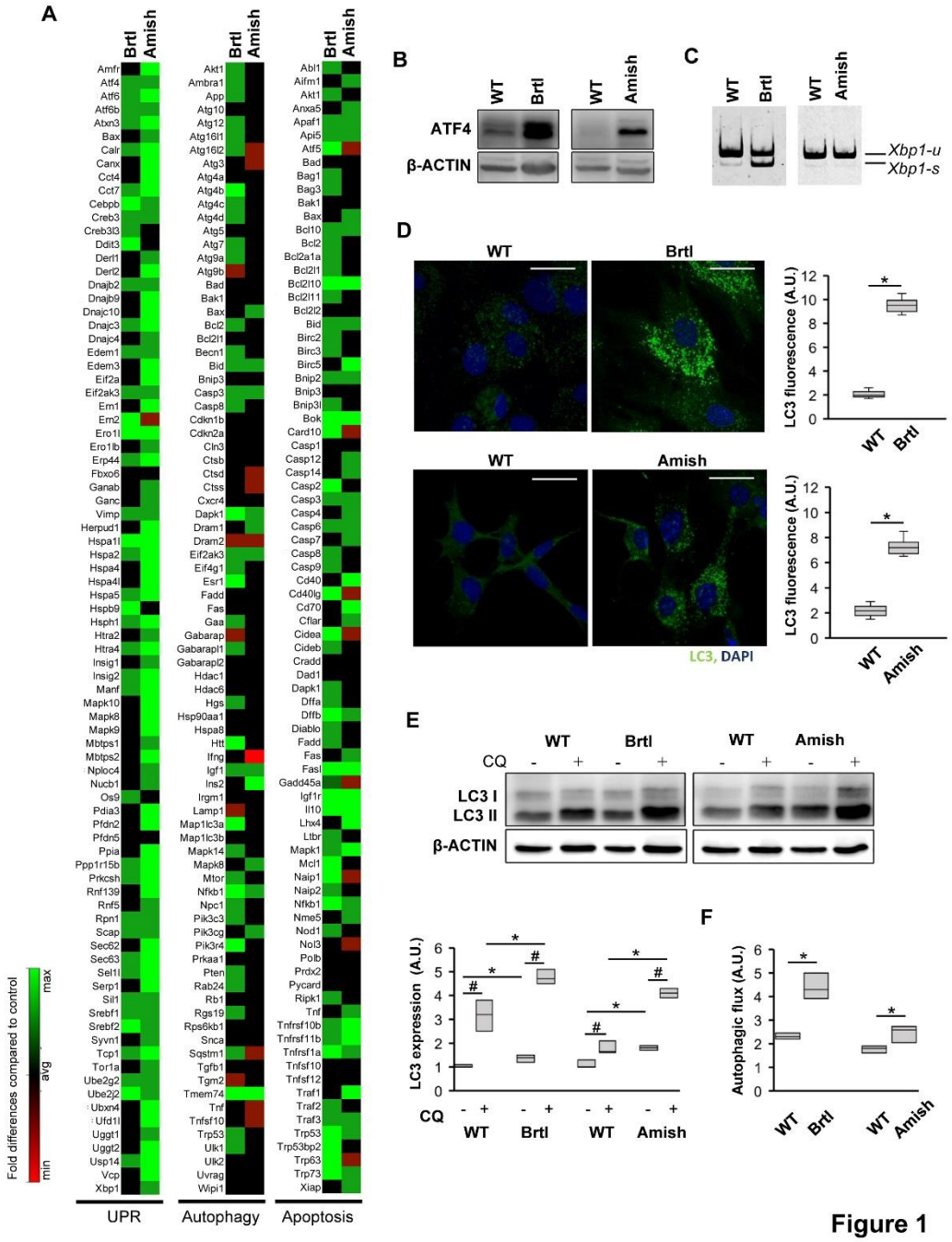

Figure 1

Figure 1: Osteoblasts homeostasis is altered in the Brtl and Amish models. (**A**) qPCR-based array heat map of relative expression of genes involved in UPR, autophagic and apoptotic pathways in Brtl and Amish OBs. Results are expressed as fold differences compared to control. The upregulation of 40 and 77 genes involved in UPR, 39 and 12 genes involved in autophagy and 54 and 38 genes involved in apoptosis were upregulated in Brtl and Amish, respectively. (**B**) Representative ATF4 western blot image. The protein was upregulated in both OI models. (**C**) RT-PCR amplification of *Xpb1* mRNA from control (WT) and mutant OBs. The spliced *Xbp1* form (*Xbp1-s*) of *Xbp1* transcript (*Xbp1-u*) was detected in Brtl. (**D**) Representative immunofluorescence images and quantification of LC3 in WT and mutant OBs. Quantitation of the total area of punctate signal per cell indicated the activation of autophagy. Nuclei were stain with DAPI. Magnification 40X, zoom 4X. *p<0.05 WT VS mutant. (**E**) Representative LC3 western blot performed on WT and mutant cell lysates obtained following chloroquine (CQ) incubation. β-actin was used for normalization. Bands quantitative analysis revealed LC3-II upregulation in chloroquine treated Brtl and Amish OBs compared to their controls. *p<0.05 WT VS mutant; # p<0.05 untreated VS chloroquine treated. (**F**) Autophagic flux, evaluated as the ratio between LC3II level in chloroquine treated samples and the untreated ones, was increased in both models. *p<0.05 WT VS mutant.

4-PBA improves osteoblasts homeostasis by alleviating cellular stress

To investigate whether modulation of cell stress would rescue cellular homeostasis, OBs were treated with the chemical chaperone 4-PBA. Following drug administration, consistent changes in the gene expression pattern of both models was observed (**Fig. 2A**). In particular, BIP-encoding gene *Hspa5* and its nucleotide exchange factor *Sil1*, together with the effectors of the PERK UPR branch (*Eif2ak3*, *Atf4*), were downregulated, revealing a beneficial effect of 4-PBA in reducing ER stress response. OBs from the two models displayed a normalization or a decrease in the level of expression of chaperones such as *Calr*, calreticulin, and *Tcp1*, a member of the chaperonin-containing TCP1 complex (CCT) that assists protein folding. In Brtl cells in particular, the normalization of protein disulphide isomerase *Erp44* and, interestingly, the upregulation of quality control protein-coding genes such as *Uggt1* and *Uggt2*, was observed (**Fig. 2A**). In Amish OBs, 4-PBA led to a more pronounced general reduction of UPR genes expression, decreasing chaperones (*Calr*, *Canx*, *Cct4*, *Cct7*), proteins involved in folding and quality control (*Dnajb2*, *Dnajb10*, *Dnajc3*, *Dnajc4)*, and the majority of heat shock proteins (*Hspa1l*, *Hspa4*, *Hspa5*, *Hsph1*). In addition, the expression of all the previously overexpressed genes

promoting ubiquitination and proteasomal degradation (*Amfr*, *Derl1* and *2*, *Edem1*, *Herpud1*, *Nploc4*, *Nucb1*, *Rnf139*, *Rnf5*, *Sec62*, *Syvn1*, *Ube2j2*, *Ubxn4*, *Ufd1l*, *Usp14*, *Vcp Vimp*) was lowered or restored to control level, suggesting that the need of a degradation pathway for unfolded proteins was diminished (**Fig. 2A**). Validation of array results pointed out that *XbpI* splicing, increased in untreated Brtl OB, was significantly reduced upon 4-PBA administration, further indicating the efficacy of the compound in alleviating cell stress (**Fig. 2B**). The impact of 4-PBA on expression of stress genes was also mirrored by substantial improvement in cellular morphology. The ER cisternae, enlarged in mutant cells from both models, appeared normalized after treatment, as revealed by transmission electron microscopy imaging (TEM) (**Fig. 2C**).

Along with UPR genes, we demonstrated the beneficial effect of 4-PBA on apoptotic gene expression. We observed a substantial decrease in the number of relevant upregulated genes in both models following 4-PBA administration (**Fig. 2A**). Expression of TNF family genes (*Tnfrsf10b*, *Tnfrsf11b*, *Tnfrsf1a* in Brtl; *Tnf*, *Tnfrsf1a* in Amish) was lowered by 4-PBA, together with genes that mediate the apoptotic cascade, in particular caspases (*Casp2*, *3*, *6*, *8* and *9* in Brtl; *Casp1*, *2*, *3*, *4*, *7* in Amish). Furthermore, Brtl cells displayed reduced expression levels of death domain receptors such as *Dapk1* and *Fadd* (**Fig. 2A**). Expression of apoptosis regulation factors was also reduced in both models upon treatment, in particular decreased expression of *Bcl* genes and their regulators suggests a general mitigation of the pathway activation. Reduction of cleaved caspase 3 expression by immunofluorescence analysis (**Fig. 2D**) further supported the findings at the transcript level that 4-PBA administration attenuates the apoptotic cascade in OI OBs from both murine models.

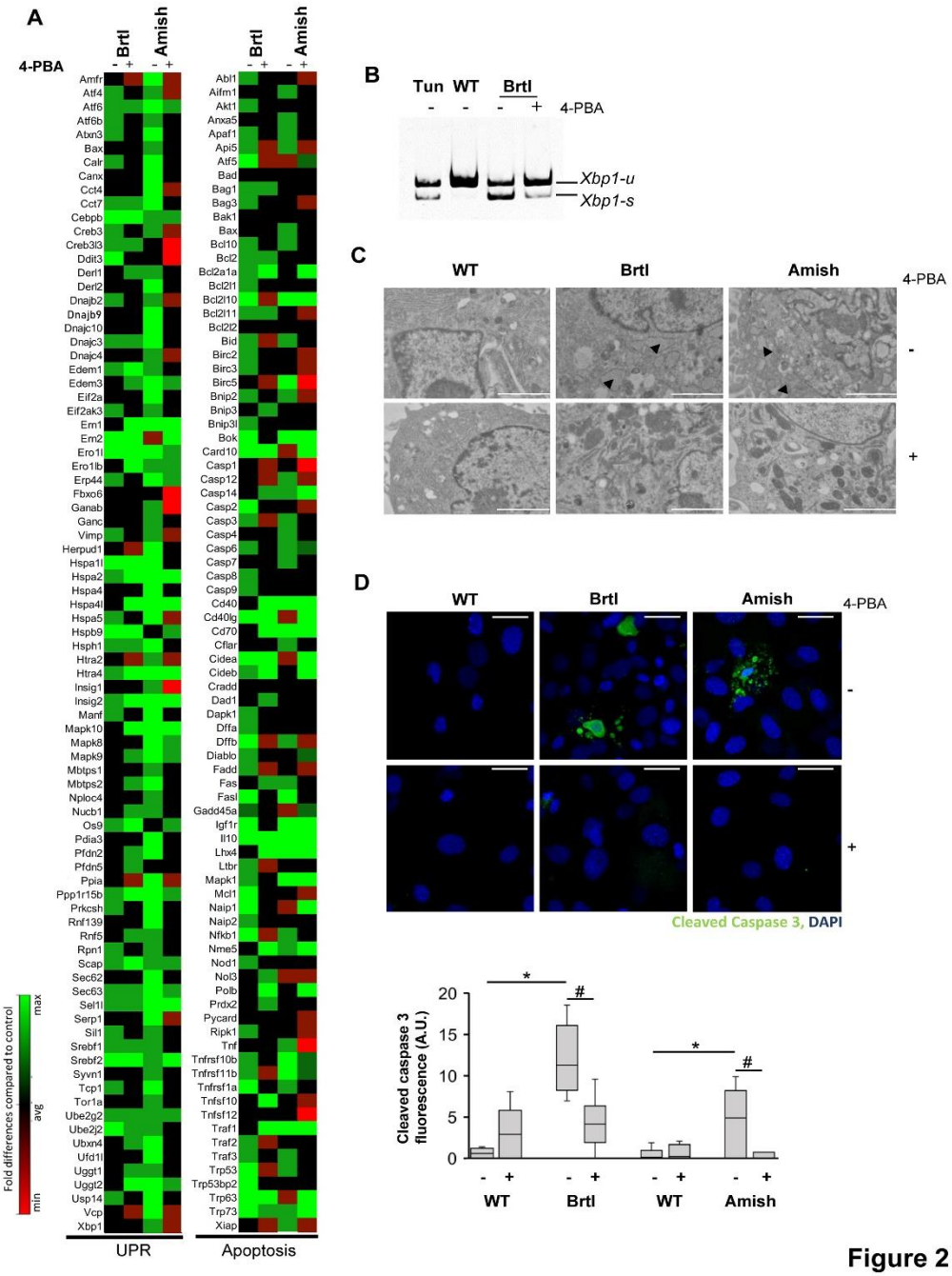

Figure 2

Figure 2: 4-PBA ameliorates Brtl and Amish osteoblast homeostasis. (**A**) qPCR-based array heat map of relative expression of genes involved in UPR, autophagic and apoptotic pathways in Brtl and Amish OBs in the absence (-) or presence (+) of 4-PBA. Results are expressed as fold differences compared to control. 4-PBA mainly reduced or normalized the upregulated genes. (**B**) RT-PCR amplification of *Xbp1* mRNA from control and Brtl untreated (-) and 4-PBA (+) treated OBs. *Xbp1-s* is reduced by 4-PBA. cDNA from OBs

treated with the stress inducing compound tunicamycin were used as positive control for ER stress. (**C**) Transmission electron microscopy representative images of OI OBs in absence (-) or presence (+) of 4-PBA. The analyses revealed ER enlargement (arrowhead) in mutant cells that was rescued by 4-PBA treatment. Magnification 20000X. (**D**) Representative immunofluorescence images and quantification of cleaved caspase 3 in WT and mutant OBs in absence (-) or presence (+) of 4-PBA. Quantitation of the total area of punctate signal indicated increased cleaved caspase 3 level in mutant OBs, pointing to the activation of apoptosis. 4-PBA treatment reduced the apoptotic marker signal in mutated cells. Nuclei were stained with DAPI. Magnification 40X, zoom 4X. *$p<0.05$ WT VS mutant, # $p<0.05$ 4-PBA treated VS untreated.

4-PBA reduces intracellular protein aggregation and stimulates secretion

Since TEM imaging highlighted a considerable ER enlargement in OI samples (**Fig. 2C**), we investigated the effect of 4-PBA on ER proteostasis by treating cells with the protein aggregate-binding fluorescent molecule Thioflavin T (ThT). Enhanced ThT fluorescence was found in Brtl and Amish OBs compared to controls, demonstrating the intracellular accumulation of misfolded material (**Fig. 3A**). Following 4-PBA treatment, mutated cells exhibited reduced ThT fluorescence. The reduction of ER protein accumulation (**Fig. 3A**) was further supported by increased general protein secretion (**Fig. 3B**), also detectable in WT cells.

Scanning electron microscopy (SEM) analysis was performed to visualize the 4-PBA effect on cellular morphology. While control OBs appeared as a flat layer, Brtl and Amish untreated cells had an enlarged and rugged globular shape that was normalized following 4-PBA administration (**Fig. 3C**). The rounded Amish cells were characterized by an abnormal accumulation of calcium, colocalizing with phosphorus and oxygen, as revealed by energy-dispersive X-ray spectroscopy (**Fig. 3D**).

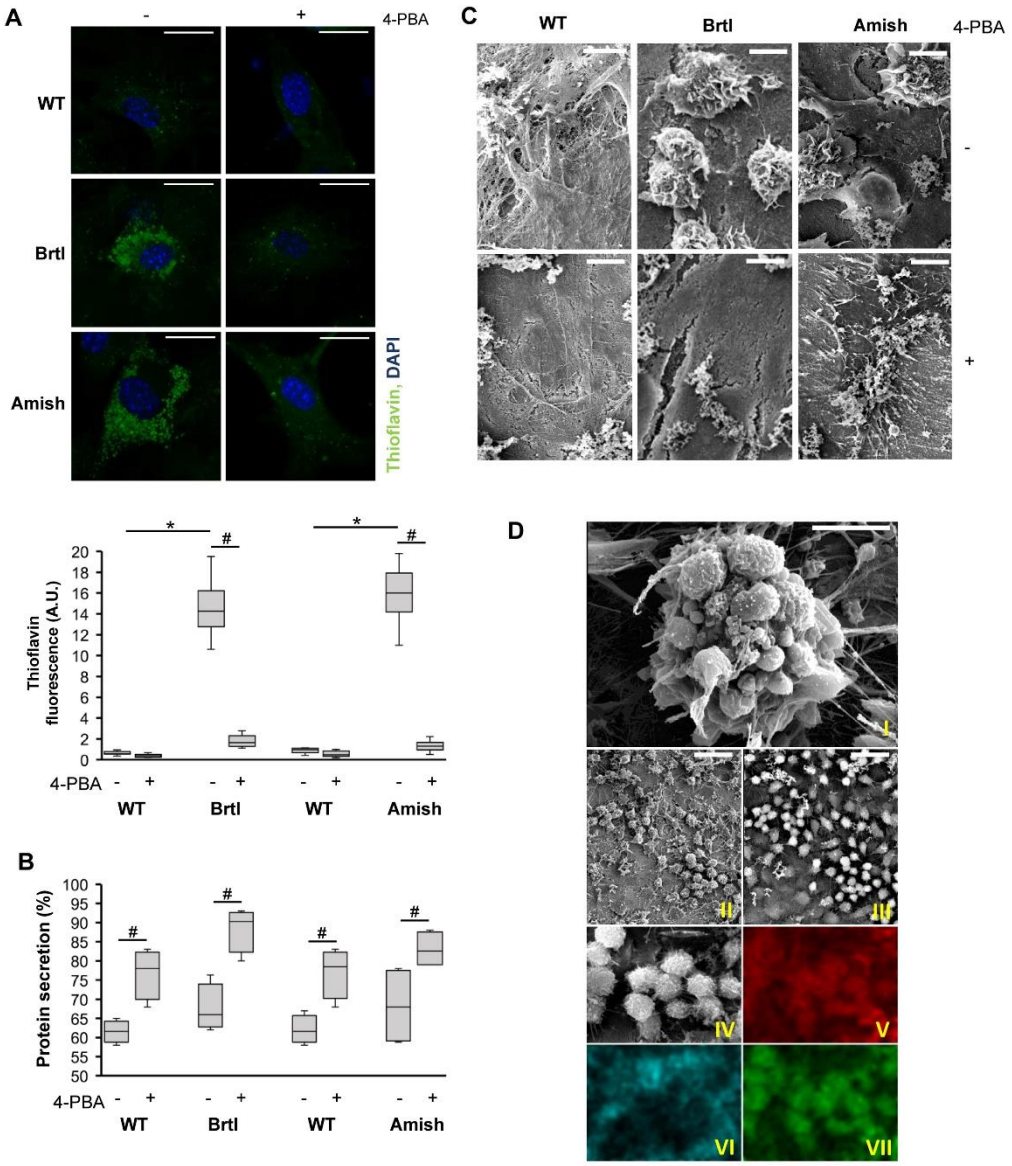

Figure 3

Figure 3: 4-PBA reduces intracellular protein aggregation and stimulates secretion. (**A**) ER proteostasis was evaluated by thioflavin T (ThT) immunofluorescence. Representative images and ThT quantification are shown. ThT fluorescence was increased in mutant cells compared to control, highlighting the intracellular accumulation of misfolded proteins. 4-PBA treatment significantly reduced ThT fluorescence, proving its ability in stimulating proteostasis. *p<0.05 WT VS mutant, # p<0.05 4-PBA treated VS untreated. (**B**) Protein secretion was evaluated in absence (-) or presence (+) of 4-PBA. The drug stimulated protein secretion in WT, Brtl and Amish cells. # p<0.05 4-PBA treated VS untreated. (**C**) Scanning electron microscopy representative images of Brtl, Amish and control OBs in the absence (−) or presence (+) of 4-PBA. Morphology analyses showed the presence of rounded

cells in mutant samples respect to the dark flat layer of control cells. 4-PBA improved mutant cells morphology. Magnification 2500X. (**D**) Amish OBs morphology was evaluated by SEM. **I.** The analyses revealed the presence of rounded cells with a rough surface. Magnification 5000X. **II.** Rounded cells. Magnification 500X. **III.** Ca^{2+} accumulation in Amish OBs is highlighted by a higher signal in backscattered electron imaging. Magnification 500X. **IV.** A cluster of Amish OBs in conventional secondary electrons is shown. Magnification 1200X. **V-VI-VII.** Energy-dispersive X-ray spectroscopy showed in false colour the corresponding mapping of calcium (red), sodium (light blue) and phosphorus (green). Note the perfect colocalization of calcium and phosphorus, compared with the unrelated distribution of sodium.

Collagen accumulation in ER is diminished upon 4-PBA administration

4-PBA stimulation of protein secretion leaves open the question about its specific effect on collagen molecules. A strong ER collagen accumulation was observed in Brtl and Amish cells compared to controls by its colocalization with the PDI marker and not with the Golgi marker GM130 (**Fig. 4**, **Supplementary fig. 2**). The increased LAMP1 signal and COLI-LAMP1 colocalization in Brtl and Amish cells are also indicative of the cellular attempt to cope with collagen accumulation by enhancing the degradative pathway (**Fig. 4, Supplementary fig. 1**). Importantly, incubation with 4-PBA substantially prevented intracellular collagen accumulation, as demonstrated by normalized intracellular collagen signal in the two models and substantially reduced COLI-PDI and COLI-LAMP1 colocalization (**Fig. 4**). No difference in collagen overglycosylation was detectable upon treatment based on collagen electrophoretic analysis (**Supplementary fig. 3**).

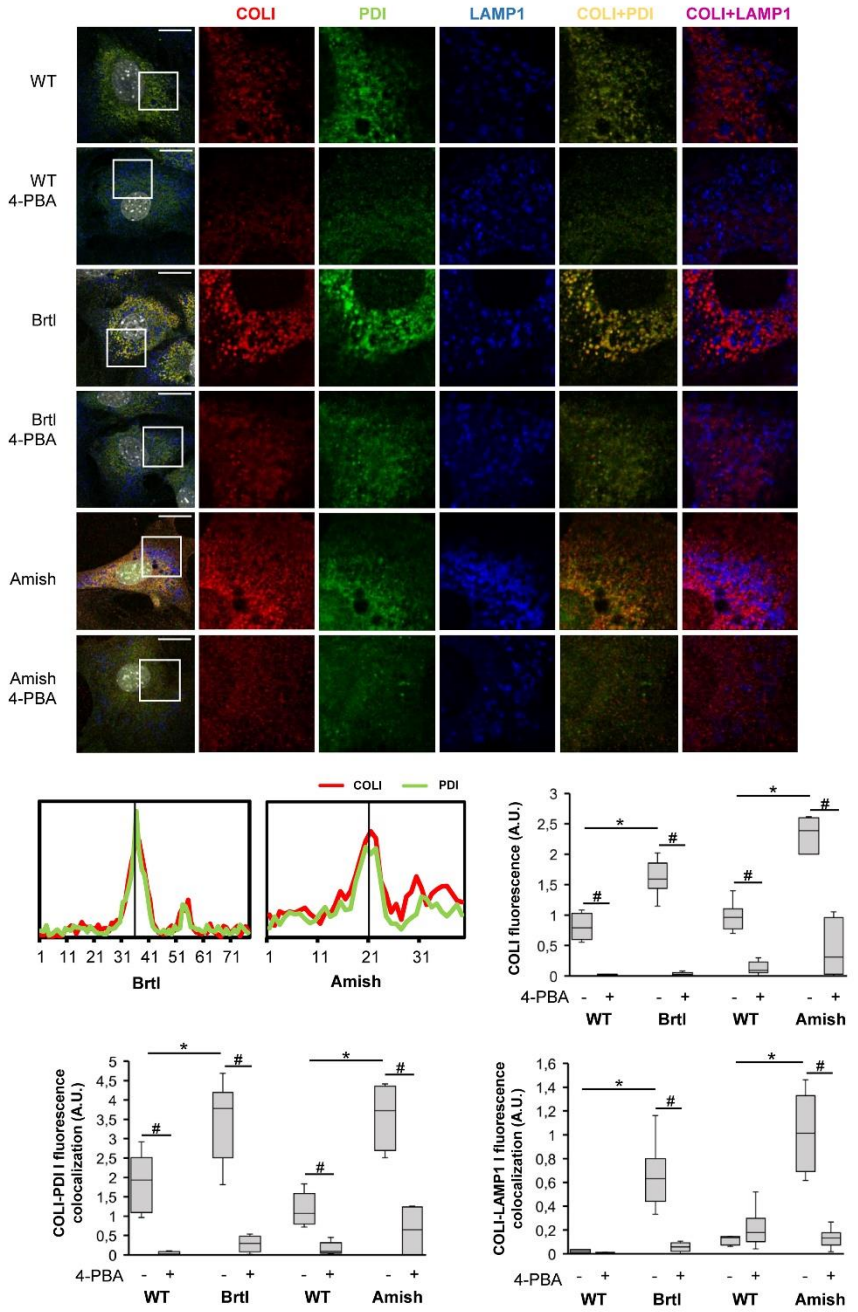

Figure 4: Collagen accumulation in the ER in OI OBs is relieved upon 4-PBA administration. (**A**) Representative images and quantification of multiple immunofluorescences of collagen (COLI), the ER marker PDI and the lysosomal marker LAMP1 on mutant and control OBs in the absence (−) or presence (+) of 4-PBA. Collagen accumulation is evident in mutant cells and reduced by 4-PBA treatment. Collagen molecules colocalize with PDI indicating its retention in the ER that is reduced by the treatment. LAMP1 expression is increased in mutant samples and reduced by the treatment.

Importantly, collagen colocalization with LAMP1 in mutant OBs was rescued by 4-PBA treatment. Nuclei were stained with DAPI. Magnification 63X, zoom 3X and 8X. Colocalization graphs of COLI-PDI signal in Brtl and Amish OBs is shown below the images indicating two overlapping peaks. *p<0.05 WT VS mutant, # p<0.05 4-PBA treated VS untreated.

Collagen matrix incorporation and maturation are improved by 4-PBA treatment

Since 4-PBA led to a substantial reduction of intracellular collagen content in mutated cells, we examined *Col1a1* expression by qPCR at different time points during mineralization and collagen protein synthesis by ^{3}H proline incorporation. 4-PBA reduced collagen expression in Brtl, Amish and control OBs, both at the transcript and protein level (**Fig. 5A-B**). Nevertheless, the treatment with 4-PBA specifically increased collagen secretion in mutated cells (**Fig. 5C**). Matrix analyses revealed that the incorporation of collagen into mutant decellularized matrix increased after treatment in comparison to treated control (**Fig. 5D**). In untreated samples SEM imaging showed that control cells were surrounded by an abundant matrix of uniform collagen fibers, on which small proteoglycans were deposited in an organized fashion, while the matrix deposited by mutated cells appeared less organized, and thinner immature fibrils were present (**Fig. 5E**). 4-PBA administration in mutant cells resulted in a more mature matrix (**Fig. 5F**) characterized by the presence of thicker collagen fibrils (**Fig. 5E**).

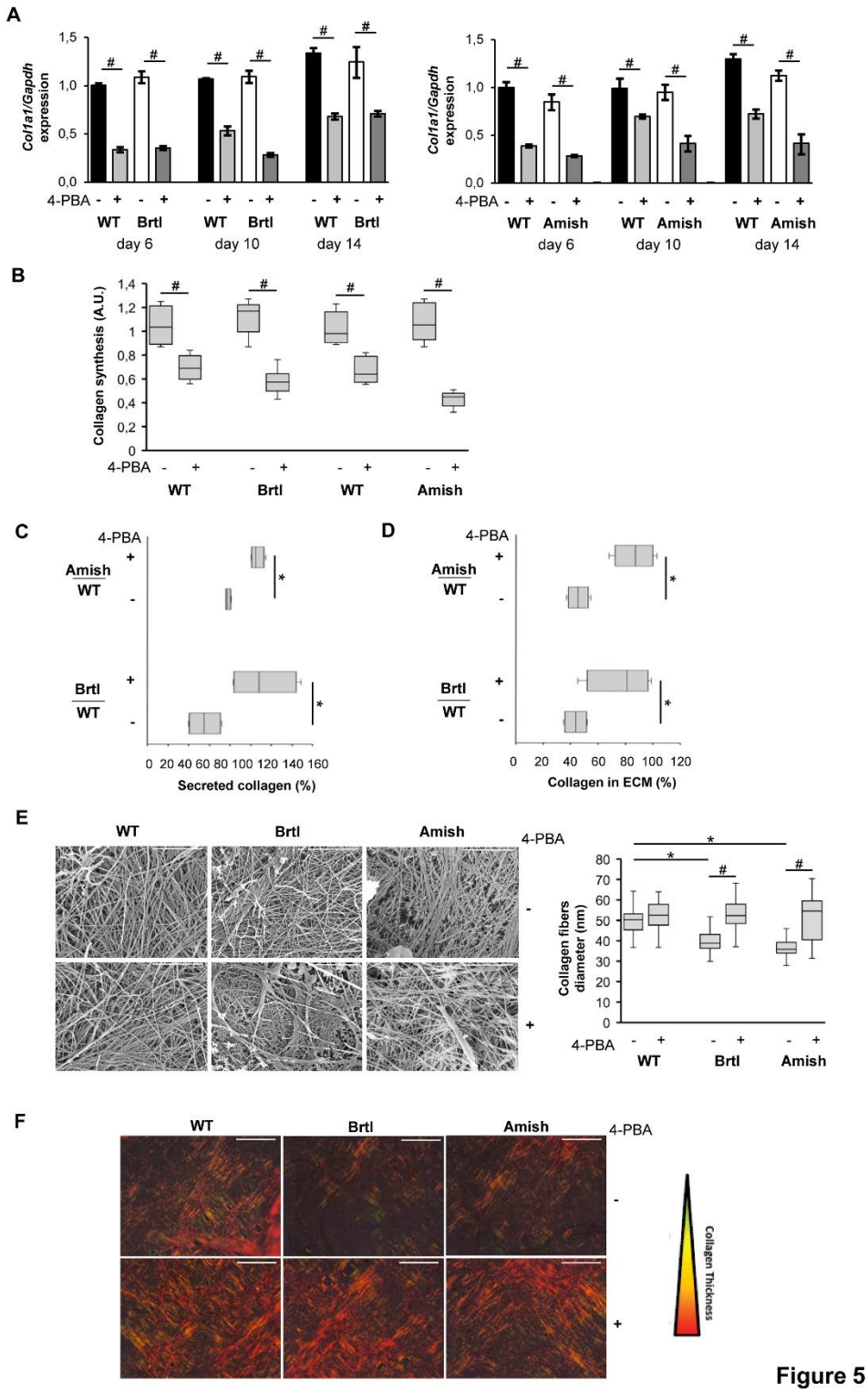
A
Col1a1/Gapdh expression
1,5
1,0
0,5
0,0
4-PBA - + - + - + - + - + - +
WT Brtl WT Brtl WT Brtl
day 6 day 10 day 14
WT Amish WT Amish WT Amish
B
Collagen synthesis (A.U.)
1,4
1,2
1
0,8
0,6
0,4
0,2
0
WT Brtl WT Amish
C
4-PBA
Amish / WT
Brtl / WT
0 20 40 60 80 100 120 140 160
Secreted collagen (%)
D
Collagen in ECM (%)
E
WT Brtl Amish
4-PBA
Collagen fibers diameter (nm)
80
70
60
50
40
30
20
10
0
F
Collagen Thickness

Figure 5

Figure 5: Collagen maturation and incorporation into the matrix are improved by 4-PBA treatment. (**A**) qPCR analysis of *Col1a1* expression in mutated and control OBs at 6, 10 and 14 days of culture in osteogenic media in the absence (−) or presence (+) of 4-PBA. The drug reduced collagen expression in all samples at each time point. *p<0.05 WT VS mutant, # p<0.05 4-PBA treated VS untreated. (**B**) Collagen synthesis in mutated and control OBs in standard culture conditions was evaluated by ^{3}H proline incorporation assay in the absence (−) or presence (+) of 4-PBA. The drug administration diminished collagen content in all samples, but more consistently in control. (**C**) Collagen secretion was also evaluated. At basal level, mutated cells presented impaired secretion compared to WT, while treatment with 4-PBA specifically increased collagen secretion in both Brtl and Amish OBs. (**D**) The amount of collagen incorporated into the ECM was evaluated in mutated and control OBs grown in osteogenic media for 21 days in absence (-) or presence (+) of 4-PBA. Collagen content was reduced in both Brtl and Amish samples but that upon treatment the incorporation of collagen in mutant decellularized matrix increased with respect treated control. (**E**) SEM images of mutant and control collagen fibrils produced by OBs. Mutated fibrils appeared thinner and their size was increased when treated with 4-PBA. Magnification 10000X. *p<0.05 WT VS mutant, # p<0.05 4-PBA treated VS untreated. (**F**) Sirius red staining highlighting collagen fibers in OBs matrix. Immature fibers are green, mature fibers are red. While mutated untreated cells present more immature fibers than control, 4-PBA treatment improves collagen fibrils maturation. Magnification 10X.

4-PBA promotes mineralization in Brtl and Amish OBs

The effect of 4-PBA on matrix mineralization was also investigated. Mineral staining by alizarin red highlighted an impaired mineral deposition in mutated cells, as well as a boost in mineral deposition after 4-PBA administration in both models (**Fig. 6A**). Accordingly, the activity of the alkaline phosphatase (ALP) enzyme was increased upon treatment (**Fig. 6B**). Enhanced expression of the early osteoblast differentiation markers zinc-finger transcription factor (*Osx*) and alkaline phosphatase (*Alp*) was also stimulated by 4-PBA during mineralization (**Fig. 6C-D**).

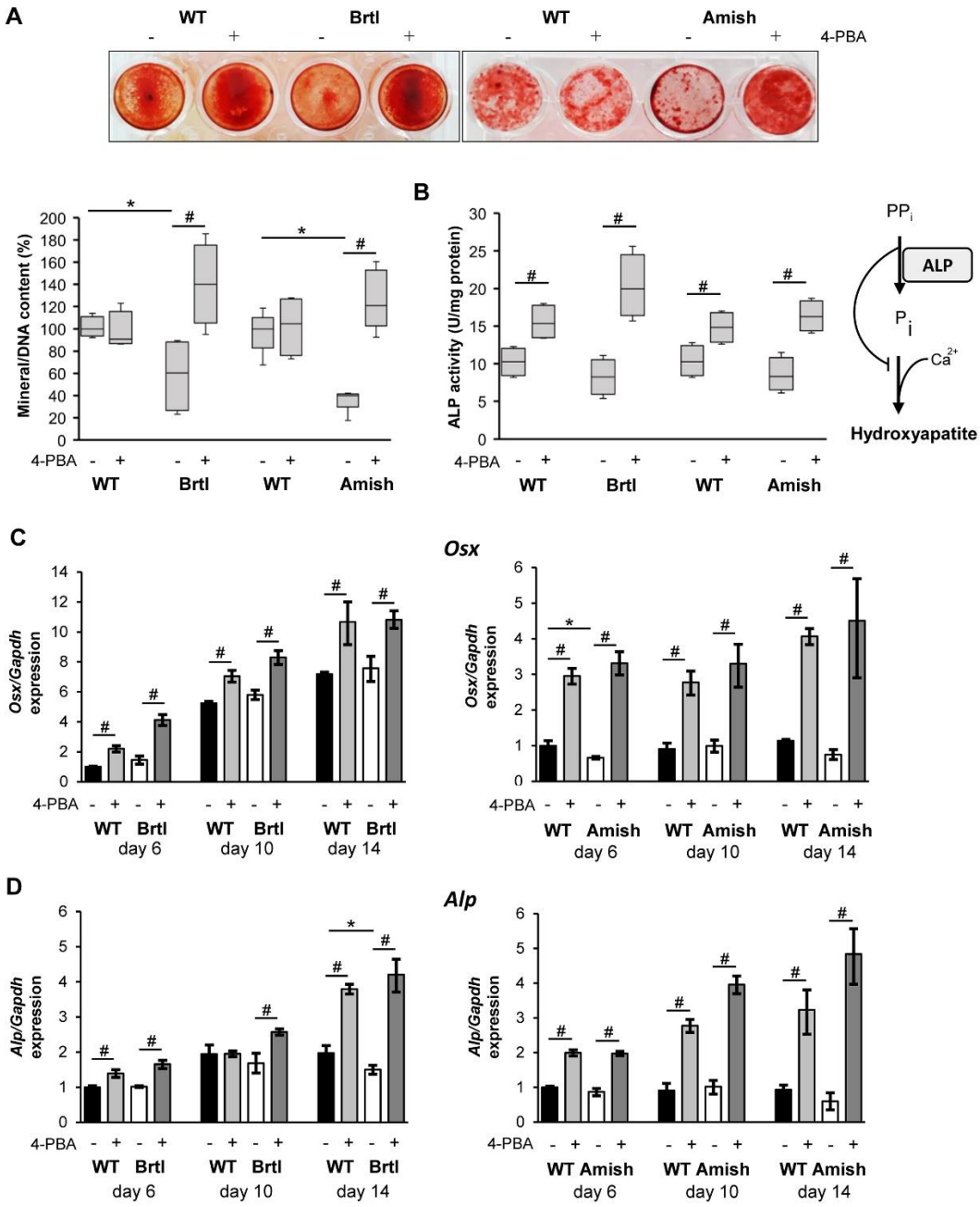

Figure 6

Figure 6: 4-PBA promotes mineralization in Brtl and Amish OBs. (**A**) Alizarin red staining of primary OBs cultured in osteogenic medium in absence (−) or presence (+) of 4-PBA. OBs mineral content was quantified. A decreased mineral staining in Brtl and Amish cells was evident. Upon 4-PBA treatment, an increased mineral content was found, demonstrating the positive action of the drug in stimulating OBs mineralization. (**B**) ALP

activity in osteogenic medium in absence (−) or presence (+) of 4-PBA was evaluated by enzymatic assay. A significant enhancement of ALP activity was detected in mutant and control cells following 4-PBA administration. (**C-D**) Real time PCR analyses of *Alp* and *Osx* expression in Brtl and Amish OBs at day 6, 10 and 14 of culture in osteogenic medium in absence (−) or presence (+) of 4-PBA. 4-PBA promoted genes expression in mutant and WT cells at all time points analyzed. *$p<0.05$ WT VS mutant, # $p<0.05$ 4-PBA treated VS untreated.

Discussion

In the present work, we have addressed the consequences of the presence of mutant collagen in OI osteoblasts and its role as a target for chaperone-based therapy to ameliorate cell homeostasis and matrix quality. OI phenotype is traditionally mainly attributed to the presence of structural abnormal collagen in the bone ECM, where it hampers structural integrity impairing cell-matrix interaction and providing a defective scaffold for mineral deposition [32]. Thus, an extensive literature is available on bone extracellular matrix analysis both in humans and murine OI models, using both *in vitro* and *in vivo* approaches. However, the identification of proteins involved in collagen post-translational modifications and osteoblast differentiation as causal for recessive forms of OI, and the discovery that mutations in collagen I and in non-collagen genes can result in partial retention of procollagen in the ER cisternae, have shifted more attention to the intracellular environment [32, 56-58]. Indeed, collagen type I misfolding and intracellular accumulation is known to happen in cells of some OI patients and in OI animal models [10, 11, 23, 25, 47, 59-62]. The consequent activation of unfolded protein response and apoptosis was demonstrated in patient fibroblasts [23, 24, 59, 60], highlighting a malfunction associated to intracellular mutant collagen with a potential role in OI clinical pathology.

Human dermal fibroblasts are frequently used as a cellular model to study OI since they produce abundant collagen and are relatively easier to obtain than patient' osteoblasts. Nevertheless, OBs represent the critical affected cells in OI and, although the primary sequence of type I collagen in skin and bone is identical, bone collagen has a unique pattern of post-translational modifications, in particular of lysine hydroxylation, resulting in a tissue-specific chemical profile of pyridinoline and pyrrole crosslinking [63-65]. Consistently, collagen produced by OI osteoblasts has a more delayed electrophoretic migration than found in fibroblast collagen [62], suggesting a cell-specific metabolism of mutant collagen. Furthermore, besides

secreting matrix collagen, OBs also secrete mineralization precursors and initiators through matrix vesicles [66, 67].

Thus, here we investigated the stress response to intracellular collagen retention in primary osteoblasts from two dominant OI murine models, Brtl and Amish, carrying glycine substitutions in α1 or α2 type I collagen chains, respectively. OI bone cells activated UPR, autophagy, and finally apoptosis in response to the stress of mutant collagen (**Fig. 1A**), reproducing findings from patient fibroblasts [23]. The transcriptomic investigation allowed us to better dissect the stress response elicited by collagen accumulations. In the Brtl model, a higher number of autophagic and apoptotic genes were deregulated, whereas in Amish the altered expression primarily involved UPR genes. Nevertheless, being the mutant collagen constitutively produced in both models, the activation of cell apoptosis was demonstrated in both Brtl and Amish OBs. The differential intracellular response may be due to the stoichiometry of collagen, indeed 75% of mutant collagen is synthetized in cells carrying α1(I) mutations and 50% in presence of α2(I) defects. A common expression pattern of molecular chaperones and heat shock proteins is shared by both models. The UPR activation occurs through the PERK branch in Brtl and Amish (**Fig. 1A-B**), in agreement with human fibroblasts carrying α1(I) or α2(I) mutations [23]. The IRE1α branch is also enhanced in Brtl OBs, while the unchanged level of spliced *Xbp1* (*Xbp1-s*), one of its effectors, in Amish OBs is in agreement with previously reported findings [11]. Nevertheless, we cannot exclude IRE1α cascade activation in this model, given the upregulation of several *Xbp1-s* target genes, including *Dnajc3*, *Dnajb9*, *Edem1* and *Serp1*, in Amish cells [68] (**Fig. 1A**). Despite the activation of the autophagic pathway in both models, putatively in an attempt to clear the engulfed ER, increased expression of several members of the caspases family suggests that cellular response to ER stress moves towards apoptosis, with a stronger pathway activation in Brtl OBs, indicated by higher level of the terminal cleaved caspase 3 (**Fig. 2D**).

The response to ER stress is an important modifier of disease severity in many human pathologies [69], including skeletal diseases such as those with mutations in the ECM components matrilin 3, COMP and collagen X [2-5, 8, 70]. For instance, the onset of a metaphyseal chondrodysplasia phenotype in mice in which ER stress was artificially triggered in hypertrophic chondrocytes demonstrated the potential for a direct pathological role of ER stress in the etiology of the disease [71]. Studies in mouse models indicate that the effect of ER stress signaling (ERSS) and the nature of the cellular strategies induced to ameliorate pathological ER stress are crucial factors in determining cell fate and clinical disease features [7]. Importantly, ERSS can affect cellular proliferation and differentiation, and cell-autonomous adaptation strategies can generate a spectrum of cellular consequences, ranging from recovery to death. ERSS alters both the transcriptome and proteome of a cell, affecting its metabolic status and, likely, impairing its secretory abilities with a secondary extracellular effect that may contribute to the phenotypic variety of the disease. Indeed, in the Brtl mouse, differential expression of chaperones, proteasomal subunits, metabolic enzymes, and proteins related to cellular fate revealed a superior ability to adapt to cellular stress in surviving Brtl mutant mice compared to lethal mice with the same molecular defect, and indicated the potential relevance of the cell response to the stress as an OI phenotype modulator [16, 72].

Based on these observations, targeting ER stress holds intriguing potential as a strategy to mitigate the phenotype in bone diseases caused by mutations in ECM components. ER stress targeting in skeletal disease has been already attempted and, for instance, an ECM amelioration was obtained in a mouse model of short-limbed dwarfism following treatment with carbamazepine, a compound stimulating autophagy and proteasomal degradation and, consequently, lowering misfolded proteins accumulation in the ER and UPR activation [73].

4-PBA, an ammonia scavenger drug which is FDA-approved for urea cycle disorders and hyperammonemia [74, 75] and a member of the histone deacetylase inhibitor family [76], has recently gained increasing attention for its chaperone-like activity

[77] and its efficacy in lowering ER stress markers and apoptosis in several non-skeletal [33-37, 42] and skeletal diseases, including OI [9, 23, 24, 78]. We recently demonstrated that 4-PBA treatment alleviates cell stress in dominant and recessive OI fibroblasts by restoring ER cisternae size, switching off activation of the PERK UPR branch and normalizing the expression of the apoptotic marker cleaved caspase 3 [23, 24].

Here we also confirmed the beneficial effects of 4-PBA in OBs from two OI murine models (**Fig. 2**). Using immunofluorescence imaging, we showed that 4-PBA treatment caused a significant decrease in the collagen accumulated in the ER (**Fig. 4**), thanks both to the ability of 4-PBA to down regulate collagen synthesis (**Fig. 5A-B**) and to increase collagen secretion (**Fig. 5C**). No difference in collagen overmodification after treatment was evident by electrophoretic analysis (**Supplementary fig. 3**), indicating there was likely no effect on the delay in folding caused by the collagen substitution. A consistent effect on collagen secretion upon 4-PBA administration was previously shown in fibroblasts from a patient with a very C-terminal α1-G859S substitution, while a smaller effect was reported in cells containing other mutations spread along the N-terminal and mid-helical portion of the triple helical domain [23]. Interestingly, Brtl and Amish mutations fall at different helical positions, α1-G349 and α2-G610 respectively, nevertheless 4-PBA significantly stimulate collagen secretion in both. It is, therefore, tempting to speculate a stronger effect of the drug on cells, such as OBs, characterized by higher collagen production. It is important that 4-PBA action extends also to general protein secretion. The altered ER homeostasis due to mutant collagen retention is likely impairing proper folding of other ER proteins on which the chaperone effect of 4-PBA seems to play a role. Indeed, the drug stimulated general protein secretion while reducing protein aggregates in osteoblasts in both models (**Fig. 3A-B**), as was reported in fibroblasts from both dominant and recessive patients [23, 24]. An intriguing mechanism has recently been proposed to explain the action of 4-PBA in regulating protein secretion. The COPII coat protein Sec24, a component of the

secretory path necessary for the translocation of proteins from the ER to the Golgi, was recently identified as a 4-PBA target. The authors showed that 4-PBA action on Sec24 promotes COPII packaging of ER proteins, stimulating sorting and reducing trafficking stringency [79]. It will be interesting to evaluate this mechanism in OI cells as well.

Whether and how 4-PBA administration affects ECM is still a puzzling question. The use of this drug in mice in presence of type IV collagen mutation was beneficial in lowering ER stress markers and increasing collagen IV secretion and incorporation into kidney basement membrane but without improving its ultrastructure [80]. In a very recent work, 4-PBA has been shown to reduce the amount of misfolded type I collagen in ECM laid down by OI fibroblasts and to either augment iPSCs differentiation ability toward OBs or favour mineral deposition in fibroblast-derived iPSCs differentiated to OB [81].

Importantly, we demonstrated for the first time a positive effect of 4-PBA on ameliorating the quality of ECM deposited by primary osteoblasts (**Fig. 5-6**). Our data suggested that upon 4-PBA incubation, collagen fibers deposited by mutant OBs appear more mature and better organised (**Fig. 5E-F**). Even though 4-PBA reduced collagen expression (**Fig. 5A-B**), a selective effect on mutated cells was evident. After treatment, collagen secretion and ECM incorporation were significantly increased in mutant OB compared to controls (**Fig. 5D**).

Together with collagen deposition, mineralization is another fundamental process of bone formation that was impaired in Brtl and Amish OBs *in vitro* (**Fig. 6A**). 4-PBA administration promotes ALP enzyme activity, stimulates mineral deposition and increases calcium deposits in Brtl and Amish OBs (**Fig. 6A-B**), providing the molecular bases for the increased bone mineralization in the treated OI zebrafish model Chihuahua [43].

It is relevant that histone acetylation is an important epigenetic mechanism that controls bone-associated gene expression because 4-PBA was reported to act as a histone deacetylase inhibitor, allowing the transcription of osteogenetic genes,

promoting cell proliferation/maturation and ALP activity in OBs cultures [82-86]. Indeed, an increased level of acetylation of histone H3 was found in Brtl and Amish OBs upon treatment (**Supplementary fig. 4**), supporting the drug effect on *Osx* and *Alp* at the transcriptional level.

In conclusion, our findings demonstrated the efficacy of 4-PBA both in restoring OI osteoblast homeostasis, and in improving extracellular matrix collagen organization and mineralization. This *in vitro* investigation supports further *in vivo* studies in animal models of the promising roles of chemical chaperons in the treatment of OI to determine their effects on bone tissue strength, cellularity, mineralization and growth.

Materials and Methods

Mouse strain and genotyping

CD1/129Sv/B6 *Col1a1*$^{+/G349C}$ (Brtl) [46] and CD1/CH3/B6 *Col1a2*$^{+/G610C}$ (Amish) [47] mice, carrying a heterozygous G349C substitution in the collagen I α1 chain and a G610C substitution in the collagen I α2 chain, respectively, were used for this study. The Amish mice were kindly provided by Prof Charlotte Phillips, University of Missouri-Colombia, USA. Mutant mice and WT littermates were maintained under standard experimental animal care protocol following Italian Laws in the centralized animal facility of the University of Pavia, Italy. All the experiments were approved by the OPBA (Office for the Animals Welfare) of the University of Pavia and by the Italian Ministry of Health (protocol n. 243/2018-PR, 27/03/18), complied with the ARRIVE guidelines and were carried out in accordance with the EU Directive 2010/63/EU for animal experiments. Genomic DNA was extracted from tail clip and genotyping was performed by PCR as previously reported [46, 47].

Calvarial osteoblast culture

Murine osteoblasts were isolated from 2-4 days old WT and mutant pups [87]. Cells from at least three animals with the same genotype were pooled together to obtain a sufficient number for experiments. After sacrifice, calvariae were removed, cleaned from fibrous tissues and sutures, washed twice with Phosphate Buffer Saline (PBS) at 37°C for 10 min in a shaker water bath and sequentially digested with 200 U/mL collagenase type II (GIBCO) at 37°C for 15 min. Cells obtained from the first two digestions were discharged, whereas cells from digestions 3, 4 and 5 were passed through a 70-μm polypropylene mesh filter and cultured in α-Modified Eagle's Medium (α-MEM, Lonza) supplemented with 10% fetal bovine serum (FBS, Euroclone), 50 μg/ml sodium ascorbate (Fluka) 4 mM glutamine (Euroclone), 100 μg/ml penicillin and streptomycin (Euroclone) at 37°C in humidified atmosphere containing 5% CO_2. Cells were used at passage 1.

For each experiment, except when differently stated, $1.5x10^4/cm^2$ were plated, cultured with no media change with the addition every other day of 50 µg/ml ascorbic acid and harvested after 5 days. For drug treatment, cells were incubated for 15 hours with 5 mM 4-phenylbutyrate (4-PBA, Sigma-Aldrich) before harvesting. To inhibit lysosome-autophagosome fusion, cells were incubated with 10 µM chloroquine (Sigma-Aldrich) for 6 hours. To induce ER stress, osteoblasts were treated with 2 µg/mL tunicamycin for 16 hours before harvesting. For mineralization studies, cells were cultured in α-MEM with 20% FBS, antibiotics, 100 µg/ml L-ascorbic acid (Sigma-Aldrich), and 10 mM β-glycerophosphate (Sigma-Aldrich) (osteogenic medium). The medium was changed three times a week. Harvest was performed at different time points, as detailed below.

Transcriptomic analyses

Total RNA was extracted from OBs from 3 independent cells preparations per genotype in absence or presence of 4-PBA with QIAzol Lysis Reagent (Qiagen) and purified by miRNeasy Mini Kit (Qiagen) according to the manufacturer's protocol. RNA concentration was determined by nanodrop and its integrity was verified on agarose gel. cDNA synthesis was performed using RT^2 First Strand kit (Qiagen) according to the manufacturer's protocol. The expression of key genes involved in UPR, autophagy and apoptosis was evaluated by Unfolded Protein Response RT^2 Profiler PCR Array, Autophagy RT^2 Profiler PCR Array and Apoptosis RT^2 Profiler PCR Array (Qiagen) using RT^2 SYBR Green Mastermix, according to the manufacturer's instructions. Arrays were performed on the QuantStudio3 thermocycler (Thermofisher). Data were analyzed using GeneGlobe Data Analysis Center software (Qiagen), five housekeeping genes (*Actb*, *B2m*, *Gapdh*, *Gusb*, *Hsp90ab1*) were used for normalization.

Xbp1 splicing analyses

cDNA from control and mutant cells, cultured in absence or presence of 4-PBA or in presence of the stress inducer tunicamycin, was used for PCR amplification across the region of the *Xbp1* cDNA (NM_013842.3) containing the intronic target of IRE1α ribonuclease using 0.4 μM sense (nt 720-740; 5'-GAACCAGGAGTTAAGAACACG-3') and antisense (nt 924-905; 3'-AGGCAACAGTGT CAGAGTCC-5') primers. Reactions were cycled as follows: 3 min at 95°C, followed by 35 cycles of 95°C for 40 sec, 60°C for 45 sec and 72°C for 40 sec, lastly a 10 min extension at 72°C was applied. The *Xbp1* unspliced form (205 bp) and the *Xbp1* spliced form (179 bp) were visualized on 8% TBE acrylamide gel. Biological triplicates were performed.

Protein lysates

Cultured osteoblasts were collected in PBS upon scraping, centrifuged at 1000 × g for 4 min, lysed and sonicated in RIPA buffer (150 mM NaCl, 1% IGEPAL® CA-630, 0.5% sodium deoxycholate, 0.1% SDS, and 50 mM Tris, pH 8) supplemented with protease inhibitors (5 μl/ml phenylmethanesulfonylfluoride and 2 mM Na_3VO_4, pH 10). Proteins were quantified by QuantumProtein Bicinchoninic Protein Assay Kit (Euroclone). Bovine serum albumine (BSA) (Sigma-Aldrich) was used as standard.

Western blot

Proteins from osteoblasts lysates (10 μg) were run on SDS-PAGE in 10% and 15% acrylamide gels for ATF4 and LC3, respectively. The proteins were electrotransferred to a PVDF membrane (GE Healthcare) at 100 Volt for 2 h on ice in 19 mM Tris-HCl, 192 mM glycine and 20% (v/v) methanol. The membranes were then blocked with 5% (w/v) BSA in 20 mM Tris-HCl, 500 mM NaCl, pH 7.5 (TBS), 0.05% (v/v) Tween-20 (Sigma-Aldrich) (TBS-T) at RT for 1 h. The membranes were incubated with 1:1000 primary antibody against the specific proteins LC3A/B (Cell

Signaling), ATF4 (Novus Biological) in 5% BSA in TBS-T o/n at 4°C. The secondary antibody (Cell Signaling) was added at dilution of 1:2000 in 5% BSA in TBS-T for 1 h at RT. The signal was detected by ECL western blotting detection reagents (GE Healthcare) and images were acquired with ImageQuant LAS 4000 (GE Healthcare), using the ImageQuant LAS 4000 1.2 software. Band intensities were evaluated by densitometry, using ImageQuant TL analysis software. Biological triplicates were performed. For each gel, the intensity of the control band was set equal to one and the expression of the mutant samples was expressed as fold difference. Actin was used for protein loading normalization.

Fluorescence Activated Cell Sorting (FACS)

Apoptosis was evaluated by Fluorescence Activated Cell Sorting (FACS) using Annexin V/Dead Cell Apoptosis Kit (Invitrogen), following manufacturer's instruction in four independent OBs preparations. Cells incubated with 20 μM thapsigargin (Sigma-Aldrich) for 24 h in serum-free D-MEM were used as positive control for the activation of apoptosis. Samples were analyzed by Attune NxT Acoustic Flow Cytometer (Thermo Fisher), 1×10^4 events for each sample were considered measuring the fluorescence emission at 515-545 nm (FITC) and 675-715 nm (PI), to avoid fluorescence spillover.

Transmission electron microscopy analysis

For transmission electron microscopy analysis, following trypsinization osteoblasts were centrifuged at 1000 × g for 3 min. Incubation with 1% glutaraldehyde in culture medium for 2 h at room temperature (RT) was used to fix the cell pellet, which was then rinsed in PBS and in H_2O. Finally, OB were fixed in 2% (w/v) OsO_4 in H_2O for 2 h at RT, rinsed in distilled water and embedded in 2% agarose. The specimens were dehydrated in acetone and infiltrated with Epoxy resin overnight (o/n) and polymerized in gelatin capsules at 60°C for 48 h. Thin sections (60-70 nm thick) were cut on a Reichert OM-U3 ultramicrotome with a diamond knife and collected

on 300-mesh nickel grids. Saturated aqueous uranyl acetate by lead citrate was used to stain the grids. A Zeiss EM900 electron microscope, operated at 80 kV with objective aperture of 30 µm was used for the analysis.

Thioflavin T labelling

OBs from three independent preparations were plated on sterile glass coverslips (Marienfeld) in 24 well plate and cultured for 4 days before incubation with 5 µM thioflavin (ThT, Sigma-Aldrich) for 15 h in presence or absence of 4-PBA. Cells were then fixed with 4% paraformaldehyde (PFA) in PBS for 20 min at RT. 4',6-diamidino-2-phenylindole (DAPI, Sigma-Aldrich) was used for staining nuclei. Images were acquired by SP8- Leica confocal microscope (Leica). The total area of punctate signal per cell was measured using the Leica software LAS4.5.

Protein secretion

OBs from three independent preparations were plated in 24 well plate and labelled with 5 µCi/ml [^{35}S] EXPRESS35S Protein Labeling Mix (PerkinElmer) in D-MEM without L-methionine, L-cystine, and L-glutamine for one h at 37°C. The precipitation of the medium and cell layer total proteins was carried out with 10% trichloroacetic acid. Following acetone washing the pellet was resuspended in 60 mM Tris-HCl, pH 6.8, 10% sodium dodecyl sulphate. The radioactivity (counts for minute, CPM) of the samples was quantified using a liquid scintillation analyzer (TRI-CARB 2300 TR). The percentage of protein secretion was calculated based on the ratio between the CPM in the media and the CPM in medium and cell layer.

Immunofluorescence

2×10^4 OB were plated on sterile glass coverslips (Marienfeld) in 24 well plate. After 4 days cells were treated for 15 h with 5 mM 4-PBA.

LC3 and cleaved caspase 3

For LC3 immunofluorescence, after 5 days cells were treated for 6 h with 10 μM chloroquine. On day 5, the medium was removed and cells were fixed with 10% neutral buffered formalin for 30 min at RT, washed 3 times with PBS and blocked 1 h in 1% BSA in PBS containing 0.3% TritonX100. LC3 primary antibody (Cell Signaling) and cleaved caspase 3 primary antibody (Cell Signaling) were used at 1:500 dilution in 1% BSA, 0.3% TritonX100 in PBS and the incubation was carried out o/n at 4°C. Following PBS washing, cells were incubated with secondary antibody (AlexaFluor 488 conjugated F(ab') fragment anti- rabbit IgG, Immunological Sciences) diluted 1:2000 and 1:400, respectively, in 1% BSA, 0.3% TritonX100 in PBS for 2 h at RT.

Collagen intracellular co-localization

For collagen localization studies, the medium was removed and cells were fixed for 45 min in 10% neutral buffered formalin and blocked with 0.5% BSA, 0.05% saponin, 50 mM NaCl and 15 mM glycine pH 7.4. For collagen colocalization with the ER marker PDI and with the Golgi marker GM130, cells were sequentially incubated o/n with COLI (1:100, SP1D8 hybridoma bank in mouse), PDI (1:200, Cell Signaling) and AlexaFluor 647 conjugated anti-GM130 antibody (1:100, BD Pharmingen) antibodies. The secondary antibodies AlexaFluor 546 goat anti- mouse IgG (Invotrogen) and AlexaFluor 488 conjugated F(ab') fragment anti- rabbit IgG (Immunological Sciences) were used. For collagen colocalization with the ER marker PDI and with the lysosome marker LAMP1, cells were sequentially incubated o/n with COLI (1:100, SP1D8 hybridoma bank in mouse), LAMP1 (1:200, Abcam) PDI AlexaFluor 647 conjugate (1:100, Invitrogen) antibodies. The secondary antibodies AlexaFluor 546 anti- mouse IgG (Immunological Sciences), and AlexaFluor 488 conjugated F(ab') fragment were used. All the antibodies were diluted in the previously described blocking buffer.

For both experiments, nuclei were stained with DAPI and images were acquired by confocal microscope TCS SP8 (Leica). The total area of punctate signal per cell and signals colocalization were measured by the Leica software LAS 4.5.

Scanning electron microscopy analysis

OBs were plated on sterile glass coverslips and cultured for 14 days with and without 2.5 mM 4-PBA. Cells were fixed for 1 h in Karnovsky fixative (8% paraformaldehyde, 0.4 M cacodylate buffer, 25% glutaraldehyde, 5% calcium chloride) and dehydrated in ethanol and hexamethyldisilazane. The specimens were mounted on appropriate stubs with a colloidal silver glue, gold coated with an Emitech K550 sputter-coater and observed with a Philips XL-30 FEG scanning electron microscope (Philips XL30FEG) fitted with secondary electron (SE) and backscattered electron (BSE) probes, and with an EDAX Sirion 200/400 dispersive X-ray spectroscopy apparatus. Elemental maps were obtained on selected specimens by X-ray dispersive spectroscopy and filtered using Adobe Photoshop.

Collagen analysis

To analyze the effect of 4-PBA on collagen synthesis, cells were labelled for 15 hours in absence or presence of 5 mM 4-PBA using 28.57 µCi of ^{3}H-Pro/ml. Collagen extraction from the media and cell layer was performed as previously reported [88]. Collagen was resuspended in Laemmli buffer (62 mM Tris-HCl, pH 6.8, 10% glycerol, 2% sodium dodecyl sulphate, 0.02% bromophenol blue) and the radioactivity (counts for minute, CPM) was measured using a liquid scintillation analyzer (PerkinElmer TRI-CARB 2300 TR).

Mineralized matrix decellularization and collagen quantification

Matrix decellularization was performed in four independent OBs preparations for each genotype as described in [89]. Briefly, cells were cultured for 21 days in osteogenic medium to allow matrix deposition. Following PBS washing, the matrix

was decellularized by incubation for 1 h in 50 mM tris-HCl buffer pH 8.0 containing 2 M KCl and 0.2% TritonX-100. The decellularized matrix was extensively washed with 10 mM Tris-buffer pH 8.0 and DNA extraction was performed to confirm decellularization. Collagen extraction and quantification from medium and decellularized matrix was performed using Sircol™ Soluble Collagen Assay (Biocolor), according to the manufacturer's protocol.

Mineralization assays and alkaline phosphatase activity

On day 21 of culture in osteogenic medium, cells were fixed in 10% formalin solution neutral buffered (Sigma-Aldrich) for 1 h and alizarin red staining was performed. Cells were incubated with 58 mM Alizarin Red S pH 4.1-4.3 (Merck) for 45 min. Mineral extraction was carried out by 10% acetic acid extraction and absorbance was measured at 405 nm [90]. Alizarin Red standards (30 µM to 4 mM) were used for calibration curve. DNA was used for normalization.

For the measurement of ALP activity, cells were maintained in osteogenic medium for 21 days in osteogenic media. ALP activity was measured in OB media using an alkaline phosphatase detection kit (Abnova) following manufacturer's instruction and normalized to total protein content.

Gene expression analysis by real time PCR

On day 6, 10 and 14 of culture in osteogenic medium, total RNA was extracted from three independent OBs preparations for each strain using QIAzol® Lysis Reagent (Qiagen) according to the manufacturer's protocol. RNA concentration was determined by Nanodrop. DNase digestion was performed using DNA-Free Kit DNase Treatment & Removal (Invitrogen). cDNA was synthetized using High Capacity cDNA Reverse Transctiption kit (Applied Biosystems). qPCR was performed on the QuantStudio3 thermocycler (Thermofisher) using PowerUp Syber Green Master Mix (Applied Biosystems) with custom primers for m*Alp* and m*Osx* with m*Gapdh* as normalizer (primers sequences available upon request), and using

Taqman Universal PCR Master Mix No Amp Erase UNG to analyze m*Col1a1* expression (Mm00801666_g1) with m*Gapdh* (Mm99999915_g1) as normalizer. All reactions were performed in triplicate. Relative expression levels were calculated using the ΔΔCt method.

Sirius red staining

OB were plated on sterile glass coverslips (Marienfeld) and after 4 days cells were treated for 15 h with 5mM 4-PBA. On day 5, the medium was removed and cells were fixed with 10% neutral buffered formalin for 30 min at RT, rinsed in PBA and H_2O and then stained for 1 h with 0.1% sirius red (Direct Red-80, Sigma-Aldrich) in saturated aqueous solution of picric acid. The specimens were then washed once in H_2O for 5 min and twice in acidified water for 20 sec, they were dehydrated in ethanol, washed twice in xylene for 1 min and mounted on Superfrost® Plus slides (VWR) with DPX Mountant for histology (Sigma-Aldrich). To evaluate Sirius red birefringence, stained cells were analyzed under polarized light by LeicaDM2500 equipped with L ICT/P polarizer and a digital color camera LEICA DFC295 (Leica).

Statistical analysis

Biological triplicates for each genotype and treatment were performed. Quantitative variables were expressed as mean ± standard deviation (SD). One-way repeated measures ANOVA was applied to evaluate genotype and treatment effect followed by post-hoc tests with the Bonferroni's correction. All data passed tests for normality and equal variance. A p value <0.05 was considered significant.

Author's contributions

Conceptualization: A.F., R.B.; Methodology: N.G., B.C., G.B., J.M., S.S., M.B., M.R., J.M., A.R., A.F., R.B.; Formal analysis: N.G., M.R., M.B., A.F., R.B.; Resources: A.R., M.R., M.B., A.F., R.B.; Data curation: N.G., A.F., R.B.; Writing original draft: N.G., A.F., R.B.; Writing - review & editing: all the coauthors; Supervision: A.F., R.B.; Project administration: A.F., R.B.; Funding acquisition: A.F., R.B.

Our colleague G.B. sadly passed away before manuscript submission.

Acknowledgments

We thank Dr. Patrizia Vaghi and Dr. Amanda Oldani, Centro Grandi Strumenti, University of Pavia, Italy, for the confocal analysis support; the animal facility "Centro di servizio per la gestione unificata delle attività di stabulazione e di radiobiologia" of the University of Pavia, Pavia, Italy to host the animals; the OPBA of the University of Pavia for supporting in animal protocol drawing up.

Declaration of Competing Interest

The authors report no conflict of interest.

Funding

This work was supported by Italian Ministry of Education, University and Research (MIUR) [Dipartimenti di Eccellenza (2018-2022)] to A.F. and by Fondazione Cariplo (2016-0417) to R.B.

Bibliography

1. Iozzo, R.V. and M.A. Gubbiotti, *Extracellular matrix: The driving force of mammalian diseases.* Matrix Biol, 2018. **71-72**: p. 1-9.
2. Leighton, M.P., et al., *Decreased chondrocyte proliferation and dysregulated apoptosis in the cartilage growth plate are key features of a murine model of epiphyseal dysplasia caused by a matn3 mutation.* Hum Mol Genet, 2007. **16**(14): p. 1728-41.
3. Nundlall, S., et al., *An unfolded protein response is the initial cellular response to the expression of mutant matrilin-3 in a mouse model of multiple epiphyseal dysplasia.* Cell Stress Chaperones, 2010. **15**(6): p. 835-49.
4. Piróg-Garcia, K.A., et al., *Reduced cell proliferation and increased apoptosis are significant pathological mechanisms in a murine model of mild pseudoachondroplasia resulting from a mutation in the C-terminal domain of COMP.* Hum Mol Genet, 2007. **16**(17): p. 2072-88.
5. Posey, K.L., et al., *Chondrocyte-specific pathology during skeletal growth and therapeutics in a murine model of pseudoachondroplasia.* J Bone Miner Res, 2014. **29**(5): p. 1258-68.
6. Marini, J.C., et al., *Consortium for osteogenesis imperfecta mutations in the helical domain of type I collagen: regions rich in lethal mutations align with collagen binding sites for integrins and proteoglycans.* Hum Mutat, 2007. **28**(3): p. 209-21.
7. Tsang, K.Y., et al., *In vivo cellular adaptation to ER stress: survival strategies with double-edged consequences.* J Cell Sci, 2010. **123**(Pt 13): p. 2145-54.
8. Boot-Handford, R.P. and M.D. Briggs, *The unfolded protein response and its relevance to connective tissue diseases.* Cell Tissue Res, 2010. **339**(1): p. 197-211.
9. Chan, W.C.W., et al., *Activating the unfolded protein response in osteocytes causes hyperostosis consistent with craniodiaphyseal dysplasia.* Hum Mol Genet, 2017. **26**(23): p. 4572-4587.
10. Lisse, T.S., et al., *ER stress-mediated apoptosis in a new mouse model of osteogenesis imperfecta.* PLoS Genet, 2008. **4**(2): p. e7.

11. Mirigian, L.S., et al., *Osteoblast Malfunction Caused by Cell Stress Response to Procollagen Misfolding in α2(I)-G610C Mouse Model of Osteogenesis Imperfecta.* J Bone Miner Res, 2016. **31**(8): p. 1608-1616.
12. Tonelli, F., et al., *Crtap and p3h1 knock out zebrafish support defective collagen chaperoning as the cause of their osteogenesis imperfecta phenotype.* Matrix Biol, 2020.
13. Forlino, A., et al., *New perspectives on osteogenesis imperfecta.* Nat Rev Endocrinol, 2011. **7**(9): p. 540-57.
14. Marini, J.C., et al., *Consortium for osteogenesis imperfecta mutations in the helical domain of type I collagen: regions rich in lethal mutations align with collagen binding sites for integrins and proteoglycans.* Hum Mutat, 2007. **28**(3): p. 209-21.
15. Rauch, F., et al., *Osteogenesis imperfecta type V: marked phenotypic variability despite the presence of the IFITM5 c.-14C>T mutation in all patients.* J Med Genet, 2013. **50**(1): p. 21-4.
16. Forlino, A., et al., *Differential expression of both extracellular and intracellular proteins is involved in the lethal or nonlethal phenotypic variation of BrtlIV, a murine model for osteogenesis imperfecta.* Proteomics, 2007. **7**(11): p. 1877-91.
17. Gagliardi, A., et al., *Cytoskeleton and nuclear lamina affection in recessive osteogenesis imperfecta: A functional proteomics perspective.* J Proteomics, 2017. **167**: p. 46-59.
18. Van Dijk, F.S. and D.O. Sillence, *Osteogenesis imperfecta: clinical diagnosis, nomenclature and severity assessment.* Am J Med Genet A, 2014. **164A**(6): p. 1470-81.
19. Taga, Y., et al., *Site-specific quantitative analysis of overglycosylation of collagen in osteogenesis imperfecta using hydrazide chemistry and SILAC.* J Proteome Res, 2013. **12**(5): p. 2225-32.
20. Forlino, A. and J.C. Marini, *Osteogenesis imperfecta.* Lancet, 2016. **387**(10028): p. 1657-71.
21. Kuznetsova, N.V., et al., *Structure, stability and interactions of type I collagen with GLY349-CYS substitution in alpha 1(I) chain in a murine Osteogenesis Imperfecta model.* Matrix Biol, 2004. **23**(2): p. 101-12.

22. Forlino, A., et al., *Selective retention and degradation of molecules with a single mutant alpha1(I) chain in the Brtl IV mouse model of OI.* Matrix Biol, 2007. **26**(8): p. 604-14.
23. Besio, R., et al., *4-PBA ameliorates cellular homeostasis in fibroblasts from osteogenesis imperfecta patients by enhancing autophagy and stimulating protein secretion.* Biochim Biophys Acta Mol Basis Dis, 2018. **1864**(5 Pt A): p. 1642-1652.
24. Besio, R., et al., *Cellular stress due to impairment of collagen prolyl hydroxylation complex is rescued by the chaperone 4-phenylbutyrate.* Dis Model Mech, 2019. **12**(6).
25. Gioia, R., et al., *Impaired osteoblastogenesis in a murine model of dominant osteogenesis imperfecta: a new target for osteogenesis imperfecta pharmacological therapy.* Stem Cells, 2012. **30**(7): p. 1465-76.
26. Morello, R., *Osteogenesis imperfecta and therapeutics.* Matrix Biol, 2018. **71-72**: p. 294-312.
27. Papapoulos, S.E., *Bisphosphonates: how do they work?* Best Pract Res Clin Endocrinol Metab, 2008. **22**(5): p. 831-47.
28. Ward, L.M., et al., *Alendronate for the treatment of pediatric osteogenesis imperfecta: a randomized placebo-controlled study.* J Clin Endocrinol Metab, 2011. **96**(2): p. 355-64.
29. Rauch, F., et al., *The effects of intravenous pamidronate on the bone tissue of children and adolescents with osteogenesis imperfecta.* J Clin Invest, 2002. **110**(9): p. 1293-9.
30. Bishop, N., et al., *Risedronate in children with osteogenesis imperfecta: a randomised, double-blind, placebo-controlled trial.* Lancet, 2013. **382**(9902): p. 1424-32.
31. Papapoulos, S.E. and S.C. Cremers, *Prolonged bisphosphonate release after treatment in children.* N Engl J Med, 2007. **356**(10): p. 1075-6.
32. Marini, J.C., et al., *Osteogenesis imperfecta.* Nat Rev Dis Primers, 2017. **3**: p. 17052.
33. Yam, G.H., et al., *Sodium 4-phenylbutyrate acts as a chemical chaperone on misfolded myocilin to rescue cells from endoplasmic reticulum stress and apoptosis.* Invest Ophthalmol Vis Sci, 2007. **48**(4): p. 1683-90.

34. Ono, K., et al., *A chemical chaperone, sodium 4-phenylbutyric acid, attenuates the pathogenic potency in human alpha-synuclein A30P + A53T transgenic mice.* Parkinsonism Relat Disord, 2009. **15**(9): p. 649-54.

35. van der Velden, L.M., et al., *Folding defects in P-type ATP 8B1 associated with hereditary cholestasis are ameliorated by 4-phenylbutyrate.* Hepatology, 2010. **51**(1): p. 286-96.

36. van den Berghe, P.V., et al., *Reduced expression of ATP7B affected by Wilson disease-causing mutations is rescued by pharmacological folding chaperones 4-phenylbutyrate and curcumin.* Hepatology, 2009. **50**(6): p. 1783-95.

37. Gong, B., et al., *Sodium 4-phenylbutyrate ameliorates the effects of cataract-causing mutant gammaD-crystallin in cultured cells.* Mol Vis, 2010. **16**: p. 997-1003.

38. Rubenstein, R.C. and P.L. Zeitlin, *A pilot clinical trial of oral sodium 4-phenylbutyrate (Buphenyl) in deltaF508-homozygous cystic fibrosis patients: partial restoration of nasal epithelial CFTR function.* Am J Respir Crit Care Med, 1998. **157**(2): p. 484-90.

39. Rubenstein, R.C., M.E. Egan, and P.L. Zeitlin, *In vitro pharmacologic restoration of CFTR-mediated chloride transport with sodium 4-phenylbutyrate in cystic fibrosis epithelial cells containing delta F508-CFTR.* J Clin Invest, 1997. **100**(10): p. 2457-65.

40. Gregor, M.F. and G.S. Hotamisligil, *Thematic review series: Adipocyte Biology. Adipocyte stress: the endoplasmic reticulum and metabolic disease.* J Lipid Res, 2007. **48**(9): p. 1905-14.

41. Granell, S., et al., *Obesity-linked variants of melanocortin-4 receptor are misfolded in the endoplasmic reticulum and can be rescued to the cell surface by a chemical chaperone.* Mol Endocrinol, 2010. **24**(9): p. 1805-21.

42. Basseri, S., et al., *The chemical chaperone 4-phenylbutyrate inhibits adipogenesis by modulating the unfolded protein response.* J Lipid Res, 2009. **50**(12): p. 2486-501.

43. Gioia, R., et al., *The chaperone activity of 4PBA ameliorates the skeletal phenotype of Chihuahua, a zebrafish model for dominant osteogenesis imperfecta.* Hum Mol Genet, 2017.

44. Enderli, T.A., et al., *Animal models of osteogenesis imperfecta: applications in clinical research.* Orthop Res Rev, 2016. **8**: p. 41-55.
45. Brommage, R. and C. Ohlsson, *High Fidelity of Mouse Models Mimicking Human Genetic Skeletal Disorders.* Front Endocrinol (Lausanne), 2019. **10**: p. 934.
46. Forlino, A., et al., *Use of the Cre/lox recombination system to develop a non-lethal knock-in murine model for osteogenesis imperfecta with an alpha1(I) G349C substitution. Variability in phenotype in BrtlIV mice.* J Biol Chem, 1999. **274**(53): p. 37923-31.
47. Daley, E., et al., *Variable bone fragility associated with an Amish COL1A2 variant and a knock-in mouse model.* J Bone Miner Res, 2010. **25**(2): p. 247-61.
48. Sillence, D.O., D.L. Rimoin, and D.M. Danks, *Clinical variability in osteogenesis imperfecta-variable expressivity or genetic heterogeneity.* Birth Defects Orig Artic Ser, 1979. **15**(5B): p. 113-29.
49. Kozloff, K.M., et al., *Brittle IV mouse model for osteogenesis imperfecta IV demonstrates postpubertal adaptations to improve whole bone strength.* J Bone Miner Res, 2004. **19**(4): p. 614-22.
50. Marini, J.C., *Osteogenesis imperfecta: comprehensive management.* Adv Pediatr, 1988. **35**: p. 391-426.
51. Masci, M., et al., *Bone mineral properties in growing Col1a2(+/G610C) mice, an animal model of osteogenesis imperfecta.* Bone, 2016. **87**: p. 120-9.
52. Bi, X., et al., *Correlations Between Bone Mechanical Properties and Bone Composition Parameters in Mouse Models of Dominant and Recessive Osteogenesis Imperfecta and the Response to Anti-TGF-β Treatment.* J Bone Miner Res, 2017. **32**(2): p. 347-359.
53. Uveges, T.E., et al., *Cellular mechanism of decreased bone in Brtl mouse model of OI: imbalance of decreased osteoblast function and increased osteoclasts and their precursors.* J Bone Miner Res, 2008. **23**(12): p. 1983-94.
54. Mertz, E.L., et al., *Makings of a brittle bone: Unexpected lessons from a low protein diet study of a mouse OI model.* Matrix Biol, 2016. **52-54**: p. 29-42.
55. Klionsky, D.J., et al., *Guidelines for the use and interpretation of assays for monitoring autophagy (3rd edition).* Autophagy, 2016. **12**(1): p. 1-222.

56. Marini, J.C., et al., *Components of the collagen prolyl 3-hydroxylation complex are crucial for normal bone development.* Cell Cycle, 2007. **6**(14): p. 1675-81.
57. Cabral, W.A., et al., *Type I collagen triplet duplication mutation in lethal osteogenesis imperfecta shifts register of alpha chains throughout the helix and disrupts incorporation of mutant helices into fibrils and extracellular matrix.* J Biol Chem, 2003. **278**(12): p. 10006-12.
58. Besio, R., et al., *Bone biology: insights from osteogenesis imperfecta and related rare fragility syndromes.* FEBS J, 2019. **286**(15): p. 3033-3056.
59. Bateman, J.F., et al., *Collagen defects in lethal perinatal osteogenesis imperfecta.* Biochem J, 1986. **240**(3): p. 699-708.
60. Bateman, J.F., et al., *Substitution of arginine for glycine 664 in the collagen alpha 1(I) chain in lethal perinatal osteogenesis imperfecta. Demonstration of the peptide defect by in vitro expression of the mutant cDNA.* J Biol Chem, 1988. **263**(24): p. 11627-30.
61. Stacey, A., et al., *Perinatal lethal osteogenesis imperfecta in transgenic mice bearing an engineered mutant pro-alpha 1(I) collagen gene.* Nature, 1988. **332**(6160): p. 131-6.
62. Sarafova, A.P., et al., *Three novel type I collagen mutations in osteogenesis imperfecta type IV probands are associated with discrepancies between electrophoretic migration of osteoblast and fibroblast collagen.* Hum Mutat, 1998. **11**(5): p. 395-403.
63. Eyre, D.R. and M.A. Weis, *Bone collagen: new clues to its mineralization mechanism from recessive osteogenesis imperfecta.* Calcif Tissue Int, 2013. **93**(4): p. 338-47.
64. Eyre, D.R., M.A. Weis, and J.J. Wu, *Advances in collagen cross-link analysis.* Methods, 2008. **45**(1): p. 65-74.
65. Hanson, D.A. and D.R. Eyre, *Molecular site specificity of pyridinoline and pyrrole cross-links in type I collagen of human bone.* J Biol Chem, 1996. **271**(43): p. 26508-16.
66. Montessuit, C., J.P. Bonjour, and J. Caverzasio, *Expression and regulation of Na-dependent P(i) transport in matrix vesicles produced by osteoblast-like cells.* J Bone Miner Res, 1995. **10**(4): p. 625-31.

67. Anderson, H.C., *Matrix vesicles and calcification.* Curr Rheumatol Rep, 2003. **5**(3): p. 222-6.
68. Horiuchi, K., T. Tohmonda, and H. Morioka, *The unfolded protein response in skeletal development and homeostasis.* Cell Mol Life Sci, 2016. **73**(15): p. 2851-69.
69. Chow, C.Y., et al., *The genetic architecture of the genome-wide transcriptional response to ER stress in the mouse.* PLoS Genet, 2015. **11**(2): p. e1004924.
70. Hamamura, K., et al., *Chondroprotective effects of Salubrinal in a mouse model of osteoarthritis.* Bone Joint Res, 2015. **4**(5): p. 84-92.
71. Rajpar, M.H., et al., *Targeted induction of endoplasmic reticulum stress induces cartilage pathology.* PLoS Genet, 2009. **5**(10): p. e1000691.
72. Bianchi, L., et al., *Differential response to intracellular stress in the skin from osteogenesis imperfecta Brtl mice with lethal and non lethal phenotype: a proteomic approach.* J Proteomics, 2012. **75**(15): p. 4717-33.
73. Mullan, L.A., et al., *Increased intracellular proteolysis reduces disease severity in an ER stress-associated dwarfism.* J Clin Invest, 2017. **127**(10): p. 3861-3865.
74. Iannitti, T. and B. Palmieri, *Clinical and experimental applications of sodium phenylbutyrate.* Drugs R D, 2011. **11**(3): p. 227-49.
75. Brusilow, S.W., *Phenylacetylglutamine may replace urea as a vehicle for waste nitrogen excretion.* Pediatr Res, 1991. **29**(2): p. 147-50.
76. Monneret, C., *Histone deacetylase inhibitors.* Eur J Med Chem, 2005. **40**(1): p. 1-13.
77. Kolb, P.S., et al., *The therapeutic effects of 4-phenylbutyric acid in maintaining proteostasis.* Int J Biochem Cell Biol, 2015. **61**: p. 45-52.
78. Tang, Y.H., et al., *4-Phenylbutyric acid presents therapeutic effect on osteoarthritis via inhibiting cell apoptosis and inflammatory response induced by endoplasmic reticulum stress.* Biotechnol Appl Biochem, 2018. **65**(4): p. 540-546.
79. Ma, W., E. Goldberg, and J. Goldberg, *ER retention is imposed by COPII protein sorting and attenuated by 4-phenylbutyrate.* Elife, 2017. **6**.
80. Jones, F.E., et al., *4-Sodium phenyl butyric acid has both efficacy and counter-indicative effects in the treatment of Col4a1 disease.* Hum Mol Genet, 2019. **28**(4): p. 628-638.

81. Takeyari, S., et al., *4-phenylbutyric acid enhances the mineralization of osteogenesis imperfecta iPSC-derived osteoblasts.* J Biol Chem, 2020.
82. Lee, H.W., et al., *Histone deacetylase 1-mediated histone modification regulates osteoblast differentiation.* Mol Endocrinol, 2006. **20**(10): p. 2432-43.
83. Schroeder, T.M. and J.J. Westendorf, *Histone deacetylase inhibitors promote osteoblast maturation.* J Bone Miner Res, 2005. **20**(12): p. 2254-63.
84. Duncan, H.F., et al., *Histone deacetylase inhibitors induced differentiation and accelerated mineralization of pulp-derived cells.* J Endod, 2012. **38**(3): p. 339-45.
85. Hesse, E., et al., *Zfp521 controls bone mass by HDAC3-dependent attenuation of Runx2 activity*. J Cell Biol, 2010. **191**(7): p. 1271-83.
86. Hu, X., et al., *Histone deacetylase inhibitor trichostatin A promotes the osteogenic differentiation of rat adipose-derived stem cells by altering the epigenetic modifications on Runx2 promoter in a BMP signaling-dependent manner*. Stem Cells Dev, 2013. **22**(2): p. 248-55.
87. Bianchi, L., et al., *Altered cytoskeletal organization characterized lethal but not surviving Brtl+/- mice: insight on phenotypic variability in osteogenesis imperfecta.* Hum Mol Genet, 2015. **24**(21): p. 6118-33.
88. Forlino, A., F. Tonelli, and R. Besio, *Steady-State and Pulse-Chase Analyses of Fibrillar Collagen.* Methods Mol Biol, 2019. **1952**: p. 45-53.
89. Jeon, J., M.S. Lee, and H.S. Yang, *Differentiated osteoblasts derived decellularized extracellular matrix to promote osteogenic differentiation.* Biomater Res, 2018. **22**: p. 4.
90. Gregory, C.A., et al., *An Alizarin red-based assay of mineralization by adherent cells in culture: comparison with cetylpyridinium chloride extraction.* Anal Biochem, 2004. **329**(1): p. 77-84.

Supplementary

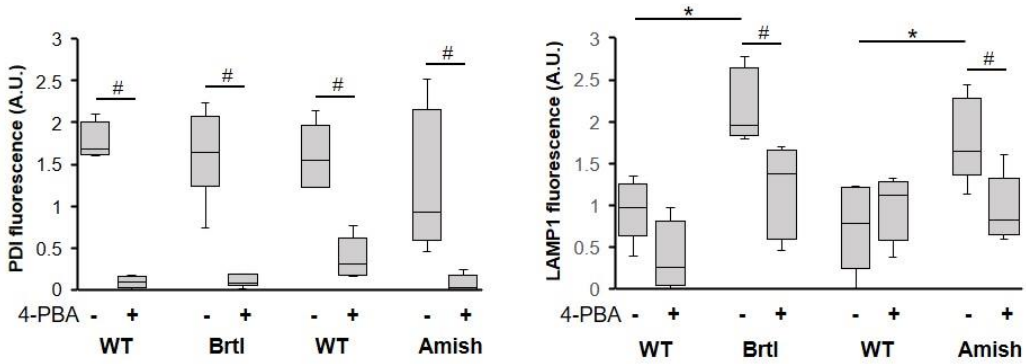

Supplementary figure 1: Quantification of the ER marker PDI and the lysosomal marker LAMP1 in mutant and control OBs in the absence (−) or presence (+) of 4-PBA. The quantification refers to multiple immunofluorescence experiments reported in Fig. 4A. *p<0.05 WT VS mutant, # p<0.05 4-PBA treated VS untreated.

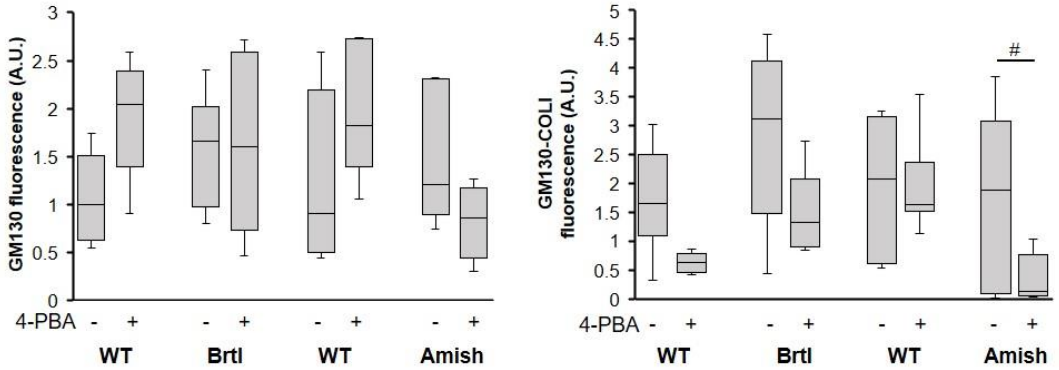

Supplementary figure 2: Quantification of immunofluorescence of the Golgi marker GM130 and of its colocalization with collagen (COLI) in mutant and control OBs in the absence (−) or presence (+) of 4-PBA. The Golgi signal was unchanged by genotype and treatment. # p<0.05 4-PBA treated VS untreated.

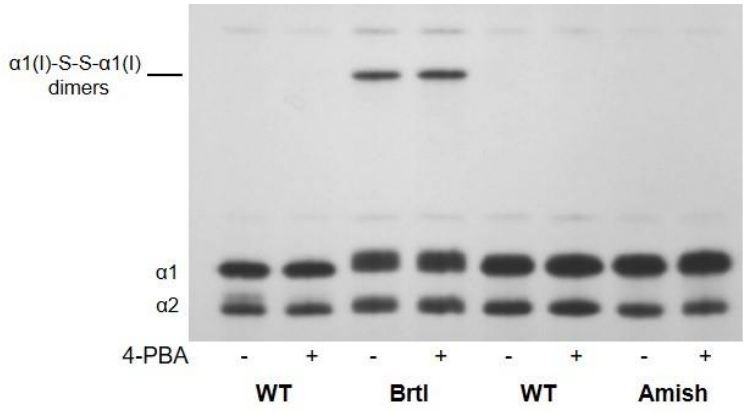

Supplementary figure 3: Electrophoretic analyses of type I collagen extracted from Brtl and Amish OB' cell layer and their littermate controls in absence (−) or presence (+) of 4-PBA. Brtl collagen presented a typical broadening and a slower migration of α1 and α2 bands, indicating the presence of overmodification. In all samples 4-PBA did not have an effect on collagen migration.

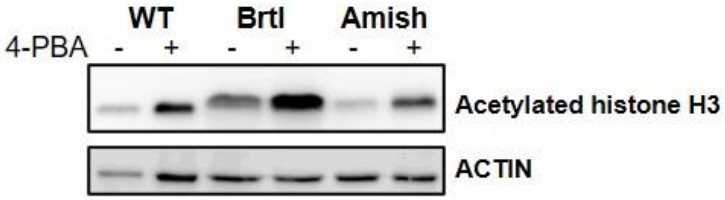

Supplementary figure 4: Histone H3 acetylation was investigated by western blot analyses. 4-PBA increased the level of the H3 modification in both Brtl and Amish OBs.

Supplementary materials

Collagen analysis

To analyze the effect of 4-PBA on collagen, cells were labelled for 15 hours in absence and in presence of 5 mM 4-PBA using 28.57 µCi of ^{3}H-Pro/ml. Collagen extraction from cell layer was performed as previously reported [85]. Collagen was resuspended in Laemmli buffer (62 mM Tris-HCl, pH 6.8, 10% glycerol, 2% sodium dodecyl sulphate, 0.02% bromophenol blue) and the radioactivity (counts for minute, CPM) was measured using a liquid scintillation analyzer (PerkinElmer TRI-CARB 2300 TR). Equal amounts of ^{3}H-labeled collagen were loaded on 6% SDS-Urea-PAGE in non-reducing condition. The gels were fixed in 45% methanol, 9% glacial acetic acid, incubated for one hour with enhancer (PerkinElmer, 6NE9701), washed in deionized water, and dried. ^{3}H gel radiographs were obtained by direct exposure of dried gels to hyperfilm (Amersham) at − 80 °C. The radiography films were digitalized by VersaDoc 3000 (BioRad)**.**

Chapter 4

Osteoblasts mineralization and collagen matrix is conserved upon specific Col1a2 silencing

COL1A1 or *COL1A2* dominant mutations are responsible for classical OI forms, for which a definitive cure is not available and gene therapy approach correcting or silencing the mutant allele would be required. Since individuals lacking α2(I) chain and synthetizing collagen α1(I) homotrimers do not show a bone phenotype, bone specific *COL1A2* silencing seems a promising strategy for the treatment of these patients.

As a side project, I collaborated to this work, in which we silenced *Col1a2 in vitro* in murine embryonic fibroblasts (MEFs) and in primary murine OBs, and *in vivo* in a murine model of OI, using *Col1a2*-silencing RNAs (siRNAs).

The siRNAs specifically targeted *Col1a2* mRNA and strongly reduced α2(I) chain expression, in MRFs and in primary OBs, whose anabolic activity was preserved.

In nude mice transplanted with biphasic calcium phosphate implants loaded with murine mesenchymal stem and injected with siRNA, we demonstrated α2(I) chain silencing at mRNA and at protein level. Staining with Masson's Trichrome highlighted the presence of newly formed collagen in the matrix, thus showing that *Col1a2* silencing did not prevent collagen matrix formation *in vivo*.

In conclusion, we identified an efficient siRNA for specific *in vitro* and *in vivo* suppression of *Col1a2* expression. The optimization of a bone specific delivery system will open a new era in the OI gene therapy, at least for those forms with dominant mutations in the COL1A2 gene.

I participated to this work as a side project, in particular I took part in the Masson Trichrome histological sections preparation and analysis and I contributed to the review and editing process of the paper.

Osteoblasts mineralization and collagen matrix is conserved upon specific *Col1a2* silencing

Silvia Maruelli[a,1], Roberta Besio[a,1], Julie Rousseau[b], Nadia Garibaldi[a], Jérôme Amiaud[b], Bénédicte Brulin[b], Pierre Layrolle[b], Virginie Escriou[c], Antonio Rossi[a], Valerie Trichet[b] and Antonella Forlino[a]

***a* - Department of Molecular Medicine,** *Biochemistry Unit, University of Pavia, Pavia, Italy*
***b* - INSERM,** *Université de Nantes, UMR1238, Phy-Os, Bone sarcomas and remodeling of calcified tissues, Faculty of Medicine, University of Nantes, Nantes, France*
***c* - Université de Paris,** *UTCBS, CNRS, INSERM, F-75006 Paris, France*

Correspondence to Antonella Forlino:*at: Department of Molecular Medicine, Biochemistry Unit, University of Pavia, Via Taramelli 3B, 27100 Pavia, Italy. aforlino@unipv.it.*
https://doi.org/10.1016/j.mbplus.2020.100028

Abstract

Classical osteogenesis imperfecta (OI) is an inherited rare brittle bone disease caused by dominant mutations in the *COL1A1* or *COL1A2* genes, encoding for the α chains of collagen type I. The definitive cure for the disease will require a gene therapy approach, aimed to correct or suppress the mutant allele. Interestingly, individuals lacking α2(I) chain and synthetizing collagen $\alpha1(I)_3$ homotrimers do not show bone phenotype, making appealing a bone specific *COL1A2* silencing approach for OI therapy. To this aim, three different *Col1a2*-silencing RNAs (siRNAs), −3554, −3825 and −4125, selected at the 3′-end of the murine *Col1a2* transcript were tested *in vitro* and *in vivo*. In murine embryonic fibroblasts *Col1a2*-siRNA-3554 was able to efficiently and specifically target the *Col1a2* mRNA and to strongly reduce α2(I) chain expression. Its efficiency and specificity were also demonstrated in primary murine osteoblasts, whose mineralization was preserved. The efficiency of *Col1a2*-siRNA-3554 was proved also *in vivo*. Biphasic calcium phosphate implants loaded with murine mesenchymal stem cells were intramuscularly transplanted in nude mice and injected with *Col1a2*-siRNA-3554 three times a week for three weeks. Collagen α2 silencing was demonstrated both at mRNA and protein level and Masson's Trichrome staining confirmed the presence of newly formed collagen matrix. Our data pave the way for further investigation of *Col1a2* silencing and siRNA delivery to the bone tissue as a possible strategy for OI therapy.

Introduction

Dominant mutations in the *COL1A1* or *COL1A2* genes, encoding for the two α chains of collagen type I, are responsible for the classical form of the rare bone disease osteogenesis imperfecta (OI). Individuals affected by OI are characterized by bone deformity, frequent fractures and growth delay [1,2]. No definitive treatment is so far available and the therapeutic options, based either on surgical interventions or drug administration, are for the most focused on ameliorating patient's quality of life [3–5]. Only a gene therapy approach, aimed to correct or suppress the expression of the mutant allele, could be effective to cure patients.

Interestingly, individuals heterozygous for null *COL1A1* allele have a mild form of the disease [6] and null *COL1A2* allele in heterozygosis where never described, suggesting an undetectable bone phenotype [1]. This observation points to allele specific silencing approach as an appealing strategy for the disease.

Indeed, for defects in *COL1A1* or *COL1A2*, the specific silencing of the mutant allele could transform

Please cite this article as: S. Maruelli, R. Besio, J. Rousseau, et al., Osteoblasts mineralization and collagen matrix is conserved upon specific *Col1a2* silencing..., https://doi.org/10.1016/j.mbplus.2020.100028

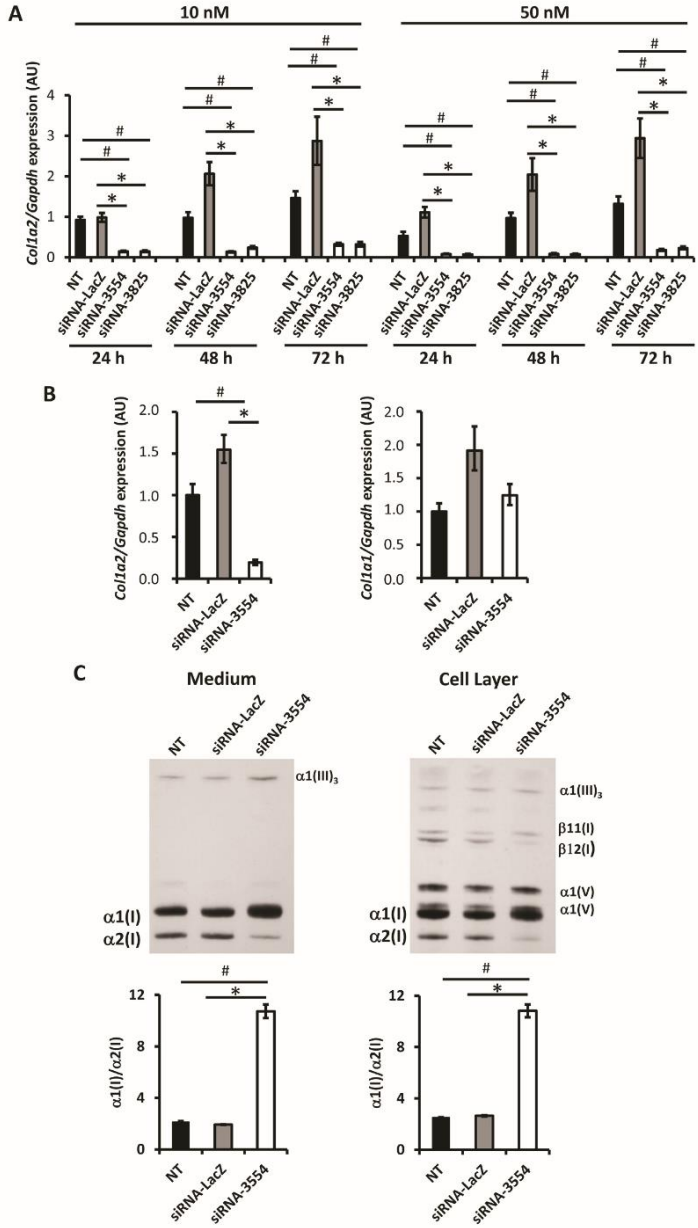

Please cite this article as: S. Maruelli, R. Besio, J. Rousseau, et al., Osteoblasts mineralization and collagen matrix is conserved upon specific *Col1a2* silencing..., https://doi.org/10.1016/j.mbplus.2020.100028

a severe phenotype into a mild osteoporotic form or even cure the disease. In classical dominant OI, over 85% of the mutations are single nucleotide substitutions changing one of the glycine, present every three residues in the helical domain and necessary for proper chains folding, with a bulkier amino acid [7]. RNA interference (RNAi) techniques based on small interfering RNA (siRNA) and short hairpin RNA (shRNA) were proved to be effective in allele specific down regulation of gene expression in several monogenic disorders [8–15]. RNA therapeutics are easy to design, cost effective, generally stable and easy to combine with carriers [16]. The first therapy based on RNA interference gene silencing, termed Onpattro®, has been approved by the US Food and Drug Administration in 2018 [17]. This lipid complex suspension, for intravenous use, contains a transthyretin-directed siRNA and is indicated for the treatment of the polyneuropathy of hereditary transthyretin-mediated amyloidosis in adults [18].

The siRNAs are short chemical synthesized double strand RNAs, they can be delivered into the cells where they can be stabilized for weeks upon association to the RISC complex, although they are diluted during cell division. The shRNAs are short double strand RNA molecules with a hairpin structure transcribed upon their subcloning in a plasmid or viral vector used to transfect the host cells. shRNAs have the advantage to be continuously synthesized by the cell machinery upon integration in the host genome, but the templates are subjected to random DNA integration.

A single nucleotide difference in the highly repetitive and GC rich collagen sequence represents the first challenge in allele specific targeting of the collagen type I genes. Nevertheless, siRNA/shRNA were successfully used in OI. The transfection of allele specific siRNA specifically suppressing the mutant *Col1a1* allele in primary fibroblasts from the OI murine model *Brtl*/+, carrying in heterozygosis the α1(I)-G349C substitution, led to about 60% down-regulation of gene expression, affecting only 20% the expression of the wild type allele. Mutant specific *Col1a1*-shRNA suppressed about 50% the gene expression, reducing to 60% the level of the mutated protein without compromising cells proliferation [19]. A limiting factor of these strategies is the requirement of specific silencing molecules for the hundreds of different mutations known to cause dominant OI (www.le.ac.uk/genetics/collagen/). To overcome this limitation, a mutation-independent approach in human bone derived cells using siRNA/shRNA targeting heterozygous single nucleotide polymorphisms in *COL1A2* [20] or insertion/ deletion polymorphisms in both the *COL1A1* and *COL1A2* genes [21] were successfully attempted *in vitro*.

Interestingly, individuals carrying in homozygosis null *COL1A2* allele are affected by a form of Ehlers Danlos syndrome (EDS) associated to vascular impairment, but they do not manifest bone phenotype [22]. Such observation suggests that a skeletal specific silencing of both mutant and normal *COL1A2* allele could indeed ameliorate the OI skeletal outcome in these individuals.

In this report, we evaluate the effect of *Col1a2* specific transcript silencing and α2 collagen protein suppression on osteoblast mineralization *in vitro* and on matrix formation *in vivo* in mice.

Results

Col1a2-siRNA efficiently and specifically reduces gene expression *in vitro* in murine embryonic fibroblasts

Three siRNAs targeting the murine *Col1a2* gene were selected *in silico* at the 3′-end of the collagen I gene, encoding for the C-terminal propeptide domain and characterized by limited repetitive and GC rich sequence. The siRNAs target positions in the *Col1a2* gene (NM_007743.3) were selected at the nucleotide 3554–3572 for siRNA-3554, 3825-3845 for siRNA-3825 and 4215-4233 for siRNA-4215. Their efficiency at two different concentrations, 10 nM and 50 nM, was first evaluated 48 h post transfection (hpt) in primary murine embryonic fibroblasts (MEFs). qPCR showed that siRNA-3554 silenced about 90% of the *Col1a2* expression at both concentrations while siRNA-3825 63% and 81% at 10 and 50 nM, respectively **(Supplementary Fig. 1A)**. On the contrary, siRNA-4215 did not significantly change *Col1a2* expression, at least at the lower concentration, and its use was discontinued. The siRNA-LacZ, used as control, did not affect

Fig. 1. Efficient and specific *Col1a2*-siRNAs suppress collagen α2 chain protein expression in primary murine embryonic fibroblasts. **(A)** The stability of *Col1a2* silencing of the 2 most effective siRNAs (siRNA-3554 and – 3825) at 10 or 50 nM was evaluated 24, 48 and 72 h post transfection in MEFs plated 1×10^4 cells/well. qPCR analyses showed *Col1a2* relative expression. **(B)** The *Col1a2* specificity was evaluated for the more promising molecule, siRNA-3554, analyzing the *Col1a1* and *Col1a2* expression by qPCR. **(C)** Representative images of SDS-Urea-PAGE analyses of ^{3}H-proline labelled type I collagen extracted from medium and cell layer of transfected cells. The densitometric analyses of collagen type I α1 and α2 was performed and the α1/α2 ratio evaluated. In the collagen fraction extracted from cell layer a contribution of collagen type V in the α1(I) quantitation cannot be excluded. Not transfected cells (NT) and cells transfected with siRNA-LacZ were used as negative controls. A biological duplicate of the experiment was performed and each experiment was performed in triplicate. * p value <.05 *vs* siRNA-LacZ, # p value <.05 *vs* NT.

Please cite this article as: S. Maruelli, R. Besio, J. Rousseau, et al., Osteoblasts mineralization and collagen matrix is conserved upon specific *Col1a2* silencing..., https://doi.org/10.1016/j.mbplus.2020.100028

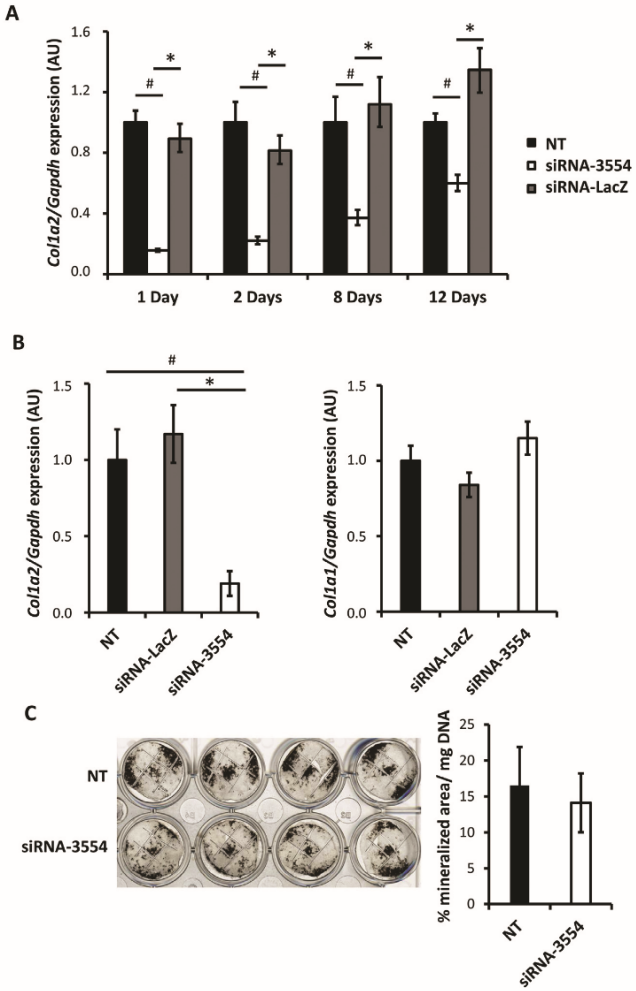

Fig. 2. Efficient and specific *Col1a2* silencing in primary murine osteoblasts does not impair mineralization. **(A)** The stability of *Col1a2* silencing was evaluated in murine osteoblasts untrasfected (NT) and upon 10 nM siRNA-3554 or siRNA-LacZ transfection at 1, 2, 8 and 12 days post transfection by qPCR quantitation of *Col1a2* expression. **(B)** Similarly, the *Col1a2* silencing specificity was evaluated by qPCR quantitation of *Col1a2 and Col1a1* expression in murine osteoblasts NT and upon 10 nM siRNA-3554 or siRNA-LacZ transfection. **(C)** NT and transfected osteoblasts were stained by Von Kossa following 19 days growth in mineralization media. Mineral was quantified and normalized to DNA amount. A biological duplicate of the experiment was performed and each experiment was run at least in triplicate. * *p* value <.05 *vs* siRNA-LacZ, # p value <.05 *vs* NT.

Col1a2 expression, as expected **(Supplementary Fig. 1A)**.

To determine the temporal stability of the 2 most effective siRNAs, the *Col1a2* gene expression was evaluated 24, 48 and 72 hpt. To this purpose two different cell densities, 1×10^4 and 2×10^4 cells/well, to mimic sub-confluent and confluent status, and two different siRNAs concentrations, 10 and

Please cite this article as: S. Maruelli, R. Besio, J. Rousseau, et al., Osteoblasts mineralization and collagen matrix is conserved upon specific *Col1a2* silencing..., https://doi.org/10.1016/j.mbplus.2020.100028

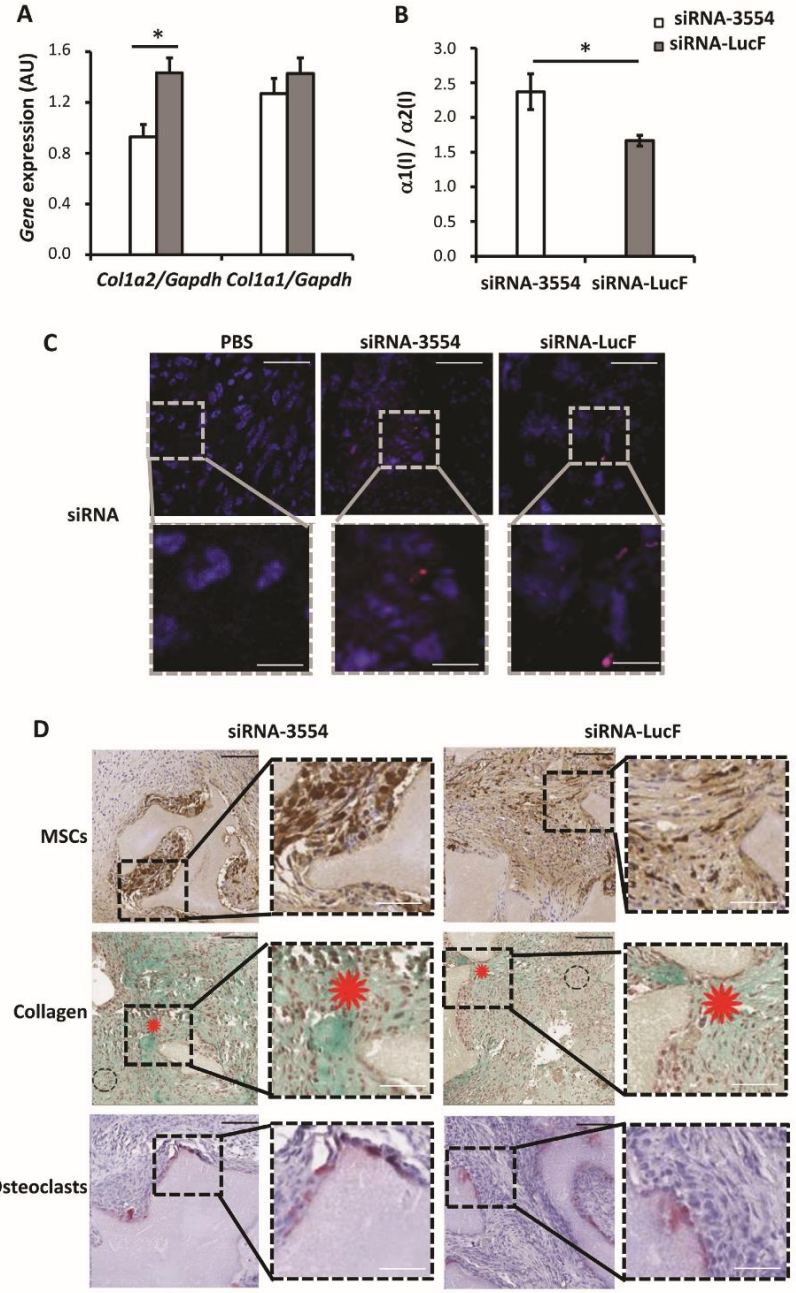

Please cite this article as: S. Maruelli, R. Besio, J. Rousseau, et al., Osteoblasts mineralization and collagen matrix is conserved upon specific *Col1a2* silencing..., https://doi.org/10.1016/j.mbplus.2020.100028

50 nM, were used. At the lowest cell density and at both siRNA concentrations, the *Col1a2* expression was reduced about 85% at all time points **(**Fig. 1A**)**.

At the highest cell density only the 50 nM siRNAs concentration showed good efficiency for both siRNA molecules **(Supplementary Fig. 1B)**.

Unfortunately, at the higher siRNA concentration the cell health was compromised and a large number of cells detached from the well, thus all the following experiments were performed using 10 nM and the 1×10^4 cell density was chosen. The siRNA-3554 was selected for its higher efficacy at the selected concentration.

Given the high similarity of the *Col1a1* and *Col1a2* genes, the siRNA-3554 specificity for *Col1a2* was tested by qPCR. At 48 hpt siRNA-3554 suppressed *Col1a2* without affecting the *Col1a1* expression **(**Fig. 1B**).**

siRNA-3554 reduces α2(I) expression

To assess whether the silencing of the *Col1a2* gene by siRNA-3554 leads to the α2 chain protein down-regulation, 48 hpt the ^{3}H-proline labelled collagen was extracted from medium and cell layer at steady state. SDS-PAGE analysis demonstrated a strong reduction of the α2(I) chain in cells transfected with the siRNA-3554 compared to the cells transfected with siRNA-LacZ, used as control. The densitometric ratio of the α1 and α2 bands intensity was clearly higher in siRNA-3554 treated cells, with respect to the 2:1 expected value based on the collagen stoichiometry (2 α1 and 1 α2 chains). This result supported the successful α2(I) chain down regulation **(**Fig. 1C**)**.

siRNA-3554 is efficient and specific in osteoblast cells

OI is mainly a bone disease and osteoblasts are the main affected cells, thus the efficiency and specificity of the siRNA-3554 were tested in primary murine osteoblasts. Cells were transfected in 24 well plates at cell density of 2×10^4 cells/well using 10 nM siRNA. The higher cell density was chosen based on the lower growth rate of osteoblasts compared to MEFs [23].

A silencing time course experiment with siRNA-3554 was performed. A down-regulation of *Col1a2* expression of 82%, 73%, 67% and 56% with respect siRNA-LacZ transfection and 84%, 78%, 63% and 40% with respect siRNA-3554 transfection was obtained at 1, 2, 8, 12 days post transfection (dpt), respectively **(**Fig. 2A**)**. At 2 dpt cells transfected with the siRNA-3554 showed a specific ~ 80% silencing of the *Col1a2* expression, with no change in the *Col1a1* expression **(**Fig. 2B**)**. No effect on the expression of *Col1a1* was detected at all time points in the time course experiment confirming the specificity of siRNA-3554 for *Col1a2* also in primary osteoblasts (**Supplementary Fig. 2A**).

Osteoblast mineralization is conserved following siRNA-3554 transfection

Mineralization is a fundamental step in bone formation [24], thus the mineralization of primary osteoblasts transfected with siRNA-3554 was evaluated. Osteoblasts mineralization was induced 24 hpt and after 19 days Von Kossa staining was performed to visualize the mineral nodules **(**Fig. 2C**)**. Interestingly, transfected and control cells produced the same amount of mineralized area normalized to DNA content, indicating that the silencing of the *Col1a2* is not affecting the process **(**Fig. 2C**)**.

In vivo siRNA-3554 efficiency and specificity

To have a proof-of-principle of the *in vivo* efficiency of siRNA-3554, biphasic calcium phosphate (BCP) implants loaded with mouse mesenchymal stem cells (MSCs) expressing the enhanced green fluorescent protein (*EGFP*) were prepared and transplanted intramuscularly in Rj:NMRI-nude mice. These implants were chosen based on their well known ability to favor bone formation [25,26]. Following implantation, siRNA-3554 and siRNA-LucF were injected at the implant site three times a week for three weeks, PBS injection was

Fig. 3. Specific *Col1a2* silencing in mouse mesenchymal stem cells injected in intramuscular biphasic calcium phosphate implants in nude mice allows collagen deposition. **(A)** *Col1a2* and *Col1a1* qPCR analysis was performed on RNA obtained from biphasic calcium phosphate (BCP) implants extracted from nude mice 28 days after transplantation and following siRNA-3554 ($n = 4$) or siRNA-LucF (n = 4) injections for three weeks. **(B)** The α1/α2 collagen chains ratio was evaluated by quantification of collagen bands in SDS-Urea-PAGE of pepsin digested collagen from BCP implants extracted 28 days after transplantation following siRNA-3554 or siRNA-LucF injections. (C) siRNA presence was evaluated in intramuscular BCP implants injected with PBS, siRNA-3554 or siRNA-LucF extracted 28 days after transplantation. Fluorescent signal (pink) revealed siRNA-3554-ATTO 655 and siRNA-LucF-ATTO 655 that were used for the last three siRNA injections. (D) Histological analysis of intramuscular BCP implants injected with siRNA-3554 or siRNA-LucF extracted 28 days after transplantation. EGFP-MSCs are stained in brown following immunohistochemistry using anti-EGFP antibody. Masson's Trichrome staining revealed collagen in green, as indicated by red asterisks. Picnotic nuclei are indicated by dasher circles. TRAP staining revealed the presence of osteoclasts (pink) in the implants. * p value <.05. High magnification images are provided for all the panels in the inserts. Black scale bar = 100 μm, white scale bar = 30 μm. (For interpretation of the references to colour in this figure legend, the reader is referred to the web version of this article.)

Please cite this article as: S. Maruelli, R. Besio, J. Rousseau, et al., Osteoblasts mineralization and collagen matrix is conserved upon specific *Col1a2* silencing..., https://doi.org/10.1016/j.mbplus.2020.100028

performed as control. The three last injections were performed with fluorescent siRNAs (ATTO 655-labelled siRNA). At the sacrifice the implants appeared as a compact mass of cells and particles **(Supplementary Fig. 3A)** and contained both EGFP positive cells and siRNAs in all siRNA injected samples **(**Fig. 3C,D**)**.

Col1a2 expression was significantly silenced (48%) in the implants injected with the siRNA-3554, and the silencing was specific since no effect on *Col1a1* was detectable **(**Fig. 3A**)**.

The analyses of collagen type I extracted from the implants revealed an increased α1 / α2 chains ratio following injection with siRNA-3554, supporting α2 suppression **(**Fig. 3B**, Supplementary Fig. 3B)**.

Bone formation upon siRNAs injection was evaluated by Masson's Trichrome histological staining. The presence of newly formed collagen matrix (red asterisks) was proved in all samples, demonstrating that the silencing of *Col1a2* did not prevent collagen matrix formation *in vivo* **(**Fig. 3D**)**. Of note, the area of the new collagen matrix was comparable in all samples (100 ± 17.14% in PBS-treated; 106.4 ± 24.5% in siRNA-3554; 117.5 ± 61% siRNA-LucF) (Fig. 3D, Supplementary Fig. 3C). Areas of picnotic nuclei were detectable (dashed circles) in siRNAs injected samples, suggesting a necrotic effect of lipoplex injections. Importantly, also osteoclasts were detected by TRAP staining, indicating that remodeling occurs upon siRNAs injection. Furthermore, the siRNAs did not affect the number of macrophages, markers of inflammation, as shown by immunohistochemistry using antibody against CD68 (**Supplementary Fig. 4**). Thus, data showed that the *Col1a2* silencing was present in our *in vivo* model both at molecular and protein level.

Discussion

Type I collagen is a heterotrimer composed of two α1(I) and one α2(I) chains. While the complete deficiency of α1(I) chain appears to be incompatible with life [27], the synthesis of α1(I) homotrimers lacking α2(I) was described in several situations. α1 (I)-trimers were isolated from normal human skin where they account for <5% of the total collagen [28], and their presence was also detected during embryogenesis [29,30], in tumors [31,32], in fibrotic tissues [33,34], in stressed mesangial cells [35], and in a variety of pathological conditions [36–38].

Homozygous null mutations in *COL1A2* also lead to α1(I) homotrimers assembly and to a range of phenotypes with an effect on tissue properties still poorly understood. *COL1A2* mutations impairing α2 (I) chain assembly in the triple helix, without affecting gene transcription and translation, are associated to severe osteogenesis imperfecta phenotype both in humans and murine models [39,40]. On the contrary, *COL1A2* defects affecting transcript stability and compromising α2(I) translation cause a mild EDS syndrome in patients, with hypermobility in childhood and cardiac valve disease in adulthood, but no bone phenotype [22]. To explain the very different effects of mutations in *COL1A2,* it is tempting to speculate that those mutations in the α2(I) C-propeptide associated to mutant α2(I) translation cause its intracellular accumulation inducing a cellular stress that we already described as a key player in OI skeletal outcome and a modulator of osteoblasts differentiation [41,42]. Of note, in the OI murine model *oim/oim*, in which mutant α2(I) translation is not impaired, but its assembly in collagen type I heterotrimer is compromised, the osteoblasts differentiation ability is affected [43].

The majority of the published silencing reports in OI comes from studies using *in vitro* approaches, only very limited data are available from *in vivo* studies in OI murine models [44–47]. Indeed, the availability of both *in vitro* and *in vivo* models is particularly relevant in studies aimed to identify novel therapeutic approaches. The *in vitro* approach is an important tool that allows to dissect and analyze specific cellular pathways without the interference of the whole tissue/organ environment, on the other hand the use of *in vivo* models is a mandatory step before clinical trials.

Using *Col1a2* silencing we demonstrated that in the absence of α2(I) the mineralization *in vitro* and collagen formation *in vivo* are not affected. *Col1a2*-siRNA transfection allowed osteoblasts mineralization, although we cannot exclude a rebound effect of *Col1a2* gene expression level from day 12 to day 19 post transfection. Indeed, a local delivery of *Col1a2*-siRNA *in vivo* to BCP beads loaded with mesenchymal stem cells preserved collagen deposition [48].

The *in vivo* silencing of the *Col1a2* expression, although specific, was less effective than in *in vitro*, and similarly, a lower reduction of the α2(I) chain was detected. A possible reason for this difference could be linked to some intrinsic limitations of the system, such as the difficulty to reach the cells inside the implant and the formation of a connective tissue capsule around the implant that could impair siRNAs entrance/uptake into the target cells. Nevertheless, collagen formation in the implant was not compromised by the *Col1a2*-siRNA injection. However, efficient *in vivo* model of new bone formation would need further optimization.

The ultimate cure for dominant OI would be the correction of the DNA mutation, but for the more severe forms the silencing of the mutant allele may represent an interesting and probably more feasible option. The highly repetitive primary sequence of type I collagen, along with over a thousand distinct single base substitutions identified in OI patients, presents a significant challenge to an allele-specific targeting approach to treat this disease [7]. In OI patients carrying over 600 point mutations in

Please cite this article as: S. Maruelli, R. Besio, J. Rousseau, et al., Osteoblasts mineralization and collagen matrix is conserved upon specific *Col1a2* silencing..., https://doi.org/10.1016/j.mbplus.2020.100028

COL1A2, the bone phenotype could in principle be treated by a mutation independent silencing approach. Our data represent a proof of principle of the feasibility of the approach, but the issue of siRNA bone delivery remains to be addressed. Indeed, atelocollagen-mediated systemic administration of siRNAs successfully inhibited bone metastasis [49]. The complexation of siRNAs with polyethylenimine also was demonstrated to be effective following systemic administration to deliver the siRNAs into different organs, but no data on specific bone targeting are available yet [50,51].

Systemic delivery of siRNA is a quite promising therapeutic approach, but it should be taken into consideration that in clinical trial a high number of repeated siRNA injections could result in a decreased patient compliance and consequent impediment to patient treatment [52].

In conclusion, following the *in silico* design of three siRNAs molecules targeting the murine *Col1a2*, we successfully identified a siRNA that efficiently and specifically suppresses *in vitro* and *in vivo* the *Col1a2* expression. The optimization of a bone specific delivery system will open a new era in the treatment of OI, at least for those forms with dominant mutations in the *COL1A2* gene.

Materials and methods

Animals

C57Bl/6 control mice were purchased from Harlan Laboratories and maintained in the animal facility at the Department of Molecular Medicine of the University of Pavia according to the current laws on the animal care. All the experiments were approved by the Italian Ministry of Health (protocol n.1116/2015-PR, 21/10/2015), complied with the ARRIVE guidelines and carried out in accordance with the EU Directive 2010/63/EU for animal experiments. Rj:NMRI-nude mice were purchased from Elevages Janvier SAS and maintained in the animal facility at the faculty of Medicine of the University of Nantes. The local Ethic Committee (CEEA.2012.27) approved the animal experimentation protocol for the research.

In silico siRNA selection and synthesis

The Basic Local Alignment Search Tool (BLAST) was used to identify three siRNAs 19–21 nucleotides long, specifically targeting the 3′-end of the murine *Col1a2* (NM_007743.3) gene encoding for the C-propeptide domain of the α2 chain of type I collagen: siRNA-3554 (5'-GGACUAUGAAGUUGAUGCA-3′) targeting exon 49 (NM_007743.3, 3633–3652), siRNA-3825 (5'-GCCAACAAGCATGTCTGGTTA-3′) targeting exon 50 (NM_007743.3, 3904–3925), and siRNA-4215 (5'-GAATTCCGTGTGGAGGTTG-3′) targeting exon 52 (NM_007743.3, 4303–4322). The three siRNAs targeting murine *Col1a2* and two negative controls for *in vitro* and *in vivo* experiments: siRNA-LacZ (5'-GUGACCAGCGAAUACCUGU-3′) and siRNA-LucF (5'-CUUACGCUGAGUACUUCGA-3′) respectively, were purchased from Eurogentec (Seraing, Belgio) with the addition of a dTdT nucleotide at their 3′-end.

Isolation and culture of primary murine embryonic fibroblasts

Murine embryonic fibroblasts were obtained from E13.5–14.5 C57Bl/6 embryos. Briefly, upon sacrifice the body was transferred in a sterile tube, minced and sequentially digested with 1 g/l trypsin in 0.4 g/l EDTA, 1.7 g/l NaCl for 5 min at 37 °C. Cells obtained from four successive digestions were passed through a 40 µm polypropylene mesh (Millipore, Burlington, Massachusetts, USA) added with Dulbecco modified Eagle's medium (D-MEM, Lonza, Basilea, Switzerland) supplemented with 10% fetal bovine serum (FBS), 4 mM glutamine, 100 µg/ml penicillin and 0.1 mg/ml streptomycin and pooled. The cells obtained from each embryo were plated in 10 cm petri dish and incubated at 37 °C. Cells at passages P3-P6 were used for all the experiments.

Isolation and culture of primary murine calvarial osteoblasts

Murine calvarial osteoblasts were isolated from 1 to 2 days old mice. Pups were euthanized, the cranium was dissected, cleaned from the surrounding connective tissue, cut in half and collected in α-Minimal Essential Medium (α –MEM, Sigma Aldrich, St. Louis, Missouri, USA) supplemented with 10% FBS, 4 mM glutamine, 100 µg/ml penicillin and 0.1 mg/ml streptomycin and 25 µg/ml sodium ascorbate (Fisher Scientific, Hampton, New Hampshire, USA). Calvaria were then pooled and sequentially digested with 200 U/ml collagenase type II (Thermo Fisher Scientific, Waltham, Massachusetts, USA) at 37 °C in an oscillating water bath for 20 min. Cells obtained from the first two digestions were discharged, while cells from the following three digestions were passed through a 70 µm polypropylene mesh, added with α -MEM containing 10% FBS and pooled. Cells were plated in 10 cm petri dish at a density of 2×10^5 cells/dish. The medium was changed twice a week and cells were used at passage P1.

Culture of murine mesenchymal stem cells

Mouse mesenchymal stem cells (MSCs) were obtained from Invitrogen (GIBCO® Mouse C57BL/6 mesenchymal stem cells; Catalog no. S1502–100)

Please cite this article as: S. Maruelli, R. Besio, J. Rousseau, et al., Osteoblasts mineralization and collagen matrix is conserved upon specific *Col1a2* silencing..., https://doi.org/10.1016/j.mbplus.2020.100028

and cultured as specified in the guidelines. They have been modified to express the enhanced green fluorescent protein (EGFP) using lentivirus as previously described [53].

Cell transfection

For MEFs transfection experiments cells were plated in 24 well plate at a density of 1×10^4 or 2×10^4 cells/well. After 24 h the cells were transfected using Interferin (PolyPlus transfection, Illkirch, France) following manufacturer's recommendation. For each siRNA two concentrations were tested, 10 and 50 mM respectively, and the RNA was collected 48 h after the transfection. For the two more efficient and specific siRNAs, siRNA-3554 and siRNA-3825 and the negative control siRNA-LacZ a time course was performed and the RNA was collected 24, 48 and 72 h after transfection with 10 nM siRNA.

For primary osteoblasts, cells were plated in 24 well plate at a density of 2×10^4 cells/well and transfected after 24 h. siRNA-3554 was used at a concentration of 10 nM and the RNA was collected 1, 2, 8, 12 days post transfection. Each experiment was performed in duplicate.

Biphasic calcium phosphate implants

The biphasic calcium phosphate (BCP) implant was composed by 40 mg of synthetic bone graft substitute bioactive calcium phosphate 0.5–1 mm granules (MBCP®, Biomatlante, Vigneux-de-Bretagne, France) incubated for 1 h at RT with 1.4×10^6 GIBCO® Mouse MSCs modified to express EGFP (EGFP-MSCs) in 60 µl of phosphate buffered saline (PBS). The lipoplex complex for the siRNA delivery was obtained as follow: a solution containing 0.67 µg/µl of siRNAs and 0.67 µg/µl of DNA plasmid pSL301 was mixed with 8 mM cationic liposome DMAPAP/DOPE (charge ratio 1:6) and incubated 20 min at room temperature to allow the siRNA encapsulation [54].

Rj:NMRI-nude female mice 5 week old were used. The mice were anesthetized by inhalation of 2% isoflurane and injected with 10 µg Buprécare intramuscularly. The leg was incised at the level of the tibia and a pocket in the muscle tissue was created. The implant was then inserted in both legs, and the cut was sutured with a non-resorbable suture thread. The week after, the siRNA lipoplex complex was injected on the implants three times a week for three weeks. Fluorescent labelled (ATTO655) siRNAs were injected the last week. The mice were injected with 10 µg of siRNA-3554 or siRNA-LucF or with PBS ($n = 4$/ group). The animals were then sacrificed 28 days after the implantation. The BCP implants were removed from the mice following euthanasia. The implants were used to evaluate collagen type I gene expression and protein levels and for histological analysis.

Gene expression analysis

The RNA from MEFs and osteoblasts was collected at the different time points detailed above using the RNeasy Plus Mini Kit (Qiagen, Hilden, Germany) according to the manufacturer instruction.

The RNA from BCP implants was extracted, following removal of the surrounding connective tissue, using Tri-Reagent (Sigma Aldrich). Briefly, the implants were crushed with the use of a pestle in 1.5 ml tube (Argos EW-44468-19) in a final volume of 1 ml of Tri-Reagent and the extraction followed the manufacturer instruction. After DNase treatment, cDNA was synthesized from 100 ng of RNA using the High Capacity cDNA Reverse Transcription kit (Applied Biosystem, Foster City, California, USA). qPCR analysis was performed using TaqMan probes, and Universal PCR Master Mix (Applied Biosystems) using the MX3000P qPCR (Stratagene, San Diego, California, USA). All samples were run in triplicate. Expression levels for *Col1a1* (Mm00801666_g1) and *Col1a2* (Mm00483888_m1) were evaluated. *Gapdh* (Mm99999915_g1) was used as housekeeping. Relative expression levels were calculated using the ΔΔCt method.

Type I collagen analysis

MEFs were plated in 6 well plate at a density of 1.2×10^5 cells/well. After 24 h the cells were transfected with 10 nM siRNA-3554 or siRNA-LacZ as described above. The day after transfection the cells were pre-labelled with D-MEM, 1% FBS containing 0.1 mg/ml ascorbic acid for 2 h to stimulate collagen production. The labelling was performed for 18 h in D-MEM pre-labelling medium using 20 µCi of ^{3}H-Pro/well. Collagen was then extracted and analyzed as previously described [55]. For the analysis of collagen from biphasic calcium phosphate, dissected implants were washed in PBS and decalcified in 0.5 M EDTA pH 7.1. Collagen was extracted by pepsin digestion as described previously and lyophilized [55]. The pellet was resuspended in Laemmli buffer (62.5 mM Tris HCl, pH 6.8, 10% glycerol, 2% sodium dodecyl sulphate (SDS), 0.02% bromophenol blue), denatured at 80 °C for 5 min and separated on 6% SDS-PAGE gels in presence of 0.5 M urea. The gels were stained with Coomassie Picric Staining [56], and digitalized by Versadoc (Biorad, Hercules, California, USA). The bands intensity was measured using Quantity one software (Biorad).

Osteoblasts mineralization assay

24 h after transfection, the mineralization media α-MEM, 10% FBS, 100 µg/ml penicillin, 0.1 mg/ml streptomycin, 5×10^{-8} M dexamethasone (Sigma Aldrich), 0.2 mM ascorbic acid (Fisher Scientific)

Please cite this article as: S. Maruelli, R. Besio, J. Rousseau, et al., Osteoblasts mineralization and collagen matrix is conserved upon specific *Col1a2* silencing..., https://doi.org/10.1016/j.mbplus.2020.100028

and 10 mM β-glycerophosphate (Sigma Aldrich) was added for 19 days, changing the media three times a week. The cells were then fixed in 10% formalin solution neutral buffer (Sigma Aldrich) for 30 min at RT and Von Kossa staining was performed. Images were acquired with a digital scanner at 2400 dpi resolution and analyzed with the Leica application suite V4.5 software. The percentage of mineralized area was calculated on the total well area and normalized on total DNA per well.

Histological and immunohistochemical analysis

The BCP implants were fixed for 24 h in 4% buffered paraformaldehyde (PFA), decalcified in 4% EDTA (Alfa Aesar, Haverhill, Massachusetts, USA) dehydrated and included in paraffin as previously described [57]. 3 µm sections were obtained using microtome RM2265 (Leica, Wetzlar, Germania, USA). Slides were stained with Masson's Trichrome combining hematoxylin for cell nuclei (blue/black), fuchsine for cytoplasm, muscle and erythrocytes (red) and light green solution for collagen (green), and with Tartrate-Resistant Acid Phosphatase (TRAP) commercial staining kit (Phosphatase Leukocyte Staining Kit, Sigma Aldrich) for osteoclasts.

Immunohistochemistry was performed to evaluate the presence of both EGFP expressing cells and macrophages. Briefly, after dewaxing and rehydration, heat-induced epitope retrieval was performed using 10 mM Tris HCl, 1 mM EDTA pH 9.0. Sections were treated with 3% H_2O_2 for 15 min at room temperature and the non-specific antibody binding was blocked using 2% normal donkey serum and 1% bovine serum albumin in 1× TBS Tween for 25 min at room temperature. Primary antibodies rat anti-mouse CD68 (1:100, FA-11, Biorad, France) and rabbit anti-EGFP (1:2000, ab290, Abcam, France) were incubated over night at 4 °C to detect macrophages and mouse EGFP-MSCs implanted with the BCP particles, respectively. Finally, a biotinylated goat anti-mouse IgG secondary antibody (Dako) and streptavidin/ horse radish peroxydase complexes (Dako) were used and revealed by a short incubation with 3,3′- diaminobenzidine (K3468, Agilent, Denmark). Nuclei were counterstained with a Gill-Hematoxylin solution. After dehydration and mounting with petex, slides were acquired using Nanozoomer 2.0 Hamamatsu slide scanner. Quantitative analysis of the collagen tissue stained by Masson's Trichrome was then performed. The collagen area and the total area of the implants were manually defined and quantified using Leica application suite V 4.5 (n = 4). The collagen amount was expressed as percentage of the total area.

Statistical analysis

All results were expressed as mean ± standard deviation. Statistical comparisons were based on Student's t-test. A $p < .05$ was considered significant.

Declaration of competing interest

The authors declare that they have no known competing financial interests or personal relationships that could have appeared to influence the work reported in this paper.

Acknowledgements

We thank Dr. Marco Manca, Department of Molecular Medicine, Biochemistry Unit, University of Pavia, Italy, for initial experiments on murine embryonic fibroblasts and the OPBA of the University of Pavia for support in animal protocol drawing up.

Funding

The work was supported by AFM-Telethon, France (2012-1607) to AF and VT, Care4Brittle-Bone, The Netherlands (2015-0003) to AF and the European Community, FP7, 'Sybil' project, Europe (Grant No. 602300) and Italian Ministry of Education, University and Research (MIUR), Italy [Dipartimenti di Eccellenza (2018–2022)] to AR and AF.

Appendix A. Supplementary data

Supplementary data to this article can be found online at https://doi.org/10.1016/j.mbplus.2020.100028.

Received 4 November 2019;
Received in revised form 24 January 2020;
Accepted 24 January 2020
Available online xxxx

Keywords:
Collagen;
Osteogenesis imperfecta;
siRNA;
Silencing;
Gene therapy

These authors contributed equally to this work.

Abbreviations used:
BCP, biphasic calcium phosphate; D-MEM, Dulbecco-modified Eagle's medium; EDS, Ehlers Danlos syndrome;

EGFP, enhanced green fluorescent protein; FBS, fetal bovine serum; MEF, murine embryonic fibroblast; MSC, mesenchymal stem cell; NMD, nonsense mediated RNA decay; OI, osteogenesis imperfecta; PBS, phosphate buffered saline; RNAi, RNA interference; SDS, sodium dodecyl sulphate; shRNA, short hairpin RNA; siRNA, small interfering RNA; TRAP, tartrate-resistant acid phosphatase.

1These authors contributed equally to this work.

References

[1] A. Forlino, J.C. Marini, Osteogenesis imperfecta, Lancet 387 (2016) 1657–1671.
[2] R. Besio, C.W. Chow, F. Tonelli, J.C. Marini, A. Forlino, Bone biology: insights from osteogenesis imperfecta and related rare fragility syndromes, The FEBS Journal 286 (2019) 3033–3056.
[3] R. Besio, A. Forlino, Treatment options for osteogenesis imperfecta, Expert Opinion on Orphan Drugs 3 (2015) 165–181.
[4] V. Rossi, B. Lee, R. Marom, Osteogenesis imperfecta: advancements in genetics and treatment, Current Opinion in Pediatrics 31 (2019) 708–715.
[5] R. Morello, Osteogenesis imperfecta and therapeutics, Matrix Biology: Journal of the International Society for Matrix Biology 71–72 (2018) 294–312.
[6] M.C. Willing, S.P. Deschenes, R.L. Slayton, E.J. Roberts, Premature chain termination is a unifying mechanism for COL1A1 null alleles in osteogenesis imperfecta type I cell strains, American Journal of Human Genetics 59 (1996) 799–809.
[7] J.C. Marini, A. Forlino, W.A. Cabral, A.M. Barnes, J.D. San Antonio, S. Milgrom, J.C. Hyland, J. Korkko, D.J. Prockop, A. De Paepe, P. Coucke, S. Symoens, F.H. Glorieux, P.J. Roughley, A.M. Lund, K. Kuurila-Svahn, H. Hartikka, D.H. Cohn, D. Krakow, M. Mottes, U. Schwarze, D. Chen, K. Yang, C. Kuslich, J. Troendle, R. Dalgleish, P.H. Byers, Consortium for osteogenesis imperfecta mutations in the helical domain of type I collagen: regions rich in lethal mutations align with collagen binding sites for integrins and proteoglycans, Human Mutation 28 (2007) 209–221.
[8] D. Schiroli, M.J. Gomara, E. Maurizi, S.D. Atkinson, L. Mairs, K.A. Christie, D.F. Cobice, C.M. McCrudden, M.A. Nesbit, I. Haro, T. Moore, Effective in vivo topical delivery of siRNA and gene silencing in intact corneal epithelium using a modified cell-penetrating peptide, Molecular Therapy–Nucleic Acids 17 (2019) 891–906.
[9] K. Zaleta-Rivera, A. Dainis, A.J.S. Ribeiro, P. Cordero, G. Rubio, C. Shang, J. Liu, T. Finsterbach, V.N. Parikh, S. Sutton, K. Seo, N. Sinha, N. Jain, Y. Huang, R.J. Hajjar, M.A. Kay, D. Szczesna-Cordary, B.L. Pruitt, M.T. Wheeler, E.A. Ashley, Allele-specific silencing ameliorates restrictive cardiomyopathy attributable to a human myosin regulatory light chain mutation, Circulation 140 (2019) 765–778.
[10] E. Giorgio, M. Lorenzati, P. Rivetti di Val Cervo, A. Brussino, M. Cernigoj, E. Della Sala, A. Bartoletti Stella, M. Ferrero, M. Caiazzo, S. Capellari, P. Cortelli, L. Conti, E. Cattaneo, A. Buffo, A. Brusco, Allele-specific silencing as treatment for gene duplication disorders: proof-of-principle in autosomal dominant leukodystrophy, Brain 142 (2019) 1905–1920.
[11] P.A. Keire, S.L. Bressler, E.R. Mulvihill, B.C. Starcher, I. Kang, T.N. Wight, Inhibition of versican expression by siRNA facilitates tropoelastin synthesis and elastic fiber formation by human SK-LMS-1 leiomyosarcoma smooth muscle cells in vitro and in vivo, Matrix Biology: Journal of the International Society for Matrix Biology 50 (2016) 67–81.
[12] D. Schuppan, M. Ashfaq-Khan, A.T. Yang, Y.O. Kim, Liver fibrosis: direct antifibrotic agents and targeted therapies, Matrix Biology: Journal of the International Society for Matrix Biology 68–69 (2018) 435–451.
[13] O. Molokanova, K. Schonig, S.Y. Weng, X. Wang, M. Bros, M. Diken, S. Ohngemach, M. Karsdal, D. Strand, A. Nikolaev, L. Eshkind, D. Schuppan, Inducible knockdown of procollagen I protects mice from liver fibrosis and leads to dysregulated matrix genes and attenuated inflammation, Matrix Biology: Journal of the International Society for Matrix Biology 66 (2018) 34–49.
[14] Z. Sun, I. Velazquez-Quesada, D. Murdamoothoo, C. Ahowesso, A. Yilmaz, C. Spenle, G. Averous, W. Erne, F. Oberndorfer, A. Oszwald, R. Kain, C. Bourdon, P. Mangin, C. Deligne, K. Midwood, C. Abou-Faycal, O. Lefebvre, A. Klein, M. van der Heyden, M.P. Chenard, G. Christofori, C. Mathelin, T. Loustau, T. Hussenet, G. Orend, Tenascin-C increases lung metastasis by impacting blood vessel invasions, Matrix Biology: Journal of the International Society for Matrix Biology 83 (2019) 26–47.
[15] R.M. Melero-Fernandez de Mera, U.T. Arasu, R. Karna, S. Oikari, K. Rilla, D. Vigetti, A. Passi, P. Heldin, M.I. Tammi, A. J. Deen, Effects of mutations in the post-translational modification sites on the trafficking of hyaluronan synthase 2 (HAS2), Matrix Biology: Journal of the International Society for Matrix Biology 80 (2018) 85–103.
[16] M.F. Coutinho, L. Matos, J.I. Santos, S. Alves, RNA therapeutics: how far have we gone? Adv. Exp. Med. Biol. 1157 (2019) 133–177.
[17] Y. Weng, H. Xiao, J. Zhang, X.J. Liang, Y. Huang, RNAi therapeutic and its innovative biotechnological evolution, Biotechnology Advances 37 (2019) 801–825.
[18] D. Adams, A. Gonzalez-Duarte, W.D. O'Riordan, C.C. Yang, M. Ueda, A.V. Kristen, I. Tournev, H.H. Schmidt, T. Coelho, J. L. Berk, K.P. Lin, G. Vita, S. Attarian, V. Plante-Bordeneuve, M.M. Mezei, J.M. Campistol, J. Buades, T.H. Brannagan 3rd, B.J. Kim, J. Oh, Y. Parman, Y. Sekijima, P.N. Hawkins, S.D. Solomon, M. Polydefkis, P.J. Dyck, P.J. Gandhi, S. Goyal, J. Chen, A.L. Strahs, S.V. Nochur, M.T. Sweetser, P.P. Garg, A. K. Vaishnaw, J.A. Gollob, O.B. Suhr, Patisiran, an RNAi therapeutic, for hereditary transthyretin amyloidosis, The New England Journal of Medicine 379 (2018) 11–21.
[19] J. Rousseau, R. Gioia, P. Layrolle, B. Lieubeau, D. Heymann, A. Rossi, J.C. Marini, V. Trichet, A. Forlino, Allele-specific Col1a1 silencing reduces mutant collagen in fibroblasts from Brtl mouse, a model for classical osteogenesis imperfecta, European Journal of Human Genetics 22 (2013) 667–674.
[20] K. Lindahl, C.J. Rubin, A. Kindmark, O. Ljunggren, Allele dependent silencing of COL1A2 using small interfering RNAs, International Journal of Medical Sciences 5 (2008) 361–365.
[21] K. Lindahl, A. Kindmark, N. Laxman, E. Astrom, C.J. Rubin, O. Ljunggren, Allele dependent silencing of collagen type I using small interfering RNAs targeting 3'UTR Indels - a novel therapeutic approach in osteogenesis imperfecta, International Journal of Medical Sciences 10 (2013) 1333–1343.
[22] U. Schwarze, R. Hata, V.A. McKusick, H. Shinkai, H.E. Hoyme, R.E. Pyeritz, P.H. Byers, Rare autosomal recessive

Please cite this article as: S. Maruelli, R. Besio, J. Rousseau, et al., Osteoblasts mineralization and collagen matrix is conserved upon specific *Col1a2* silencing..., https://doi.org/10.1016/j.mbplus.2020.100028

cardiac valvular form of Ehlers-Danlos syndrome results from mutations in the COL1A2 gene that activate the nonsense-mediated RNA decay pathway, American Journal of Human Genetics 74 (2004) 917–930.
[23] H. Saeed, H. Taipaleenmaki, A.M. Aldahmash, B.M. Abdallah, M. Kassem, Mouse embryonic fibroblasts (MEF) exhibit a similar but not identical phenotype to bone marrow stromal stem cells (BMSC), Stem Cell Reviews and Reports 8 (2011) 318–328.
[24] M.F. Young, Skeletal biology: where matrix meets mineral, Matrix Biology 52–54 (2016) 1–6.
[25] B.S. Kim, M.K. Choi, J.H. Yoon, J. Lee, Evaluation of bone regeneration with biphasic calcium phosphate substitute implanted with bone morphogenetic protein 2 and mesenchymal stem cells in a rabbit calvarial defect model, Oral Surgery, Oral Medicine, Oral Pathology, Oral Radiology 120 (2015) 2–9.
[26] A.L. Gamblin, M.A. Brennan, A. Renaud, H. Yagita, F. Lezot, D. Heymann, V. Trichet, P. Layrolle, Bone tissue formation with human mesenchymal stem cells and biphasic calcium phosphate ceramics: the local implication of osteoclasts and macrophages, Biomaterials 35 (2014) 9660–9667.
[27] A. Schnieke, K. Harbers, R. Jaenisch, Embryonic lethal mutation in mice induced by retrovirus insertion into the alpha 1(I) collagen gene, Nature 304 (1983) 315–320.
[28] J. Uitto, Collagen polymorphism: isolation and partial characterization of alpha 1(I)-trimer molecules in normal human skin, Archives of Biochemistry and Biophysics 192 (1979) 371–379.
[29] A.S. Narayanan, D.F. Meyers, R.C. Page, H.G. Welgus, Action of mammalian collagenases on type I trimer collagen, Collagen and Related Research 4 (1984) 289–296.
[30] S.A. Jimenez, R.I. Bashey, M. Benditt, R. Yankowski, Identification of collagen alpha1(I) trimer in embryonic chick tendons and calvaria, Biochemical and Biophysical Research Communications 78 (1977) 1354–1361.
[31] J.H. Rupard, S.J. Dimari, I. Damjanov, M.A. Haralson, Synthesis of type I homotrimer collagen molecules by cultured human lung adenocarcinoma cells, The American Journal of Pathology 133 (1988) 316–326.
[32] E. Makareeva, S. Han, J.C. Vera, D.L. Sackett, K. Holmbeck, C.L. Phillips, R. Visse, H. Nagase, S. Leikin, Carcinomas contain a matrix metalloproteinase-resistant isoform of type I collagen exerting selective support to invasion, Cancer Research 70 (2010) 4366–4374.
[33] M. Rojkind, M.A. Giambrone, L. Biempica, Collagen types in normal and cirrhotic liver, Gastroenterology 76 (1979) 710–719.
[34] H.P. Ehrlich, H. Brown, B.S. White, Evidence for type V and I trimer collagens in Dupuytren's contracture palmar fascia, Biochemical Medicine 28 (1982) 273–284.
[35] M.A. Haralson, H.R. Jacobson, R.L. Hoover, Collagen polymorphism in cultured rat kidney mesangial cells, Laboratory Investigation 57 (1987) 513–523.
[36] S. Yamagata, T. Yamagata, FBJ virus-induced osteosarcoma contains type I, type I trimer, type III as well as type V collagens, Journal of Biochemistry 96 (1984) 17–26.
[37] L. Moro, B.D. Smith, Identification of collagen alpha1(I) trimer and normal type I collagen in a polyoma virus-induced mouse tumor, Archives of Biochemistry and Biophysics 182 (1977) 33–41.
[38] A.S. Narayanan, R.C. Page, D.F. Meyers, Characterization of collagens of diseased human gingiva, Biochemistry 19 (1980) 5037–5043.
[39] S.D. Chipman, H.O. Sweet, D.J. McBride Jr., M.T. Davisson, S.C. Marks Jr., A.R. Shuldiner, R.J. Wenstrup, D.W. Rowe, J. R. Shapiro, Defective pro alpha 2(I) collagen synthesis in a recessive mutation in mice: a model of human osteogenesis imperfecta, Proceedings of the National Academy of Sciences of the United States of America 90 (1993) 1701–1705.
[40] J.M. Pace, M. Wiese, A.S. Drenguis, N. Kuznetsova, S. Leikin, U. Schwarze, D. Chen, S.H. Mooney, S. Unger, P.H. Byers, Defective C-propeptides of the proalpha2(I) chain of type I procollagen impede molecular assembly and result in osteogenesis imperfecta, The Journal of Biological Chemistry 283 (2008) 16061–16067.
[41] R. Besio, N. Garibaldi, L. Leoni, L. Cipolla, S. Sabbioneda, M. Biggiogera, M. Mottes, M. Aglan, G.A. Otaify, S.A. Temtamy, Rossi, A & Forlino A Cellular stress due to impairment of collagen prolyl hydroxylation complex is rescued by the chaperone 4-phenylbutyrate, Disease Models & Mechanisms 12 (2019).
[42] R. Besio, G. Iula, N. Garibaldi, L. Cipolla, S. Sabbioneda, M. Biggiogera, J.C. Marini, A. Rossi, A. Forlino, 4-PBA ameliorates cellular homeostasis in fibroblasts from osteogenesis imperfecta patients by enhancing autophagy and stimulating protein secretion, Biochimica et Biophysica Acta - Molecular Basis of Disease (1864) 1642–1652.
[43] H. Li, X. Jiang, J. Delaney, T. Franceschetti, I. Bilic-Curcic, J. Kalinovsky, J.A. Lorenzo, D. Grcevic, D.W. Rowe, I. Kalajzic, Immature osteoblast lineage cells increase osteoclastogenesis in osteogenesis imperfecta murine, The American Journal of Pathology 176 (2010) 2405–2413.
[44] J.S. Khillan, S.W. Li, D.J. Prockop, Partial rescue of a lethal phenotype of fragile bones in transgenic mice with a chimeric antisense gene directed against a mutated collagen gene, Proceedings of the National Academy of Sciences of the United States of America 91 (1994) 6298–6302.
[45] P.A. Dawson, J.C. Marini, Hammerhead ribozymes selectively suppress mutant type I collagen mRNA in osteogenesis imperfecta fibroblasts, Nucleic Acids Research 28 (2000) 4013–4020.
[46] G. Grassi, A. Forlino, J.C. Marini, Cleavage of collagen RNA transcripts by hammerhead ribozymes in vitro is mutation-specific and shows competitive binding effects, Nucleic Acids Research 25 (1997) 3451–3458.
[47] I. Toudjarska, M.W. Kilpatrick, J. Niu, R.J. Wenstrup, P. Tsipouras, Delivery of a hammerhead ribozyme specifically downregulates mutant type I collagen mRNA in a murine model of osteogenesis imperfecta, Antisense & Nucleic Acid Drug Development 11 (2001) 341–346.
[48] M.A. Brennan, A. Renaud, J. Amiaud, M.T. Rojewski, H. Schrezenmeier, D. Heymann, V. Trichet, P. Layrolle, Preclinical studies of bone regeneration with human bone marrow stromal cells and biphasic calcium phosphate, Stem Cell Research & Therapy 5 (2014) 114.
[49] F. Takeshita, Y. Minakuchi, S. Nagahara, K. Honma, H. Sasaki, K. Hirai, T. Teratani, N. Namatame, Y. Yamamoto, K. Hanai, T. Kato, A. Sano, T. Ochiya, Efficient delivery of small interfering RNA to bone-metastatic tumors by using atelocollagen in vivo, Proceedings of the National Academy of Sciences of the United States of America 102 (2005) 12177–12182.
[50] B. Urban-Klein, S. Werth, S. Abuharbeid, F. Czubayko, A. Aigner, RNAi-mediated gene-targeting through systemic application of polyethylenimine (PEI)-complexed siRNA in vivo, Gene Therapy 12 (2005) 461–466.

Please cite this article as: S. Maruelli, R. Besio, J. Rousseau, et al., Osteoblasts mineralization and collagen matrix is conserved upon specific *Col1a2* silencing..., https://doi.org/10.1016/j.mbplus.2020.100028

[51] A. Aigner, Delivery systems for the direct application of siRNAs to induce RNA interference (RNAi) in vivo, Journal of Biomedicine & Biotechnology 2006 (2006) 71659.
[52] T. Tanaka, L.S. Mangala, P.E. Vivas-Mejia, R. Nieves-Alicea, A. P. Mann, E. Mora, H.D. Han, M.M. Shahzad, X. Liu, R. Bhavane, J. Gu, J.R. Fakhoury, C. Chiappini, C. Lu, K. Matsuo, B. Godin, R.L. Stone, A.M. Nick, G. Lopez-Berestein, A.K. Sood, M. Ferrari, Sustained small interfering RNA delivery by mesoporous silicon particles, Cancer Research 70 (2010) 3687–3696.
[53] J. Rousseau, V. Escriou, P. Perrot, G. Picarda, C. Charrier, D. Scherman, D. Heymann, F. Redini, V. Trichet, Advantages of bioluminescence imaging to follow siRNA or chemotherapeutic treatments in osteosarcoma preclinical models, Cancer Gene Therapy 17 (2010) 387–397.
[54] M. Khoury, P. Louis-Plence, V. Escriou, D. Noel, C. Largeau, C. Cantos, D. Scherman, C. Jorgensen, F. Apparailly, Efficient new cationic liposome formulation for systemic delivery of small interfering RNA silencing tumor necrosis factor alpha in experimental arthritis, Arthritis and Rheumatism 54 (2006) 1867–1877.
[55] A. Forlino, F. Tonelli, R. Besio, Steady-state and pulse-chase analyses of fibrillar collagen, Methods in Molecular Biology 1952 (2019) 45–53.
[56] J.L. Stephano, M. Gould, L. Rojas-Galicia, Advantages of picrate fixation for staining polypeptides in polyacrylamide gels, Analytical Biochemistry 152 (1986) 308–313.
[57] C. Paganini, L. Monti, R. Costantini, R. Besio, S. Lecci, M. Biggiogera, K. Tian, J.M. Schwartz, C. Huber, V. Cormier-Daire, B.G. Gibson, K.A. Pirog, A. Forlino, A. Rossi, Calcium activated nucleotidase 1 (CANT1) is critical for glycosaminoglycan biosynthesis in cartilage and endochondral ossification, Matrix Biology: Journal of the International Society for Matrix Biology 81 (2018) 70–90.

Please cite this article as: S. Maruelli, R. Besio, J. Rousseau, et al., Osteoblasts mineralization and collagen matrix is conserved upon specific *Col1a2* silencing..., https://doi.org/10.1016/j.mbplus.2020.100028

BIBLIOGRAPHY

1. *Istologia di V. Monesi*. 6° ed.: Piccin.
2. Adamo, S., et al., *Istologia di V. Monesi*. 6° ed. 2016: Piccin.
3. Rutkovskiy, A., K.O. Stensløkken, and I.J. Vaage, *Osteoblast Differentiation at a Glance.* Med Sci Monit Basic Res, 2016. **22**: p. 95-106.
4. Jubb, Kennedy, and Palmer, *Pathology of Domestic Animals: Volume 1 - Chapter 2, Bones and Joints*. Sixth edition ed. 2016.
5. Ricard-Blum, S., *The collagen family.* Cold Spring Harb Perspect Biol, 2011. **3**(1): p. a004978.
6. Orgel, J.P., et al., *Microfibrillar structure of type I collagen in situ.* Proc Natl Acad Sci U S A, 2006. **103**(24): p. 9001-5.
7. Gelse, K., E. Pöschl, and T. Aigner, *Collagens--structure, function, and biosynthesis.* Adv Drug Deliv Rev, 2003. **55**(12): p. 1531-46.
8. Holmes, R., et al., *Influence of telopeptides on the structural and physical properties of polymeric and monomeric acid-soluble type I collagen.* Mater Sci Eng C Mater Biol Appl, 2017. **77**: p. 823-827.
9. Marini, J.C., et al., *Osteogenesis imperfecta.* Nat Rev Dis Primers, 2017. **3**: p. 17052.
10. Forlino, A. and J.C. Marini, *Osteogenesis imperfecta.* Lancet, 2016. **387**(10028): p. 1657-71.
11. Canty, E.G. and K.E. Kadler, *Procollagen trafficking, processing and fibrillogenesis.* J Cell Sci, 2005. **118**(Pt 7): p. 1341-53.
12. Krane, S.M., *The importance of proline residues in the structure, stability and susceptibility to proteolytic degradation of collagens.* Amino Acids, 2008. **35**(4): p. 703-10.
13. Jenkins, C.L., et al., *Effect of 3-hydroxyproline residues on collagen stability.* J Am Chem Soc, 2003. **125**(21): p. 6422-7.
14. Vranka, J.A., L.Y. Sakai, and H.P. Bächinger, *Prolyl 3-hydroxylase 1, enzyme characterization and identification of a novel family of enzymes.* J Biol Chem, 2004. **279**(22): p. 23615-21.
15. Forlino, A., et al., *New perspectives on osteogenesis imperfecta.* Nat Rev Endocrinol, 2011. **7**(9): p. 540-57.
16. Tonelli, F., et al., *Crtap and p3h1 knock out zebrafish support defective collagen chaperoning as the cause of their osteogenesis imperfecta phenotype.* Matrix Biol, 2020.
17. Marini, J.C., et al., *Components of the collagen prolyl 3-hydroxylation complex are crucial for normal bone development.* Cell Cycle, 2007. **6**(14): p. 1675-81.
18. Morello, R., et al., *CRTAP is required for prolyl 3- hydroxylation and mutations cause recessive osteogenesis imperfecta.* Cell, 2006. **127**(2): p. 291-304.
19. van Dijk, F.S., et al., *PPIB mutations cause severe osteogenesis imperfecta.* Am J Hum Genet, 2009. **85**(4): p. 521-7.
20. Smith, T., et al., *Hsp47 and cyclophilin B traverse the endoplasmic reticulum with procollagen into pre-Golgi intermediate vesicles. A role for Hsp47 and cyclophilin B in the export of procollagen from the endoplasmic reticulum.* J Biol Chem, 1995. **270**(31): p. 18323-8.

21. Heard, M.E., et al., *Sc65-Null Mice Provide Evidence for a Novel Endoplasmic Reticulum Complex Regulating Collagen Lysyl Hydroxylation.* PLoS Genet, 2016. **12**(4): p. e1006002.
22. Gruenwald, K., et al., *Sc65 is a novel endoplasmic reticulum protein that regulates bone mass homeostasis.* J Bone Miner Res, 2014. **29**(3): p. 666-75.
23. Kozlov, G., et al., *Structural basis of cyclophilin B binding by the calnexin/calreticulin P-domain.* J Biol Chem, 2010. **285**(46): p. 35551-7.
24. Yao, Q., et al., *Roles of cyclophilins in cancers and other organ systems.* World J Surg, 2005. **29**(3): p. 276-80.
25. Makareeva, E., N.A. Aviles, and S. Leikin, *Chaperoning osteogenesis: new protein-folding disease paradigms.* Trends Cell Biol, 2011. **21**(3): p. 168-76.
26. Ishida, Y. and K. Nagata, *Hsp47 as a collagen-specific molecular chaperone.* Methods Enzymol, 2011. **499**: p. 167-82.
27. Omari, S., et al., *Mechanisms of procollagen and HSP47 sorting during ER-to-Golgi trafficking.* Matrix Biol, 2020.
28. Ishikawa, Y., P. Holden, and H.P. Bächinger, *Heat shock protein 47 and 65-kDa FK506-binding protein weakly but synergistically interact during collagen folding in the endoplasmic reticulum.* J Biol Chem, 2017. **292**(42): p. 17216-17224.
29. Chen, Y., et al., *FKBP65-dependent peptidyl-prolyl isomerase activity potentiates the lysyl hydroxylase 2-driven collagen cross-link switch.* Sci Rep, 2017. **7**: p. 46021.
30. Duran, I., et al., *A Chaperone Complex Formed by HSP47, FKBP65, and BiP Modulates Telopeptide Lysyl Hydroxylation of Type I Procollagen.* J Bone Miner Res, 2017. **32**(6): p. 1309-1319.
31. Sepulveda, D., et al., *Interactome Screening Identifies the ER Luminal Chaperone Hsp47 as a Regulator of the Unfolded Protein Response Transducer IRE1α.* Mol Cell, 2018. **69**(2): p. 238-252.e7.
32. Davis, E.C., et al., *Identification of tropoelastin as a ligand for the 65-kD FK506-binding protein, FKBP65, in the secretory pathway.* J Cell Biol, 1998. **140**(2): p. 295-303.
33. Besio, R., et al., *Bone biology: insights from osteogenesis imperfecta and related rare fragility syndromes.* FEBS J, 2019. **286**(15): p. 3033-3056.
34. Widmer, C., et al., *Molecular basis for the action of the collagen-specific chaperone Hsp47/SERPINH1 and its structure-specific client recognition.* Proc Natl Acad Sci U S A, 2012. **109**(33): p. 13243-7.
35. Köhler, A., et al., *New specific HSP47 functions in collagen subfamily chaperoning.* FASEB J, 2020.
36. Ishikawa, Y., et al., *Intracellular mechanisms of molecular recognition and sorting for transport of large extracellular matrix molecules.* Proc Natl Acad Sci U S A, 2016. **113**(41): p. E6036-E6044.
37. Saito, K., et al., *TANGO1 facilitates cargo loading at endoplasmic reticulum exit sites.* Cell, 2009. **136**(5): p. 891-902.
38. McCaughey, J. and D.J. Stephens, *ER-to-Golgi Transport: A Sizeable Problem.* Trends Cell Biol, 2019. **29**(12): p. 940-953.
39. Zanetti, G., et al., *The structure of the COPII transport-vesicle coat assembled on membranes.* Elife, 2013. **2**: p. e00951.
40. Keller, P. and K. Simons, *Post-Golgi biosynthetic trafficking.* J Cell Sci, 1997. **110 (Pt 24)**: p. 3001-9.

41. Polishchuk, R.S., et al., *Correlative light-electron microscopy reveals the tubular-saccular ultrastructure of carriers operating between Golgi apparatus and plasma membrane.* J Cell Biol, 2000. **148**(1): p. 45-58.
42. Polishchuk, E.V., et al., *Mechanism of constitutive export from the golgi: bulk flow via the formation, protrusion, and en bloc cleavage of large trans-golgi network tubular domains.* Mol Biol Cell, 2003. **14**(11): p. 4470-85.
43. Leblond, C.P., *Synthesis and secretion of collagen by cells of connective tissue, bone, and dentin.* Anat Rec, 1989. **224**(2): p. 123-38.
44. Marchi, F. and C.P. Leblond, *Radioautographic characterization of successive compartments along the rough endoplasmic reticulum-Golgi pathway of collagen precursors in foot pad fibroblasts of [3H]proline-injected rats.* J Cell Biol, 1984. **98**(5): p. 1705-9.
45. Trelstad, R.L. and K. Hayashi, *Tendon collagen fibrillogenesis: intracellular subassemblies and cell surface changes associated with fibril growth.* Dev Biol, 1979. **71**(2): p. 228-42.
46. Kadler, K., *Extracellular matrix 1: Fibril-forming collagens.* Protein Profile, 1995. **2**(5): p. 491-619.
47. Yamauchi, M. and M. Shiiba, *Lysine hydroxylation and cross-linking of collagen.* Methods Mol Biol, 2008. **446**: p. 95-108.
48. Bradshaw, A.D., et al., *Pressure overload-induced alterations in fibrillar collagen content and myocardial diastolic function: role of secreted protein acidic and rich in cysteine (SPARC) in post-synthetic procollagen processing.* Circulation, 2009. **119**(2): p. 269-80.
49. Kadler, K.E., A. Hill, and E.G. Canty-Laird, *Collagen fibrillogenesis: fibronectin, integrins, and minor collagens as organizers and nucleators.* Curr Opin Cell Biol, 2008. **20**(5): p. 495-501.
50. Birk, D.E., *Type V collagen: heterotypic type I/V collagen interactions in the regulation of fibril assembly.* Micron, 2001. **32**(3): p. 223-37.
51. Blaschke, U.K., et al., *Collagen XI nucleates self-assembly and limits lateral growth of cartilage fibrils.* J Biol Chem, 2000. **275**(14): p. 10370-8.
52. Gordon, M.K. and R.A. Hahn, *Collagens.* Cell Tissue Res, 2010. **339**(1): p. 247-57.
53. Fleischmajer, R., et al., *Dermal collagen fibrils are hybrids of type I and type III collagen molecules.* J Struct Biol, 1990. **105**(1-3): p. 162-9.
54. Taye, N., S.Z. Karoulias, and D. Hubmacher, *The "other" 15-40%: The Role of Non-Collagenous Extracellular Matrix Proteins and Minor Collagens in Tendon.* J Orthop Res, 2020. **38**(1): p. 23-35.
55. Li, Y., et al., *Biomechanical stimulation of osteoblast gene expression requires phosphorylation of the RUNX2 transcription factor.* J Bone Miner Res, 2012. **27**(6): p. 1263-74.
56. Komori, T., *Regulation of Proliferation, Differentiation and Functions of Osteoblasts by Runx2.* Int J Mol Sci, 2019. **20**(7).
57. Collins, F.L., et al., *The Potential of Probiotics as a Therapy for Osteoporosis.* Microbiol Spectr, 2017. **5**(4).
58. Qiu, Z.Y., et al., *Mineralized Collagen: Rationale, Current Status, and Clinical Applications.* Materials (Basel), 2015. **8**(8): p. 4733-4750.

59. Montessuit, C., J.P. Bonjour, and J. Caverzasio, *Expression and regulation of Na-dependent P(i) transport in matrix vesicles produced by osteoblast-like cells.* J Bone Miner Res, 1995. **10**(4): p. 625-31.
60. Anderson, H.C., *Matrix vesicles and calcification.* Curr Rheumatol Rep, 2003. **5**(3): p. 222-6.
61. Blair, H.C., et al., *Osteoblast Differentiation and Bone Matrix Formation In Vivo and In Vitro.* Tissue Eng Part B Rev, 2017. **23**(3): p. 268-280.
62. Harrison, G., I.M. Shapiro, and E.E. Golub, *The phosphatidylinositol-glycolipid anchor on alkaline phosphatase facilitates mineralization initiation in vitro.* J Bone Miner Res, 1995. **10**(4): p. 568-73.
63. Orimo, H., *The mechanism of mineralization and the role of alkaline phosphatase in health and disease.* J Nippon Med Sch, 2010. **77**(1): p. 4-12.
64. Hodge, A.J., *Molecular models illustrating the possible distributions of 'holes' in simple systematically staggered arrays of type I collagen molecules in native-type fibrils.* Connect Tissue Res, 1989. **21**(1-4): p. 137-47.
65. Gorski, J.P., *Acidic phosphoproteins from bone matrix: a structural rationalization of their role in biomineralization.* Calcif Tissue Int, 1992. **50**(5): p. 391-6.
66. Young, M.F., et al., *Structure, expression, and regulation of the major noncollagenous matrix proteins of bone.* Clin Orthop Relat Res, 1992(281): p. 275-94.
67. Rosset, E.M. and A.D. Bradshaw, *SPARC/osteonectin in mineralized tissue.* Matrix Biol, 2016. **52-54**: p. 78-87.
68. Ganss, B., R.H. Kim, and J. Sodek, *Bone sialoprotein.* Crit Rev Oral Biol Med, 1999. **10**(1): p. 79-98.
69. Sodek, J., B. Ganss, and M.D. McKee, *Osteopontin.* Crit Rev Oral Biol Med, 2000. **11**(3): p. 279-303.
70. Hauschka, P.V., et al., *Osteocalcin and matrix Gla protein: vitamin K-dependent proteins in bone.* Physiol Rev, 1989. **69**(3): p. 990-1047.
71. Willems, B.A., et al., *The realm of vitamin K dependent proteins: shifting from coagulation toward calcification.* Mol Nutr Food Res, 2014. **58**(8): p. 1620-35.
72. Zhu, J.X., et al., *Temporal and spatial gene expression of major bone extracellular matrix molecules during embryonic mandibular osteogenesis in rats.* Histochem J, 2001. **33**(1): p. 25-35.
73. Zoch, M.L., T.L. Clemens, and R.C. Riddle, *New insights into the biology of osteocalcin.* Bone, 2016. **82**: p. 42-9.
74. Ishida, M. and S. Amano, *Osteocalcin fragment in bone matrix enhances osteoclast maturation at a late stage of osteoclast differentiation.* J Bone Miner Metab, 2004. **22**(5): p. 415-29.
75. Dallas, S.L., M. Prideaux, and L.F. Bonewald, *The osteocyte: an endocrine cell ... and more.* Endocr Rev, 2013. **34**(5): p. 658-90.
76. Nicholls, J.J., et al., *The skeletal consequences of thyrotoxicosis.* J Endocrinol, 2012. **213**(3): p. 209-21.
77. Okamoto, K., et al., *Osteoimmunology: The Conceptual Framework Unifying the Immune and Skeletal Systems.* Physiol Rev, 2017. **97**(4): p. 1295-1349.
78. Ono, T. and T. Nakashima, *Recent advances in osteoclast biology.* Histochem Cell Biol, 2018. **149**(4): p. 325-341.
79. Silva, B.C. and J.P. Bilezikian, *Parathyroid hormone: anabolic and catabolic actions on the skeleton.* Curr Opin Pharmacol, 2015. **22**: p. 41-50.

80. Nakashima, T., et al., *Evidence for osteocyte regulation of bone homeostasis through RANKL expression.* Nat Med, 2011. **17**(10): p. 1231-4.
81. Takayanagi, H., et al., *Induction and activation of the transcription factor NFATc1 (NFAT2) integrate RANKL signaling in terminal differentiation of osteoclasts.* Dev Cell, 2002. **3**(6): p. 889-901.
82. Asagiri, M., et al., *Autoamplification of NFATc1 expression determines its essential role in bone homeostasis.* J Exp Med, 2005. **202**(9): p. 1261-9.
83. Kajiya, H., *Calcium signaling in osteoclast differentiation and bone resorption.* Adv Exp Med Biol, 2012. **740**: p. 917-32.
84. Marini, J.C., et al., *Consortium for osteogenesis imperfecta mutations in the helical domain of type I collagen: regions rich in lethal mutations align with collagen binding sites for integrins and proteoglycans.* Hum Mutat, 2007. **28**(3): p. 209-21.
85. Fratzl-Zelman, N., et al., *Bone mass and mineralization in osteogenesis imperfecta.* Wien Med Wochenschr, 2015. **165**(13-14): p. 271-7.
86. Sillence, D.O., A. Senn, and D.M. Danks, *Genetic heterogeneity in osteogenesis imperfecta.* J Med Genet, 1979. **16**(2): p. 101-16.
87. Sillence, D.O., D.L. Rimoin, and D.M. Danks, *Clinical variability in osteogenesis imperfecta-variable expressivity or genetic heterogeneity.* Birth Defects Orig Artic Ser, 1979. **15**(5B): p. 113-29.
88. Ishikawa, Y. and H.P. Bächinger, *A molecular ensemble in the rER for procollagen maturation.* Biochim Biophys Acta, 2013. **1833**(11): p. 2479-91.
89. Barnes, A.M., et al., *Deficiency of cartilage-associated protein in recessive lethal osteogenesis imperfecta.* N Engl J Med, 2006. **355**(26): p. 2757-64.
90. Van Dijk, F.S., et al., *CRTAP mutations in lethal and severe osteogenesis imperfecta: the importance of combining biochemical and molecular genetic analysis.* Eur J Hum Genet, 2009. **17**(12): p. 1560-9.
91. Baldridge, D., et al., *Generalized connective tissue disease in Crtap-/- mouse.* PLoS One, 2010. **5**(5): p. e10560.
92. Cabral, W.A., et al., *A founder mutation in LEPRE1 carried by 1.5% of West Africans and 0.4% of African Americans causes lethal recessive osteogenesis imperfecta.* Genet Med, 2012. **14**(5): p. 543-51.
93. Caparrós-Martin, J.A., et al., *Clinical and molecular analysis in families with autosomal recessive osteogenesis imperfecta identifies mutations in five genes and suggests genotype-phenotype correlations.* Am J Med Genet A, 2013. **161A**(6): p. 1354-69.
94. Besio, R., et al., *Cellular stress due to impairment of collagen prolyl hydroxylation complex is rescued by the chaperone 4-phenylbutyrate.* Dis Model Mech, 2019. **12**(6).
95. Barnes, A.M., et al., *Lack of cyclophilin B in osteogenesis imperfecta with normal collagen folding.* N Engl J Med, 2010. **362**(6): p. 521-8.
96. Christiansen, H.E., et al., *Homozygosity for a missense mutation in SERPINH1, which encodes the collagen chaperone protein HSP47, results in severe recessive osteogenesis imperfecta.* Am J Hum Genet, 2010. **86**(3): p. 389-98.
97. Kawasaki, K., et al., *Deletion of the collagen-specific molecular chaperone Hsp47 causes endoplasmic reticulum stress-mediated apoptosis of hepatic stellate cells.* J Biol Chem, 2015. **290**(6): p. 3639-46.

98. Alanay, Y., et al., *Mutations in the gene encoding the RER protein FKBP65 cause autosomal-recessive osteogenesis imperfecta.* Am J Hum Genet, 2010. **86**(4): p. 551-9.
99. Barnes, A.M., et al., *Absence of FKBP10 in recessive type XI osteogenesis imperfecta leads to diminished collagen cross-linking and reduced collagen deposition in extracellular matrix.* Hum Mutat, 2012. **33**(11): p. 1589-98.
100. Puig-Hervás, M.T., et al., *Mutations in PLOD2 cause autosomal-recessive connective tissue disorders within the Bruck syndrome--osteogenesis imperfecta phenotypic spectrum.* Hum Mutat, 2012. **33**(10): p. 1444-9.
101. Kelley, B.P., et al., *Mutations in FKBP10 cause recessive osteogenesis imperfecta and Bruck syndrome.* J Bone Miner Res, 2011. **26**(3): p. 666-72.
102. Lv, F., et al., *Novel Mutations in PLOD2 Cause Rare Bruck Syndrome.* Calcif Tissue Int, 2018. **102**(3): p. 296-309.
103. Oganesian, A., et al., *The NH2-terminal propeptide of type I procollagen acts intracellularly to modulate cell function.* J Biol Chem, 2006. **281**(50): p. 38507-18.
104. Pace, J.M., et al., *Defective C-propeptides of the proalpha2(I) chain of type I procollagen impede molecular assembly and result in osteogenesis imperfecta.* J Biol Chem, 2008. **283**(23): p. 16061-7.
105. Martínez-Glez, V., et al., *Identification of a mutation causing deficient BMP1/mTLD proteolytic activity in autosomal recessive osteogenesis imperfecta.* Hum Mutat, 2012. **33**(2): p. 343-50.
106. Imamura, Y., B.M. Steiglitz, and D.S. Greenspan, *Bone morphogenetic protein-1 processes the NH2-terminal propeptide, and a furin-like proprotein convertase processes the COOH-terminal propeptide of pro-alpha1(V) collagen.* J Biol Chem, 1998. **273**(42): p. 27511-7.
107. Li, S.W., et al., *The C-proteinase that processes procollagens to fibrillar collagens is identical to the protein previously identified as bone morphogenic protein-1.* Proc Natl Acad Sci U S A, 1996. **93**(10): p. 5127-30.
108. Uzel, M.I., et al., *Multiple bone morphogenetic protein 1-related mammalian metalloproteinases process pro-lysyl oxidase at the correct physiological site and control lysyl oxidase activation in mouse embryo fibroblast cultures.* J Biol Chem, 2001. **276**(25): p. 22537-43.
109. Syx, D., et al., *Defective Proteolytic Processing of Fibrillar Procollagens and Prodecorin Due to Biallelic BMP1 Mutations Results in a Severe, Progressive Form of Osteogenesis Imperfecta.* J Bone Miner Res, 2015. **30**(8): p. 1445-56.
110. Scott, I.C., et al., *Bone morphogenetic protein-1 processes probiglycan.* J Biol Chem, 2000. **275**(39): p. 30504-11.
111. Vadon-Le Goff, S., D.J. Hulmes, and C. Moali, *BMP-1/tolloid-like proteinases synchronize matrix assembly with growth factor activation to promote morphogenesis and tissue remodeling.* Matrix Biol, 2015. **44-46**: p. 14-23.
112. Moffatt, P., et al., *Bril: a novel bone-specific modulator of mineralization.* J Bone Miner Res, 2008. **23**(9): p. 1497-508.
113. Li, F., et al., *Pigment epithelium derived factor suppresses expression of Sost/Sclerostin by osteocytes: implication for its role in bone matrix mineralization.* J Cell Physiol, 2015. **230**(6): p. 1243-9.
114. Li, F., et al., *Pigment epithelium-derived factor (PEDF) reduced expression and synthesis of SOST/sclerostin in bone explant cultures: implication of PEDF-osteocyte gene regulation in vivo.* J Bone Miner Metab, 2019. **37**(5): p. 773-779.

115. Li, F., et al., *Pigment epithelium-derived factor enhances differentiation and mineral deposition of human mesenchymal stem cells.* Stem Cells, 2013. **31**(12): p. 2714-23.
116. Hu, K. and B.R. Olsen, *Osteoblast-derived VEGF regulates osteoblast differentiation and bone formation during bone repair.* J Clin Invest, 2016. **126**(2): p. 509-26.
117. Sekiya, A., et al., *Pigment epithelium-derived factor (PEDF) shares binding sites in collagen with heparin/heparan sulfate proteoglycans.* J Biol Chem, 2011. **286**(30): p. 26364-74.
118. Semler, O., et al., *A mutation in the 5'-UTR of IFITM5 creates an in-frame start codon and causes autosomal-dominant osteogenesis imperfecta type V with hyperplastic callus.* Am J Hum Genet, 2012. **91**(2): p. 349-57.
119. Glorieux, F.H., et al., *Type V osteogenesis imperfecta: a new form of brittle bone disease.* J Bone Miner Res, 2000. **15**(9): p. 1650-8.
120. Cheung, M.S., F.H. Glorieux, and F. Rauch, *Natural history of hyperplastic callus formation in osteogenesis imperfecta type V.* J Bone Miner Res, 2007. **22**(8): p. 1181-6.
121. Homan, E.P., et al., *Mutations in SERPINF1 cause osteogenesis imperfecta type VI.* J Bone Miner Res, 2011. **26**(12): p. 2798-803.
122. Patoine, A., et al., *Topological mapping of BRIL reveals a type II orientation and effects of osteogenesis imperfecta mutations on its cellular destination.* J Bone Miner Res, 2014. **29**(9): p. 2004-16.
123. Farber, C.R., et al., *A novel IFITM5 mutation in severe atypical osteogenesis imperfecta type VI impairs osteoblast production of pigment epithelium-derived factor.* J Bone Miner Res, 2014. **29**(6): p. 1402-11.
124. Nakashima, K., et al., *The novel zinc finger-containing transcription factor osterix is required for osteoblast differentiation and bone formation.* Cell, 2002. **108**(1): p. 17-29.
125. Fiscaletti, M., et al., *Novel variant in Sp7/Osx associated with recessive osteogenesis imperfecta with bone fragility and hearing impairment.* Bone, 2018. **110**: p. 66-75.
126. Lapunzina, P., et al., *Identification of a frameshift mutation in Osterix in a patient with recessive osteogenesis imperfecta.* Am J Hum Genet, 2010. **87**(1): p. 110-4.
127. Cabral, W.A., et al., *Absence of the ER Cation Channel TMEM38B/TRIC-B Disrupts Intracellular Calcium Homeostasis and Dysregulates Collagen Synthesis in Recessive Osteogenesis Imperfecta.* PLoS Genet, 2016. **12**(7): p. e1006156.
128. Moon, R.T., et al., *The promise and perils of Wnt signaling through beta-catenin.* Science, 2002. **296**(5573): p. 1644-6.
129. Laine, C.M., et al., *WNT1 mutations in early-onset osteoporosis and osteogenesis imperfecta.* N Engl J Med, 2013. **368**(19): p. 1809-16.
130. Lindert, U., et al., *MBTPS2 mutations cause defective regulated intramembrane proteolysis in X-linked osteogenesis imperfecta.* Nat Commun, 2016. **7**: p. 11920.
131. Symoens, S., et al., *Deficiency for the ER-stress transducer OASIS causes severe recessive osteogenesis imperfecta in humans.* Orphanet J Rare Dis, 2013. **8**: p. 154.
132. Martinek, N., et al., *Is SPARC an evolutionarily conserved collagen chaperone?* J Dent Res, 2007. **86**(4): p. 296-305.
133. Termine, J.D., et al., *Osteonectin, a bone-specific protein linking mineral to collagen.* Cell, 1981. **26**(1 Pt 1): p. 99-105.

134. Mendoza-Londono, R., et al., *Recessive osteogenesis imperfecta caused by missense mutations in SPARC.* Am J Hum Genet, 2015. **96**(6): p. 979-85.
135. Delany, A.M., et al., *Osteonectin-null mutation compromises osteoblast formation, maturation, and survival.* Endocrinology, 2003. **144**(6): p. 2588-96.
136. van Dijk, F.S., et al., *PLS3 mutations in X-linked osteoporosis with fractures.* N Engl J Med, 2013. **369**(16): p. 1529-36.
137. Fahiminiya, S., et al., *Osteoporosis caused by mutations in PLS3: clinical and bone tissue characteristics.* J Bone Miner Res, 2014. **29**(8): p. 1805-14.
138. Thouverey, C., et al., *Proteomic characterization of biogenesis and functions of matrix vesicles released from mineralizing human osteoblast-like cells.* J Proteomics, 2011. **74**(7): p. 1123-34.
139. Neugebauer, J., et al., *Plastin 3 influences bone homeostasis through regulation of osteoclast activity.* Hum Mol Genet, 2018. **27**(24): p. 4249-4262.
140. Kämpe, A.J., et al., *PLS3 Deletions Lead to Severe Spinal Osteoporosis and Disturbed Bone Matrix Mineralization.* J Bone Miner Res, 2017. **32**(12): p. 2394-2404.
141. Balasubramanian, M., et al., *Novel PLS3 variants in X-linked osteoporosis: Exploring bone material properties.* Am J Med Genet A, 2018. **176**(7): p. 1578-1586.
142. Garbes, L., et al., *Mutations in SEC24D, encoding a component of the COPII machinery, cause a syndromic form of osteogenesis imperfecta.* Am J Hum Genet, 2015. **96**(3): p. 432-9.
143. Zhang, H., et al., *Novel mutations in the SEC24D gene in Chinese families with autosomal recessive osteogenesis imperfecta.* Osteoporos Int, 2017. **28**(4): p. 1473-1480.
144. Moosa, S., et al., *Mutations in SEC24D cause autosomal recessive osteogenesis imperfecta.* Clin Genet, 2016. **89**(4): p. 517-519.
145. Kuchta, K., et al., *FAM46 proteins are novel eukaryotic non-canonical poly(A) polymerases.* Nucleic Acids Res, 2016. **44**(8): p. 3534-48.
146. Diener, S., et al., *Exome sequencing identifies a nonsense mutation in Fam46a associated with bone abnormalities in a new mouse model for skeletal dysplasia.* Mamm Genome, 2016. **27**(3-4): p. 111-21.
147. Watanabe, T., et al., *regulates BMP-dependent pre-placodal ectoderm differentiation in.* Development, 2018. **145**(20).
148. Dagoneau, N., et al., *Null leukemia inhibitory factor receptor (LIFR) mutations in Stuve-Wiedemann/Schwartz-Jampel type 2 syndrome.* Am J Hum Genet, 2004. **74**(2): p. 298-305.
149. Doyard, M., et al., *mutations are responsible for autosomal recessive osteogenesis imperfecta.* J Med Genet, 2018. **55**(4): p. 278-284.
150. Cormier-Daire, V., et al., *Presentation of six cases of Stüve-Wiedemann syndrome.* Pediatr Radiol, 1998. **28**(10): p. 776-80.
151. Moosa, S., et al., *Autosomal-Recessive Mutations in MESD Cause Osteogenesis Imperfecta.* Am J Hum Genet, 2019. **105**(4): p. 836-843.
152. Hsieh, J.C., et al., *Mesd encodes an LRP5/6 chaperone essential for specification of mouse embryonic polarity.* Cell, 2003. **112**(3): p. 355-67.
153. Li, Y., et al., *Mesd binds to mature LDL-receptor-related protein-6 and antagonizes ligand binding.* J Cell Sci, 2005. **118**(Pt 22): p. 5305-14.

154. Koduri, V. and S.C. Blacklow, *Requirement for natively unstructured regions of mesoderm development candidate 2 in promoting low-density lipoprotein receptor-related protein 6 maturation.* Biochemistry, 2007. **46**(22): p. 6570-7.
155. Hartikka, H., et al., *Heterozygous mutations in the LDL receptor-related protein 5 (LRP5) gene are associated with primary osteoporosis in children.* J Bone Miner Res, 2005. **20**(5): p. 783-9.
156. Dubail, J., et al., *Homozygous loss-of-function mutations in CCDC134 are responsible for a severe form of osteogenesis imperfecta.* J Bone Miner Res, 2020.
157. Huang, J., et al., *CCDC134, a novel secretory protein, inhibits activation of ERK and JNK, but not p38 MAPK.* Cell Mol Life Sci, 2008. **65**(2): p. 338-49.
158. Capitani, M. and M. Sallese, *The KDEL receptor: new functions for an old protein.* FEBS Lett, 2009. **583**(23): p. 3863-71.
159. van Dijk, F.S., et al., *Interaction between KDELR2 and HSP47 as a Key Determinant in Osteogenesis Imperfecta Caused by Bi-allelic Variants in KDELR2.* Am J Hum Genet, 2020. **107**(5): p. 989-999.
160. Briggs, M.D., et al., *New therapeutic targets in rare genetic skeletal diseases.* Expert Opin Orphan Drugs, 2015. **3**(10): p. 1137-1154.
161. Boot-Handford, R.P. and M.D. Briggs, *The unfolded protein response and its relevance to connective tissue diseases.* Cell Tissue Res, 2010. **339**(1): p. 197-211.
162. Cabral, W.A., et al., *Type I collagen triplet duplication mutation in lethal osteogenesis imperfecta shifts register of alpha chains throughout the helix and disrupts incorporation of mutant helices into fibrils and extracellular matrix.* J Biol Chem, 2003. **278**(12): p. 10006-12.
163. Nagai, N., et al., *Embryonic lethality of molecular chaperone hsp47 knockout mice is associated with defects in collagen biosynthesis.* J Cell Biol, 2000. **150**(6): p. 1499-506.
164. Bateman, J.F., et al., *Collagen defects in lethal perinatal osteogenesis imperfecta.* Biochem J, 1986. **240**(3): p. 699-708.
165. Bateman, J.F., et al., *Substitution of arginine for glycine 664 in the collagen alpha 1(I) chain in lethal perinatal osteogenesis imperfecta. Demonstration of the peptide defect by in vitro expression of the mutant cDNA.* J Biol Chem, 1988. **263**(24): p. 11627-30.
166. Sarafova, A.P., et al., *Three novel type I collagen mutations in osteogenesis imperfecta type IV probands are associated with discrepancies between electrophoretic migration of osteoblast and fibroblast collagen.* Hum Mutat, 1998. **11**(5): p. 395-403.
167. Mirigian, L.S., et al., *Osteoblast Malfunction Caused by Cell Stress Response to Procollagen Misfolding in α2(I)-G610C Mouse Model of Osteogenesis Imperfecta.* J Bone Miner Res, 2016. **31**(8): p. 1608-1616.
168. Daley, E., et al., *Variable bone fragility associated with an Amish COL1A2 variant and a knock-in mouse model.* J Bone Miner Res, 2010. **25**(2): p. 247-61.
169. Lisse, T.S., et al., *ER stress-mediated apoptosis in a new mouse model of osteogenesis imperfecta.* PLoS Genet, 2008. **4**(2): p. e7.
170. Moore, K.A. and J. Hollien, *The unfolded protein response in secretory cell function.* Annu Rev Genet, 2012. **46**: p. 165-83.
171. Ni, M. and A.S. Lee, *ER chaperones in mammalian development and human diseases.* FEBS Lett, 2007. **581**(19): p. 3641-51.

172. Hetz, C., E. Chevet, and S.A. Oakes, *Proteostasis control by the unfolded protein response.* Nat Cell Biol, 2015. **17**(7): p. 829-38.
173. Hendershot, L.M., *The ER function BiP is a master regulator of ER function.* Mt Sinai J Med, 2004. **71**(5): p. 289-97.
174. Flynn, G.C., et al., *Peptide-binding specificity of the molecular chaperone BiP.* Nature, 1991. **353**(6346): p. 726-30.
175. Meunier, L., et al., *A subset of chaperones and folding enzymes form multiprotein complexes in endoplasmic reticulum to bind nascent proteins.* Mol Biol Cell, 2002. **13**(12): p. 4456-69.
176. Zhang, J.X., et al., *Quality control in the secretory pathway: the role of calreticulin, calnexin and BiP in the retention of glycoproteins with C-terminal truncations.* Mol Biol Cell, 1997. **8**(10): p. 1943-54.
177. Freedman, R.B., P. Klappa, and L.W. Ruddock, *Protein disulfide isomerases exploit synergy between catalytic and specific binding domains.* EMBO Rep, 2002. **3**(2): p. 136-40.
178. Ellgaard, L. and L.W. Ruddock, *The human protein disulphide isomerase family: substrate interactions and functional properties.* EMBO Rep, 2005. **6**(1): p. 28-32.
179. Lewy, T.G., J.M. Grabowski, and M.E. Bloom, *BiP: Master Regulator of the Unfolded Protein Response and Crucial Factor in Flavivirus Biology.* Yale J Biol Med, 2017. **90**(2): p. 291-300.
180. Carrara, M., et al., *Crystal structures reveal transient PERK luminal domain tetramerization in endoplasmic reticulum stress signaling.* EMBO J, 2015. **34**(11): p. 1589-600.
181. Zhou, J., et al., *The crystal structure of human IRE1 luminal domain reveals a conserved dimerization interface required for activation of the unfolded protein response.* Proc Natl Acad Sci U S A, 2006. **103**(39): p. 14343-8.
182. Chessler, S.D. and P.H. Byers, *BiP binds type I procollagen pro alpha chains with mutations in the carboxyl-terminal propeptide synthesized by cells from patients with osteogenesis imperfecta.* J Biol Chem, 1993. **268**(24): p. 18226-33.
183. Rutkowski, D.T. and R.J. Kaufman, *A trip to the ER: coping with stress.* Trends Cell Biol, 2004. **14**(1): p. 20-8.
184. Shi, Y., et al., *Identification and characterization of pancreatic eukaryotic initiation factor 2 alpha-subunit kinase, PEK, involved in translational control.* Mol Cell Biol, 1998. **18**(12): p. 7499-509.
185. Fusakio, M.E., et al., *Transcription factor ATF4 directs basal and stress-induced gene expression in the unfolded protein response and cholesterol metabolism in the liver.* Mol Biol Cell, 2016. **27**(9): p. 1536-51.
186. Yoshida, H., et al., *XBP1 mRNA is induced by ATF6 and spliced by IRE1 in response to ER stress to produce a highly active transcription factor.* Cell, 2001. **107**(7): p. 881-91.
187. Lee, A.H., N.N. Iwakoshi, and L.H. Glimcher, *XBP-1 regulates a subset of endoplasmic reticulum resident chaperone genes in the unfolded protein response.* Mol Cell Biol, 2003. **23**(21): p. 7448-59.
188. Calfon, M., et al., *IRE1 couples endoplasmic reticulum load to secretory capacity by processing the XBP-1 mRNA.* Nature, 2002. **415**(6867): p. 92-6.
189. Haze, K., et al., *Mammalian transcription factor ATF6 is synthesized as a transmembrane protein and activated by proteolysis in response to endoplasmic reticulum stress.* Mol Biol Cell, 1999. **10**(11): p. 3787-99.

190. Wang, M., et al., *Role of the unfolded protein response regulator GRP78/BiP in development, cancer, and neurological disorders.* Antioxid Redox Signal, 2009. **11**(9): p. 2307-16.
191. Bateman, J.F., et al., *Abnormal type I collagen metabolism by cultured fibroblasts in lethal perinatal osteogenesis imperfecta.* Biochem J, 1984. **217**(1): p. 103-15.
192. Ishida, Y., et al., *Autophagic elimination of misfolded procollagen aggregates in the endoplasmic reticulum as a means of cell protection.* Mol Biol Cell, 2009. **20**(11): p. 2744-54.
193. Klionsky, D.J., *Autophagy: from phenomenology to molecular understanding in less than a decade.* Nat Rev Mol Cell Biol, 2007. **8**(11): p. 931-7.
194. Mizushima, N., et al., *Autophagy fights disease through cellular self-digestion.* Nature, 2008. **451**(7182): p. 1069-75.
195. Omari, S., et al., *Noncanonical autophagy at ER exit sites regulates procollagen turnover.* Proc Natl Acad Sci U S A, 2018. **115**(43): p. E10099-E10108.
196. Shore, G.C., F.R. Papa, and S.A. Oakes, *Signaling cell death from the endoplasmic reticulum stress response.* Curr Opin Cell Biol, 2011. **23**(2): p. 143-9.
197. D'Arcy, M.S., *Cell death: a review of the major forms of apoptosis, necrosis and autophagy.* Cell Biol Int, 2019. **43**(6): p. 582-592.
198. Zinszner, H., et al., *CHOP is implicated in programmed cell death in response to impaired function of the endoplasmic reticulum.* Genes Dev, 1998. **12**(7): p. 982-95.
199. Urano, F., et al., *Coupling of stress in the ER to activation of JNK protein kinases by transmembrane protein kinase IRE1.* Science, 2000. **287**(5453): p. 664-6.
200. Han, D., et al., *IRE1alpha kinase activation modes control alternate endoribonuclease outputs to determine divergent cell fates.* Cell, 2009. **138**(3): p. 562-75.
201. Hetz, C., et al., *Proapoptotic BAX and BAK modulate the unfolded protein response by a direct interaction with IRE1alpha.* Science, 2006. **312**(5773): p. 572-6.
202. Morello, R., *Osteogenesis imperfecta and therapeutics.* Matrix Biol, 2018. **71-72**: p. 294-312.
203. Soares, A.P., et al., *Bisphosphonates: Pharmacokinetics, bioavailability, mechanisms of action, clinical applications in children, and effects on tooth development.* Environ Toxicol Pharmacol, 2016. **42**: p. 212-7.
204. Besio, R. and A. Forlino, *Treatment options for osteogenesis imperfecta* 2015.
205. Papapoulos, S.E., *Bisphosphonates: how do they work?* Best Pract Res Clin Endocrinol Metab, 2008. **22**(5): p. 831-47.
206. Adami, S., et al., *Intravenous neridronate in adults with osteogenesis imperfecta.* J Bone Miner Res, 2003. **18**(1): p. 126-30.
207. Shapiro, J.R., et al., *The effect of intravenous pamidronate on bone mineral density, bone histomorphometry, and parameters of bone turnover in adults with type IA osteogenesis imperfecta.* Calcif Tissue Int, 2003. **72**(2): p. 103-12.
208. Shapiro, J.R., et al., *Bone mineral density and fracture rate in response to intravenous and oral bisphosphonates in adult osteogenesis imperfecta.* Calcif Tissue Int, 2010. **87**(2): p. 120-9.
209. Rauch, F., et al., *The effects of intravenous pamidronate on the bone tissue of children and adolescents with osteogenesis imperfecta.* J Clin Invest, 2002. **110**(9): p. 1293-9.

210. Ward, L.M., et al., *Alendronate for the treatment of pediatric osteogenesis imperfecta: a randomized placebo-controlled study.* J Clin Endocrinol Metab, 2011. **96**(2): p. 355-64.
211. Bishop, N., et al., *Risedronate in children with osteogenesis imperfecta: a randomised, double-blind, placebo-controlled trial.* Lancet, 2013. **382**(9902): p. 1424-32.
212. Papapoulos, S.E. and S.C. Cremers, *Prolonged bisphosphonate release after treatment in children.* N Engl J Med, 2007. **356**(10): p. 1075-6.
213. Alharbi, M., et al., *Pamidronate treatment of children with moderate-to-severe osteogenesis imperfecta: a note of caution.* Horm Res, 2009. **71**(1): p. 38-44.
214. Nicolaou, N., et al., *Changing pattern of femoral fractures in osteogenesis imperfecta with prolonged use of bisphosphonates.* J Child Orthop, 2012. **6**(1): p. 21-7.
215. Honma, M., et al., *RANKL subcellular trafficking and regulatory mechanisms in osteocytes.* J Bone Miner Res, 2013. **28**(9): p. 1936-49.
216. Xiong, J., et al., *Matrix-embedded cells control osteoclast formation.* Nat Med, 2011. **17**(10): p. 1235-41.
217. Bargman, R., et al., *RANKL inhibition improves bone properties in a mouse model of osteogenesis imperfecta.* Connect Tissue Res, 2010. **51**(2): p. 123-31.
218. Bone, H.G., et al., *10 years of denosumab treatment in postmenopausal women with osteoporosis: results from the phase 3 randomised FREEDOM trial and open-label extension.* Lancet Diabetes Endocrinol, 2017. **5**(7): p. 513-523.
219. Guerrini, M.M. and H. Takayanagi, *The immune system, bone and RANKL.* Arch Biochem Biophys, 2014. **561**: p. 118-23.
220. Hoyer-Kuhn, H., et al., *Safety and efficacy of denosumab in children with osteogenesis imperfect--a first prospective trial.* J Musculoskelet Neuronal Interact, 2016. **16**(1): p. 24-32.
221. Semler, O., et al., *First use of the RANKL antibody denosumab in osteogenesis imperfecta type VI.* J Musculoskelet Neuronal Interact, 2012. **12**(3): p. 183-8.
222. Hoyer-Kuhn, H., O. Semler, and E. Schoenau, *Effect of denosumab on the growing skeleton in osteogenesis imperfecta.* J Clin Endocrinol Metab, 2014. **99**(11): p. 3954-5.
223. Neer, R.M., et al., *Effect of parathyroid hormone (1-34) on fractures and bone mineral density in postmenopausal women with osteoporosis.* N Engl J Med, 2001. **344**(19): p. 1434-41.
224. Kawai, M., et al., *Emerging therapeutic opportunities for skeletal restoration.* Nat Rev Drug Discov, 2011. **10**(2): p. 141-56.
225. Gatti, D., et al., *Teriparatide treatment in adult patients with osteogenesis imperfecta type I.* Calcif Tissue Int, 2013. **93**(5): p. 448-52.
226. Leali, P.T., et al., *Efficacy of teriparatide.* Clin Cases Miner Bone Metab, 2017. **14**(2): p. 153-156.
227. Holm, J., et al., *Atypical femoral fracture in an osteogenesis imperfecta patient successfully treated with teriparatide.* Endocr Pract, 2014. **20**(10): p. e187-90.
228. Orwoll, E.S., et al., *Evaluation of teriparatide treatment in adults with osteogenesis imperfecta.* J Clin Invest, 2014. **124**(2): p. 491-8.
229. Lewiecki, E.M., *Role of sclerostin in bone and cartilage and its potential as a therapeutic target in bone diseases.* Ther Adv Musculoskelet Dis, 2014. **6**(2): p. 48-57.

230. Sinder, B.P., et al., *Adult Brtl/+ mouse model of osteogenesis imperfecta demonstrates anabolic response to sclerostin antibody treatment with increased bone mass and strength.* Osteoporos Int, 2014. **25**(8): p. 2097-107.
231. Sinder, B.P., et al., *Rapidly growing Brtl/+ mouse model of osteogenesis imperfecta improves bone mass and strength with sclerostin antibody treatment.* Bone, 2015. **71**: p. 115-23.
232. Roschger, A., et al., *Effect of sclerostin antibody treatment in a mouse model of severe osteogenesis imperfecta.* Bone, 2014. **66**: p. 182-8.
233. Grafe, I., et al., *Sclerostin Antibody Treatment Improves the Bone Phenotype of Crtap(-/-) Mice, a Model of Recessive Osteogenesis Imperfecta.* J Bone Miner Res, 2016. **31**(5): p. 1030-40.
234. Cardinal, M., et al., *Sclerostin antibody reduces long bone fractures in the oim/oim model of osteogenesis imperfecta.* Bone, 2019. **124**: p. 137-147.
235. Olvera, D., et al., *Low Dose of Bisphosphonate Enhances Sclerostin Antibody-Induced Trabecular Bone Mass Gains in Brtl/+ Osteogenesis Imperfecta Mouse Model.* J Bone Miner Res, 2018. **33**(7): p. 1272-1282.
236. Tang, Y., et al., *TGF-beta1-induced migration of bone mesenchymal stem cells couples bone resorption with formation.* Nat Med, 2009. **15**(7): p. 757-65.
237. Song, B., K.D. Estrada, and K.M. Lyons, *Smad signaling in skeletal development and regeneration.* Cytokine Growth Factor Rev, 2009. **20**(5-6): p. 379-88.
238. Erlebacher, A. and R. Derynck, *Increased expression of TGF-beta 2 in osteoblasts results in an osteoporosis-like phenotype.* J Cell Biol, 1996. **132**(1-2): p. 195-210.
239. Grafe, I., et al., *Excessive transforming growth factor-β signaling is a common mechanism in osteogenesis imperfecta.* Nat Med, 2014. **20**(6): p. 670-5.
240. Bianchi, L., et al., *Altered cytoskeletal organization characterized lethal but not surviving Brtl+/- mice: insight on phenotypic variability in osteogenesis imperfecta.* Hum Mol Genet, 2015. **24**(21): p. 6118-33.
241. Trachtman, H., et al., *A phase 1, single-dose study of fresolimumab, an anti-TGF-β antibody, in treatment-resistant primary focal segmental glomerulosclerosis.* Kidney Int, 2011. **79**(11): p. 1236-43.
242. Cabral, W.A. and J.C. Marini, *High proportion of mutant osteoblasts is compatible with normal skeletal function in mosaic carriers of osteogenesis imperfecta.* Am J Hum Genet, 2004. **74**(4): p. 752-60.
243. Panaroni, C., et al., *In utero transplantation of adult bone marrow decreases perinatal lethality and rescues the bone phenotype in the knockin murine model for classical, dominant osteogenesis imperfecta.* Blood, 2009. **114**(2): p. 459-68.
244. Horwitz, E.M., et al., *Isolated allogeneic bone marrow-derived mesenchymal cells engraft and stimulate growth in children with osteogenesis imperfecta: Implications for cell therapy of bone.* Proc Natl Acad Sci U S A, 2002. **99**(13): p. 8932-7.
245. Le Blanc, K., et al., *Fetal mesenchymal stem-cell engraftment in bone after in utero transplantation in a patient with severe osteogenesis imperfecta.* Transplantation, 2005. **79**(11): p. 1607-14.
246. Götherström, C., et al., *Pre- and postnatal transplantation of fetal mesenchymal stem cells in osteogenesis imperfecta: a two-center experience.* Stem Cells Transl Med, 2014. **3**(2): p. 255-64.
247. Sagar, R., et al., *Fetal stem cell transplantation and gene therapy.* Best Pract Res Clin Obstet Gynaecol, 2019. **58**: p. 142-153.

248. Keating, A., *Mesenchymal stromal cells: new directions.* Cell Stem Cell, 2012. **10**(6): p. 709-716.
249. Phinney, D.G. and M.F. Pittenger, *Concise Review: MSC-Derived Exosomes for Cell-Free Therapy.* Stem Cells, 2017. **35**(4): p. 851-858.
250. Katsuda, T., et al., *The therapeutic potential of mesenchymal stem cell-derived extracellular vesicles.* Proteomics, 2013. **13**(10-11): p. 1637-53.
251. Huang, Y.C., O. Parolini, and L. Deng, *The potential role of microvesicles in mesenchymal stem cell-based therapy.* Stem Cells Dev, 2013. **22**(6): p. 841-4.
252. Valadi, H., et al., *Exosome-mediated transfer of mRNAs and microRNAs is a novel mechanism of genetic exchange between cells.* Nat Cell Biol, 2007. **9**(6): p. 654-9.
253. Théry, C., M. Ostrowski, and E. Segura, *Membrane vesicles as conveyors of immune responses.* Nat Rev Immunol, 2009. **9**(8): p. 581-93.
254. Phinney, D.G., et al., *Mesenchymal stem cells use extracellular vesicles to outsource mitophagy and shuttle microRNAs.* Nat Commun, 2015. **6**: p. 8472.
255. Otsuru, S., et al., *Transplanted bone marrow mononuclear cells and MSCs impart clinical benefit to children with osteogenesis imperfecta through different mechanisms.* Blood, 2012. **120**(9): p. 1933-41.
256. Otsuru, S., et al., *Extracellular vesicles released from mesenchymal stromal cells stimulate bone growth in osteogenesis imperfecta.* Cytotherapy, 2018. **20**(1): p. 62-73.
257. Shapiro, J.R., *Genetic approach to treatment of osteogenesis imperfecta* 2013: Oxford, UK.
258. Chamberlain, J.R., et al., *Gene targeting in stem cells from individuals with osteogenesis imperfecta.* Science, 2004. **303**(5661): p. 1198-201.
259. Lindahl, K., et al., *Allele dependent silencing of collagen type I using small interfering RNAs targeting 3'UTR Indels - a novel therapeutic approach in osteogenesis imperfecta.* Int J Med Sci, 2013. **10**(10): p. 1333-43.
260. Lindahl, K., et al., *Allele dependent silencing of COL1A2 using small interfering RNAs.* Int J Med Sci, 2008. **5**(6): p. 361-5.
261. Rousseau, J., et al., *Allele-specific Col1a1 silencing reduces mutant collagen in fibroblasts from Brtl mouse, a model for classical osteogenesis imperfecta.* Eur J Hum Genet, 2014. **22**(5): p. 667-74.
262. Zhang, G., et al., *A delivery system targeting bone formation surfaces to facilitate RNAi-based anabolic therapy.* Nat Med, 2012. **18**(2): p. 307-14.
263. Millington-Ward, S., et al., *RNAi of COL1A1 in mesenchymal progenitor cells.* Eur J Hum Genet, 2004. **12**(10): p. 864-6.
264. McNamara, J.O., et al., *Cell type-specific delivery of siRNAs with aptamer-siRNA chimeras.* Nat Biotechnol, 2006. **24**(8): p. 1005-15.
265. Deyle, D.R., et al., *Normal collagen and bone production by gene-targeted human osteogenesis imperfecta iPSCs.* Mol Ther, 2012. **20**(1): p. 204-13.
266. Gao, X., et al., *Treatment of autosomal dominant hearing loss by in vivo delivery of genome editing agents.* Nature, 2018. **553**(7687): p. 217-221.
267. Mendell, J.R. and L.R. Rodino-Klapac, *Duchenne muscular dystrophy: CRISPR/Cas9 treatment.* Cell Res, 2016. **26**(5): p. 513-4.
268. Karimian, A., et al., *CRISPR/Cas9 technology as a potent molecular tool for gene therapy.* J Cell Physiol, 2019. **234**(8): p. 12267-12277.
269. Spira, A.I. and M.A. Carducci, *Differentiation therapy.* Curr Opin Pharmacol, 2003. **3**(4): p. 338-43.

270. Brusilow, S.W., *Phenylacetylglutamine may replace urea as a vehicle for waste nitrogen excretion.* Pediatr Res, 1991. **29**(2): p. 147-50.
271. Iannitti, T. and B. Palmieri, *Clinical and experimental applications of sodium phenylbutyrate.* Drugs R D, 2011. **11**(3): p. 227-49.
272. Monneret, C., *Histone deacetylase inhibitors.* Eur J Med Chem, 2005. **40**(1): p. 1-13.
273. Strahl, B.D. and C.D. Allis, *The language of covalent histone modifications.* Nature, 2000. **403**(6765): p. 41-5.
274. Leandro, P. and C.M. Gomes, *Protein misfolding in conformational disorders: rescue of folding defects and chemical chaperoning.* Mini Rev Med Chem, 2008. **8**(9): p. 901-11.
275. Arakawa, T., et al., *Small molecule pharmacological chaperones: From thermodynamic stabilization to pharmaceutical drugs.* Biochim Biophys Acta, 2006. **1764**(11): p. 1677-87.
276. Kolb, P.S., et al., *The therapeutic effects of 4-phenylbutyric acid in maintaining proteostasis.* Int J Biochem Cell Biol, 2015. **61**: p. 45-52.
277. Rubenstein, R.C., M.E. Egan, and P.L. Zeitlin, *In vitro pharmacologic restoration of CFTR-mediated chloride transport with sodium 4-phenylbutyrate in cystic fibrosis epithelial cells containing delta F508-CFTR.* J Clin Invest, 1997. **100**(10): p. 2457-65.
278. Gregor, M.F. and G.S. Hotamisligil, *Thematic review series: Adipocyte Biology. Adipocyte stress: the endoplasmic reticulum and metabolic disease.* J Lipid Res, 2007. **48**(9): p. 1905-14.
279. Basseri, S., et al., *The chemical chaperone 4-phenylbutyrate inhibits adipogenesis by modulating the unfolded protein response.* J Lipid Res, 2009. **50**(12): p. 2486-501.
280. Granell, S., et al., *Obesity-linked variants of melanocortin-4 receptor are misfolded in the endoplasmic reticulum and can be rescued to the cell surface by a chemical chaperone.* Mol Endocrinol, 2010. **24**(9): p. 1805-21.
281. Burrows, J.A., L.K. Willis, and D.H. Perlmutter, *Chemical chaperones mediate increased secretion of mutant alpha 1-antitrypsin (alpha 1-AT) Z: A potential pharmacological strategy for prevention of liver injury and emphysema in alpha 1-AT deficiency.* Proc Natl Acad Sci U S A, 2000. **97**(4): p. 1796-801.
282. Teckman, J.H., *Lack of effect of oral 4-phenylbutyrate on serum alpha-1-antitrypsin in patients with alpha-1-antitrypsin deficiency: a preliminary study.* J Pediatr Gastroenterol Nutr, 2004. **39**(1): p. 34-7.
283. Yam, G.H., et al., *Sodium 4-phenylbutyrate acts as a chemical chaperone on misfolded myocilin to rescue cells from endoplasmic reticulum stress and apoptosis.* Invest Ophthalmol Vis Sci, 2007. **48**(4): p. 1683-90.
284. Gong, B., et al., *Sodium 4-phenylbutyrate ameliorates the effects of cataract-causing mutant gammaD-crystallin in cultured cells.* Mol Vis, 2010. **16**: p. 997-1003.
285. van der Velden, L.M., et al., *Folding defects in P-type ATP 8B1 associated with hereditary cholestasis are ameliorated by 4-phenylbutyrate.* Hepatology, 2010. **51**(1): p. 286-96.
286. van den Berghe, P.V., et al., *Reduced expression of ATP7B affected by Wilson disease-causing mutations is rescued by pharmacological folding chaperones 4-phenylbutyrate and curcumin.* Hepatology, 2009. **50**(6): p. 1783-95.

287. Ono, K., et al., *A chemical chaperone, sodium 4-phenylbutyric acid, attenuates the pathogenic potency in human alpha-synuclein A30P + A53T transgenic mice.* Parkinsonism Relat Disord, 2009. **15**(9): p. 649-54.
288. Lee, H.W., et al., *Histone deacetylase 1-mediated histone modification regulates osteoblast differentiation.* Mol Endocrinol, 2006. **20**(10): p. 2432-43.
289. Schroeder, T.M. and J.J. Westendorf, *Histone deacetylase inhibitors promote osteoblast maturation.* J Bone Miner Res, 2005. **20**(12): p. 2254-63.
290. Murray, L.S., et al., *Chemical chaperone treatment reduces intracellular accumulation of mutant collagen IV and ameliorates the cellular phenotype of a COL4A2 mutation that causes haemorrhagic stroke.* Hum Mol Genet, 2014. **23**(2): p. 283-92.
291. Fisher, S., P. Jagadeeswaran, and M.E. Halpern, *Radiographic analysis of zebrafish skeletal defects.* Dev Biol, 2003. **264**(1): p. 64-76.
292. Gioia, R., et al., *The chaperone activity of 4PBA ameliorates the skeletal phenotype of Chihuahua, a zebrafish model for dominant osteogenesis imperfecta.* Hum Mol Genet, 2017. **26**(15): p. 2897-2911.
293. Li, H., et al., *Defective autophagy in osteoblasts induces endoplasmic reticulum stress and causes remarkable bone loss.* Autophagy, 2018. **14**(10): p. 1726-1741.
294. Bonadio, J., et al., *Transgenic mouse model of the mild dominant form of osteogenesis imperfecta.* Proc Natl Acad Sci U S A, 1990. **87**(18): p. 7145-9.
295. Jepsen, K.J., et al., *Type-I collagen mutation compromises the post-yield behavior of Mov13 long bone.* J Orthop Res, 1996. **14**(3): p. 493-9.
296. Pereira, R., et al., *Transgenic mice expressing a partially deleted gene for type I procollagen (COL1A1). A breeding line with a phenotype of spontaneous fractures and decreased bone collagen and mineral.* J Clin Invest, 1993. **91**(2): p. 709-16.
297. Khillan, J.S., et al., *Transgenic mice that express a mini-gene version of the human gene for type I procollagen (COL1A1) develop a phenotype resembling a lethal form of osteogenesis imperfecta.* J Biol Chem, 1991. **266**(34): p. 23373-9.
298. Enderli, T.A., et al., *Animal models of osteogenesis imperfecta: applications in clinical research.* Orthop Res Rev, 2016. **8**: p. 41-55.
299. Stacey, A., et al., *Perinatal lethal osteogenesis imperfecta in transgenic mice bearing an engineered mutant pro-alpha 1(I) collagen gene.* Nature, 1988. **332**(6160): p. 131-6.
300. Bateman, J.F., et al., *The study of collagen structure and function by site-directed mutagenesis of collagen genes.* Ann N Y Acad Sci, 1990. **580**: p. 324-9.
301. Chen, F., et al., *First mouse model for combined osteogenesis imperfecta and Ehlers-Danlos syndrome.* J Bone Miner Res, 2014. **29**(6): p. 1412-23.
302. Chipman, S.D., et al., *Defective pro alpha 2(I) collagen synthesis in a recessive mutation in mice: a model of human osteogenesis imperfecta.* Proc Natl Acad Sci U S A, 1993. **90**(5): p. 1701-5.
303. McBride, D.J., J.R. Shapiro, and M.G. Dunn, *Bone geometry and strength measurements in aging mice with the oim mutation.* Calcif Tissue Int, 1998. **62**(2): p. 172-6.
304. Camacho, N.P., et al., *The material basis for reduced mechanical properties in oim mice bones.* J Bone Miner Res, 1999. **14**(2): p. 264-72.
305. Forlino, A., et al., *Use of the Cre/lox recombination system to develop a non-lethal knock-in murine model for osteogenesis imperfecta with an alpha1(I) G349C*

substitution. Variability in phenotype in BrtlIV mice. J Biol Chem, 1999. **274**(53): p. 37923-31.
306. Marini, J.C., et al., *Serine for glycine substitutions in type I collagen in two cases of type IV osteogenesis imperfecta (OI). Additional evidence for a regional model of OI pathophysiology.* J Biol Chem, 1993. **268**(4): p. 2667-73.
307. Marini, J.C., *Osteogenesis imperfecta: comprehensive management.* Adv Pediatr, 1988. **35**: p. 391-426.
308. Kozloff, K.M., et al., *Brittle IV mouse model for osteogenesis imperfecta IV demonstrates postpubertal adaptations to improve whole bone strength.* J Bone Miner Res, 2004. **19**(4): p. 614-22.
309. Uveges, T.E., et al., *Cellular mechanism of decreased bone in Brtl mouse model of OI: imbalance of decreased osteoblast function and increased osteoclasts and their precursors.* J Bone Miner Res, 2008. **23**(12): p. 1983-94.
310. Gioia, R., et al., *Impaired osteoblastogenesis in a murine model of dominant osteogenesis imperfecta: a new target for osteogenesis imperfecta pharmacological therapy.* Stem Cells, 2012. **30**(7): p. 1465-76.
311. Kuznetsova, N.V., et al., *Structure, stability and interactions of type I collagen with GLY349-CYS substitution in alpha 1(I) chain in a murine Osteogenesis Imperfecta model.* Matrix Biol, 2004. **23**(2): p. 101-12.
312. Forlino, A., et al., *Selective retention and degradation of molecules with a single mutant alpha1(I) chain in the Brtl IV mouse model of OI.* Matrix Biol, 2007. **26**(8): p. 604-14.
313. Fertala, A., et al., *Collagen II containing a Cys substitution for Arg-alpha1-519: abnormal interactions of the mutated molecules with collagen IX.* Biochemistry, 2001. **40**(48): p. 14422-8.
314. Kojima, T., et al., *The retention of abnormal type I procollagen and correlated expression of HSP 47 in fibroblasts from a patient with lethal osteogenesis imperfecta.* J Pathol, 1998. **184**(2): p. 212-8.
315. Forlino, A., et al., *Differential expression of both extracellular and intracellular proteins is involved in the lethal or nonlethal phenotypic variation of BrtlIV, a murine model for osteogenesis imperfecta.* Proteomics, 2007. **7**(11): p. 1877-91.
316. Bianchi, L., et al., *Differential response to intracellular stress in the skin from osteogenesis imperfecta Brtl mice with lethal and non lethal phenotype: a proteomic approach.* J Proteomics, 2012. **75**(15): p. 4717-33.
317. Goldman, R.D., et al., *The function of intermediate filaments in cell shape and cytoskeletal integrity.* J Cell Biol, 1996. **134**(4): p. 971-83.
318. Cassimeris, L., *The oncoprotein 18/stathmin family of microtubule destabilizers.* Curr Opin Cell Biol, 2002. **14**(1): p. 18-24.
319. Bamburg, J.R., *Proteins of the ADF/cofilin family: essential regulators of actin dynamics.* Annu Rev Cell Dev Biol, 1999. **15**: p. 185-230.
320. Streeten, E.A., et al., *Quantitative trait loci for BMD identified by autosome-wide linkage scan to chromosomes 7q and 21q in men from the Amish Family Osteoporosis Study.* J Bone Miner Res, 2006. **21**(9): p. 1433-42.
321. Agarwala, R., L.G. Biesecker, and A.A. Schäffer, *Anabaptist genealogy database.* Am J Med Genet C Semin Med Genet, 2003. **121C**(1): p. 32-7.
322. Masci, M., et al., *Bone mineral properties in growing Col1a2(+/G610C) mice, an animal model of osteogenesis imperfecta.* Bone, 2016. **87**: p. 120-9.

323. Mertz, E.L., et al., *Makings of a brittle bone: Unexpected lessons from a low protein diet study of a mouse OI model.* Matrix Biol, 2016. **52-54**: p. 29-42.
324. Jeong, Y., et al., *Hindlimb Skeletal Muscle Function and Skeletal Quality and Strength in +/G610C Mice With and Without Weight-Bearing Exercise.* J Bone Miner Res, 2015. **30**(10): p. 1874-86.
325. Bi, X., et al., *Correlations Between Bone Mechanical Properties and Bone Composition Parameters in Mouse Models of Dominant and Recessive Osteogenesis Imperfecta and the Response to Anti-TGF-β Treatment.* J Bone Miner Res, 2017. **32**(2): p. 347-359.